Environmental Degradation of Historical Materials in Jeddah, Saudi Arabia

Fahed Ayed N Aloufi

A thesis submitted to the University of Bristol in accordance with regulations of the degree of Doctor of Philosophy at the

Interface Analysis Centre, Faculty of Science

February 2020

42,608 Words

Declaration of authorship

I declare that the work in this dissertation was carried out in accordance with the requirements of the University's Regulations and Code of Practice for Research Degree Programmes and that it has not been submitted for any other academic award. Except where indicated by specific reference in the text, the work is the candidate's own work. Work done in collaboration with, or with the assistance of, others, is indicated as such. Any views expressed in the dissertation are those of the author.

Signed: ……

Date: ……

“Happiness can be found even in the darkest times, when one only remembers to turn on the light.”

Albus Dumbledore, Harry Potter and the Prisoner of Azkaban

Abstract

The work presented in this thesis involved a study of the effects of atmospheric pollution aerosol particulates on the degradation of building materials used to construct the declared UNESCO world heritage site located in Jeddah, Saudi Arabia. The novelties of this work were to identify the type of atmospheric aerosol pollutants deposited on building surfaces at the historical site and its environmental impacts on the degradation of the building materials. Stone, mortar and plaster specimens were collected from six historic houses as well as fresh stone sample from the quarry where the stone blocks were produced. The composition and alteration characteristics of the stone, mortar, plaster and quarry materials were determined to provide information about the chemical compositions and their decay mechanisms. Light Optical Microscopy (OM), X-Ray Diffraction (XRD), Laser Raman Spectroscopy (LRS) and Scanning Electron Microscopy combined with Energy-Dispersion X-ray Spectroscopy (SEM-EDS) were the analytical techniques used for this purpose. The results revealed that the stone used throughout the historic buildings comprised of calcareous limestone. Calcite, ($CaCO_3$), Aragonite, ($CaCO_3$), Gypsum, ($CaSO_4.2H_2O$), Quartz, (SiO_2) and Halite, (NaCl), were the primary phases identified in the stone samples. The mortar mixture that was used to bind the stones consisted of lime, local sand and crushed seashells. The chemical binding agent used to produce the mortar was non-hydraulic lime. Calcite, ($CaCO_3$), Gypsum, ($CaSO_4.2H_2O$), Orthoclase Feldspar, ($KAlSi_3O_8$), Quartz, (SiO_2) and Halite, (NaCl) were the main phases identified. The binding plaster was determined to be a mixture of lime, gypsum, local sand and crushed seashells, again with non-hydraulic lime as the active binding agent. The decorative facade samples consisted of the phase gypsum ($CaSO_4.2H_2O$). Calcite, ($CaCO_3$), Aragonite, ($CaCO_3$), Gypsum, ($CaSO_4.2H_2O$), Quartz, (SiO_2) and Halite, (NaCl), were the main phases identified. On plaster surfaces, anthropogenic particulate matter (PM) and, sea salt was detected. During the investigation, the anthropogenic particles detected were microscale metallic particles determined to comprise of Fe, Zn and Cu. Other contaminant elements identified included sodium, chloride, sulphur and phosphorus. The observation of metallic particles was unusual and not to our knowledge, previously reported in any aerosol pollution survey in Jeddah.

Atmospheric pollution play an important role in the degradation of historical buildings. The observed aerosol PM's on the samples collected from both building surfaces in the historical quarter and air filter samples were rich in spherical and irregularly structured metallic particles. There was good agreement between air and solid samples, indicating that particles were relatable and had a similar provenance. Metallic particles were distinct in their composition, being comprised of Fe, Zn, and Cu with lesser amounts of C, Mn, Ca, K, Ti and S.

Laboratory studies carried out on calcite single crystals and stone substrates illustrated that during environmental corrosion of these particles on building surface, the associated volume expansion from metal oxidation would be sufficient to cause brittle failure (micro-cracking) of the surface layers of building material. Furthermore, a higher frequency of cracking was observed in calcite single crystal than seen in limestone substrates. This would further exacerbate the increase degradation rates that are already expected to be occurring from increased level of atmospheric CO_2.

Acknowledgments

First, I would like to give my grateful thanks and praise to Allah the almighty in whom I depend and believe in. The accomplishment of this work has been made possible by his will and mercy, and may his peace and blessings be upon his prophet Mohammed.

I would also like to sincerely give thanks to my two academic supervisors: Professor Tom Scott and Dr Adel El-Turke. Without their encouragement and professional supervision, it would have been impossible for me to finish this thesis.

The assistance of my colleagues at the Interface Analysis Centre, especially Dr Keith Hallam, Dr Peter Heard, Dr John Day, Dr Christopher Jones and Dr Charilaos Paraskevoulakos for advice and keeping the equipment running, is gratefully acknowledged. The assistance of everyone else at the University of Bristol is gratefully acknowledged.

I would like to thank my mother, Gomaiah, and father, Ayed, and the rest of my family for their continued prayers and support. This thesis would not have been completed without their love and understanding.

I would like to utilise this opportunity to express my deepest thanks to my government of Saudi Arabia for trusting me and providing financial assistance and support which has enabled me to carry out this research.

Also, I would like to thank all my friends and colleagues in United Kingdom and Saudi Arabia for their encouragement, friendship and help which has contributed to this work in several ways.

Finally, may Allah accept this work for his sake

Publications

Publications:

Fahed Ayed N Aloufi, Adel El-Turke, Tom Scott. (2017) Analysis of the constituent materials of historical buildings in Jeddah, Saudi Arabia. (In Preparation).

Fahed Ayed N Aloufi, Adel El-Turke, Tom Scott. (2019) Identification and Characterisation of Particulate Matter (PM) on Historical Site and Southern Industrial Area in Jeddah, Saudi Arabia. (In Preparation).

Conferences (posters and presentations):

Fahed Ayed N Aloufi, Adel El-Turke, Tom Scott. (2017) Analysis of the constituent materials of historical buildings in Jeddah, Saudi Arabia. European Geoscience Union in Vienna, Austria 23–28, April 2017, (Presentation).

Fahed Ayed N Aloufi, Adel El-Turke, Tom Scott. (2019) Identification and Characterisation of Particulate Matter (PM) on historical site and Southern industrial area in Jeddah, Saudi Arabia. 5th International Conference on Pollution Control & Sustainable Environment in London, UK March 14-16, 2019. (Poster).

Contents

List of Figures

List of Tables

List of Abbreviations

UNESCO	United Nations Educational, Scientific and Cultural Organisation
WHO	World Health Organisation
IAC	Interface Analysis Centre
PM	Particulate Matter
ppb	parts per billion
ppm	parts per million
NAPAP	National Acid Precipitation Assessment Program
RH	Relative Humidity
OM	Optical Microscope
XRD	X-Ray Diffraction
NIR	Near Infra-red (Spectroscopy)
CCD	Charge-Coupled Device
FEG	Field Emission Gun
SEM	Scanning Electron Microscopy
Fe	Iron
Cu	Copper
Zn	Zinc
SE	Secondary Electron
EDX/EDAX	Energy Dispersive of X-Ray
eV	Electron Volt
DB	Dual Beam
FIB	Focused Ion Beam
LRS	Laser Raman (Spectroscopy)
JCPDS	Joint Committee on Powder Diffraction Standards
keV	Kilo-electron Volt
a.u.	Arbitrary Unit
mg	milligram
µm	micrometer
nm	nanometer
GAMEP	The General Authority of Meteorology and Environment Protection
IEA	International Energy Agency
SCC	Stress Corrosion Cracking
BE	Binding Energy
T	Temperature
°C	The degree Celsius
TGA/DSC	Thermo-Gravimetric Analysis/ Differential Scanning Calorimetry
XRT	X- Ray Tomography
XRF	X-Ray Fluorescence
ASTM	American Society for Testing and Materials

CHAPTER 1
INTRODUCTION

1.1 Background

Jeddah is one of the most significant commercial cities in the Kingdom of Saudi Arabia [1]. The city has snowballed in size over the last five decades driven by commercial and industrial development. However, the city's first structures were built over 2,500 years ago with numerous ancient buildings still standing today and representing a national treasure [2]. As the city grows, environmental issues also grow and require sensitive consideration regarding building materials and structures [3]. Moreover, there are concerns that increasing levels of pollution are leading to the accentuation and acceleration of the degradation of the city's most ancient buildings [4]. The natural and man-made materials used in buildings throughout the world can be affected in various ways by chemical, physical and environmental reactions. However, the rate at which the degradation of materials occurs depends significantly on the type of material and the environment in which the materials are used [5, 6]. Such processes vary in effect depending on climatic and environmental conditions, but atmospheric pollutants are widely recognised to contribute to material degradation and contribute to failure.

Atmospheric pollution is the consequence of human activities that introduce various pollutants into the atmosphere. These pollutants may include gases and aerosol particles from heavy industries, vehicles and power stations as well as particles from domestic burning of substances, which typically contain carbon [7, 8]. The different compounds introduced into the atmosphere lead to various potentially harmful changes in the environment relative to the extent of the pollution. As such, changes in the natural and the polluted atmosphere vary significantly in space and with time. Equally, pollutants from industrial activities that are well-recognised as having harmful effects on the environment (and hence degradation of building materials) such as sulphur dioxide, nitrogen oxides and ash particles will also vary in concentration, on different timescales from daily to seasonally [9].

The parameters mentioned, either combined or in isolation, have different potentials to cause damage to buildings. Rapid rates of degradation increase the maintenance costs and reduce the lifespan of buildings [10]. In addition, pollution also affects humans and other living organisms. Additionally, historical buildings are treated with high regard because they represent the cultural heritage of the country therefore the governments (including that of Saudi Arabia) may not be willing to lose such structures and instead have a duty of care to preserve them for future generations. Such buildings are arguably most vulnerable to degradation as they have stood for centuries and have already been affected by variable climatic conditions. It is therefore essential to focus more attention on these historic buildings with the aim of extending their lifespan, as documented in the literature [11]. This PhD study investigates the environmental effects of anthropogenic pollution on the declared United Nations Educational, Scientific and Cultural Organisation (UNESCO) world heritage site located in Jeddah, Saudi Arabia, and provides an initial assessment of the primary mechanisms for their degradation driven by anthropogenic air pollution.

1.2 Environmental Pollution

The environment is a unique system, with intricate interconnections and feedback loops that hosts all living and non-living things on the planet. The physical environment includes air, water, land, animals, and plants; buildings and other infrastructure; and all the natural resources that provide all the basic needs for social and economic development [12, 13, 14]. Indeed, it has been profoundly and unequivocally stated that man influences the environment and the environment influences man [15].

Certainly, the human population of the world is becoming increasingly aware and sensitive of the demonstrable fact that we have begun to significantly perturb global climate and weather systems through our insatiable burning of fossil fuels. Man's quest for energy through the use of fossil fuels is responsible for about 65% of atmospheric sulphur dioxide, constituent NO_x and particulate matter. Other emitted pollutants including carbon dioxide are the major contributors to environmental pollution and climate change [16]. These emissions constitute the majority of what we consider air pollution (notwithstanding volcanic events or release from wetlands and cattle).

SO_x and NO_x can dissolve in rainwater (becoming acid rain) leading to accelerated destruction of historical buildings and other materials - especially these containing carbonate minerals, which readily dissolve in acidic conditions. Infrastructural degradation and corrosion when it is exposed to a pollution, can be physical or chemical in nature. The environment over time is becoming increasingly polluted both by natural and man-made factors [17].

1.3 Historical Buildings

Historic sites are typically focal points for tourism. Tourists come to visit these sites out of a sense of nostalgia for past eras, wishing to learn about their cultural heritage. The question of whether to protect these historic buildings or monuments is a function of the meaning they bring to our societies as places that define and mark history. A building may also be considered historic because it signifies something particular about local culture and trade. This includes preserving knowledge of local building materials and construction methods typical of their time in history. There are so many factors to be considered in determining what is historic; usually historic status is qualified by guidelines set in place by local, state, or international organisations like UNESCO [18, 19, 20, 21].

The local, state and federal governments in Saudi Arabia are responsible for the designation of historic properties. Each of these tiers of government is saddled with the authority to designate landmarks which are dependent on their own set criteria for designation. Generally, for a building or other property to qualify for designation as a historic property, it must be at least 100 years old and must have some level of historic relevance [22]. There is ongoing responsibility to preserve these heritage sites for future generations.

1.4 Scope of the Study

In this study, Jeddah city was chosen for investigation because Jeddah is considered to be one of the most historically significant cities in Saudi Arabia. It has a long and complex history and accordingly, has many notable historic buildings dated to be over 300 years old (Figure 1.4.1). Jeddah is currently one of the most visited places in Saudi Arabia. It is a coastal city located on the western side of Hijaz and is known as the transport gateway into the two main Islamic holy cities of Medina and Mecca [1].

Figure 1.4.1 Google maps image representing the location of the historical site in the city of Jeddah.

1.5 Statement of the Problem

The historical building site in Jeddah is surrounded by industrial activity e.g. the industrial area to the south, the oil refinery, the Jeddah port and the desalination plant (Figure 1.4.1). In addition, the historical buildings in Jeddah have been neglected for a long time without any condition monitoring scheme. Significant degradation has now been observed on the buildings as shown in Figure 1.5.1., leading to this current study.

As can be seen from the photos, the buildings are in an advanced state of degradation, that will be costly to restore. These buildings now require urgent attention to be preserved as historic treasures for future generations.

Figure 1.5.1 An example of historical buildings degradation in Jeddah.

1.6 Research Hypothesis

The degradation of these historic buildings is occurring at a faster rate than expected. It would seem that the rate of degradation has accelerated commensurately with increasing industrial activity in the city. Well known pollutants, such as gases, are known to cause degradation of building materials, however particulate pollutants, especially metallic particles, are not well understood in this regard. It is hypothesized that metallic aerosol particles, driven from industrial activity, have the detrimental effect of enhancing rates of degradation of building material surfaces.

1.7 Aims and Objectives of the Study

The main research objectives of the work carried out throughout this study are:

- To characterise the chemical composition of the historic building materials, including stone, mortar and plaster.
- To characterise the surface state of degraded building surfaces to determine the dominant contributors to degradation.
- To characterise aerosol air pollutants collected in the historic quarter of Jeddah at different locations.
- To investigate the scientific mechanisms by which pollutant particles may influence the degradation of building materials.

1.8 Significance of the Study

The information gathered from this study will underpin the generation of new guidelines for the Health and Meteorological departments and the Saudi Commission for Tourism and National Heritage which is responsible for the preservation and management of all historical sites in Saudi Arabia.

Moreover, this study will provide significant data on the particulate air pollutants present in Jeddah day to day and their role in the degradation of these historic buildings. Subsequently, this will inform strategies for protecting, preserving or restoring these ancient monuments.

It is expected that this study, though focused on Jeddah, will be applicable to most any city in the same climatic zone and will therefore have a wide-reaching international significance.

1.9 Structure of the Thesis

The thesis has nine chapters:

1. Chapter one provides the general background and rationale of the research.

2. Chapter two is a literature review that covers environmental pollution.

3. Chapter three provides a deep understanding of the degradation of building materials and the effects of metal oxidation.

4. Chapter four gives the experimental procedures (sample collection and preparation) and analytical techniques used for data collection.

5. Chapter five discusses the results from the characterising the building materials (stone, mortar and plaster).

6. Chapter six discusses the in-situ aerosol air pollutants measured in the historic areas of Jeddah. This details information about the locations of collection, the amounts of heavy metals, and finally the analyses of the aerosol pollutants.

7. Chapter seven explains the role of metallic particles in the degradation of building materials. It also outlines the preparation of the samples used in this part of the study.

8. Chapter eight is a general discussion of the findings and how they relate to the work of other scholars and conclusions that were made.

9. Chapter nine provides the proposed outline for future work.

1.10 References

[1] Baik, A., Boehm, J., Robson, S., (2014). Jeddah Historical Building Information Modeling" JHBIM" Old Jeddah-Saudi Arabia. ISPRS-International Archives of the Photogrammetry, Remote Sensing and Spatial Information Sciences, 2, pp 41-47. Available at: DOI: 10.5194/isprsannals-II-5-41-2014.

[2] Saudi Network, (2008). Jeddah. [online] Available at: http://www.the-saudi.net/saudi arabia/jeddah/index.htm [Accessed 2018].

[3] Struhala, K., Stránská, Z., Pěnčík, J., Matějka, L., (2014). Environmental assessment of thermal insulation composite material. The International Journal of Life Cycle Assessment, 19(12), pp 1908-1918.

[4] Klokkernes, T., (1991). The influence of air-pollution on ancient monuments, buildings, and museum objects. In: PACT. s.l.: Conseil de l'Europe, 33, pp121-128.

[5] Diks, R. M. M., Ottengraf, S. P. P., Van den Oever, A. H. C., (1994). The influence of NaCl on the degradation rate of dichloromethane by Hyphomicrobium sp.Biodegradation, 5(2), pp129-141.

[6] Webb, A. H., Bawden, R. J., Busby, A. K., Hopkins, J. N., (1992). Studies on the effects of air pollution on limestone degradation in Great Britain. Atmospheric Environment. Part B. Urban Atmosphere, 26(2), pp 165-181. Available at: https://doi.org/10.1016/0957-1272(92)90020-S.

[7] Jaramillo, P., Muller, N. Z., (2016). Air pollution emissions and damages from energy production in the US: 2002–2011. Energy Policy, 90(1), pp 202-211. Available at: DOI: 10.1016/j.enpol.2015.12.035.

[8] Sýkorová, I., Havelcová, M., Zeman, A., Trejtnarová, H., (2011). Carbon air pollution reflected in deposits on chosen building materials of Prague Castle. Science of the Total Environment, 409(21), pp 4606-4611. Available at: https://doi.org/10.1016/j.scitotenv.2011.07.025

[9] Jones, C., (2009). Photocatalytic oxidation of SO_2 and NO_x pollutant gases using titania compounds and nanostructures (Doctoral dissertation, University of Bristol).

[10] Cowell, D., Apsimon, H., (1996). Estimating the cost of damage to buildings by acidifying atmospheric pollution in Europe. Atmospheric Environment, 30(17), pp 2959-2968. Available at: https://doi.org/10.1016/1352-2310(96)00003-9.

[11] Varotsos, C., Tzanis, C., Cracknell, A., (2009). The enhanced deterioration of the cultural heritage monuments due to air pollution. Environmental Science and Pollution Research, 16(5), pp 590-592. Available at: DOI: 10.1007/s11356-009-0114-8.

[12] Conserve Energy Future (2019). What is Environmental Degradation? [Online] Available at: www.conserve-energy-future.com [Accessed 15/03/2019].

[13] Idiata, D., (2016). Understanding the Role of Green Infrastructure (GI) in Tackling Climate Change in Today's World. International Journal of Environment and Sustainability [IJES] ISSN 1927-9566, 5 (1), pp 35-45. Available at: DOI: 10.24102/ijes.v5i1.661.

[14] MSD-Ministry of Social Development (2003), Social Report. Physical Environment. [Online] Available at: www. socialreport.msd.gov.nz [Accessed 15/03/2019].

[15] Fu, Q., Heath, A.C., Bucholz, K.K., Nelson, E.C., (2002). A twin study of genetic and environmental influences on suicidality in men.32(1), pp 11-24. Available at: DOI: https://doi.org/10.1017/S0033291701004846.

[16] Idiata, D.J., Omoruyi, S.O., Aiwize, E. A., (2010). Sustainable Power: Impact of Generator Driven Economy on the Environment. Journal of Innovative Research in Engineering and Science, 1(1), pp 55-61. October, Maiden Edition. Global Research Publishing.

[17] Ahmad, Z., (2006). Principles of Corrosion Engineering and Corrosion control. Butterworth- Heinemann/IChemE Series, Great Britain.

[18] Deskfood, (2011). What makes a building historic? Colorado Preservation, Inc. January 28. [online] Available at: www.coloradopreservation.org [Accessed 22/03/2019].

[19] Alderson, W.T., Low, S.P., (1985). Interpretation of Historic Sites. Rowman Altamira. ISBN 9780761991625.

[20] Levy, B.A; Lloyd, S.M and Schreiber, S.P., (2002). Great Tours! Thematic Tours and Guide Training for Historic Sites. Rowman Altamira. ISBN 9780759116757. pp.12.

[21] Kozak, M., Andreu, L., (2013). Progress in Tourism Marketing, pp. 134.

[22] Landmark Society of Western New York. (2019). [online] Available at: http://landmarksociety.org/resources/faq/ [Accessed 22/03/2019].

CHAPTER 2
ATMOSPHERIC POLLUTION

2.1 Background

Atmospheric pollution alters the environment and its composition; greatly affecting and threatening the lives of humans, animals and our built environment. The environment can be defined as the combination of all living species, weather, climate, and manmade or natural resources that affect human survival and economic activity.

Atmospheric pollution affects our health in various ways. The link between human health and the environment has been widely studied. Environmental risks have been proven to have significant impacts on human health directly by exposure of people to harmful agents [1]. Furthermore, there are various effects of atmospheric pollution on the degradation of historical buildings and monuments and have led to the deterioration of ancient objects. Pollution, therefore, is not only confined to ecological degradation but also degradation of our cultural and historical environment [2].

2.2 Environmental Pollution

Environmental pollution is among the greatest threats that humans and other living creatures face. Environmental pollution can be defined as the contamination of the physical and organic elements of the earth and atmospheric systems leading to changes in the environmental processes. Major pollutants like sulphur dioxide, chlorofluorocarbons and nitrogen oxides are naturally occurring substances, though they are discussed in this context as impure contaminants, due to their concentrations. Compounds that have a higher level of concentration than the average, natural background level are considered pollutants.

2.2.1 Air Pollution

Air pollution is a global challenge which has many effects. The purity of the air around us and the resultant effects of emissions released into our surroundings need special attention [3].

The effects of air pollution on architecture has been recognized widely over the last few decades. The heightened interest in this important environmental issue has fostered a welcome increase in research on material damage by air pollutants [4]. Air pollutants, coupled with climatic factors, are of major importance for the degradation of many materials used in cultural monuments [5]. Air quality is influenced by both manmade and natural causes.

Air pollution is clearly a major problem. It occurs when excess harmful gaseous elements, particulates and biological molecules enter the atmosphere [6]. Such elements end up inside organisms, affecting their health in numerous ways. The main problem with toxic pollutants is indoor pollution and poor urban air quality.

2.2.1.1 Atmospheric Particulates

The main sources of atmospheric particulate matter (PM) are: smoke from cars and trucks; open fires; outdoor smoking activities; agricultural aerosols and coal and oil-burners [7]. The main elements include potassium from biomass products, sodium chloride (sea salt), calcium from cement, aluminium, selenium, cobalt and arsenic from burning coal, iron, zinc, copper, lead, other metals that come from factories and carbon from petrol, diesel and biomass [3]. These particulates infuse the air to form the primary pollutants. However, secondary sources of PM include sulphates, nitrates, ammonium and organic aerosols from the combustion of gases. Such particles mostly originate from power plants and other processes in big industries, such as paper factories and oil refineries.

Particulates in air refer to the microscopic particles of solid or liquid elements that exist in the atmosphere. The mixture of air and particulate matter is often referred to as an aerosol. The sources of such suspensions can either be anthropogenic or can be natural; they have different impacts on

the precipitation as well as on the general climate of a given area. They may also affect health. PM can be directly or indirectly emitted into the atmosphere. The directly emitted PM is referred to as 'primary aerosols,' while the obliquely emitted Particle Matter (PM) is referred to as 'secondary aerosols'.

The investigation of the composition of Particle Matter ($PM_{2.5}$ and PM_{10}) was conducted at seven different sites in Jeddah using X-ray fluorescence with the aim of finding the chemical compositions of aerosols, studied by Khodeir et al. Their study analysed 84 samples of $PM_{2.5}$ with 17 variables and 80 samples of PM_{10} with 20 variables. It found that the mean concentration of the particles was 28.4 ± 25.4 μg m^{-3} for $PM_{2.5}$ and 87.3 ± 47.3 μg m^{-3} for $PM_{10.}$ Table 2.2.1 provides a summary of elemental concentrations (μg m^{-3}) according to site and levels of each element in the air [8].

Table 2.2.1 Sampling sites in Jeddah and PM concentrations (μg m^{-3}) [8].

Site Name	Location type [a]	Number of samples ($PM_{2.5}$, PM_{10})	$PM_{2.5}$ (mean+S.D.)	PM_{10} (mean+S.D.)	$PM_{2.5}/PM_{10}$
1. Al-Muhammadiyah	residential	7, 7	15.8±3.1	47.0±6.5	0.34
2. Al-Rehab	residential	7, 7	18.0±4.0	68.9±20.5	0.26
3. Al-Rughama	suburban	7, 6	73.2±65.1	141±124	0.52
4. University Campus	urban	43, 40	23.8±11.7	84.9±33.1	0.27
5. Al-Nuzlah Al Yamaneyyah	urban	6, 6	29.1±14.1	73.5±10.1	0.40
6. Pitrumin	urban	7, 7	31.1±5.8	107±28.7	0.29
7. Al-Alfiyyah	residential	7, 7	24.5±11.8	99.4±43.9	0.25

[a]Urban = residential + commercial area

Suburban = urban area located at the city border

According to Hussein et al, the monthly average concentration of (PM_{10}) ranges from 10 μg m^{-3} to 280 μg m^{-3}, and the trend shows that the level was increasing in 2012 within the Jeddah district. The research found that PM_{10} had a daily variation of 17.5–1400 μg m^{-3}, where the daily concentration ratio of $PM_{2.5}$ to PM_{10} was 2:5 [9].

The particulates in the air are also affected by weather changes, such as precipitation and wind directions. Wind sector analysis in the industrial area around Jeddah found it to be the main source of PM passing over the city. According to Hussein et al., the sea breeze is one of the greatest influencers of PM number concentrations (TC). Particulate matter concentrations (PM_{10}, $PM_{2.5}$, and PM_1) and number concentration (TC) of particles in the diameter size range 0.25–32 µm were measured by an optical scattering spectrometer (EDM-180D, Grimm Aerosol). The results showed that the circulating winds can lead to low concentrations of the atmospheric pollutants by dilution in Jeddah. Figures 2.2.1 and 2.2.2 present data demonstrating the dispersing of PM concentrations with temperature, pressure, and relative humidity variations. The PM_{10} concentrations increase with increasing ambient temperature above 40°C and below that they were generally constant. The $PM_{2.5}$ and PM_1 had their maximum values during ambient temperature between 25°C and 30°C whereas TC was maximum during ambient temperature between 30°C and 35°C. The PM_{10} concentrations decrease with increasing relative humidity. Conversely, the $PM_{2.5}$, PM_1 and TC concentrations increase with the increasing the relative humidity. The relationship between pressure and the PM concentrations and TC was inconclusive. From this study, it can be concluded that circulating wind can reduce the concentration of pollutants by dispersing them across the continent and out to sea. [9].

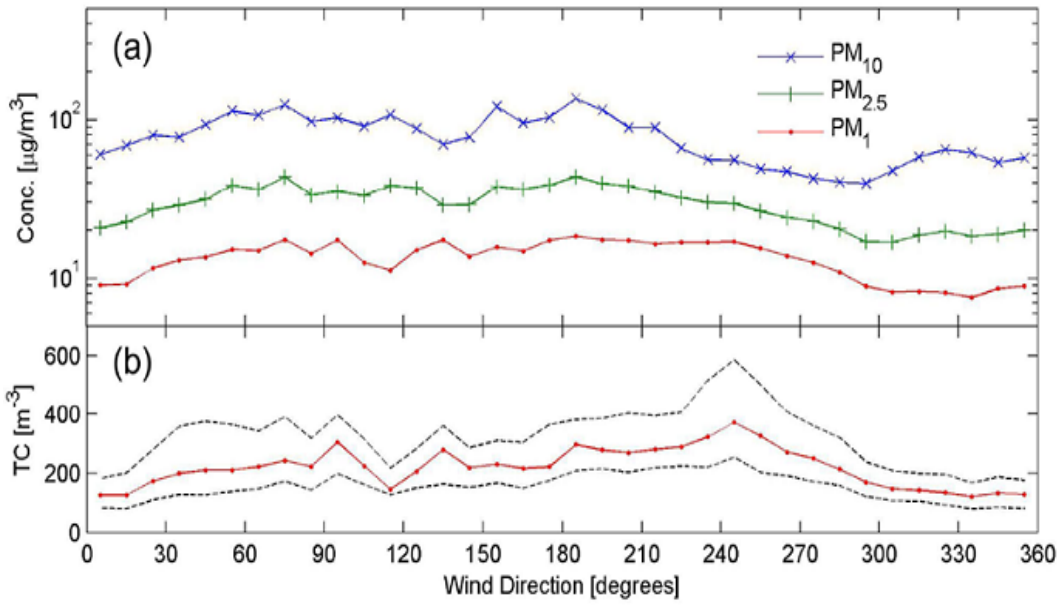

Figure 2.2.1 Trends in PM concentrations and particle size count for PM 0.25 and PM 32 µm with respect to the direction of the wind [9].

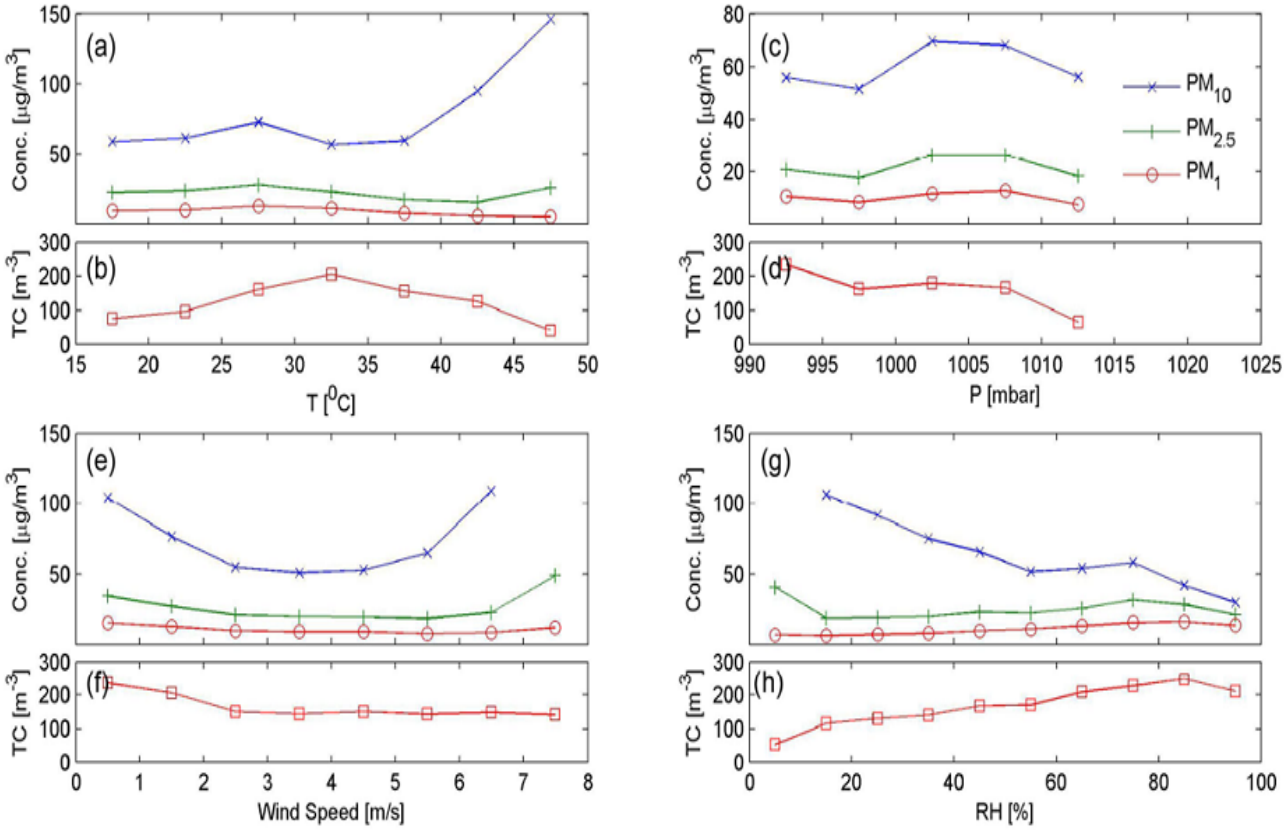

Figure 2.2.2 Trend with respect to ambient temperature (a–b), barometric pressure (c–d), the speed of wind (e–f) and relative humidity (g–h) [9].

Most fuel-users, such as those in industries, motor vehicles, and aeroplanes find it more efficient to use residual fuels because of their low cost, yet the resultant pollutant emission effects are at very high levels. For example, the oil sector in Saudi Arabia accounts for 47% of GDP, 90% of revenues and 90% of export earnings. In addition to oil sector, domestic oil consumption in Saudi Arabia has increased drastically in the past few decades, from 0.41 million barrels per day in 1970 to 3.07 in 2013 [7]. Table 2.2.2 summarizes the levels and growth rates for the consumption of oil, real income, population and CO_2 emissions for Saudi Arabia and some industrialized economy over the period from 1971 to 2013.

Table 2.2.2 CO_2 Emissions and consumption of oil, 1971–2013 [7].

	Variables names	1971	2013	% Growth 1971–2013	Average annual % growth				
		Level	Level		1971 2013	1971 1979	1980 1989	1990 1999	2000 2013
Saudi Arabia	Total oil (mbd)	0.41	3.07	647.8	5.2	6.9	4.36	4.84	5.1
	Transport oil (mbd)	0.03	1.3	3525.7	9.5	27.1	7.1	3.9	5.2
	CO_2 emissions (mt)[a]	66.1	632	856.3	5.8	7.2	6.4	4.2	5.2
	CO_2 emissions from transport oil (mt)	3.29	122.5	3623	9.9	28.3	8.5	2.74	5.6
	Population (millions)	5.8	28.8	375.7	3.8	5.3	5.4	2.3	2.8
	Real income (billions)[b]	60.5	520.6	760.8	5.4	14.5	−0.61	3.1	5.5
Germany	Total oil (mbd)	2.77	2.38	−17.86	−0.26	2.2	−2.4	0.89	−1.12
	CO_2 emissions (mt)	1056.4	842.8	−20.2	−0.49	1.25	−1.14	−1.53	−0.37
	Population (millions)	78.2	80.6	2.95	0.07	−0.01	0.08	0.42	−0.13
	Real income (billions)	1365	3161.9	124.6	1.99	3.1	1.9	2.2	1.17
Japan	Total oil (mbd)	4.3	4.5	6.2	0.49	4.1	−0.76	1.3	−1.5
	CO_2 emissions (mt)	857.1	1397.4	56	1.2	2.5	0.57	1.7	0.53
	Population (millions)	104.3	127.3	20.5	0.46	1.17	0.6	0.28	0.03
	Real income (billions)	1582	4784.5	202.4	2.6	4.7	4.4	1.5	0.94
Canada	Total oil (mbd)	1.51	2.38	57.7	1.2	3.1	−0.74	1.58	1.1
	CO_2 emissions (mt)	371.4	616.7	66	1.28	2.9	0.98	1.27	0.54
	Population (millions)	21.6	35.1	62.4	1.2	1.4	1.2	1.1	1.0
	Real income (billions)	417.4	1319.3	216.1	2.8	4.3	2.9	2.4	2.2
China	Total oil (mbd)	0.75	10.7	1324.2	7.4	14.5	2.6	6.7	6.6
	CO_2 emissions (mt)	749.7	9524.3	978	6.2	7.8	5.2	3.3	7.8
	Population (millions)	818.3	1357.4	61.4	1.2	1.89	1.45	1.14	0.57
	Real income (billions)	118.3	4864	4010.1	9.1	6.1	9.7	10	9.8
U.S.A	Total oil (mbd)	15.2	18.9	24.1	0.64	2.6	−0.54	1.21	−0.2
	CO_2 emissions (mt)	4682.8	5931.4	616.7	0.59	1.52	0.31	1.25	−0.27
	Population (millions)	205.1	316.1	52.2	1.01	1.03	0.93	1.23	0.89
	Real income (billions)	4333.8	14,450.3	233.4	2.86	3.6	3.1	3.2	1.9
World	Total oil (mbd)	47.9	91.3	90.75	1.67	3.92	0.29	1.53	1.3
	CO_2 emissions (mt)	15,463.9	35,094.4	126.9	2.02	3.1	1.4	0.94	2.5

PM amount is greater with such heavy combustion processes that require large amounts of concentration of oxygen. The major types of PM that result from combustion are cenospheres and soot. The features of the particulates are a result of the composition of the fuels and the burning conditions (such as burning location and temperature). Natural combustion of gas does not contribute to the formation of particulates because many of these particles are over 300 μm and a cenosphere particle is defined as between 20 - 300 μm diameter. Cenospheres are products of silica and alumina produced from combustion in power plants and they are used as cement fillers in the production of low-density concrete [10, 11].

Over time, particles are added to the atmosphere either directly through different activities or naturally through winds, volcanic eruption or spatial processes that are explained by the distribution of climatic and other environmental conditions. Studies suggest that the most important aspects of particulates at any site or environment are concentration, composition and size. These three aspects are affected by atmospheric as well as meteorological factors. Moreover, they are affected by the topography, the emission sources and the parameters of the particles, including the shape and orientation, relative weight, density and relative humidity. When fuels are not allowed to burn completely, they result in the production of ambient aerosols [12]. Other processes that affect the composition of these air pollutants also include natural processes (like erosion and weathering) and industrial activities that result in condensation of atmospheric moisture or photochemical decomposition of gases. The suspended particles are in the aerosol state, and then they start undergoing a removal process in the earth's atmosphere through sedimentation, diffusion into the surface of the planet, washout, or coagulation processes [13].

One of the most dominant properties determining behaviour of PM is size distribution. For example, the degree of suspended particles penetrating the respiratory system is mainly a function of the size of the particles. For instance, the main fraction of PM deposited in breathing systems in most cases have a diameter of 0.5 μm or less [14]. Scientists concerned with different aspects of PM, both from medical and meteorological departments have demonstrated the various detrimental effects of atmospheric particulate matter.

As discussed, the particles in the air that lead to pollution mainly come from crustal sources, such as soil remobilisation and weathering, and from anthropogenic sources. The aforementioned study conducted in Jeddah instead focuses on natural and direct anthropogenic sources.

However, most of the elements considered in the study exist in both types of sources, as ultimately all PM comes from the crust originally. It was also suggested that anthropogenic sources of particulates are not very common, especially in Jeddah. A comparison of concentrations of PM present among different cities is presented in Table 2.2.3.

Table 2.2.3 Comparison of PM ($\mu g\ m^{-3}$) in different cities.

Country	**City**	**$PM_{2.5}$**	**PM_{10}**	**$PM_{2.5}/PM_{10}$**
Saudi Arabia	Jeddah [15]	28.4	87.3	0.38
Greece	Athens [16]	40.2	76	0.53
Italy	Milan [17]	45	63	0.71
Turkey	Izmir [18]	64	80	0.80
Egypt	Cairo [19]	59	136	0.43
Lebanon	Beirut [20]	38.9	103.8	0.37
China	Hong Kong [21]	57.4	73.1	0.78
Korea	Seoul [22]	49	51	0.98
India	Hyderabad [23]	50	135	0.37

While amount of particulate matter itself may not be an indicator of pollution, the ratio of the smaller to larger particle size may be indicative of a PM problem in an urban area, since these are the particles that are likely to cause respiratory distress. Seoul has a very high ratio of the $PM_{2.5}$ relative to the amount of PM_{10} which may be an indicator of poor atmospheric health. Jeddah has a relatively lower amount and ratio of the smaller, more problematic particle size compared to the less harmful larger particulate size. In dense urban populations, the overall amount of air pollution is likely to correlate with fuel consumption and incineration processes in industry.

According to the International Energy Agency (IEA) [24], the global daily crude oil consumption is over 99 million barrels, where the US is the leading consumer with 19.8 million, followed by the European Union with 15 million and Saudi Arabia is placed fifth with 3.9 million barrels per day according to 2017 estimates [25, 26].

Although atmospheric trace heavy metals produced by burning crude oil represent a relatively small fraction of atmospheric aerosols excluding Fe, it contributes to a variety of health-related and environmental subjects to the aerosol composition, extent and time of exposure [27, 28, 29].

Various industrial processes contribute to the increase in atmospheric trace metals. Activities such as smelting, grinding and blending generate aerosols from the materials they use [28]. Table 2.2.4 provides a summary of the trace metal compositions from fly ash collected from a coal-fired steam power plant.

Table 2.2.4 Trace metals in fly ash as a function of particle size [30].

Elements	**Concentration, ppm**				
	25 µm	**12.5 µm**	**10 µm**	**3.5 µm**	**1.5 µm**
Al	67,000	54,300	57,000	63,600	59,300
B	300	500	500	500	500
Be	2	1	2	2	2
Cd	<5	<5	<5	<5	100
Cr	130	130	130	300	300
Cu	150	150	200	200	200
Fe	40,000	59,000	43,500	35,500	32,300
Mn	200	240	290	390	500
Ni	300	200	200	300	300
Pb	300	200	300	300	500
V	200	200	200	200	200

Trace metals are introduced to the environment from fuel combustion, incineration, and through industrial emission sources, which are an increasing cause for concern to air pollution researchers. Lee et al in their study using X-ray fluorescence, and atomic absorption techniques, showed the composition, concentration and size of trace metals in urban environments [30]. They highlighted the need to have sensitive (ppb) trace metal analyses techniques and an awareness and monitoring of background levels near likely emission sources.

Spherical atmospheric particles are often the result of high temperature. Their existence is often considered a supporting symptom for assessing severity levels and spherical fly ash particles are also formed and released into the atmosphere as a result of the high-temperature combustion process of fossil fuels [31, 32].

The spherical particle proportions and composition may vary widely depending on the kind of fuel used and the thermal characteristics of the process. In the situation of a high-temperature furnace in a power plant, there are two types of spherical particles that can be produced. Solid fuels, e.g. coal, oil shale, peat etc., consist of largely aluminosilicate glassy material formed by the fusion of minerals within the fuel, and liquid fuel particles produced by incomplete combustion of oil which is mainly elemental carbon. These particles enter the atmosphere along with the plume of flue gases, and dispersion occurs by air currents and atmospheric turbulence, which is a function of the meteorological conditions. They are then deposited in various media by both wet and dry means - even thousands of kilometers from the source [33].

Spherical particles as a result of their form are resistant to chemical degradation and are highly persistent in the terrestrial and aquatic environments. Due to the low burning temperatures in combustion engines and the inherent absorption of oxygen, metal-oxides are the primary metal-bearing aerosol constituent from vehicle exhausts and are not the source of the spherical articles. These spherical particles can only be derived from a very high-temperature and oxygen poor industrial process. This characteristic makes them particularly adapted and efficient in the degradation of buildings, as determined in studies of atmospheric contamination from industry.

2.2.1.2 Health Implication from Atmospheric Pollution

The World Health Organisation (WHO) reports that around 7 million people worldwide have died from exposure to air pollution [34]. Air pollution resulting from particulate air contamination is regarded as a serious health challenge globally [35].

Particulate Matter (PM) may affect not only the physical processes in an environment but also the health of those who are exposed to such particles. Recent population data, reported in 2017, concerns 60 areas within Jeddah. From this demographic data, one very outstanding piece of information is on the premature mortality rate, with most deaths occurring at 50 years within the Jeddah district [36].

Therefore, there is a need to estimate the extent of premature mortality as related to the PM exposure concentration. However, the areas have similar levels of pollutants, so the cause must be mainly due to the concentration of $PM_{2.5}$. The World Health Organisation (WHO) reviewed data from different air quality reports across the globe, revealing that most measurements do not put enough effort into providing data on $PM_{2.5}$ and PM_{10} [37].

The crustal elements forming the primary PM in Jeddah mainly came from wind-blown material like local dust and soil with the larger particles being the more predominant PM type. Different studies show that emitted $PM_{2.5}$ is associated with many cases of cardiopulmonary diseases, such as lung cancer, among other health impacts. The highest health risk comes from chemical carcinogens [38]. However, because of the local conditions, including dust storms, prevailing wind conditions, and natural soil composition, the need for regional specific PM levels to decide what can be considered ‘healthy’ or more at risk, are highlighted as in the atmospheric PM – soil and dust were found to account for 27% of the $PM_{2.5}$ and 77% of the $PM_{2.5\text{-}10}$ fraction, whereas residual oil burning accounted for 63% of the $PM_{2.5}$ found in Jeddah, and this varies seasonally when dust storms occur, for example, which may be very unlike the local fluctuations in other cities worldwide.

2.3 References

[1] Tyagi, S., Garg, N., Paudel, R., (2014). Environmental Degradation: Causes and Consequences. European Researcher, 81(8-2), pp 1491-1498. Availabe at: DOI: 10.13187/er.2014.81.1491.

[2] Newcomb, D.E., Hansen, K.R., (2006). Mix Type Selection for Perpetual Pavements. [Online] Available at: www.ohio.edu [Accessed 17/04/2019].

[3] Al-Seroury, F.A., Mayhoub, A.B., (2011). Air Pollutants from Jeddah Desalination – Power Plant (KSA). AIP Conference Proceedings, 1370(256), Available at: http://dx.doi.org/10.1063/1.3638513.

[4] Brimblecombe, P., (2000). Air Pollution and Architecture: Past, Present and Future, Journal of Architectural Conservation, 6(2), pp 30-46. Available at: DOI:10.1080/13556207.2000.10785268.

[5] Doytchinov, S., Screpanti, A., Leggeri, G., (2012). Effects on Materials, including Historic and cultural Monuments. Conservation of Cultural Heritage. EAI Speciale II - Knowledge, Diagnostics and Preservation of Cultural Heritage, pp 95-100.

[6] Brook, R.D., Rajagopalan, S., Pope III, C.A., Brook, J.R., Bhatnagar, A., Diez-Roux, A.V., Holguin, F., Hong, Y., Luepker, R.V., Mittleman, M.A. and Peters, A., (2010). Particulate matter air pollution and cardiovascular disease: an update to the scientific statement from the American Heart Association. Circulation, 121(21), pp 2331-2378. Available at: doi: 10.1161/CIR.0b013e3181dbece1.

[7] Alkhathlan, K., Javid, M., (2015). Carbon emissions and oil consumption in Saudi Arabia. Renewable and Sustainable Energy Reviews, 48, pp 105-111.

[8] Khodeir, M., Shamy, M., Alghamdi, M., Zhong, M., Sun, H., Costa, M., Chen, L.C. and Maciejczyk, P., (2012). Source apportionment and elemental composition of PM2.5 and PM10 in Jeddah City, Saudi Arabia. Atmospheric pollution research, 3(3), pp 331-340.

[9] Hussein, T., Alghamdi, M.A., Khoder, M., AbdelMaksoud, A.S., Al-Jeelani, H., Goknil, M.K., Shabbaj, I.I., Almehmadi, F.M., Hyvärinen, A., Lihavainen, H. and Hämeri, K., (2014). Particulate matter and number concentrations of particles larger than 0.25 μm in the urban atmosphere of Jeddah, Saudi Arabia. Aerosol and Air Quality Research, 14(5), pp 1383-1391. Available at: DOI: 10.4209/aaqr.2014.02.0027.

[10] Kim, H.S., Islam, M., (2009). Syntactic foams as building materials consisting of inorganic hollow microspheres and starch binder, Chapter 1 in "Building Materials: Properties and Performance and Applications", Edited by Donald N. Cornejo and Jason L. Haro, Nova publishers, pp 1-56.

[11] Ranjbar, N., and Kuenzel, C., (2017). Cenospheres: A review. Fuel. 207, pp 1–12. Available at: doi:10.1016/j.fuel.2017.06.059.

[12] Bertran, C.A. and Marques, C.S., (2004). Study of the particulate matter emitted from residual oil combustion and natural gas reburning. Journal of the Brazilian Chemical Society, 15(4), pp 548-555.

[13] Borja-Aburto, V.H., Loomis, D.P., Bangdiwala, S.I., Shy, C.M. and Rascon-Pacheco, R.A., (1997). Ozone, suspended particulates, and daily mortality in Mexico City. American journal of epidemiology, 145(3), pp 258-268. Available at: https://doi.org/10.1093/oxfordjournals.aje.a009099

[14] Lee, R.E., (1972). The size of suspended particulate matter in air: size distributions of ambient aerosols must be studied in order to determine their effects on the environment. Science, 178(4061), pp.567-575. Available at: DOI: 10.1126/science.178.4061.567.

[15] Pey, J., Rodriguez, S., Querol, X., Alastuey, A., Moreno, T., Putaud, J.P., Van Dingenen, R., (2008). Variations of urban aerosols in the western Mediterranean. Atmospheric Environment, 42, pp. 9052-9062. Available at: https://doi.org/10.1016/j.atmosenv.2008.09.049.

[16] Chaloulakou, A., Kassomenos, P., Spyrellis, N., Demokritou, P., Koutrakis, P., (2003). Measurements of PM10 and PM2.5 particle concentrations in Athens, Greece. Atmospheric Environment, 37, pp 649-660. Available at: https://doi.org/10.1016/S1352-2310(02)00898-1.

[17] Marcazzan, G.M., Ceriani, M., Valli, G., Vecchi, R. (2003). Apportionment of PM10 and PM2.5 in Milan (Italy) using receptor modelling. Science of the Total Environment, 317, pp 137-147.

[18] Yatkin, S., Bayram, A., (2008). Source apportionment of PM10 and PM2.5 using positive matrix factorization and chemical mass balance in Izmir, Turkey. Science of the Total Environment, 390, pp 109-123. Available at: https://doi.org/10.1016/j.scitotenv.2007.08.059.

[19] Abu-Allaban, M., Lowenthal, D.H., Gertler, A.W., Labib, M., (2007). Sources of PM10 and PM2.5 in Cairo's ambient air. Environmental Monitoring and Assessment, 133, pp.417–425.

[20] Saliba, N.A., El Jam, F., El Tayar, G., Obeid, W., Roumie, M., (2010). Origin and variability of particulate matter (PM10 and PM2.5) mass concentrations over an eastern Mediterranean city. Atmospheric Research, 97, pp.106-114. Available at: https://doi.org/10.1016/j.atmosres.2010.03.011.

[21] Ho, K.F., Lee, S.C., Chan, C.K., Yu, J.C., Chow, J.C., Yao, X.H., (2003). Characterization of chemical species in $PM_{2.5}$ and PM_{10} aerosols in Hong Kong. Atmospheric Environment, 37, pp.31-39. Available at: https://doi.org/10.1016/S1352-2310(02)00804-X.

[22] Kim, K.H., Choi, G.H., Kang, C.H., Lee, J.H., Kim, J.Y., Youn, Y.H., Lee, S.R., (2003). The chemical composition of fine and coarse particles in relation with the Asian dust events. Atmospheric Environment, 37, 7pp.53-765. Available at: https://doi.org/10.1016/S1352-2310(02)00954-8.

[23] Gummeneni, S., Bin Yusup, Y., Chavali, M., Samadi, S.Z., (2011). Source apportionment of particulate matter in the ambient air of Hyderabad city, India. Atmospheric Research, 101, pp.752-764. Available at: https://doi.org/10.1016/j.atmosres.2011.05.002.

[24] EC - European Commission, (2019). Oil refining. [Online] Available at: https://ec.europa.eu/energy/en/topics [Accessed 17/04/2019].

[25] International Energy Agency, (2019) Oil. [Online] Available at: http://www.iea.org/aboutus/faqs/oil/ [Accessed 17/04/2019].

[26] CIA- Central Intelligence Agency. The world factbook. [Online] Available at: https://www.cia.gov/library/publications/the-world- factbook/rankorder/2246rank.html [Accessed 17/04/2019].

[27] Venter, A.D., van Zyl, P.G., Beukes, J.P., Josipovic, M., Hendriks, J., Vakkari, V., Laakso, L., (2017). Atmospheric trace metals measured at a regional background site (Welgegund) in South Africa. Atmos. Chem. Phys., 17, pp 4251–4263.

[28] Colbeck, I., (2008). Environmental chemistry of aerosols, Oxford, UK, Blackwell Publishing Ltd.

[29] Poschl, U., (2005). Atmospheric aerosols: Composition, transformation, climate and health effects, Angew. Chem. Int. Edit., 44, pp.7520–7540. Available at: https://doi.org/10.1002/anie.200501122.

[30] Lee Jr, R.E., von Lehmden, D.J., (1973). Trace Metal Pollution in the Environment, Journal of the Air Pollution Control Association, 23(10), pp 853-857, Available at: DOI: 10.1080/00022470.1973.10469854.

[31] Scott, D., Seifert, W., Westcott, V., (1994). The Particles of Wear. Scientific American Offprints, pp.10-11.

[32] Fitch, J., Gebarin, S., (2019). Origin of Spherical Particles in Lubricants. Noria Corporation. [Online] Available at: www.machinerylubrication.com/Read/719/ [Accessed 17/04/2019].

[33] Kaasik, M., Alliksaar, T., Ivask, J., Loosaar, J., (2005). Spherical Fly Ash Particles from Oil Shale Fired Power Plants in Atmospheric Precipitations. Possibilities of Quantitative Tracing. Oil Shale, 22, pp 547-562.

[34] World Health Organization. (2014). 7 million premature deaths annually linked to air pollution. World Health Organization, Geneva, Switzerland. [Online] Available at: https://www.who.int/mediacentre/news/releases/2014/air-pollution/en/ [Accessed 17/04/2019].

[35] Schwarze, P., Totlandsdal, A., Herseth, J.I., Holme, J.A., Låg, M., Refsnes, M., Øvrevik, J., Sandberg, W., Bølling, A.K., (2010). Importance of Components and Sources for Health Effects of Particulate Air Pollution. InTech, [online] Available at: http://www.intechopen.com/books/air-pollution/importance-of-components-and-sources-forhealth-effects-of-particulate-air-pollution [Accessed 17/04/2019].

[36] Harrison, R.M., Bousiotis, D., Mohorjy, A.M., Alkhalaf, A.K., Shamy, M., Alghamdi, M, Khoder, M., Costa, M., (2017). Health risk associated with airborne particulate matter and its components in Jeddah, Saudi Arabia. Science of the Total Environment, 590(1), pp.531-539. Available at: https://doi.org/10.1016/j.scitotenv.2017.02.216.

[37] IAMAT. (2018), November 15. Saudi Arabia General Health Risks: Air Pollution. From IAMAT [online] Available at: https://www.iamat.org/country/saudi-arabia/risk/air-pollution# [Accessed 17/04/2019].

[38] Lim, C.C., Thurston, G.D., Shamy, M., Alghamdi, M., Kohder, M., Mohorjy, A.M., Alkhalaf, A.K., Brocato, K., Chen, L.C., Costa, M., (2018). Temporal variation of fine and coarse particulate matter sources in Jeddah, Saudi Arabia. Published in final edited form as: J Air Waste Manag Assoc. 68(2), pp.123–138. Available at: https://doi.org/10.1080/10962247.2017.1344158.

CHAPTER 3
DEGRADATION OF BUILDING MATERIALS

3.1 Background

Over the past millennia, limestone, sandstone, marble, reinforced concrete, glass, wood, plastics, galvanised steels and stainless steels have all contributed as materials to modernize the architectural and structural design of buildings. The development of new techniques in building arose through the development of new materials and was enhanced by continued research and development on their use as construction materials, aiming for strength, robustness to the elements and low weight.

Man-made airborne pollutant emissions are recognized to have a detrimental effect on building stones, historic buildings and monuments. The degrading effect is considered a serious issue with many studies undertaken examining the different pollutants and their effects. Effects such as stone cracking, splitting, spalling, softening and staining have all been documented, with primary causations being salt crystallisation, and acid-based chemical dissolution reactions [1, 2].

Non-metallic materials are extensively used in the construction industry, typically for houses and architectural commissions. Natural building materials such as limestone and sandstone were extensively used in in historic buildings and are still used in construction today. Stone buildings are comprised of discrete blocks, bonded with mortar and the outer surfaces often covered with plaster. Both the stone and mortar materials have varying mineral constituents depending on the application. Mortar (usually water, sand and either lime or cement) and plaster (lime, cement and clay) both have variable amounts of sand and water added to the mixture based on the usage, and the mineral composition can vary slightly depending on the base building materials used, and the purpose of the mortar and plaster.

Metallic materials were introduced into building to provide grout fittings such as window frames and door handles. However, the use of metallic materials came to the fore when structural strength was required - for example in reinforced concrete or Rolled Steel Joists (RSJ) as stanchions in buildings. Some applications such as cladding also extensively use metals when prefabrication or modular construction is required.

Worldwide, humans have erected buildings on every continent using different materials and designs based on location, culture, time and available resources. The longevity of any building depends on the mechanical, corrosion and degradation performance in the environment to which they are exposed. All materials are prone to degradation, but the rate of degradation and the degree of damage or intensity necessary for failure varies. Table 3.1.1 shows some of the typical building materials and their relative susceptibility to degradation caused by air pollution [4].

Table 3.1.1 The effect of air pollution on some building materials [4].

Materials affected	**Relative sensitivity**
Bricks	Very low
Concrete	Low
Marble, limestone	High
Sandstone	Moderate
Mild steel	High
Stainless steel	Very low
Aluminum	Very low
Copper	Low

The importance of atmospheric corrosion of metals and alloys, whether for economic, safety, historic or artistic reasons, has been recognised for a long time. In recent years, public attention has been directed towards this area of research because of questions raised regarding the significance of acid rain and other environments on the ecosystem, including corrosion of metals. Five main environments may be considered [5]:

1) **Marine environment**. Often regarded as a highly corrosive atmosphere, due to high levels of chloride ions and high humidity.
2) **Industrial environment**. A relatively highly corrosive atmosphere, contain high levels of anthropogenic pollutant from industrial activities such as SO_2 and NO_2.
3) **Urban environment**. A relatively corrosive atmosphere, due to high levels of NO_2, SO_2 and CO_2 and particulates, largely originating from internal combustion engines.
4) **Rural environment**. Regarded as less corrosive, due to low levels of salt and pollutants gases.
5) **Indoor environment**. May be very aggressive, especially in swimming pools, due to high levels of chloride, humidity and temperature. However, in some circumstances buildings may also concentrate certain pollutants, for example the raised levels of formic and acetic acids in museum display cabinets [6].

Materials can physically deteriorate on their outer surfaces through the action of chemical and mechanical processes referred to as corrosion and erosion respectively [7]. Equally, deterioration can also occur internally due to phenomena known as embrittlement or fatigue induced by externally exerted forces. It is generally accepted that many 'natural' building materials, which have an inherent porosity, can be effected some distance into the material by environmental phenomena such as wetting by rainwater. The release of acidic gases such as CO_2, NO_x, SO_x etc. into the atmosphere often leads to their dissolution in rainwater. When the acid rain meets the material surfaces of a building structure or monument. It corrodes them [8]. This is most damaging for stones and mortars which have a carbonate cement; following the reaction (equation 3.1):

$$CaCO_3 + H_2SO_4 \longrightarrow CaSO_4 + CO_2 + H_2O \qquad (3.1)$$

Calcite + Sulphuric acid $\longrightarrow$ Calcium sulphate + Carbon dioxide + water

The present work is focused on the effect of atmospheric pollutants on the historical building materials found in Jeddah namely: stone, mortar and plaster.

3.2 Mechanisms of Stone Decay

Weathering is a natural process by which stone surfaces slowly decay, breaking into smaller particles. The decay of building stones is comparable to cancer - decline in the health of a building leading to its ultimate demise. The weathering of ancient buildings, and other ancient monuments or sculptures that use natural stone (or man-made porous inorganic materials), has existed since antiquity [9].

Preserving these historic treasures is a major and ongoing challenge throughout the world – trying literally to halt or slow the unrelenting and gradual work of Mother Nature. Arguably this preservation task is becoming harder (not easier) as anthropogenic climate change makes the global weather more extreme and air pollution increases the rate of degradation of building surfaces. Figure 3.2.1 gives an example of stone degradation typical in gulf countries. The photograph shows clearly how the mortar has proved more resistant to degradation than the bricks it was locking together.

Figure 3.2.1 Photograph showing a clear example of the effect of weathering on historical buildings in the United Arab Emirates.

The effects of weathering disintegrate and alter the mineral compositions of building stones which are interacting with the environment. The major categories of weathering according to Vee [10] and Beach [11] are:

- Physical weathering; which physically breaks down stone surfaces because of environmental factors that include heat, cold, water and wind. A harsh form of physical weathering is freeze-thaw cycling. Water in liquid form, penetrates the many pores within a stone or mortar. It starts freezing as temperatures drop to 32 degrees ºF and below. As the water freezes, it expands and becomes about 10 percent larger. This expansion drives the cracks and pores in stone and building materials outward. Even the hardest rocks such as granite, cannot match the extremely strong force. Physical weathering refers to processes that break down rock and stone without chemical alteration. This can include processes by which rock is cracked or shattered; for instance, when falling rocks smash into each other and break apart under the influence of gravity. Physical weathering can also refer to the slow wearing away or smoothing of rock surfaces by sandstorms that physically abrade stone surfaces, or by more general exposure to the elements.

- Chemical weathering can create decomposition, dissolving and loosening of mineral particles in a stone or mortar surface. Chemical reactions destroy the bonds that hold the rocks together, often by attacking the natural cement holding mineral particles together. This causes the surfaces to break into smaller pieces. Chemical weathering occurs when the minerals within the rocks are chemically altered. For example, rainwater and carbon dioxide in the atmosphere can (and do) combine to form carbonic acid (H_2CO_3). This acid can dissolve minerals within a rock, weakening the structure and resulting in damage and wear, then dissociates to give the hydrogen ion (H^+) and the hydrogen carbonate ion (HCO_3^-). The ability of H_2CO_3 to deliver H^+ is what classifies this molecule as an acid, thus lowering the pH of a solution (see equation 3.2). Oxidation represents another form of chemical weathering where oxygen combines with chemically reduced metallic cations the rock to form higher oxides. Iron-rich rocks provide a simple example of this, oxidation of magnetite minerals found in mafic igneous rocks results in a rusting effect, like the rust found on exposed pig iron.

Natural weathering (rain, hail, snow and ice) affects rocks by dissolving constituents and transporting soluble minerals away. The weathering reactions involve the transformation of one mineral to another mineral (e.g. feldspar to clay), and the release of some ions into solution (e.g., Ca^{2+}). Some weathering processes involve the complete dissolution of a mineral. Calcite, for example, which often forms a natural cement in sedimentary rocks, will dissolve in weak acid to produce aqueous calcium cations and bicarbonate anions. The equation is as follows [12]:

$$CaCO_3 + H^+ + HCO_3^- \longrightarrow Ca^{2+} + 2HCO_3^- \qquad (3.2)$$

Calcite + Hydrogen ions + Bicarbonate ——> Calcium ions + Bicarbonate

The aqueous products will be washed away, contributing to the destruction of the limestone.

Calcium carbonate, $CaCO_3$, is a very common mineral in sedimentary rocks. Limestone is the most familiar form of calcium carbonate, but it can also be present as a mineral cement in certain kinds of sandstones, termed 'micrites' (marine-deltaic sandstones). All calcite containing rocks are susceptible to acid attack (equation 3.3) [13].

$$CaCO_3 + H_2CO_3 \longleftrightarrow Ca^{2+} + 2HCO_3 \qquad (3.3)$$

Calcite + Carbonic acid <——> Calcium + Bicarbonate

As all surface waters are in equilibrium with atmospheric carbon dioxide there is a constant concentration of carbonic acid (H_2CO_3) in the water, including in rain waters. With anthropogenic fossil fuel burning since the onset of the industrial revolution in 1750, the global atmospheric concentration of CO_2 has increased substantially, going up 39%. The World Meteorological Organisation shows that carbon dioxide levels are now at 389 parts per million, up from ~280ppm about 250 years ago. This means there is commensurately more carbonic acid acting on buildings than ever before. In urban areas, the inherent acidity of meteoric waters can be further enhanced by the role of SO_x and NO_x which are key pollutant gases in accelerating stone weathering.

The main processes by which acid-forming gases can degrade building surfaces are:

a) Dry deposition of gases on a stone surface. In the presence of pre-existing moisture, this can lead to the fundamental processes of sulphation. It is the direct reaction between SO_2 gas deposited on or in the stone that occurs in the presence of a catalyst (e.g. iron oxide) and under conditions of high relative humidity. At ambient temperature, SO_2 may be catalyzed in solution to produce sulphuric acid, which in turn reacts with calcium carbonate to produce gypsum (equation 3.4) [14]. Gypsum may itself be dissolved in water, especially under acid conditions.

$$CaCO_3 + H_2SO_4 + H_2O \longrightarrow CaSO_4.2H_2O + CO_2 \qquad (3.4)$$

b) Direct 'wet' deposition, wherein acid-forming gases are dissolved in rainwater and it falls on building surfaces, driving stone dissolution. The wetting of stone with polluted condensation (in the form of dew, fog or cloud) can also lead to the dissolution of calcium carbonate. The effectiveness of wet deposition depends on solution's acidity: CO_2, SO_2 and NO_x may all contribute to lowering the pH. Usual atmospheric levels of CO_2 will lead to an equilibrium pH of about 5.6. Below pH 5.6, SO_2 and NO_x are the major causes of acidity rather than carbon dioxide. Physical processes may accompany the chemical processes of dissolution and sulphation.

Many other factors contribute to the degradation of stone, and can be broken down into groups depending on the available moisture (rain, fog, humidity), the temperature of air, the heating and cooling of surfaces (by wind and radiation) and the evaporation and condensation of moisture on them, the motion of the air (wind) and the presence of air constituents and contaminants (gaseous and particle). The influence of these factors depends upon the time of day and seasonal aspects and large-scale meteorological phenomena and human activities [15, 16, 17].

3.2.1 Study of Calcareous Stone

The degradation of different stone materials (rates and mechanisms) have been studied both in-situ (in the field) and ex-situ in laboratories. The use of laboratory studies provides a more controlled environment where certain parameters are fixed or removed, and the type of pollutants to be investigated can be adjusted. This provides an opportunity for studying and understanding specific degradation mechanisms of interest.

3.2.2 Field Studies

Cities and their associated environments have been recognized to be more severe than rural areas for degradation, primarily because atmospheric pollution levels are much higher. Globally there are numerous studies demonstrating the effect that acid rain and pollutants released by industrial activity have on buildings, with a few described in this section.

In the Middle East, studies have shown that not only are levels of air pollutants high, but that buildings and monuments are being affected. In Al-Salt City, Jordan, historic buildings on the road-side with limestone as the core building material were found to be affected by the soot and fumes of traffic whereas those further away from the roads were visibly less affected and less structurally damaged [18]. Cairo suffers similarly, where permanent haze caused by unregulated traffic and industrial emissions have led to acidic gases and atmospheric particulates corroding the binder used in the tall mosques, historic buildings and monuments that are a critical feature of the culture and history of the city [19]. A study in Iran demonstrated the increasing importance of awareness of environmental degradation and how atmospheric haze and water problems should be a priority of local governments for protecting architectural heritage and the mounting evidence that traffic and air pollution are only getting worse, but that there are a lack of studies conducted in the major cities to support a strategy to manage these challenges [20]. For the city of Jeddah, increasing pollution levels are well-documented. Land contamination results are traceable to oil drilling, urbanization and heavy traffic leading to roadside contamination and high carbon emissions [21].

The deterioration of limestone, sandstone and marble exposed to anthropogenic acid deposition from the environment and to natural weathering is being assessed as one of the major activities of the Materials Effects Task Groups of the National Acid Precipitation Assessment Program (NAPAP) [22, 23], and the American Society for Testing and Materials (ASTM) [24, 25].

A pair of significant studies from the USA provided quantitative measurements of average weathering rates for marble and limestone and including the capture of parameters like rainfall, pH and the composition and concentration of air pollutants (SO_4^{2-}, NO_3^-) deposited onto surfaces,

and ultimately showed the average weathering rates range from 4 to 140μm y^{-1} where rainfall events showed more mass loss than sites where there was less rainfall [26, 27]. Physical recession estimation of test stones exposed for five years to ambient conditions varied from ~20 to ~45μm yr^{-1} for limestone, and from ~15 to ~30 μm yr^{-1} for marble. Also, small accumulations of $CaSO_4$ and $Ca(NO_3)_2$ have been observed in the rain-washed outer surface after cycles of dry deposition of SO_4^{2-} and NO_3^-. The hygroscopic behavior of $Ca(NO_3)_2/CaCO_3$ particles is identical to that of pure $Ca(NO_3)_2$ particles, suggesting a negligible effect of the inclusion of slightly soluble $CaCO_3$ [28].

Numerous published academic papers have conducted field exposures of stone samples examining the processes and mechanisms causing the degradation of rain-washed limestone in different environments [29, 30]. However, these analyses have extended to include damage studies. The principal mechanism has been listed, identifying the conversion of limestone to calcium sulphate by dry deposition of sulphur dioxide and its subsequent dissolution. Stone-weathering research studies have also revealed that the stone disintegration caused by slow dissolution of $CaCO_3$ from limestone and marble surfaces are directly proportional to the amount of rainfall. Weight-loss rates of the test samples of stones and marble from North Carolina, Washington D.C., New Jersey and New York sites were found to be 0.33% of weight yearly. The study found that the limestone materials suffered losses of 1.59% of their weight in the first year and then 0.75% in the second year [31].

Many researchers have reported that urban areas are more polluted than the rural areas [32, 33]. Commensurate with this it is reported that stone degradation is also more pronounced in urban areas than in rural areas. Oolitic Portland limestone surfaces were studied in urban (central London) and rural (Garston) sites in the UK. The experiment gave the average weight loss over a two-year exposure period for the central London (urban) samples to be 0.31% and that for Garston (rural) to be 0.12% [34]. A similar study was published by Jaynes and Cooke [35]. The study was conducted on oolitic Portland limestone from Monks Park, examining samples from 25 sites in southeast England and London. The findings showed that the stone samples were degraded more rapidly in urban areas compared to rural sites. The central London test site showed significantly

higher degradation rates than any other urban areas, again coincident with the highest levels of air pollution.

In 1985, a study was conducted by the Central Electricity Generating Board (CEGB) and the Cathedral Advisory Commission in England, involving exposure of samples of Portland limestone at eight sites in both England and Scotland; urban, rural and marine environments [36]. The study concluded that the rate of limestone weight loss due to sulphur dioxide in the air was less than 1μm yr^{-1}, and oxides of nitrogen appeared to have no residual effect on weight loss.

In summary, decay of stone surfaces can result from a variety of mechanisms. The atmospheric factors, chemical and biological processes resulting from pollution encompass the primary contributors to degradation. The effectiveness of these factors depends on the time of day and seasons of the year, including meteorological phenomena and human activities. The atmospheric factors which have a direct effect on stone decay are available moisture/humidity, air temperature, wind and chemical constituents of the air [37].

Overall, the deterioration of the calcareous surfaces typical of historic buildings and monuments exposed in different environments and subsequently degrading or failing is assigned to the chemical transformation of calcite ($CaCO_3$) into dissolved gypsum ($CaSO_4.2H_2O$) in the presence of acidic rain and surface waters [38, 39, 40].

3.2.3 Contribution of Anthropogenic Combustion Processes to Building Deterioration

Studies of stone building deterioration typically involve the analysis of damaged or corroded stone samples collected from historical sites. There are a number of laboratory techniques used, such as X-ray Diffraction (XRD), Scanning Electron Microscopy interfaced with X-ray Energy Dispersive Analysis (SEM/EDS), Differential Thermal Analysis (DTA), Thermo-Gravimetric Analysis (TGA), and Infra-Red Spectrometry (IR). Utilization of this array of techniques is targeted at collecting a range of data on the state and type of stone. Included is the environmental and management history, where historical records are available. XRD, SEM/EDX and IR techniques are all surface analysis techniques, ideal for determining chemical or mineralogical changes at the

stone's surface. This makes them well suited to investigating chemical degradation effects caused by anthropogenic airborne pollutants.

Gases such as CO_2 and SO_2 and fly ash particulates are by-products from coal and oil combustion and the role it plays in the deterioration of calcareous building has been investigated in detail. Discoveries posited that coal and fly ash particulates promote the sulphation process that reduces marble and limestone to gypsum [41, 42, 43].

Many stone buildings in industrialised areas are notably blackened by pollution. Studies in the 1980s examined samples of limestone wherein a uniform black carbonaceous deposit found on the limestone deposited via biological weathering mechanisms that usually protect the outer surface, but that had a layer rich in gypsum crystals with a radial structure normal to the underlying stone surface [42]. A direct relationship was discovered by Del Monte and Vittori that the aggressive gypsum growth can occur on and within the black carbonaceous layer, and even the gypsum particles appeared to nucleate from the biologically deposited calcium oxalate layer [45].

Stone may usually contain metal oxide mineral particles, which can behave as catalysts, sometimes for the oxidation of SO_2^{2-} to SO_4^{2-}. Portland and Monks Park limestones both contain small but measurable levels of iron oxides and other compounds of Cu and Mn oxides, sufficient to facilitate the necessary oxidation process of SO_2 to sulphate [41]. Other investigations have also highlighted that smoke or soot are believed to catalyze the SO_2 oxidation process [46, 47].

The study conducted by Cheng et al. on the characterization of the degraded structural surface of City Hall in Schenectady, New York built in 1930 found that the marble grains had weakened structurally on exposed surfaces due to the sulphation of marble to gypsum. Surface analysis showed the existence of fly ash (from industrial activities) and iron oxide particles (it could be present in sand aggregate), and the authors pointed to the likelihood of a catalytic mechanism for the conversion of sulphur dioxide to sulphate [48].

Building covering system components can easily come into contact with water. Cladding can be wetted by rain and condensation, and other forms of structural coverings wetted by water infiltration. The role of water in the mechanism of deterioration of porous building materials has been recognized for centuries. The crystallization of soluble salts associated with wetting is a major mechanism in the degradation of some historical building materials, including stone, mortar and plaster. This mechanism of deterioration is caused by the pressure exerted by the formation of salt structures in voids of porous materials. The percentage of increased volume is dependent on the type of salts involved and scale of deterioration caused relates to the size and arrangement of the pores. When the pressure exceeds the internal strength of the material, and particularly when the salt formations undergo cycles of crystallization and dissolution the deterioration of materials becomes apparent. These cycles typically occur at times of varying humidity [49].

3.2.4 Laboratory Studies of Sulphation

Numerous researchers [50-61] have qualitatively reported that atmospheric gases containing the pollutant SO_X can accelerate degradation of building surfaces composed of $CaCO_3$ through the production of calcium sulphate (equation 3.5), with small amounts of $Ca(NO_3)_2$, also formed due to NO_x gases. Nonetheless, the only observations made on rates of mass loss from calcareous stone exposed in rain and SO_2 shows that the rate of reaction of limestone is related in part to the porosity, which invariably will increase the water intake resulting from precipitation. Therefore, limestone quality will influence the dissolution process and hence the rate of mass loss (degradation) [50].

$$SO_2(g) + CaCO_3(s) + 0.5O_2(g) + 2H_2O\ (1) \Rightarrow CaSO_4\text{-}2H_2O(s) + CO_2(g) \qquad (3.5)$$

Corrosion, as well as the alterations of both the physical and mineralogical properties of two texturally and physically different limestone types used for building, was investigated [51]. An oolitic porous limestone was the first type, with an effective porosity of 36% used for the facades of monuments with a very low compressive strength (2-11 MPa) while the second type was a freshwater limestone with effective porosity of less than 10% and compressive strength of up to 120 MPa. The porous limestone exhibited an intense black and white layer formation. The strength of the crust was found to be a function of the thickness (with thicker layers being stronger), but

also the mineral constituents, the morphology of the layer and its water adsorption capability. Rock samples richest in calcite formed an impermeable thick white layer with the highest strength. Other less calcium-rich surfaces showed laminar black layers with a coincident but thin gypsum-rich white layer. These formed layers were prone to spallation and flaking that drives an increased rate of material loss and back-weathering. Studies observed that when a section of the gypsum-rich crust chips off, with it also comes a detachment of a layer from the substrate. The result was a significant mass loss and a decrease in the volume and surface strength respectively. In the case of freshwater limestone, the crusts did not show a similar decay trend; only that blackened crusts were formed on the limestone surface. The crusts, so formed, were determined to be comprised of more stable compounds and do not tend to spall off from the carbonate substrate. The determined decrease in surface strength was small by comparison.

Studies conducted by Heuer et al, [52] and Wai et al, [53] on SO_2 acid rain from high elevation, showed that both rock surfaces and vegetation are vulnerable to degradation since they are encompassed by acidic clouds and fog. The same is applicable to buildings in such environments – for example, the thick smogs which periodically engulf large cities in China. Per-hour values of daily variation in measured meteorological variables that affect the SO_2 dry deposition during this period are solar radiation levels, air temperature, wind speed, relative humidity and precipitation. It was pointed out that the deposition velocity was larger over wet canopies than over dry canopies. Across the wet tree canopies, the mean dry deposition velocities of SO_2 were estimated to be 0.83 cm s^{-1} during daytime and 0.47 cm s^{-1} during the night-time; and 0.44cm s^{-1} during daytime and 0.19 cm s^{-1} during night-time over the corresponding dry canopy.

The dry deposition velocity of SO_2 for daytime was found to be relatively higher than nighttime values, indicating a temperature or solar influence. In summertime, the deposition velocity was 0.43 cm s^{-1} in the daytime and 0.13 cm s^{-1} at night, also indicating a thermal effect [54]. This indicates that the SO_2 attack of building surfaces will be more aggressive if they are already wetted.

The effect of grain size and relative humidity on the reaction between marble and SO_2 shows that there is an increase in the rate of reaction with high relative humidity and smaller grain size. For grounded marble (powdered) the reaction rate was much faster by two to three times as compared

with the solid marble [55]. Borgwardt and Harvey [56] have studied the reactivity of SO_2 with limestone at 980^o C and found that the physical properties of the original stone, particularly pore volume and surface area, strongly influenced the reaction rate. These observations are logical, indicating that reactive surface area (RSA) has an important influence on the rate of mass loss due to acid attack.

According to Siegesmund et al, and Vazquez et al, marble degradation is linked with the increase in porosity and a general increase of the maximum pore radii. In-situ damage analyses in combination with laboratory tests on marble 'bowing potential' were used to constrain factors that may influence the failure risk. Bowing is a well-established phenomenon seen in marbles used as building veneers. This shape of this rock weathering occurs because of external factors such as temperature, humidity, the system for anchoring the marble slabs or the panel dimensions [57, 58]. According to YSMA (Greece's Acropolis Restoration Service), rainwater, which is acidified by carbon dioxide, sulphur dioxide and nitrogen oxides from air pollution slowly dissolves the marble. Such damage on marble cladding can lead to the loss of cohesion and ultimately in their falling off [59].

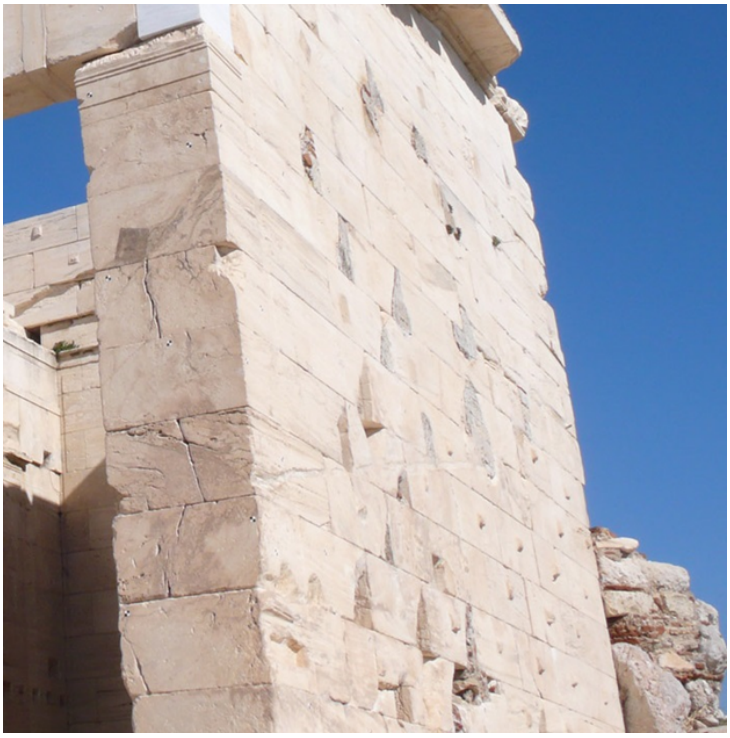

Figure 3.2.2 Photograph showing a clear example of the effect of dissolution and atmospheric pollution on Propylaia in Greece [59].

By comparison, samples of red limestone from Sweden (Kinnekulle), white Carrara marble and yellow Rome travertine were exposed to atmospheric environments containing NO_2, SO_2 and an $SO_2 + NO_2$ mixture at a relative humidity of 90%, using weight change experiments to monitor the rates of reaction. Results following 41 days of SO_2 exposure at 1.6 ppm, show that the limestone samples gained the largest weight gain, of about 0.25 mg cm^{-2}, in comparison the marble and travertine gained about 0.1 mg cm^{-2}. When the same samples were exposed to the $SO_2 + NO_2$ mixture, the weight gain results were higher for limestone and travertine with about 0.7 mg cm^{-2} and with about 0.4 mg cm^{-2} for marble. Using XRD, $CaSO_4.½H_2O$ (Hemihydrate), and $CaSO_4.2H_2O$ (Gypsum) were the main crystalline phases identified at the sample surfaces. The study reported the following observations: (1) there is an increase in the rate of reactivity of limestone as SO_2 levels increased and was greater when compared with marble. The difference was ascribed to the greater porosity of the limestone, which created a larger effective surface area for reaction. (2) When NO_2 is also present as a pollutant gas, the surface reactivity drastically increases. As Johansson et.al concluded, NO_2 plays a role as a catalyst [60].

G.C Allen et al, in their study using the surface analytical technique of X-ray Photoelectron spectroscopy (XPS) determined that the NO_2 increases the rate of attack by SO_2, but does not strictly play a catalytic part, as has been stated previously [60]. The existence of NO_2 accelerates the rate of sulphation of limestone by aiding the oxidation of sulphur dioxide to sulphur trioxide, usually a slow process. In turn, sulphur trioxide reacts with the calcareous stone to form calcium sulphate [17].

Characterisation of mortar materials used in the historical buildings in Abu Dhabi, United Arab Emirates revealed that the mortar is gypsum-based. In addition, the analysis showed that the mortar used in the buildings located at the coastal areas is lime-based mortars [61]. This result may explain why these mortar structures are more resistant to erosion or chemical transformation and degradation, since they will not be susceptible to sulphation the same way calcite-based materials are.

3.3 Metallic Corrosion

Corrosion of metals is one of the most significant problems faced by advanced industrial societies. Corrosion effects can be visible, for example, in the formation of rust on exposed iron surfaces, and invisible, such as pitting, cracking and the resulting loss of strength of metals beneath surfaces. The choice of metals for architectural uses is a complex decision. In the construction industry, stainless steels are often used in view of their advantageous mechanical, physical and chemical properties, but the choice also depends on the environmental conditions they will encounter. Table 3.3.1 shows the global cost of metal corrosion in 2013 was estimated to be US$2.5 trillion, which is equivalent to 3.4% of the global GDP [62].

Table 3.3.1 Showing the global cost of corrosion (CoC).

Economic Regions	**Agriculture CoC US$ billion**	**Industry CoC US$ billion**	**Services CoC US$ billion**	**Total CoC US$ billion**	**Total GDP US$ billion**	**CoC as GDP %**
United States	2.0	303.2	146.0	451.3	16720	2.7
India	17.7	20.3	32.3	70.3	1670	4.2
European Region	3.5	401.0	297.0	701.5	18331	3.8
Arab world	13.3	34.2	92.6	140.1	2789	5.0
China	56.2	192.5	146.2	394.9	9330	4.2
Russia	5.4	37.2	41.9	84.5	2113	4.0
Japan	0.6	45.9	5.1	51.6	5002	1.0
Four Asian Tigers + Macau	1.5	29.9	27.3	58.6	2302	2.5
Rest of the World	52.4	382.5	117.6	552.5	16057	3.4
Global	**152.7**	**1446.7**	**906.0**	**2505.4**	**74314.0**	**3.4**

Corrosion and abrasion are estimated to cost the UK economy around £80 billion per annum [63, 64]. In Saudi Arabia, the annual cost of corrosion is US$ 25 billion (2011 estimate) with most of the cost related to corrosion in its energy industry. The UAE incurs the second-highest cost of corrosion after Saudi Arabia ($14.26 billion) followed by Qatar ($8 billion) [65]. Hence, corrosion is a major problem in the Middle East.

Corrosion is the deterioration of metals or materials by chemical, biological or environmental processes. This is a natural process involving the electrochemical oxidation of metals. The mechanism of corrosion must be understood before a process can be developed for its prevention or control.

Corrosion occurs in two general ways: over the entire surface of the metal (Generalised Corrosion), or in local spots or areas (Localised Corrosion).

- Generalised Corrosion*:* Normally never happens, aside from in submerged acidic conditions or gaseous corrosion conditions. Such a uniform corrosion over the entire surface of the metal is rare and leads to overall uniform thinning, which has little effect outside of acting in conjunction with localised fatigue and stress conditions.

- Localised Corrosion*:* The most frequent, and most detrimental form of localised corrosion is pitting. Pitting is when the corrosive attack happens at one or more isolated locations on the surface and creates a pit, or small cavity, in the metal. Such a type of corrosion attack is difficult to prevent, or engineer against, and is often hard to detect before structural failure is met due to cracking. Pipes are often put in jeopardy due to pitting, typically at joints or where dissimilar metals come into contact and form a galvanic couple [66, 67].

Pitting corrosion is a form of extremely localized corrosion that leads to the creation of small holes in the metal. The driving power for pitting corrosion is the depassivation of a small area, which becomes anodic while an unknown but potentially vast area becomes cathodic, leading to very localized galvanic corrosion. The corrosion penetrates the mass of the metal, with a limited diffusion of ions. Once pits are initiated they may continue to grow by a self-sustaining

mechanism. Accordingly, much attention has been paid to explain and understand the factors controlling their initiation. A number of theories has been proposed to explain the initiation of pits. Kinetic theories explain the breakdown of passivity in terms of the competitive adsorption between chloride ions and oxygen and thermodynamic theories consider the pitting potential to be that at which the chloride ion is in equilibrium with the oxide, other manifestations include pitting corrosion, grain-boundary corrosion and stress corrosion cracking [68, 69].

There are three main components necessary for corrosion to occur:

1. Metal or metal-alloy (example: iron, or steel).
2. Oxidising agent (usually from the either O_2 or water).
3. An electrolyte (usually water).

Many metals used in industry occur naturally in ore as oxides and therefore must be separated out and converted to an elemental (metallic) state to be processed, formed and worked into objects. Whilst in an oxide state the metal compounds are at or near to thermodynamic stability but in an elemental (metallic) state they are electrochemically unsatisfied, and hence thermodynamically driven to revert to oxide compounds.

Corroding of metals, either in contact with gas or with liquid, is governed by interfacial phenomena taking place at the boundary of at least two phases. Corrosion products, whether metal oxides or other species, might appear as thin or thick films or as fine or coarse particles. These products may be either in a colloidal state or must have existed in such a state before growing into a coarse material or layer [70, 71].

3.3.1 Dry Oxidation or 'Gaseous Corrosion'

Corrosion occurs between the metal (producing positively charged ions) and a gaseous oxidant (non-metallic, providing a source of negatively charged ions) such as oxygen, halogens, hydrogen, chlorine, etc. The mechanism for this reaction is that the oxidation and reduction reaction of both

metal and the non-metal occurs simultaneously, usually called a redox reaction which occurs at the surface of the metal.

Metals in Group I and II of the periodic table very readily react with oxygen, apart from beryllium and magnesium, and have little use as materials in construction engineering. The transition metals provide the basis of engineering alloys used in the construction industry and their affinity for atmospheric oxygen is relatively low at ambient temperature, but this increases more rapidly with increasing temperature. For example, when iron is heated above 600°C in air, rapid corrosion takes place and the metal surface is uniformly corroded to form an oxide scale consisting of three layers (Figure 3.3.1) of which the FeO at the metal-oxide interface is the thickest [72].

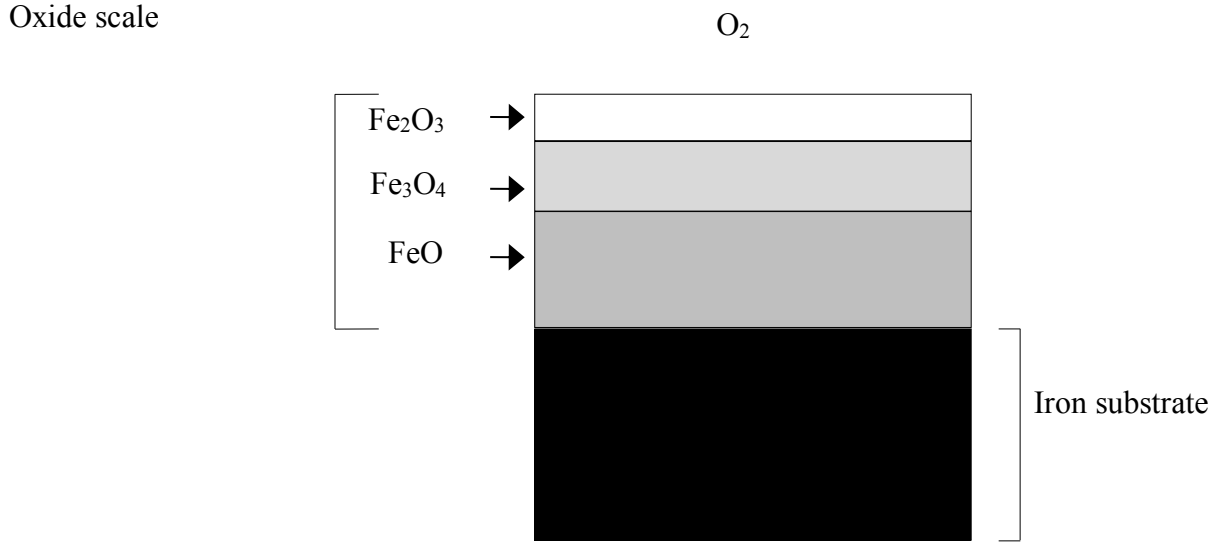

Figure 3.3.1 The complex oxide scale formed on iron at high temperature.

If the material cools, the lower FeO layer decomposes due to phase instability to give particles of iron embedded in a matrix of magnetite (equation 3.6).

$$4FeO \longrightarrow Fe_3O_4 + Fe \qquad (3.6)$$

If iron is heated to a temperature below 570°C, the FeO layer is absent, and a duplex layer of Fe_3O_4/Fe_2O_3 is formed. At even lower temperatures, only Fe_2O_3 is formed. Oxides formed at the gas/solid interface are those which are in equilibrium with the gas at the prevailing pressure and temperature.

As an oxide layer is formed between a metal and its external environment, a physical barrier is introduced, through which, reactants must pass if the oxide film is to continue thickening (i.e. for corrosion to continue). The rate of reaction may then be governed by:

1) The rate of transport of cationic reactants up through the oxide.
2) The rate of oxygen supply to the outer oxide surface.
3) The rate at which the oxygen and metal react to form an oxide.

If we assume that the Y is given as the thickness of an oxide film (layer) at time t, then $dY/dt = K_1$, which upon integration gives a linear growth law. It is a simple oxidation law, which can be represented by the following equation (3.7):

$$Y - Y_o = K_1 t \qquad (3.7)$$

Where K_1 is the linear rate constant.

A graph showing a generalized plot of the film thickness against time is shown in Figure 3.3.2. This situation is temperature dependent.

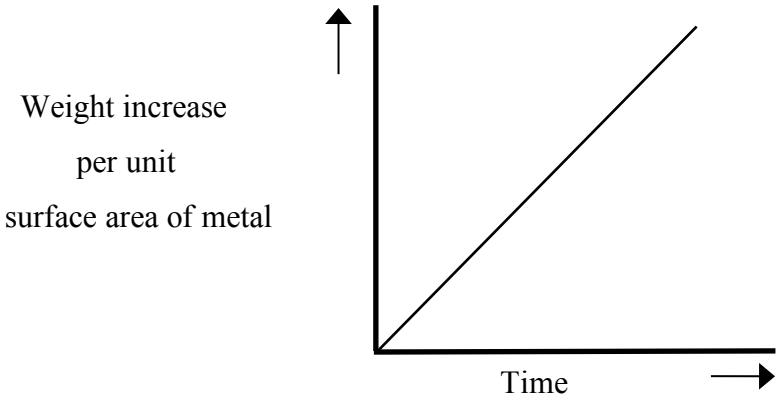

Figure 3.3.2 Linear growth rate of oxidization.

In reality, the growth of a surface oxide layer or film further hinders growth. The layer acts as a protective layer or a defensive barrier, with ions taking longer and finding it energetically harder to traverse the thickening oxide via diffusion. The 'protectiveness' of an oxide film is assumed to be proportional to its thickness shown mathematically as $dY/dt = K_2/Y$, which after integration gives a parabolic relationship (equation 3.8). This parabolic relationship is encountered frequently in metallic oxidation processes (see Figure 3.3.3).

$$(Y-Y_o)^2 = 2K_2t \qquad (3.8)$$

Where K_2 is the parabolic rate constant.

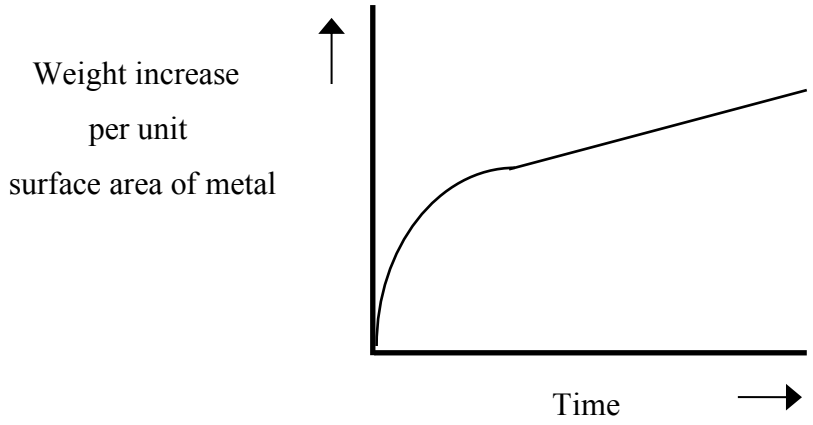

Figure 3.3.3 Parabolic-rate curve.

Furthermore, the cyclical nature of oxidative film-growth suggests that a very thin protective film produced at the surface of metals can be adherent but beyond a critical thickness, brittle spallation occurs causing the oxide to flake away, causing exposure of fresh metal to the atmosphere and resulting in renewed formation of oxide. This process will continue in a similar manner following a breakdown of the oxide layer. The outcome of such behaviour is shown in schematically Figure 3.3.4 and is often referred to as a 'saw-tooth' corrosion profile.

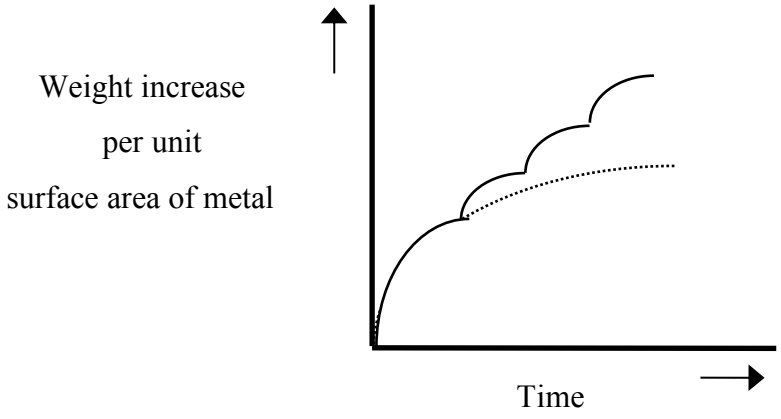

Figure 3.3.4 Cyclic film-growth and cracking.

When corrosion temperatures are low, the rate of growth protective oxide coatings can often obey a logarithmic rate law (Figure 3.3.5). Films tend to be brittle at low temperatures, which can result in cavity formation. The total film growth rate is low at low temperature; therefore, films can house cavities without cracking occurring. Given the fact that ions cannot continue to diffuse through the film at cavities, little or no reaction takes place at such points. Access of oxidants to the area for reaction thus decreases, resulting in localised film formation, at a decreasing rate over time until it is effectively halted. In such cases, the oxide is considered fully protective. An example of this is the oxide which rapidly forms on stainless steel.

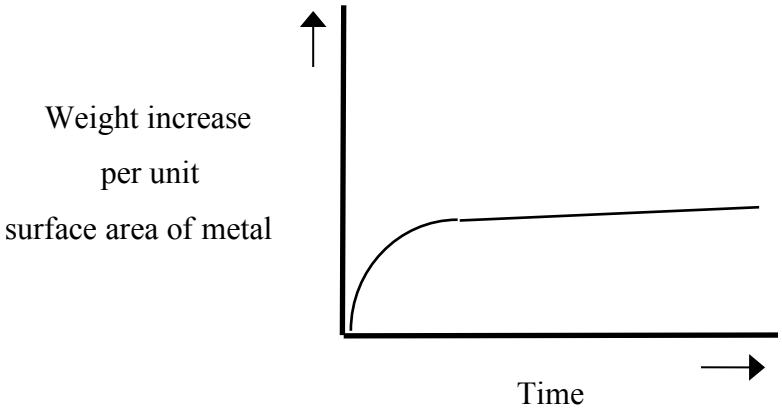

Figure 3.3.5 Logarithmic growth rate.

Real-life corrosion situations are virtually always a combination of the four corrosion rate behaviours discussed above with behaviours switching as environmental conditions change. The shape of a corrosion curve will be a function of not just the type of metal and prevailing temperature, but on factors such as relative humidity, the composition of the vapour phase and presence of pollutants.

3.3.2 Wet Oxidation

Corrosion in the presence of moisture is termed ‘wet’ oxidation. Oxidation is driven by dissolved or suspended components in water (air pollutants gases). Whilst few buildings exist intentionally under water, wet corrosion from an engineering or architectural standpoint is typically referred to as "Wet Air Oxidation" (WAO) [73]. Such WAO circumstances invoke condensing of water to occur on surfaces as droplets or, in extreme cases of high humidity, in the form of a continuous film. Metals may react with water and oxygen in combination more rapidly than with either in isolation. The order of these conditions may be proposed by the following reactions (M signifies the metal):

1) Metal + water

$$M + H_2O \longrightarrow MO + H_2 \qquad (3.9)$$

Unless the metal is very reactive or acids are present, this reaction, in which hydrogen gas is evolved, is slow or completely inhibited by a thin protective oxide film.

2) Metal + oxygenated water

$$2M + 2H_2O + O_2 \longrightarrow 2M(OH)_2 \qquad (3.10)$$

Via this ‘mixed route’ a new corrosion product is formed, which is more likely to be friable and powdery rather than protective. Iron and zinc are examples of metals which demonstrate this type

of behaviour. They remain clean and bright in both dry and unpolluted air of less than critical humidity, and even in deoxygenated water, but corrode visibly when condensation occurs.
At this stage, it is of interest to mention that the reaction of metal + oxygenated water summed up in reaction (3.10) occurs in the following sequence:

$$2M \longrightarrow 2M^{2+} + 4e^{-} \qquad (3.11)$$

Electrons chemically reduce dissolved oxygen from reaction (3.11).

$$2H_2O + O_2 + 4e^{-} \longrightarrow 4(OH^{-}) \qquad (3.12)$$

The metal hydroxide is formed by a mixture of products of reactions (3.12) and (3.13).

$$2M^{2+} + 4(OH)^{-} \longrightarrow 2M(OH)_2 \qquad (3.13)$$

This kind of reaction sequence, involving liberation, transfer and consumption of electrons, results in small but significant electrical currents flowing from one site to another under the water droplet or film, is termed electrochemical corrosion. Even with the droplet of condensed water on steel, for example, where the availability of oxygen at the drop surface predominates, the three phases occur in different regions of the droplet. The most radical form of wetting will, of course, occur during external rainfall or internal exposure to condensate from more extensively cooled surfaces. It is notable that a continuous layer of moisture on a metal surface is usually less corrosive than a series of small drops because the geometrical factors enabling reactions to proceed are eliminated and reactive contaminants are removed by dilution. Existence of water-soluble chemically active pollutants is considered to have a significant effect on corrosion in damp atmospheres. Sulphur dioxide, hydrogen sulphide, sodium chloride particles, hydrochloric acid and carbon dioxide may all be present in condensed rainwater droplets or in rainwater causing corrosion reactions other than (3.5) - (3.8) – and more vigorous.

The uniform corrosion on a metal surface is considered the primary mode of atmospheric deterioration in dry climates. Another factor that needs to be considered is the Pilling-Bedworth ratio in the corrosion of metals. This is defined as "the ratio of the volume of the elementary cell of a metal oxide to the volume of the elementary cell of the corresponding metal (from which the oxide is created)".

Metal dowels and cramps were often built into traditional masonry structures to secure stone blocks which might otherwise be subject to displacement. For example displacement of copings and cornices. The clamps have been widely used in regular Ashler type walls, which usually consist of a relatively thin face of delicate and narrow stone work, attached to a core of brick or stone. Cramps are combined to connect the face again to the core nucleus. Nails and screws have also been incorporated into the structural cavities to help maintain their structural integrity.

In 18th and 19th century buildings, dowels and cramps were usually made from wrought iron which is susceptible to corrosion if exposed to air and moisture. When a shallow mortar decomposes on the surface or cracks, moisture is able to penetrate blockwork. Narrowing the joints makes effective reassignment very difficult, so the water penetrates, causing rusting of exposed iron. Expansion caused by rust eventually leads to pressure on the stone, which results in cracking or heave. Conventional treatment includes major surgery to remove spasms, replace it with non-corrosive phosphorous bronze or stainless steel, and then repair damaged stone work.

3.4 Chapter Summary

The current thesis examines samples of ancient building materials collected from the city of Jeddah in Saudi Arabia. Evidence of surface degradation, including the mechanisms and extent, are examined using surface analysis techniques. Specific investigation is made of the influence of aerosol particulates, both natural and anthropogenic, in driving degradation. A specific hypothesis, that air pollution is accelerating material degradation, will be investigated.

The following chapter outlines the analytical techniques used for this study and the basis on which they work.

3.5 References

[1] Rovnaníková, P., (2007). Chapter 7 - Environmental pollution effects on other building materials. WIT Transactions on State of the Art in Science and Engineering. WIT Press. 28, pp 217-247.

[2] Rao, N.V., Rajasekhar, M., Chinna Rao, C., (2014). Detrimental effect of Air pollution, Corrosion on Building Materials and Historical Structures. American Journal of Engineering Research. 3(3), pp-359-364.

[3] The Steel Construction Institute. "Concise Guide to the Structural Design of Stainless Steel". SCI-P-123, (1992).

[4] Rao, N.V., Rajasekhar, M., and Rao, G.C., (2014). Detrimental effect of Air pollution, Corrosion on Building Materials and Historical Structures. American Journal of Engineering Research (AJER). (03), Issue- 03, pp-359-364 www.ajer.org.

[5] Anon., Materials Performance. 30(11), 58, (1991).

[6] Oddy, W. A., Meusem Journal. 37, 27, (1973).

[7] Rochester Institute of Technology (2019). Understanding Deterioration. www.imagepermanenceinstitute.org/resources/newsletter- archive/v2/understanding-deterioration.

[8] Idiata, D.J, Omoruyi, F.O, Agbonlahor, N.N and Ohonba, S.U (2007). Environmrntology effects of fossil fuel usage. The Nigerian Academic Forum, 13, No. 2. National Association of the Academics.

[9] Siegesmund, S., Weiss, T., Vollbrecht, A., (2002). Natural Stone, Weathering Phenomena, Conservation Strategies and Case Studies. Geological Society, London, Special Publications, 205, 1-7. Available at: https://doi.org/10.1144/GSL.SP.2002.205.01.01.

[10] Vee, V., (2018). Weathering Effects. https://sciencing.com/weathering- effects-8012412.html.

[11] Beach, E., (2017). How Does Weathering Affect Monuments? https://sciencing.com/weathering-affect-monuments-4324.html

[12] Earle, S., (2015). Physical Geology created as part of the B.C. Open Textbook Project. Gabriola Island. https://opentextbc.ca/geology/front- matter/about-bccampus/

[13] Shapley, P., (2011). Limestone and Acid Rain. University of Illinois, 2011.

[14] Georgiadis, T., and Rossi, F., (1989). Dry deposition of pollutants and effects on vegetation. 5: 111. Publisher Name Kluwer Academic Publishers. Available at: DOI https://doi.org/10.1007/BF02486509.

[15] Wu, Y., Liu, J., Zhai, J., Cong, L., Wang, Y., Ma, W, Zhang., Z and Li, C., (2018). Comparison of dry and wet deposition of particulate matter in near-surface waters during summer. 13(6). Available at: doi: 10.1371/journal.pone.0199241.

[16] Yue-Peng, Pan., Xia-Ying, Zhu., Shi-Li, Tian., Li-Li, Wang., Guo-Zhong, Zhang., Yan-Bo, Zhou., Peng, Xu., Bo, Hu., Yue-Si, Wang., (2017). Wet deposition and scavenging ratio of air pollutants during an extreme rainstorm in the North China Plain, Atmospheric and Oceanic Science Letters, 10(5), pp 348-353, DOI: 10.1080/16742834.2017.1343084.

[17] Allen, G.C., El-Turki, A., Hallam, K.R., Mclaughlin, D., and Stacey, M., (2000). Role Of NO_2 and SO_2 in degradation of limestone. British Corrosion Journal, (35) No. 135.

[18] Al-Kharabsheh, M.R.S., Al-Azab, T.A., Al Shawabkeh, A.F., Abu-Hamatteh, Z.S.H., (2008). Damage Inflicted by Traffic Pollution on Historical Buildings in Al-Salt City, Jordan, Al-Balqa's First Engineering Conference, Al-Balqa, Jordan, 1, pp 303-314.

[19] Khallaf, M. K., (2011). Effect of Air Pollution on Archaeological Buildings in Cairo' in Monitoring, Control and Effects of Air Pollution, edited by Andrzej Chmielewski, [online] eBook (PDF) ISBN: 978-953-51-6032-8 Available at: DOI: 10.5772/998 [Accessed 23/01/2020].

[20] Valizadeh, H., Parvin, M.R., (2014). Middle East's Environmental Contamination and Responsibilities of the Islamic Republic of Iran Regarding Compensation of Environmental Damages (Haze and Water Contaminations). European Online Journal of Natural and Social Sciences. 3(3), pp186-199.

[21] Kadi, M. W., (2009). Soil Pollution Hazardous to Environment": A case study on the chemical composition and correlation to automobile traffic of the roadside soil of Jeddah city, Saudi Arabia". Journal of Hazardous Materials. 168 (2–3), 1280–1283. Available at: https://doi.org/10.1016/j.jhazmat.2009.03.015.

[22] NAPAP (National Acid Precipitation Assessment Program). "Processes of Deposition to Structures", Report No 20, In Acid Deposition State of Science and Technology, 111, Terrestrial. Materials, Health and Visibility Effects, Government Printing Office. Washington. DC, USA, (1990).

[23] Tidblad, J., Kucera, V., Ferm, M., Kreislova, K., Brüggerhoff, S., Doytchinov, S., Screpanti, A., Grøntoft, T., Yates, T., Fuente, D., Roots, O., Lombardo, T., Simon, S., Faller, M., Kwiatkowski, L., Kobus, J., Varotsos, C., Tzanis, C., Krage, L., Schreiner, M., Melcher, M., Grancharov, I. and Karmanova, N., (2012). Effects of Air Pollution on Materials and Cultural Heritage: Available at: https://doi.org/10.1155/2012/496321.

[24] American Society for Testing and Materials, ASTM Standards, Part 10, 985-992, (1980a).

[25] American Society for Testing and Materials, ASTM Standards, Part 10, 781-786, (1980b).

[26] Lipfert, F. W., (1989). "Atmospheric Damage to Calcareous Stones Comparison and Reconciliation of Recent Experimental Findings". Atmos. Environ. 23, 415- 429, Available at: https://doi.org/10.1016/0004-6981(89)90587-8.

[27] Youngdah, C. A. and Doe B. R., (1986). "Effects of Atmospheric Exposure on Roughening Recession, and Chemical Alteration of Marble and Limestone Samples Surfaces in the Eastern United States". In "Materials Degradation Caused by Acid Rain". (Edited by Baboiar R), American Chemical Society, Washington DC, 318, 226-238, Available at: DOI: 10.1021/bk-1986-0318.ch019.

[28] Baedecker, P. A. Reddy, M. M. Reimann, K. J. and Sciammarell. C.A., (1992). "Effect of Acid Deposition on the Erosion of Carbonate Stone-Experimental Results from the US". National Acid Precipitation Assessment Program (NAPAP). Atmos. Environ. 26B, 147-158. Available at: https://doi.org/10.1016/0957-1272(92)90018-N.

[29] Raihan, 1, Syamsudin, F and Satrio, L (2012). Mechanical Analysis of Limestone in Jaya, Lhong, and Lhoknga. Journal of Aceh Physics Society, SS, 1(1) pp 7-8.

[30] Webb, A.H, Bawden, R.J, Busby, A.K and Hopkins, J, N (1992). Studies on the effects of air pollution on limestone degradation in Great Britain. Atmospheric Environment. Part B. Urban Atmosphere. 26 (2), pp 165-181. Available at: https://doi.org/10.1016/0957-1272(92)90020-S.

[31] Reddy, M. M. and Youngdahl, C. A., (1987). "Acid Rain and Weathering Damage to Carbonate Building Stone; Results of Material Loss Measurements". Corrosion 87. Meeting. San Francisco. California. Paper no. 415, pp 9-13,

[32] D'Amato, G., (2011). Effects of climatic changes and urban air pollution on the rising trends of respiratory allergy and asthma.Multidiscip Respir Med. 2011; 6(1): 28–37. Available at: doi: 10.1186/2049-6958-6-1-28.

[33] Salvi S and Holgate, S.T (1999). Mechanisms of particulate matter toxicity. Clin Exp Allergy. 29:1187–1194. Available at: doi: 10.1046/j.1365- 2222.1999.00576.x.

[34] Honeyborne, D. G. and Price, C. A., (1977). "Air Pollution and Decay of Limestones". BRE Report no, N 117/77, Building Research Establishment, Garston, UK.

[35] Jaynes, S. M. and Cooke, R. U., (1987). "Stone Weathering in Southeast England", 21(7), pp1601-1622. Available at: https://doi.org/10.1016/0004-6981(87)90321-0.

[36] Martin, A. and Baber, F. R., (1987). "Measurement of Material lost from Limestone Specimens to Rain". CEGB report OED/STM/87/00003/N.

[37] Tombach, I., (1982). Measurement of local climatological and air pollution factors affecting stone decay. Conservation of Historic Stone Buildings and Monuments. Available at: https://www.nap.edu/read/514/chapter/15.

[38] House of Commons, Environment Committee, Fourth Report. "Acid Rain". HMSO, London, (1984).

[39] Henley, K. J., (1967). "Some Mineralogical Aspects of Air Pollution Damage to Limestone". Proc. Clean Air Conf., Blackpool, pp 69-74,

[40] Braun, R. C., and Wilson, M. J. G., (1970). The Removal of Atmospheric Sulphur by Building Stones". 4, pp 371-378. Available at: https://doi.org/10.1016/0004-6981(70)90082-X.

[41] Del Monte, M. and Sabbioni, C., (1984). Urban Stone Sulphation and Oil-Fired Carbonaceous Particles". Sci. Total. Envir. 36, pp 369-376. Available at: https://doi.org/10.1016/0048-9697(84)90289-4.

[42] Henry, W. M., Knapp, H. T., (1980). "Compounds Forms of Fossil Fuel Fly Ash Emission". Environm. Sci. Technol. 14, 450-451.

[43] Hutchinson, A. J. Johanson, J. B. Thompson, G. E. and Wood, G. C., (1992). "The Role of Fly-Ash Particulate Material and Oxide Catalysts in Stone Degradation". 26A (15), 2795-2803, Available at: https://doi.org/10.1016/0960-1686(92)90017-F.

[44] Camuffo, D., (1986). "Deterioration Processes of Historical Monuments". In Acidification and its Policy Implications" (Edited by Schneider, T. S) Elsevier, Amsterdam. 182-211.

[45] Del Monte, M. and Vittori, O., (1986). "Air Pollution and Stone Decays. The Case of Venice". 50, 165-182, Available at:https://doi.org/10.1016/0160-9327(85)90110-3.

[46] Russell, P. A., (1979). "Carbonaceous Particulates in the Atmosphere". Illumination by Electron Microscopy. Proc. Carbonaceous Particles in the Atmosphere. Sponsored by the National Science Foundation and the Lawrence Berkeley Laboratory.133-140.

[47] Sherry, B. S. Johnson, J. B. and Wood, G. C., (1988). "Corrosion in Smoke, hydrocarbon and SO_2 Polluted Atmospheres. 1. General Behaviour of Iron". Corros. Sci. 28, 657-695.

[48] Cheng, J. R., Castillo, R., (1984). "A Study of Marble Deterioration at City Hall, Schenectady, New York" Air Pollution Control Association. 34(1), 15-19.

[49] Delgado J.M.P.Q.., de Freitas V.P.., (2013). Salt Degradation in Stone of Old Buildings. Defect and Diffusion Forum Vols. 334-335, pp 337-342. Available at: doi:10.4028/www.scientific.net/DDF.334-335.337.

[50] Lipfert, F. W., (1989). "Atmospheric Damage to Calcareous Stones Comparison and Reconciliation of Recent Experimental Findings". 23, 415- 429. Available at: https://doi.org/10.1016/0004-6981(89)90587-8.

[51] Török, A (2006). Deterioration-related changes in physical properties and mineralogy of limestone monuments. IAEG2006 Paper number 297. The Geological Society of London 20061.

[52] Heuer, K., Tonnessen, K.A, Ingersoll, G.P (2000). Comparison of precipitation. 481 chemistry in the Central Rocky Mountains, Colorado, USA, 34, 1713– 1722. Available at: https://doi.org/10.1016/S1352-2310(99)00430-6.

[53] Wai, K.M., Lin, N.H, Wang, S.H, Dokiya, Y., (2008). Rainwater chemistry at a 530 high-altitude station, Mt. Lulin, Taiwan: Comparison with a background station, 531 Mt. Fuji, J. Geophys. Res., 113, D6. Available at: https://doi.org/10.1029/2006JD008248.

[54] Xu, Y., Carmichael, G. R., (1998). Modelling the Dry Deposition Velocity of Sulfur Dioxide and Sulfate in Asia. 37. Available at: https://doi.org/10.1175/1520-0450(1998)037<1084:MTDDVO>2.0.CO;2.

[55] Gauri, K. L., Gwinn, J. A., (1983). "Deterioration of Marble in Air Containing 5-10ppm SO_2 and NO_2". Durability Bldg Mater. 1, 217-233.

[56] Borgwardt, R. H. and Harvey, R. D., (1972). "Properties of Carbonate Rocks Related to SO_2 Reactivity". Envir. Sci. Technol. 6, 350-360.

[57] Siegesmund, S, Ruedrich, J and Koch, A (2008). Marble bowing: comparative studies of three different public building facades**.** Environmental Geology. 56, (3–4), pp 473–494.

[58] Vázquez, P., Siegesmund, S., Alonso, F.J., (2011). Environ Earth Sci 63: 1603. Available at: https://doi.org/10.1007/s12665-010-0882-y.

[59] YSMA (2018). Deterioration of the marble. https://ysma.gr/en/maintenance/deterioration-of-the-marble/.

[60] Johansson, L.G. Lindqvist, O. and Mangio, R. E., (1988). "Corrosion of Calcareous Stones in Humid Air Containing SO_2 and NO_2". 5, 439-449

[61] Benjamin L. Marcus., (2012). Characterization of historic mortars and earthen building materials in Abu Dhabi Emirate, UAE. IOP Conference Series: Materials Science and Engineering.

[62] NACE International (2016). NACE study estimates the global cost of corrosion at $2.5 trillion annually**.** http://impact.nace.org/economic-impact.aspx.

[63] Lim, H.L (2012). Assessing Level and Effectiveness of Corrosion Education in the UAE. 2012. Available at: http://dx.doi.org/10.1155/2012/785701.

[64] University of Edinburgh (2017). Materials study targets industry corrosion and wear. Available at: https://www.ed.ac.uk/news/2017.

[65] Al Hashem, A (2011). Corrosion in the Gulf Cooperation Council (GCC) states: Statistics and figures. Paper presented at the Corrosion UAE, Abu Dhabi, UAE.

[66] Ahmad, Z., (2006). Principles of Corrosion Engineering and Corrosion Control, Butterworth-Heinemann, Oxford, UK.

[67] Roberge, P., (2008). Corrosion Engineering: Principles and Practice, McGraw-Hill Professional, New York, NY, USA.

[68] Fontana, M. G. and Grenne .N. D., (1967). "Corrosion Engineering". McGraw-Hill Co. New York. 51.

[69] Szklarska-Smialowska. Z., (1974). "Localised Corrosion". National Association of Corrosion Engineers. Houston.

[70] Landolt, D., (2007). Corrosion and Surface Chemistry of Metals. EPFL Press.

[71] Perez, N., (2004). Electrochemistry and Corrosion Science. Kluwer Academic Publishers.

[72] Pilling, N. B., Bedworth, R. E., J. Inst. Met. 88, 205 (1960).

[73] Patria, L., Maugans, C., Ellis, C.; Belkhodja, M., Cretenot, D., Luck, F., Copa, B., (2004). "Wet Air Oxidation Processes", Advanced Oxidation Processes for Water and Wastewater Treatment, S. Parsons Editor, pp 247–274.

[74] Farrell, D., Davies K., and McCaig. Cathodic Protection of Iron and Steel Recent applications to heritage buildings, The Building Conservation Directory, 2001.

CHAPTER 4
MATERIALS AND ANALYTICAL TECHNIQUES

4.1 Introduction

Stone, mortar and plaster were the main materials used in the construction of the historical buildings of Jeddah, Saudi Arabia. In this study, a suite of samples were collected from six historic houses in the centre of old Jeddah, as well as from the quarry. Significant paperwork and permissions were obtained from Historic Jeddah Municipality to facilitate this sampling campaign. Each material will be discussed separately hereafter with regards to the sampling process.

4.1.1 Stone

Stone is one of the most common and oldest raw materials used for construction. They are generally used for construction due to their strength, durability and resistance to weathering. Stone for the historic part of Jeddah was sourced from a nearby quarry complex, with the stone blocks processed by cutting, shaping and polishing. Stone as a construction material can be categorised into natural stone, crushed stone (hard-rock aggregate), sand and gravel [1].

4.1.2 Mortar

Mortar is a material used in masonry construction to fill the gaps between the bricks and blocks. Mortar is the bonding agent between building materials, and it is a mixture of binder (lime, cement and clay), aggregate (sand) and water [2].

Mortar is initially formulated as a workable paste which subsequently sets due to internal carbonation and hydration reactions, becoming hard. The ancient Egyptians used and made the earliest known mortar; it was made from either argillaceous or microcrystalline gypsum, anhydrite, calcite, quartz and halite, where microcrystalline anhydrite was found to improve stability, and halite, or larger gypsum crystals, to be destabilising [3].

4.1.3 Plaster

Plaster is a material used in construction to cover the rough walls and uneven surfaces. It is used for aesthetic purposes and does not have any major structural contribution to a building. Like mortar, plaster is a mixture of binding agent (lime or cement) and sand (usually fine) along with the right quantity of water [4]. Plastering helps to bring out the beauty of the structure as well as improve durability and resistance of the building when used externally [5].

All three of these above materials were used to construct the historical buildings in Jeddah. The site locations from where samples were extracted are shown in Figures 4.1.1 and 4.1.2 respectively. The main objective of this sampling work and ensuing analysis was to identify the constituent materials used to build these historical buildings, as well as to determine the mechanisms and extent of any observable degradation. A description of the samples and the analytical techniques used for the analysis of each material is described in the following sections of this chapter.

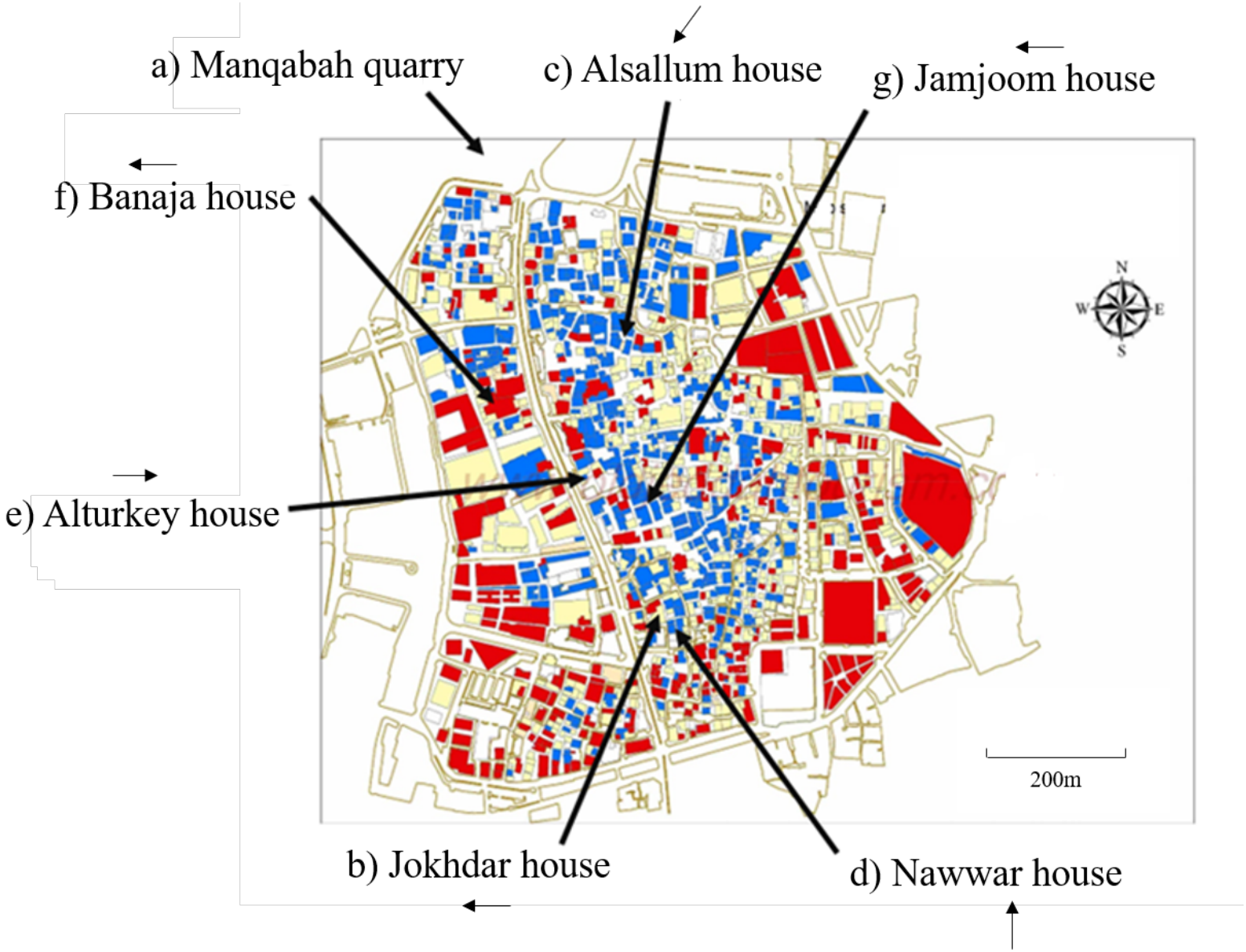

Figure 4.1.1 Map represents the locations the samples were collected from, where small arrows indicate the direction the walls were facing (a) Manqabah quarry, (b) Jokhdar house, (c) Alsallum House, (d) Nawwar house, (e) Alturkey house, (f) Banaja house, and (g) Jamjoom house.

a. Manqabah, Quarry.

b. Jokhdar House.

c. Alsallum House

d. Nawwar House

e. Alturkey House

f. Banaja House

g. Jamjoom House

Figure 4.1.2 Photographs showing the location from where the samples were collected.

4.2 Sample Collection and Preparation

A hammer and fine chisel were used for sample collection. Suitable protective equipment was worn, and the equipment was cleaned using deionised water between samples to avoid cross contamination. Each sample was individually bagged using labelled zip-lock plastic sample bags. A marker pen was used to mark the inner or bottom face of each sample. The analysis was carried out to identify the chemical composition of the materials using the following techniques; Optical Microscope (OM), X-Ray Diffraction (XRD), Scanning Electron Microscope-Energy Dispersive X-Ray Spectroscopy (SEM-EDS), Laser Raman Spectroscopy (LRS) and Dual-Beam (DB).

4.2.1 Stone

A total of four stone samples were collected from four houses, in addition, a sample from the quarry was also collected. An images and description of the samples are given in Table 4.2.1.

The quarry samples were cut from the large slabs and are considered 'fresh' material. All samples were 2-20cm^3 of material. Stone samples were extracted from houses where plaster was not used as a veneer.

Table 4.2.1 Stone samples images and description.

Sample Images	Description Sample
	Stone from the quarry (Manqabah).

	Stone from the external west facade of Jokhdar House.
	External stone of Alsallum House from the south west facade.
	Internal stone of Banaja House from the west facade.
	External stone of Jamjoom House from the west facade.

4.2.2 Mortar

Five mortar samples were collected from five historic houses, where the method of sample collection was the same as for the stone. The location, images and description are presented in Table 4.2.2.

Table 4.2.2 Mortar samples images and description.

Sample Images	Sample Description
	Original external mortar of Jokhdar House from the west facade.
	Original external mortar of Jamjoom House from the west facade.
	Original external mortar of Banaja house from the east facade, indoors.

	Original external mortar of Banaja house from the south facade, outdoors.
	Original external mortar of the Nawwar house from the north facade.

4.2.3 Plaster

Five plaster samples were collected from give historic houses. Details are presented in Table 4.2.3. A volume of 2-10cm^3 was collected at each location using the same sampling methodology as for the stone and mortar.

Table 4.2.3 Plaster samples images and description.

Sample Images	Sample Description
	Original external plaster of the Nawwar house from the north facade.
	Original external plaster of the Alturkey house from the east facade.
	Original external plaster of Jokhdar house from the east facade.

	Original external plaster of Jokhdar house from the west facade.
	Original external plaster of Jamjoom house from the west facade.

4.3 Analytical Techniques

The description and technical basis of the analytical techniques used to characterise the above collected materials are detailed in the following sections.

4.3.1 Light Optical Microscope (LOM)

The optical microscope (OM) is a device widely employed for observing and recording a material's surface topography, as shown in figure 4.3.1. The d_{min} known as the limit resolution of an optical microscope is given by equation 4.1 [6, 7].

$$d_{min} = {k\lambda}/{2NA} \quad \text{..... 4.1}$$

Where:

K= constant with value 1.22 when the object is filled with light from an appropriate condenser.

λ = wavelength of monochromatic incident light

NA = numerical aperture ranging from 0.1 – 1.3. In the visible spectrum, the red end of the wavelength for visible light ranges from ˜650 nm down to ˜400 nm at the blue end of the spectrum. At the blue end, d_{min} has 1.5 times better resolution than at the red end.

Stone, mortar and plaster samples were optically imaged using a Zeiss Axio Imager 2. The optical microscope was used. This automatically detects and configures objectives and contrast modules for Axio Imager Z2m using white light. 20x and 50x objectives were used to digitally capture the images of each sample at different magnifications.

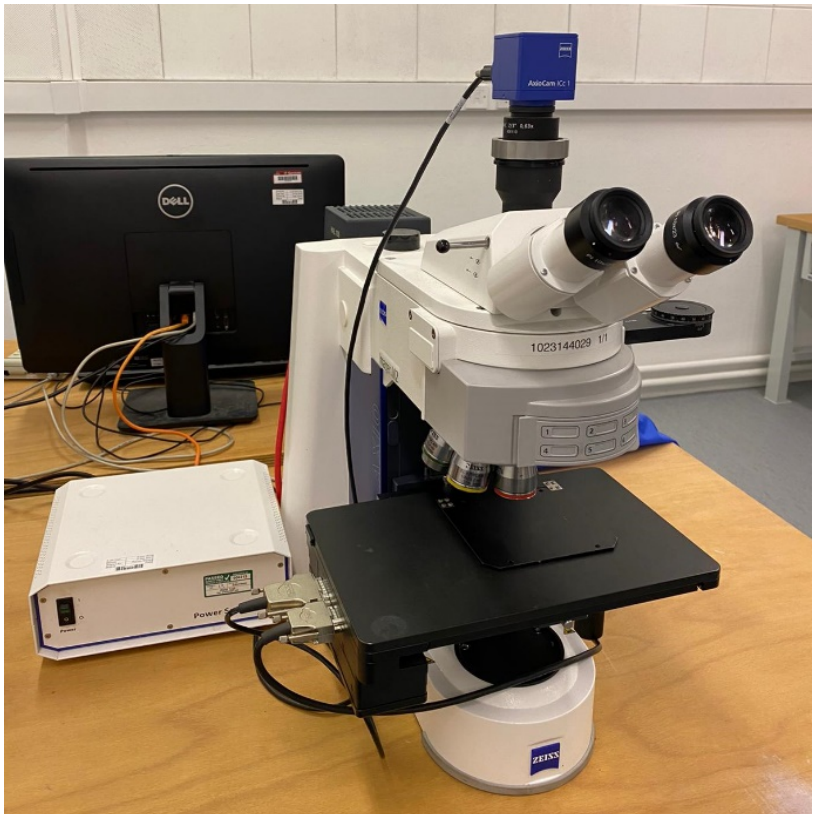

Figure 4.3.1 Photograph of the light optical microscope (LOM).

4.3.2 X-Ray Diffraction (XRD)

4.3.2.1 Introduction

X-ray diffraction is a bulk analytical tool used to probe the presence of crystalline phases in a sample, usually a powder. When a monochromatic X-ray beam is incident on a sample, the X-rays are scattered, and the angles of scatter are measured with respect to corresponding intensities, thus determining the crystallographic nature of the sample based on coherent scattering of the repeating atomic planes found in crystalline materials.

4.3.2.2 Bragg Conditions

Any crystal is made up of a Bravais lattice, which is a regular 3-dimensional array of a group of atoms. The Bragg condition is satisfied for a particular wavelength corresponding to the spacing between atomic layers (d) when the beam hits the sample at a certain angle, which then causes the beam to refract. There is a high concentration of electron density around the atoms within the lattice that result in the reflection of the x-ray beams. These reflected areas form a constructive interference producing the measurable intensity peaks at 2θ angles.

Bragg derived an equation to summarise this condition for constructive interference of a diffracted x-ray beam as:

$$n\lambda = 2dsin\theta \quad \text{..... 4.2 [8]}$$

Where:

n = an integer

λ = the x-ray wavelength

d = the spacing between the planes of high electron density

θ = the angle between the plane of electrons and the path of the incident radiation

Examining a crystalline sample that has a regular d-spacing creates only specific angles of incidence resulting in a measurable constructive interference with monochromatic X-rays. The reflected X-rays emanating from the crystal structure also produce a background signal at any angle.

Path difference for rays 1K1' and 2L2' is:

$$ML + LN = 2dsin\theta \quad \text{..... 4.3}$$

When the difference in a path is equal to a whole number (n) of the wavelengths, the scattered rays 1' and 2' are completely in phase (equation 4.2) and shown in Figure 4.3.2.

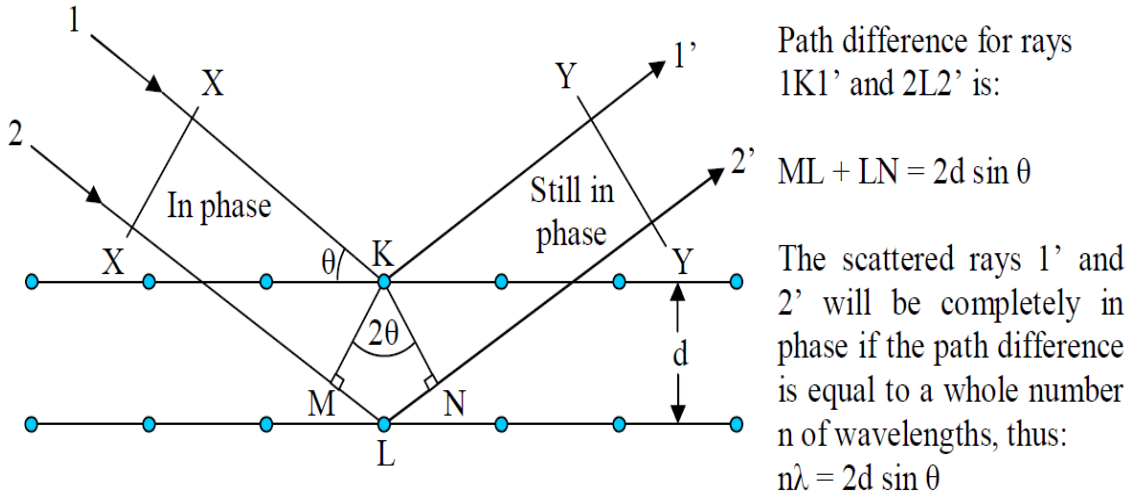

Figure 4.3.2 Visual representation of Bragg's law [8].

As previously stated, XRD is usually performed on powder samples because all of the small crystallites will be randomly oriented. However, this is not good practice for valuable building samples and hence analysis of intact surfaces was performed, recognising that crystallites present may not be randomly oriented and instead exhibit texture. This meant that only semi-quantitative analysis could be performed. Whilst the crystal phases in a sample could be identified the relative abundances could not.

4.3.2.3 Apparatus

The powdered stone, mortar and plaster samples were analysed using a Bruker D8 Advanced X-ray diffractometer with a Cu K-alpha radiation source ($\lambda = 1.5406$ Å). The 2θ range was from 5 to 80 degrees, and the step size was 2 seconds.

The equipment was operated with the X-ray source at 40kV and 30mA emission current, generating monochromatic Cu Kα X-rays [9]. Since the only emission of interest was the X-ray, there was no restriction from the atmosphere to detect signals, and hence the samples remained under ambient conditions. The X-rays were collimated using a 2mm slit before interacting with the sample. The incident angle of the beam on the sample alters as the combination of source and sample tilts in the setup used for this work and varies in steps of 0.01^{o}. The penetration depth depends on a number of factors including the elements present in the sample (the depth increases as the angle increases and means it may not be constant throughout the measurement). A photomultiplier helps to convert the measured X-ray fluorescence to an electrical signal creating a count of the incident X-rays at each angle increment [10]. The measured 2θ spectra peak values were cross-referenced with a crystallite database to determine the mineral phases present. The software used was the International Chemical Structure Database (ICSD).

4.3.3 Laser Raman Spectroscopy (LRS)

4.3.3.1 Introduction

Raman spectroscopy is used to study characteristic asymmetrical bond vibrations in systems of chemical compounds. In this interaction, vibrational energy is gained by an impinged molecule and lost by the photon. Raman is a laser analysis technique which is based on the phenomenon of Raman scattering. When a laser is fired at a surface, the majority of the incident light that is scattered or reflected maintains its wavelength (known as Rayleigh scattering), However approximately 1 in a million photos loses energy due to inelastic scattering, caused by molecular interaction with the material surface, and is known as Raman scattering. Raman and Krishnan experimentally investigated and observed this effect [11, 12].

Raman is used by chemists and materials scientists to quickly gain information about materials; principally the compounds present. It is a qualitative rather than quantitative analysis technique but can be useful for point analysis or surface mapping to determine the distribution of different materials.

4.3.3.2 Types of Scattering

For infrared spectroscopy, a range of frequencies are fired at the sample until a resonant frequency causes the sample to vibrate. This occurs when the frequency of incident radiation matches the molecule's resonant frequency, and the energy is absorbed. There is a detected loss of frequency once the radiation has passed through the sample. On the contrary, Raman spectroscopy irradiates the sample with a single frequency and measures the radiation that is scattered, not absorbed, from the molecule.

The Rayleigh procedure does not include any form of energy changes and this process is the most intense, involving elevations of energy levels but returning to the same energy state.

The Raman scattering phenomena occurs in two ways, Stokes and Anti-Stokes. Stokes scattering encompasses the excitation of a molecule to an energy vibrational state (n) by absorbing energy from a ground vibrational state (m). Anti-Stokes scattering will only occur when a molecule is already in a state of excitement as a result of thermal energy absorption, and generally is a lot weaker than Stokes scattering. However, in the Stokes scattering scenario, some energy is transferred to the scattered photon, which remains in the elevated 'n' state. The comparison of Stokes, Rayleigh and anti-Stokes is shown in Figure 4.3.3.

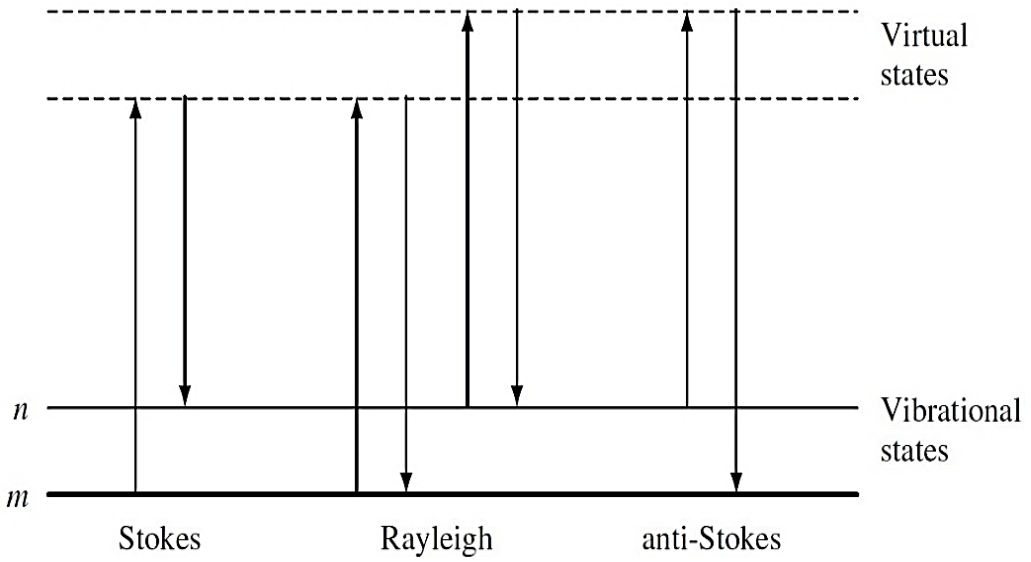

Figure 4.3.3 Diagram of the Rayleigh and Raman scattering processes [13].

As a result of collecting Raman spectra, laser-induced fluorescence can produce interference. When fluorescence occurs, the molecule absorbs a photon, which then elevates it to a higher electronic level (state) where it will continue to stay until the end of its resonant lifetime. The backward return to the ground state will involve the emission of a photon typically between 0.5-20 ns after absorption.

Fluorescence will only happen from photons having the same energy required to move the molecule to an excited electronic state. Hence, it is a function of the wavelength of the excitation source used, whereas in the Raman shift it is not so. Therefore, the fluorescence bands will move relative to the Raman peaks if the colour of the laser excitation source is varied.

4.3.3.3 Molecular Vibrations

As long as there is no change in electronic energy, the molecule's energy can be broken down into several parts, or degrees of freedom. There are three degrees of freedom that represent the movement in space of two bonded ions and three rotational types that are possible. For vibrational modes, the vibrational degrees of freedom will be given as 3N-6 if N is assumed to be the number of atoms contained in the molecule, except in the case of a linear molecule - where it becomes 3N-5, as the missing degree of the freedom of rotation converts directly to rotational freedom.

There must be changed in the polarisability of a molecule in other for a transition to become Raman active, or we can also say that there is a distortion in the energy levels with respect to the atomic nuclei. In the case of an infrared signal to occur there must be absorption, which is generally the case when there is a change in dipole moment. An example is that an O_2 molecule will only have just one vibration mode, symmetric expansion and contraction occurs along with the O-O bond. They will cause a change in the polarisation but not dipole moment (giving a Raman signal but not necessarily an IR signal). In N-O there are changes in both the polarisation and the dipole moment since both infrared and Raman active signals causes a vibration along with the bond. For example, vibrational, rotational, and translational motions of a carbon dioxide molecule are illustrated in Figure 4.3.4.

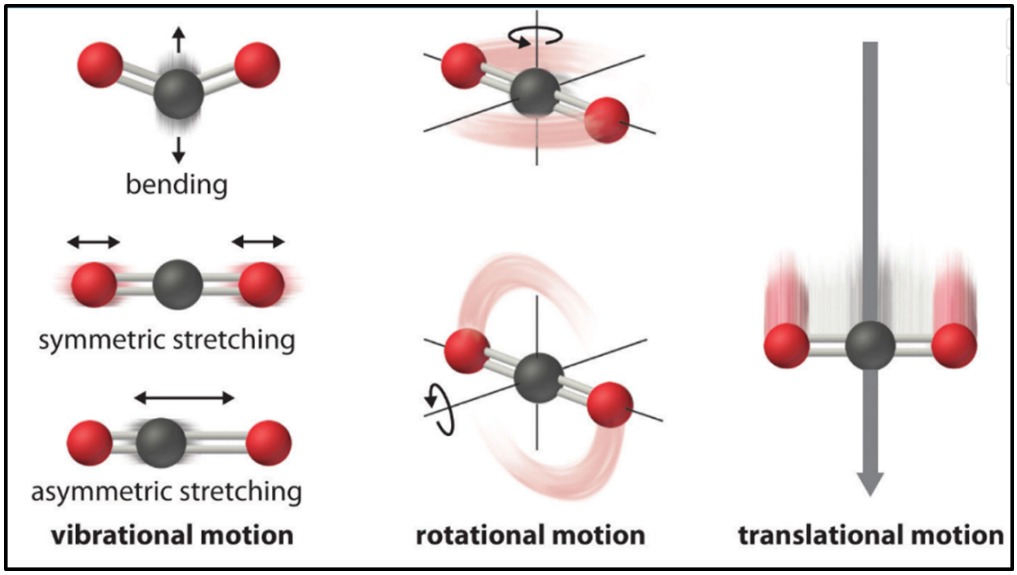

Figure 4.3.4 Molecular motion of carbon dioxide; translation, rotation, and vibration [14].

4.3.3.4 Apparatus and Equipment's Specification

The samples were characterised using Perkin RamanFlex 400 laser spectrometer which is equipped with an excitation source fitted with an NIR 785nm laser diode and a cooled Peltier CCD detector (charge couple device). A laser beam focuses on the sample using an x50 NA = 0.75 microscope objective lens to a spot of about 40µm in diameter and the scattered light is projected in a non-polarized backscattering geometry (see Figure 4.3.5). The summation of the total power on the sample is about 40mW.

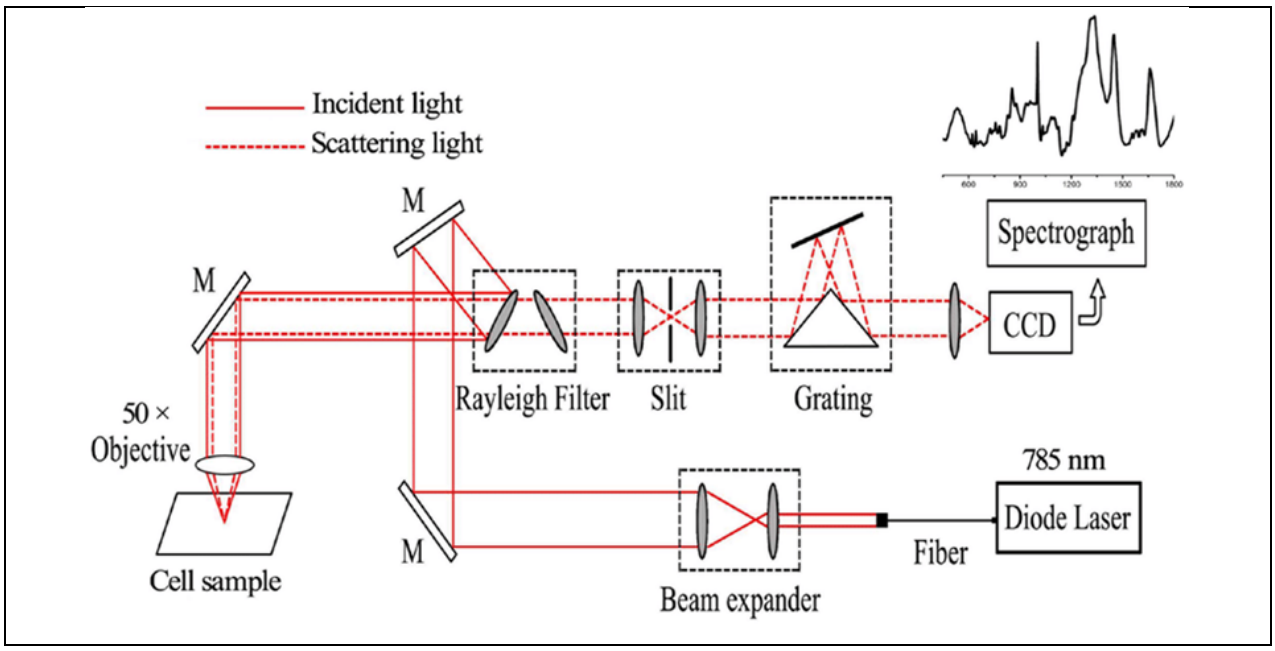

Figure 4.3.5 Diagram of the Perkin RamanFlex 400 laser spectrometer [15].

4.3.4 Scanning Electron Microscope (SEM)

4.3.4.1 Introduction

The scanning electron microscope (SEM) is a device of electron microscopy which produces images from the surface being investigated with electron bombardment. The technique is advanced compared to a conventional optical microscope as the SEM has the capacity to achieve a resolution better than 1nm. As such it is very good for studying crystal morphology on a micro-scale but the device is controlled by the incident beam diameter [16].

4.3.4.2 Instrument

Typical SEMs function by emitting an electron beam which is focused on the sample surface using one or two lenses to a spot 0.4-5nm diameter. The beam is made to pass through a deflection coil which deflects the beam in an x and y axis, as seen in Figure 4.3.6. The result is a raster like scanning over a rectangular region of the surface of the sample. Several kinds of detectors can be installed in the device to collect information from different signals to image the region examined or investigated, such as secondary backscattered electrons.

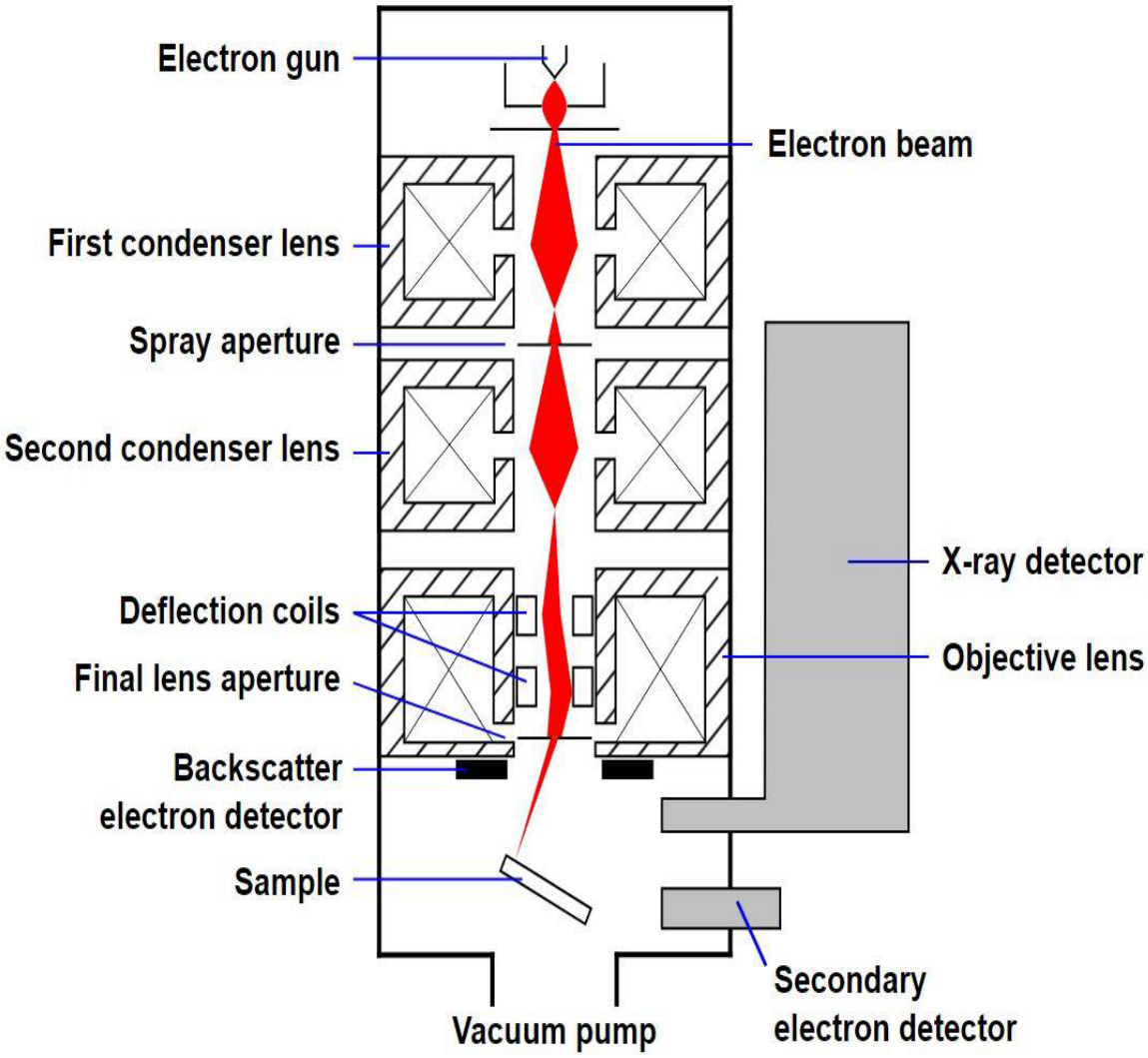

Figure 4.3.6 Schematic diagram of an SEM [17].

4.3.4.3 Electron Emission

The SEM uses interactions of the electron beams with atoms located at various depths in the sample to produce signals that are then converted into digital images (electron micrographs). Signal types employed for this investigation are either reflected or back-scattered electrons (BSE) produced from secondary electrons (SE). The secondary electron detectors are a standard detector present in all SEMs, but it is uncommon for a machine to have detectors that can measure all other possible signals, including for example – X-rays, the current absorbed by the sample, cathodoluminescence and any other electrons that may be transmitted. The SEM used in this investigation and its capabilities are discussed in section 4.3.6.

Imaging using secondary electrons relies on the emission of secondary electron from depths which are very close to the surface of the sample and are usually highly localised. However, using these electrons, the SEMs have the capacity to produce very high-resolution images of the surface exposing details less than 1nm in size. Primary electrons (PE) are electrons scattered from up to 5μm within the sample surface and are reflected to the detector. The escaping electron is the secondary electron resulting from an inelastic interaction with the primary electron beam, then captured by the detector producing a signal forming the more detailed image.

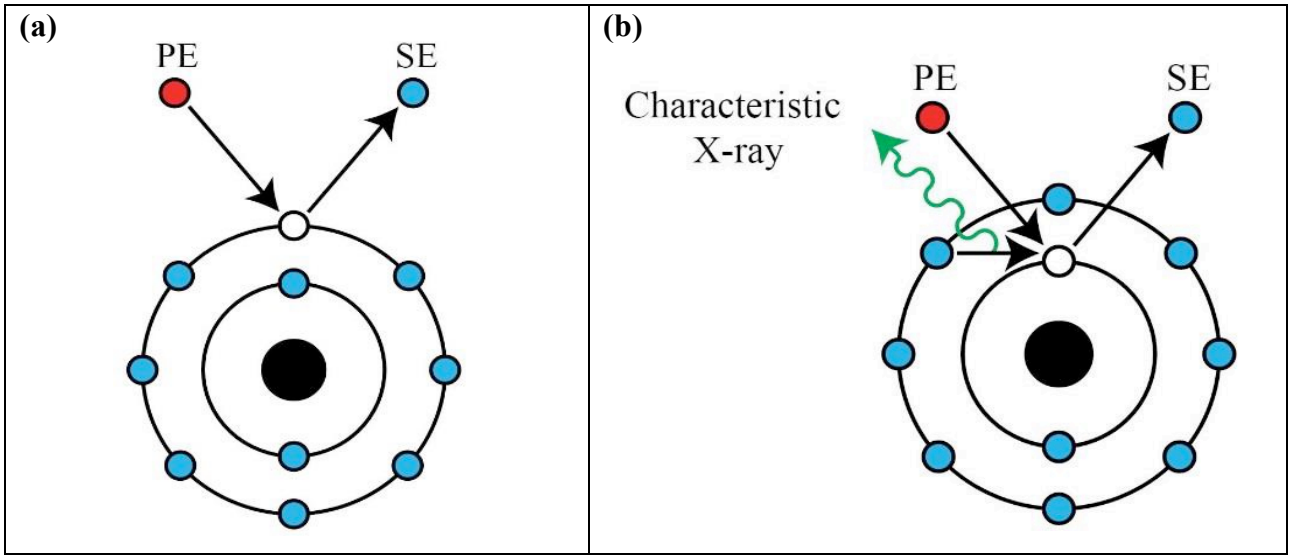

Figure 4.3.7 Mechanisms of emission of (a) secondary electrons (SE); and (B) characteristic X-rays from atoms of the sample. PE represents a primary electron [17].

When there is a removal of an inner shell electron from an atom in the sample by an incident PE, a characteristic X-ray can be produced. A higher-energy electron occupies the inner shell that was previously occupied by its own electron, leading to the energy release as shown in Figure 4.3.7. The characteristic X-rays produced are useful for identifying the composition as well as measurement of the abundance of the elements in the sample.

4.3.4.4 Sample Interaction Volume

As mentioned prior, when beams collide with the surface of samples it leads to the production of several signals that provide information from different depths, as in Figure 4.3.8. Topographic information crucial for images to be produced is provided by the secondary electrons. Characteristics X-rays are for the provision of signals from an extended region, generating information on the sample's atomic composition.

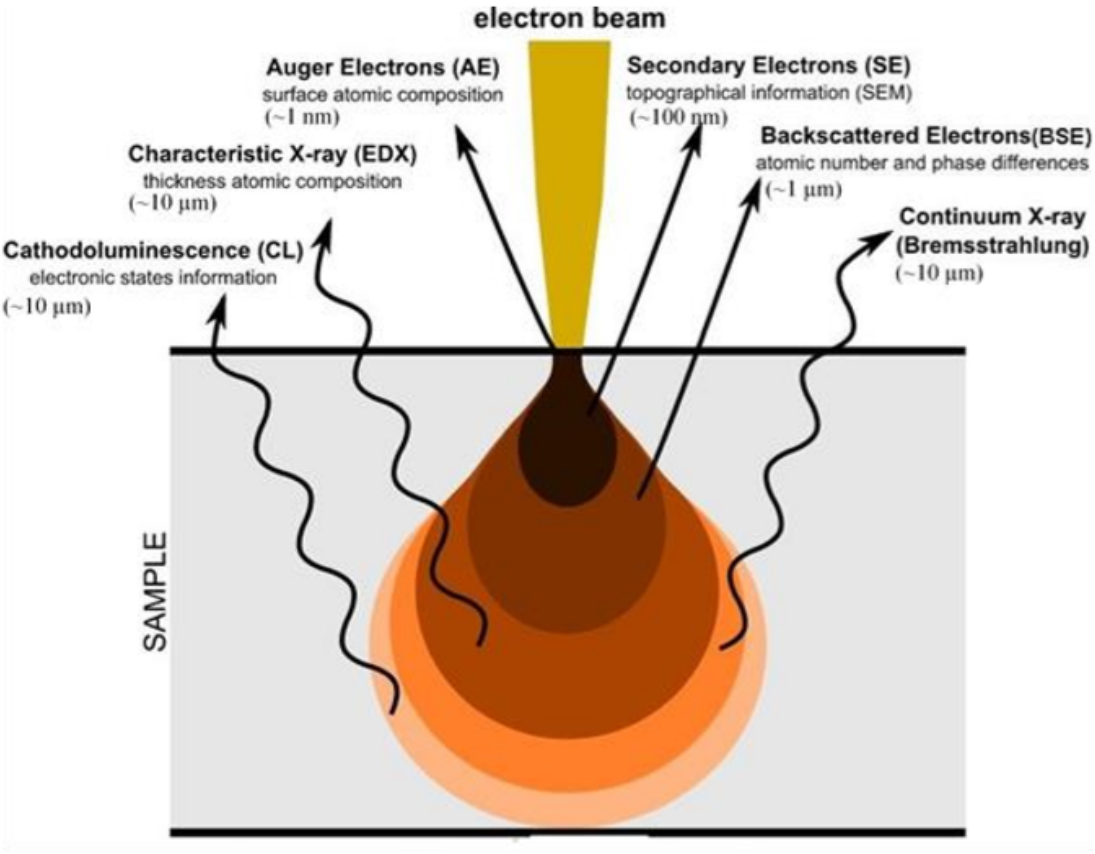

Figure 4.3.8 Signals emitted from a different depth of sample and corresponding interaction volume [18].

4.3.4.5 Sample Preparation

In sample preparation, the samples must be an appropriate size to fit into the specimen chamber and can be moved safely into position for the incident beam by manipulating the stage. Prepared samples must be suitable for high vacuum. A typical pumping range is 10^{-5} mbar before the

investigation of a sample. The probing method of the surface inherently causes the accumulation of electrostatic charge at the surface, so when a sample is conductive (i.e., metallic), little preparation is needed, other than fixing the sample onto an aluminium stub with good electrical contact which allows the surface charge to dissipate. Samples which are insulated can be imaged but result in a signal distortion on the surface, which can be particularly prominent in secondary electron imaging of samples. In order to reduce the effect of this distortion, the beam energy can be reduced but this can have the disadvantageous effect of lowering the resolution. Usually, the process of sample preparation for SEM investigation is to coat the sample in an ultra-thin gold or carbon layer. When this film thickness is kept under 10nm, the effect on the image quality is negligible.

The Zeiss Sigma VP FEG-SEM equipment was employed for this investigation. The SEM is fitted with a field emission gun converting secondary electrons and X-rays into electronic signals. Samples were subjected to analysis between 15-30 kV, with a working distance of about 8mm at which distance, the best resolution images are obtained for this equipment and setup.

4.3.5 Energy Dispersive X-Ray Spectroscopy (EDS)

Elemental analysis is carried out employing an analytical technique known as Energy Dispersive X-ray Spectroscopy (EDS) [19]. An SEM has the capacity to gather a spectrum from any element with a mass above lithium from the examined sample. Often this is useful in estimating the relative abundance of chemical elements, or to provide maps of the distributions of various elements present in a sample – particularly important when investigating samples containing complex minerals or compounds with a range of elements. These results are usually semi-quantitative at best.

There are factors that affect the accuracy of the quantitative analysis of EDS. EDS usually gives inaccurate results when analysing light elements i.e. elements having an atomic number ranging from 4-9. This challenge is a function of the low count rates resulting from insufficient beam current at the low voltage required, and minute spot sizes making it difficult for microanalysis [20].

X-rays are generated within the sample when an atom's inner shell electron is excited by the primary electron from the external electron beam. The most stable state for the atomic shell is when the shell is closest to the atomic nucleus – this is the lowest energy state, also known as the ground state (K). When an electron in this state is stimulated by one of the primary electrons, it gains energy, leaving a gap in the lower energy state. The electron maintains this excited state for a while and then returns to its original level releasing the same amount of energy that was gained earlier, as in Figure 4.3.9. This phenomenon means each element has a unique fingerprint, making it possible to identify the elements present in the sample [21].

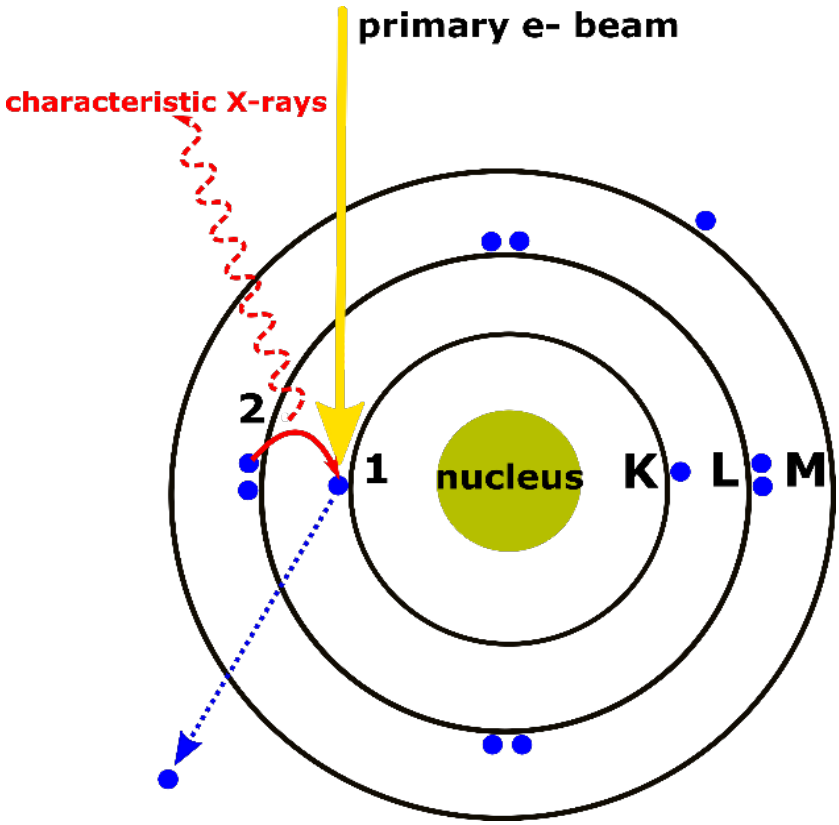

Figure 4.3.9 Schematic drawing for atomic nucleus stimulation [22, 23].

The microstructure and chemical composition were analysed using the EDAXTM Software, used in conjunction with a Carl Zeiss Sigma (FEG-SEM) acquiring spectra and maps. All EDS was undertaken with a primary energy (PE) between 15 KeV to a maximum of 25 eV. The volume of the interacting electron beam for this investigation was approximately 500nm in size [24].

The data obtained in the process was corrected using the ZAF (atomic number, absorption, fluorescence) approach. The ZAF technique is deployed when using semi-quantitative electron probe microanalysis for converting the intensity ratios into concentration units [25]. The three corrections are calculated separately, namely: atomic number correction (Z), absorption correction (A) and fluorescence correction (F). The Z factor arises from the discrepancy between the X-rays generated at higher versus lower atomic weights. The A factor is employed for calculating the X-ray absorption within the sample, and the F factor is an iterative correction for X-rays from heavier elements fluorescing lower energy X-rays, potentially obscuring the intensities, and is based on the Reed model [26].

4.3.6 Dual-Beam (DB)

The Dual-beam (DB) technique is a combination of the FIB and SEM methods in one system. Most recent dual-beam machines are fitted with a FIB column which is then combined with another SEM column to become a dual-beam platform. The technique also has transmission electron microscopy (TEM) capability for sample preparation and microstructural analysis [27]. A typical dual-beam device is shown in Figure 4.3.10 showing the FIB and SEM columns.

The dual-beam platform involves both electron and Ga^{+} ion beams interacting with the sample at the same location. A known angle is made between the incident electron and ion beams. Electrons are radiated and sputtered particles are produced and collected respectively by the corresponding detectors to produce separate SEM and FIB images.

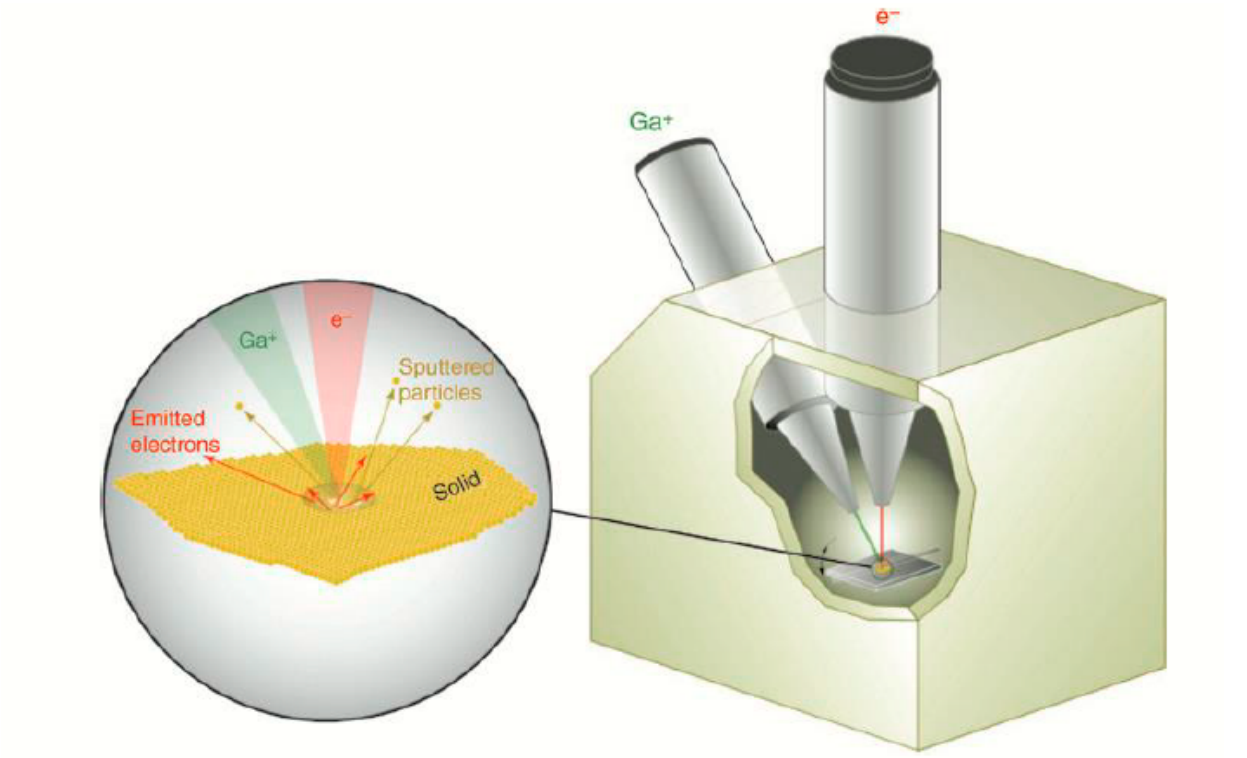

Figure 4.3.10 Schematic illustration of dual-beam and an expanded view showing electron and ion beam sample interactions [27, 29].

4.3.6.1 Ion used for Milling and Imaging

The focused ion beam (FIB) imaging technique is a material science technique used for site-specific analysis, deposition and ablation of materials. It is quite similar to the SEM investigation technique with the exception that the beam raised over the specimen is not an electron beam but a gallium ion (Ga+) beam [27].

In this study the Thermo Fisher Scientific FEI Helios NanoLab 600 combined focus ion beam was employed for trenching, sectioning and imaging of the samples. The emission of secondary electrons (SE) from the surface of the sample produced images with high spatial resolution.

4.3.6.2 Instrument

A typical FIB ion column device has a column very similar to the SEM. However, as mentioned the main discrepancy between these devices is the use of gallium ion (Ga+) beam in the rather than the electron beam in the SEM. Secondly, the other important distinction between the two techniques is that the lenses in the FIB are electrostatic, due to the large mass of Ga+ ions, rather than magnetic as in the SEM. The ion beam is produced from a liquid-metal ion by applying a strong electric field causing a positively charged ion to emerge from a gallium liquid cone on the tip of a tungsten needle while maintaining a vacuum of about $1x10^{-7}$ mbar in the column [27]. After the first refinement by spraying through the aperture, the ion beam condenses on the first electrostatic lens and the beam's stigmatism is adjusted by the upper octopole. A typical ion beam energy is between the range of 10 – 50 keV, and currents vary between 1 pA and 20 nA.

4.3.6.3 Milling, Imaging and Deposition

An example FIB raster scan over a substrate during imaging is shown in Figure 4.3.11a. Generating and collecting secondary particles with the inclusion of neutral atoms, ions and electrons are carried out by a CDEM (continuous dynode electron multiplier). Hence, the differences shown in the FIB-generated images are a function of the amount of the secondary ions and electrons reflected from the different features on the sample's surface. Figure 4.3.11b schematically highlights the physical sputtering with respect to the samples. The ion penetration depth in crystalline materials changes because of channelling in the lattice structure along open columns. Therefore, FIB can also be used for imaging crystalline grains, exposing differences in the structure's orientation with depth. A drawback to this technique is that imaging with FIB can cause damage to the sample, since Ga+ ions entering the surface of the sample lead to ion implantation. Therefore, the overall interaction volume depends on the ion energy and incident angle of the ion beam.

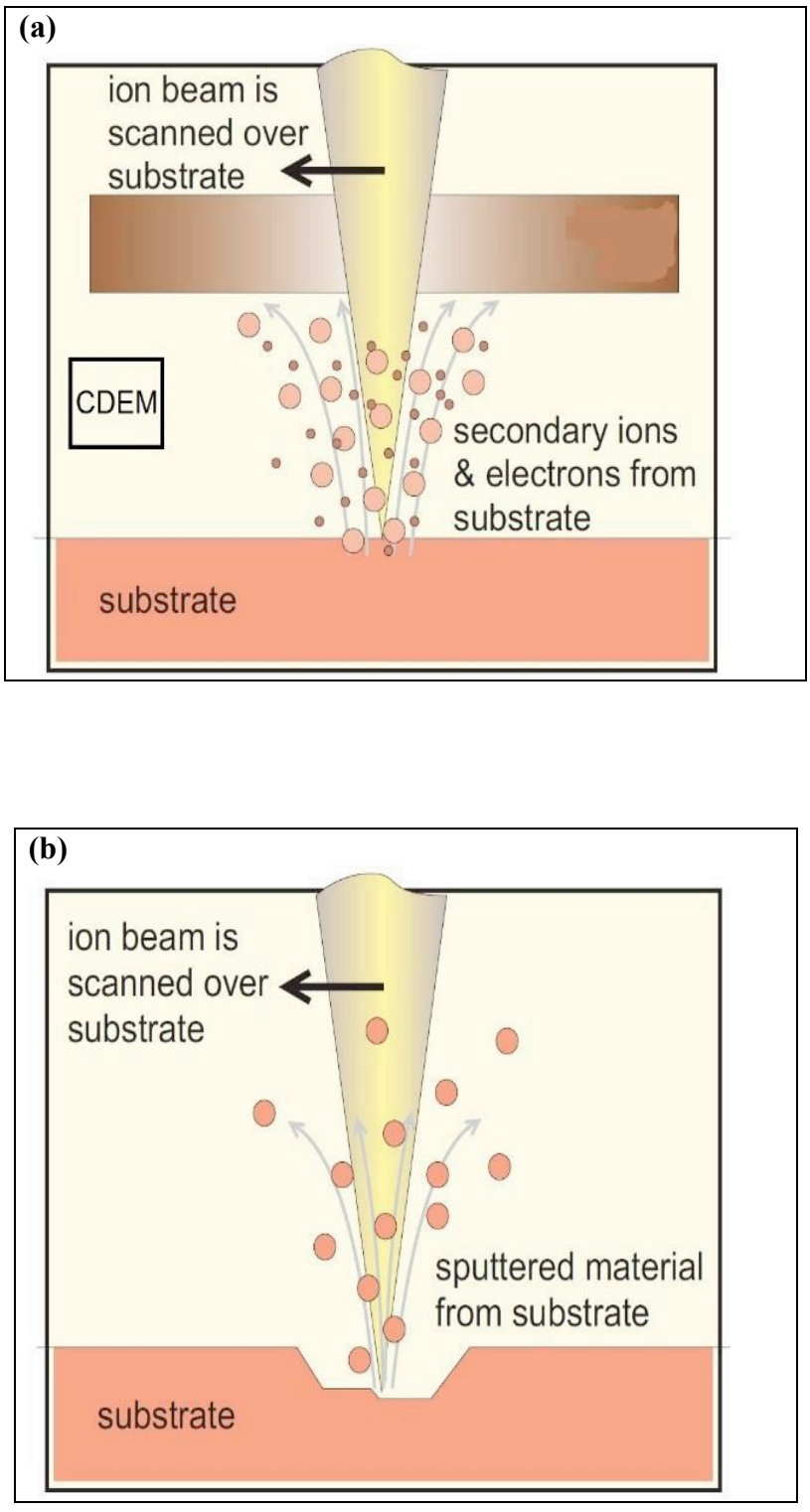

Figure 4.3.11 Principle of FIB (a) imaging and (b) milling. CDEM represents continuous dynode electron multiplier [28, 29].

4.4 References

[1] Geological Survey of Norway, (2015). Stone Construction Material. [Online] Available at: https://www.ngu.no/en [Accessed 02/04/2019].

[2] The Concrete Centre, (2019). This is Concrete. [Online] Available at: https://www.sustainableconcrete.org.uk/ [Accessed 02/04/2019].

[3] Regourd, M., Kerisel, J., Deletie, P., Hauenauer, B., (1987). Microstructure of mortars from three Egyptian pyramids. Cement and Concrete Research, 18(1), ppn81-90. [Online] Available at: https://www.sciencedirect.com/science/article/pii/000884688890124X. [Accessed 8/1/2020].

[4] Gopi, S., (2009). Basic Civil Engineering. [Online] Available at: https://www.oreilly.com/library/view/basic-civil-engineering/9788131729885/ [Accessed 02/04/2019].

[5] PRODYOGI (2018). Plastering - Requirements, Types and Specifications. [Online] Available at: https://learnandearnd5.blogspot.com/ [Accessed 02/04/2019].

[6] Liu, C., (2018). Oxidation and carburization of 9Cr-1Mo steel inboth simulant and in-service AGR coolant gases. PhD, University of Bristol.

[7] Haynes, R (1984). Optical Microscopy of Materials, Blackie & Son Ltd.

[8] Jones, C., (2009). Photocatalytic Oxidation of So_2 and No_x Pollutant Gases Using Titania Compounds and Nanostructures. PhD, University of Bristol.

[9] Suryanarayana, C., Grant Norton, M., (1998). X-Ray Diffraction: a practical approach. [Online] Springer US. Available at: https://www.springer.com/gp/book/9780306457449 [Accessed 02/04/2019].

[10] Kasai, N., Kakudo, M., (2005). X-ray diffraction by macromolecules. [Online] Springer Berlin. Available at: https://link.springer.com/book/10.1007/3-540-28353-6#about [Accessed 02/04/2019].

[11] Ewen Smith, G.D., (2005). Modern Raman Spectroscopy: A Practical Approach. John Wiley and Sons.

[12] Gardiner, D.J, P.R.G. and Bowley, H.J., (1989). Practical Raman Spectroscopy. Springer-Verlag.

[13] Fernandes, R., (2016). Green emitting diodes for solid state lighting. MSc Thesis, Advisor: Rute A Sá Ferreira, Universidade de Aveiro.

[14] Chemistry.LiberText. [Online]. Available at: https://chem.libretexts.org/Bookshelves/General_Chemistry/Book%3A_Chemistry_(Averill_and_Eldredge)/Chemical_Thermochemistry/18.4_Entropy_Changes_and_the_Third_Law_of_Thermodynamics [Accessed 16/05/2020].

[15] Huang, H., Lin, D., Chen, W., Yu, Y., Xu, J., Liang, Z., Lin, X., Dong, Z., Shi, H., (2014). Nondestructive discrimination between normal and hematological malignancy cell lines using near-infrared Raman spectroscopy and multivariate analysis. Laser Physics Letters.

[16] Stokes, D., (2008). Principles and Practice of VariablePressure/Environmental Scanning Electron Microscopy (VP-ESEM), Wiley.

[17] Goldstein, J.I, Newbury, D.E, Michael, J.R, Ritchie, N.W.M, Scott, J.H.J and Joy, D.C., (2018). Scanning Electron Microscopy and X-ray Microanalysis, 3rd ed, Springer New York.

[18] Goldstein, J.I, Newbury, D.E, Echlin, P, Joy,D.C, Romig, A.D,Lyman, C.E, Fiori, C and Lifshin, E (1992). Scanning Electron Microscopy and X-Ray Microanalysis: A Text for Biologists, Materials Scientists, and Geologists, 2nd ed., Springer US.

[19] Shindo, D and Oikawa, T., (2002). Energy Dispersive X-ray Spectroscopy, in: Anal. Electron Microsc. Mater. Sci., Springer Japan, Tokyo, 2002: pp. 81–102.

[20] Lyman, C.E, Goldstein, J.I, Romig, A.D, Echlin, P, Joy, D.C, Newbury,D.E, Williams, D.B, Armstrong, J.T, Fiori, C.E, Lifshin, E and Peters, K.R (1990). Light Element Microanalysis, in: Scanning Electron Microsc. X-Ray Microanal. Anal. Electron Microsc., Springer US, Boston, MA, 1990: pp. 117–121.

[21] Charles G., Barkla M.A. D.Sc., (2014). The Spectra of the Fluorescent Röntgen Radiations, London, Edinburgh, Dublin Philos. Mag. J. Sci. 22(1911) 396–412.

[22] Bertin, E.P (1975). Principles and Practice of X-Ray Spectrometric Analysis, Springer US.

[23] NASA, (2019), Astronomer's Toolbox. [Online] Available at: https://imagine.gsfc.nasa.gov/science/toolbox/toolbox.html [Accessed 02/04/2019].

[24] Doig, P, Lonsdale, D., Flewitt, P.E.J (1980). The Spatial Resolution of X-ray Microanalysis in the Scanning Transmission Electron Microscope, Philos.Mag. A. 41. pp 761–775.

[25] Bastin, G.F, Heijligers, H.J.M and van Loo, F.J.J., (1984). The Performance of the Modified Φ(ρz) Approach as Compared to the Love and Scott, Ruste and Standard ZAF Correction Procedures in Quantitative Electron Probe Microanalysis, Scanning. 6, pp58–68.

[26] Reed, S.J. B., (1965). Characteristic Fluorescence Corrections in Electron-probe Microanalysis, Br. J. Appl. Phys. 16, pp 913–926.

[27] Volkert, C.A., Minor, A.A., (2007). Focused Ion Beam Microscopy and Micromachining, MRS Bull. 32. pp 389–399.

[28] Reyntjens, S., Puers, R (2001). A Review of Focused Ion Beam Applications in Microsystem Technology, J. Micromechanics Microengineering. 11, pp287–300.

[29] Wang, Z.M (2013). FIB Nanostructures, Springer.

CHAPTER 5
MATERIALS CHARACTERISATION

5.1 Background

In this chapter the results gathered from the analysis of materials collected from the historical buildings - namely stone, mortar and plaster - are presented. It is very important to understand the composition of each materials used to construct these buildings [1]. Mineralogical characterisation of historical materials is presented for several reasons related to the conservation of traditional structures. The reasons for analysis and the questions posed during the conservation or restoration of an old building determine the analysis methods that will be selected. A range of mineralogical characterisation methods are available for the study of historic masonry materials. These include Optical Microscopy (OM), X-ray Diffraction (XRD), Scanning Electron Microscopy, Energy Dispersive X-ray Spectroscopy (SEM-EDS) and Laser Raman Spectroscopy (LRS) [2, 3]. The results obtained from each material collected from the different historical houses discussed in Chapter 4 are presented below.

5.2 Stone

The preparation of stone samples collected from four historical houses and additionally from the Manqabah quarry sample are shown in chapter 4 (section 4.2.1). The analysis was carried out using the following techniques:

- Optical Microscope (OM)
- X-Ray Diffraction (XRD)
- Scanning Electron Microscope-Energy Dispersive X-Ray Spectroscopy (SEM-EDS)
- Laser Raman Spectroscopy (LRS)

5.2.1 Optical Microscope

Figure 5.2.1 presents an optical micrograph of the stone surface collected from the quarry (Manqabah). The surface topography revealed a mixture of dense white and brownish colours and in addition, a black deposit was observed. The optical micrographs obtained from the stone surfaces from four houses are shown in Figure 5.2.2.

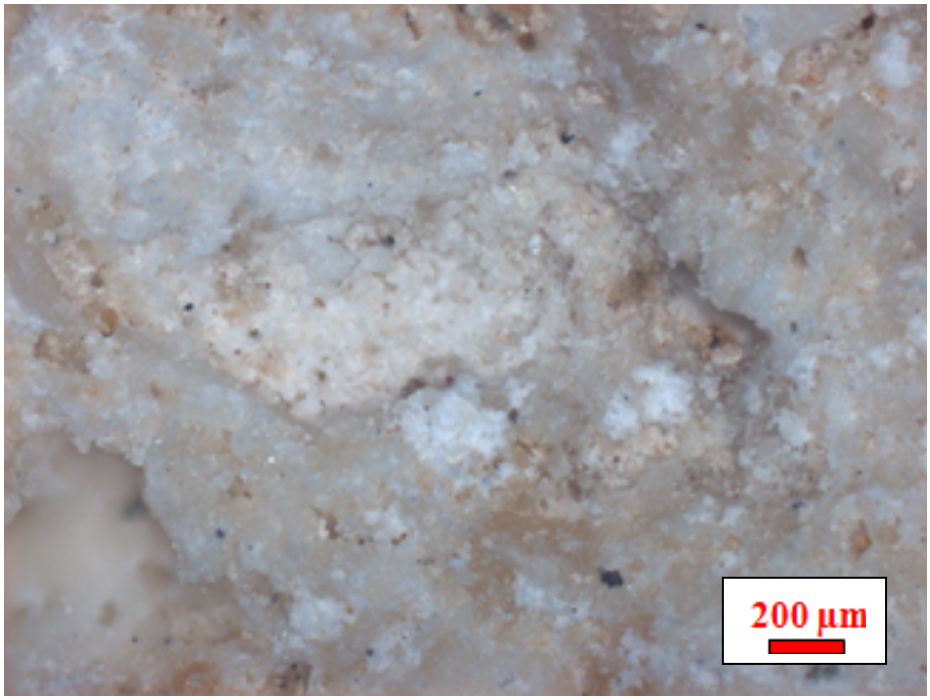

Figure 5.2.1 Optical micrograph of the stone surface collected from the Manqabah quarry.

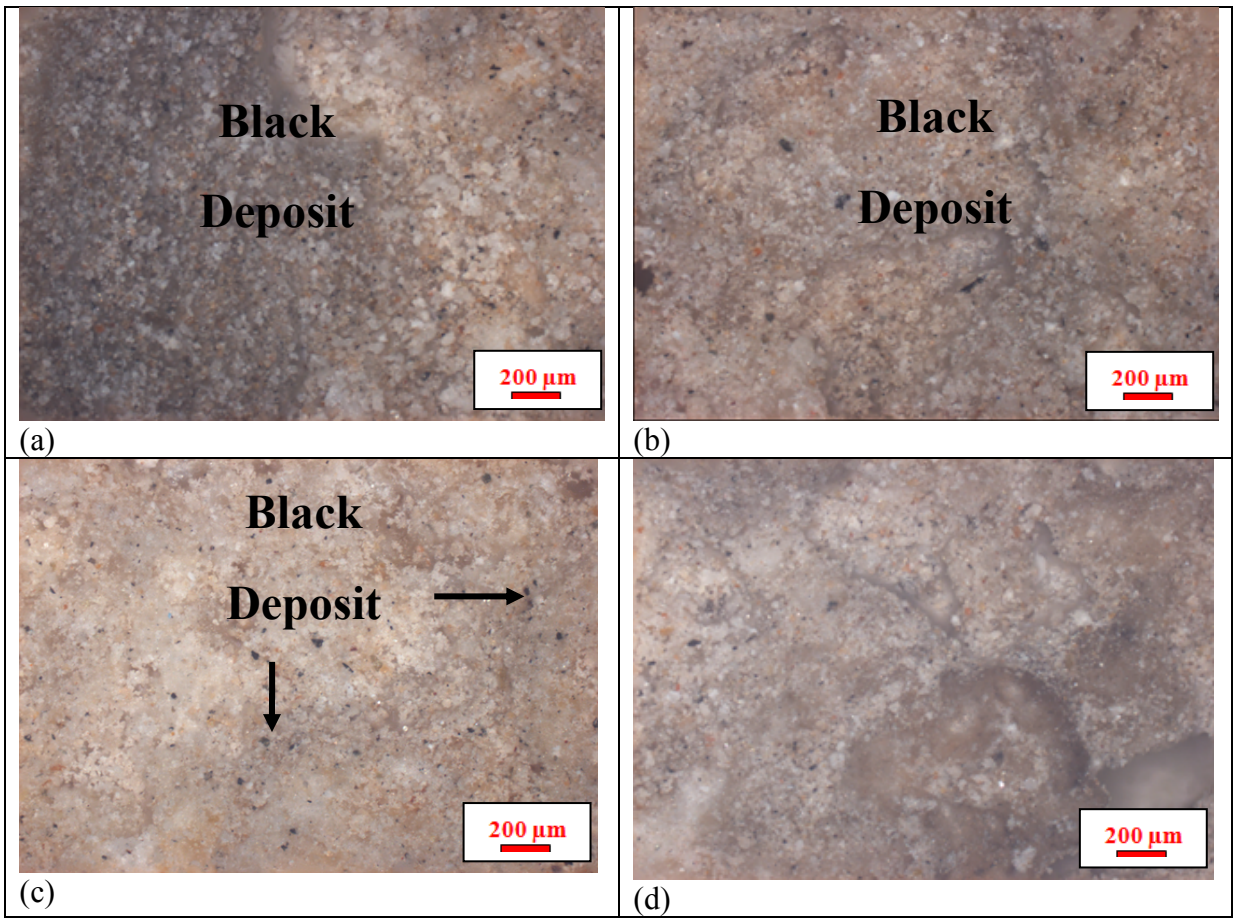

Figure 5.2.2 Optical micrographs from the stone surfaces; (a) Jokhdar house west facade, (b) Jamjoom house west facade, (c) Banaja house west facade and (d) Alsallum house south west facade.

The results revealed that the surfaces were very dense with little amounts of voids being observed (Figure 5.2.2d). The black deposit observed could be attributed to carbons or emissions from traffic congestion and industrial activities around the site.

When compared with the relatively fresh surface of the quarry sample, the discolourations and additional black precipitates strongly suggest that the surfaces are heavily contaminated.

5.2.2 X-Ray Diffraction Analysis

To identify the main phases of each stone specimen, XRD was used. Table 5.2.1 summarises the results obtained from the stone powder samples.

Table 5.2.1 Summary of the mineral phases identified in the stone samples collected from the quarry and the historical houses.

Location	Compound
Original quarry stone from Manqabah site.	$CaCO_3$ √ $CaCO_3$ NaCl
Stone from the external west facade of Jokhdar house.	$CaCO_3$ √ $CaSO_4.2H_2O$ NaCl
Stone from the external west facade of Jamjoom house.	$CaCO_3$ √ SiO_2 NaCl
Original stone from the external west facade of Banaja house.	Calcite √ $CaSO_4.2H_2O$ SiO_2 NaCl
Original stone from the external south-west facade of Alsallum house.	$CaCO_3$ √ $CaSO_4.2H_2O$ NaCl

MANQABAH QUARRY

The resultant XRD diffraction pattern for the quarry sample is shown in Figure 5.2.3. $CaCO_3$, calcite, was the main mineral phase identified and in addition, a small amount of $CaCO_3$ in the form of aragonite was identified. Aragonite is one of the three most common naturally forming crystals of calcium carbonate, the other forms being calcite and vaterite. This crystal phase being present indicates that the aragonite has not yet been transformed to calcite, the main constituent phase in limestone (a common building material globally) due to its stability over geological periods of time [4]. NaCl (halite) was also observed. This is assigned to salt deposition from the sea, however there must be investigations of the physical and chemical composition of each mineral phase to evaluate their growth and suggest provenance. Geologists call it crystal growth – morphology, and evaluating the surface topography of the crystal faces is key to understanding their growth mechanisms [5].

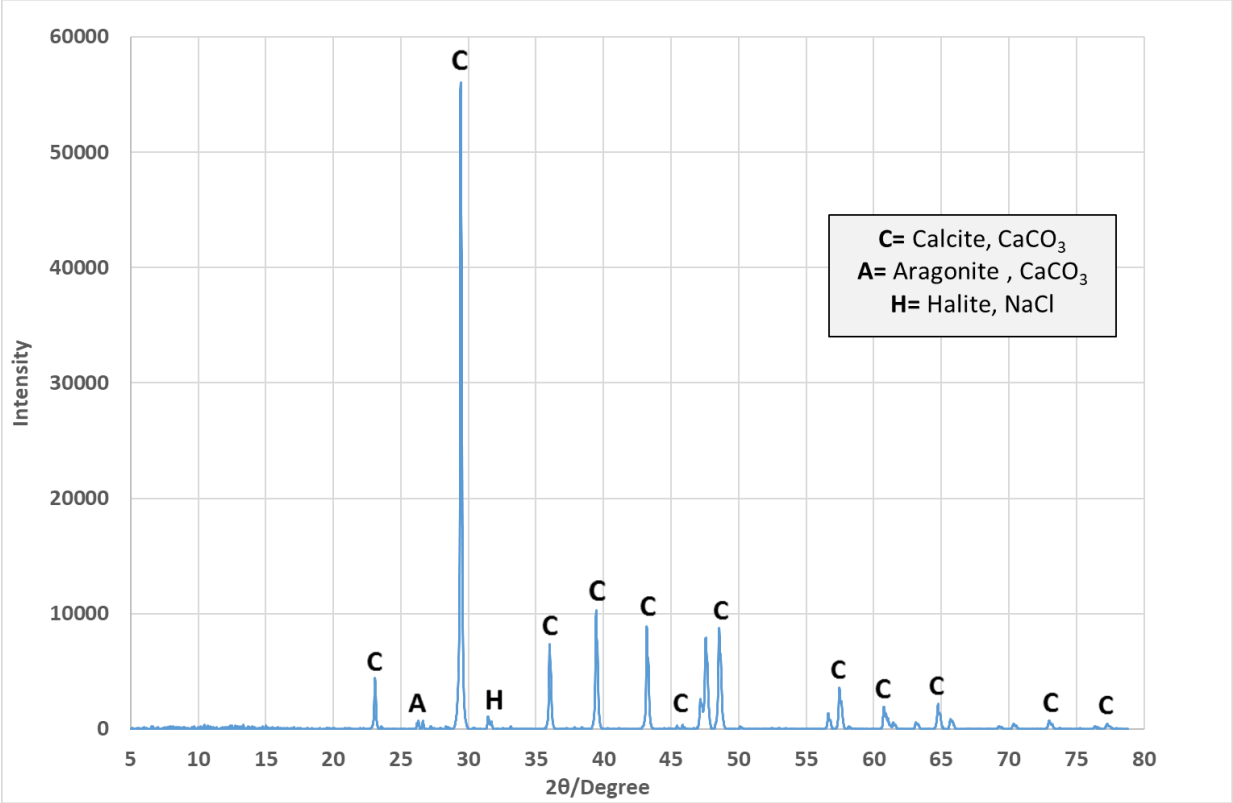

Figure 5.2.3 XRD pattern from as cut stone sample collected from Manqabah quarry.

The presence of salt crystallisation is recognized as a cause of structural deterioration of porous building materials. In particular, the crystallisation pressure of salt crystals growing in confined pores is found to be the main cause for the structural damage that occurs over time. La Russa et al observed the degradation of porous rocks induced by salt crystallisation, and found a correlation between how much salts crystallise over time with the microstructural and chromatic variations of these kinds of void-bearing materials (i.e. limestones). Any historic house located in a marine environment facing sodium chloride spray for centuries may suffer severe deterioration of its structure, due to the recrystallisation of the salt through repeating wetting and drying cycles as the expanding and shrinking crystal structure applies stress, damaging the building [6].

JOKHDAR HOUSE

$CaCO_3$, as calcite, was the main phase identified from this sample, whilst a small amount of $CaSO_4.2H_2O$, (gypsum) was observed as well as a small amount of NaCl, (halite) (Table 5.2.1 and Figure 5.2.4). This confirmed that the stone type used to construct this house was made from limestone (any rock composed mainly of calcium carbonate, especially those used in construction). The presence of gypsum is assigned to the reaction between the limestone and the atmospheric SO_2 [7, 8].

When compared with the as-cut stone from the quarry, the results showing gypsum's presence indicate that the stone was degraded by the atmospheric pollutant, sulfur dioxide.

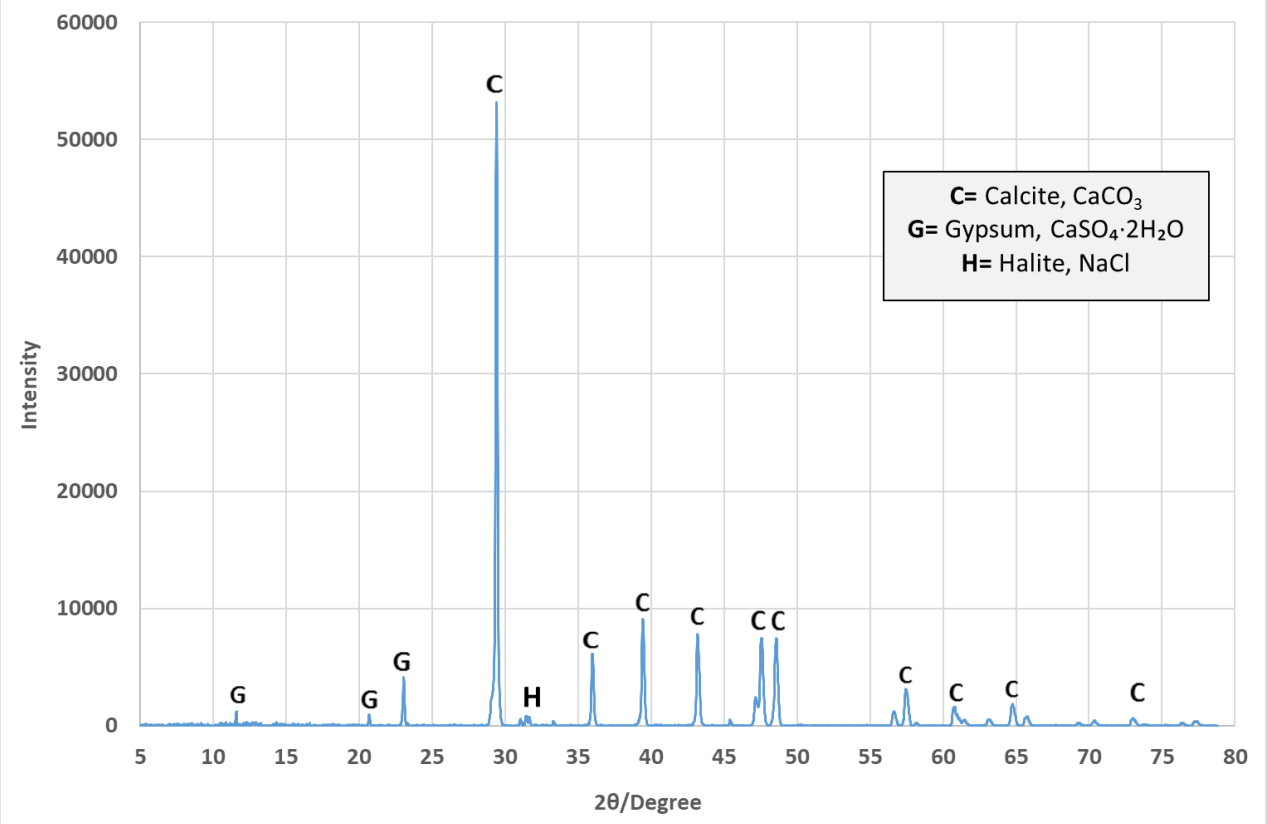

Figure 5.2.4 XRD pattern from the stone sample collected from Jokhdar house.

JAMJOOM HOUSE

The XRD diffraction pattern obtained from the Jamjoom house sample is shown in Figure 5.2.5. The diffraction pattern identified $CaCO_3$ (calcite), SiO_2, (quartz), and NaCl, (halite), as listed in Table 5.2.1. The result does not show any gypsum formation, indicating that the face of this house had no observable degradation. The presence of SiO_2 and NaCl are from aerially deposited sand and from sea salt spray, respectively [9].

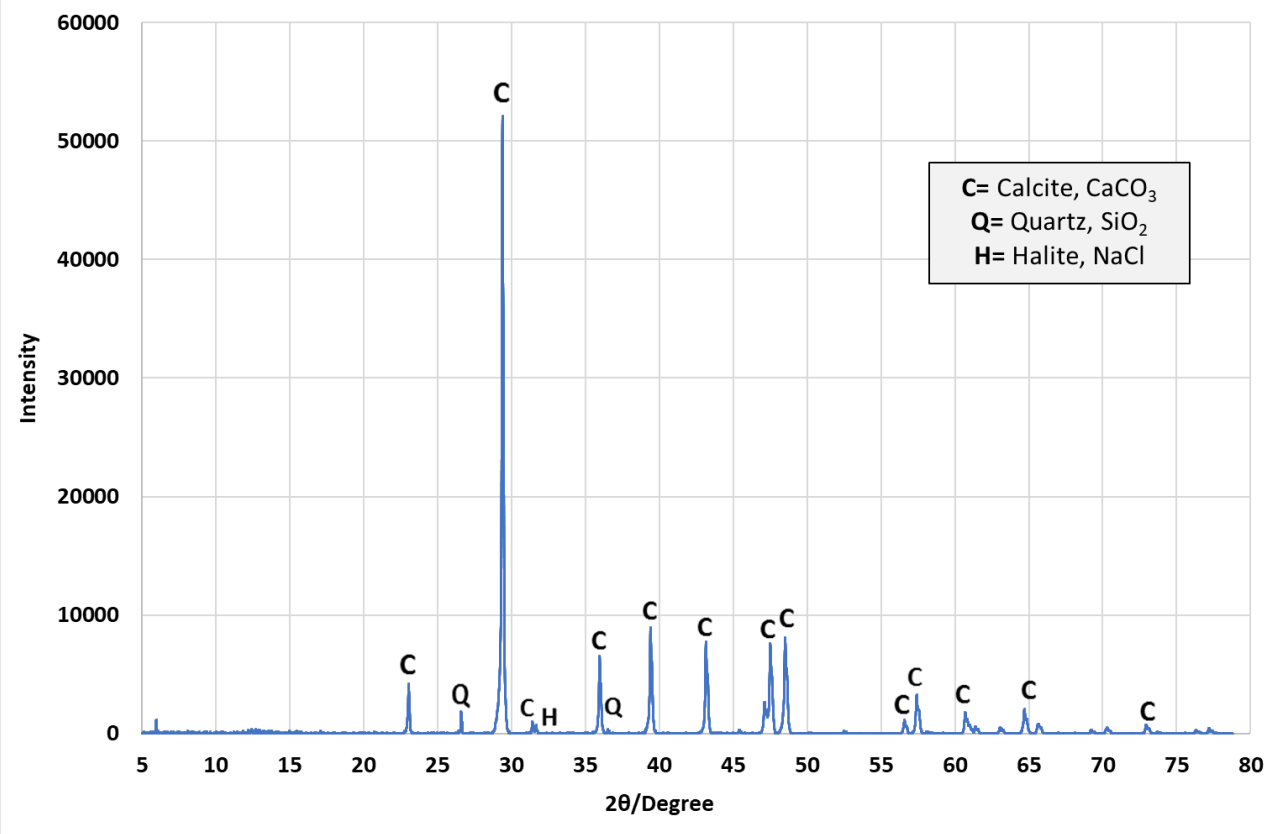

Figure 5.2.5 XRD diffraction pattern of the stone sample collected from Jamjoom house.

BANAJA HOUSE

$CaCO_3$ as calcite was determined to be the main phase of the sample from Banaja house, and small amounts of $CaSO_4.2H_2O$ (gypsum) were also observed. In addition to these main phases, SiO_2, and NaCl were identified - just like Jamjoom house (Figure 5.2.6). These findings are like those observed in the Jokhdar house sample, indicating a similar degradation process of this stone, likely from enough sulfur dioxide present in the atmosphere near this face of the house to attack the surface (Figure 5.2.4).

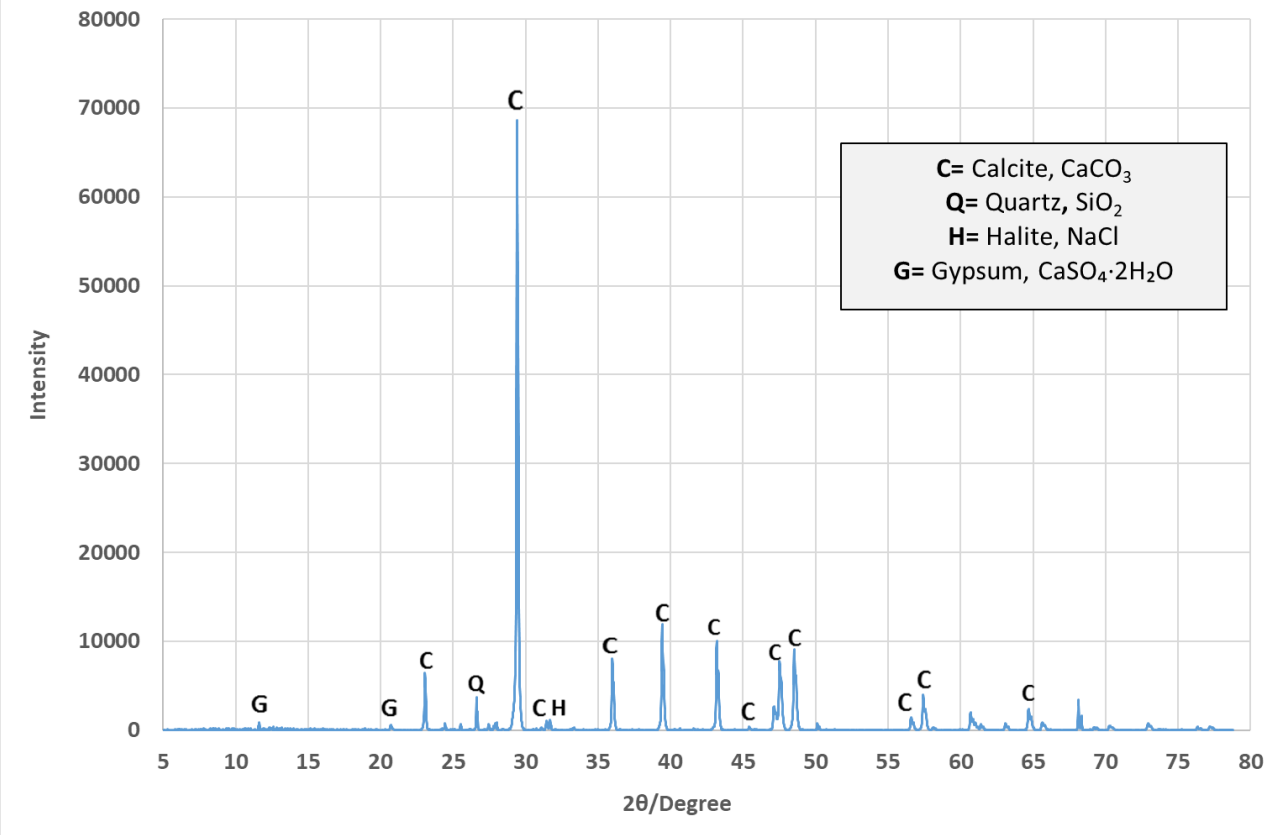

Figure 5.2.6 Typical XRD pattern of the stone sample collected from Banaja house.

ALSALLUM HOUSE

Figure 5.2.7 represents the XRD diffraction pattern from the stone sample collected from Alsallum house. Again, $CaCO_3$ (calcite) was identified as the main phase in these results. Also, just like the other samples, small amounts of gypsum were identified.

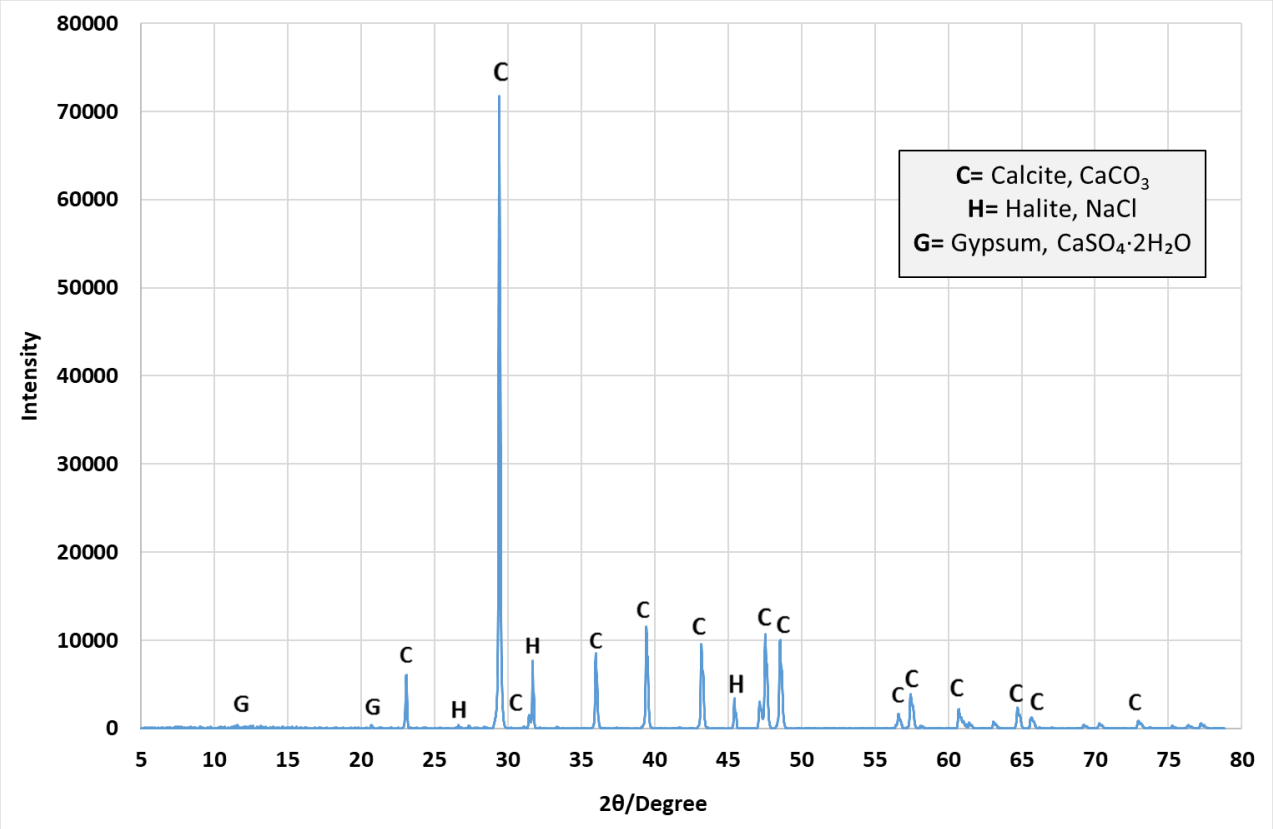

Figure 5.2.7 Typical XRD pattern of the stone sample collected from Alsallum house.

Overall, the XRD results indicate that the houses were constructed using limestone blocks, therefore it can be sensibly deduced that they were produced from the nearby Manqabah quarry, as they have very similar peaks present in their spectra, suggesting similar chemical compositions [10].

5.2.3 SEM-EDS Analysis

MANQABAH QUARRY

An SEM micrograph from the freshly cut quarry stone sample is shown in Figure 5.2.8a. The image revealed that the surface contained typical calcite crystal formations. Historically, the rhombohedral cleavage has been the most investigated growth form of calcite [5]. The elemental composition as obtained from the EDS analysis identified the elements in order of descending weight %: Ca, O, C, Na, Cl, Si, Mg, Al, Fe, P and Si, as shown in Figure 5.2.8b.

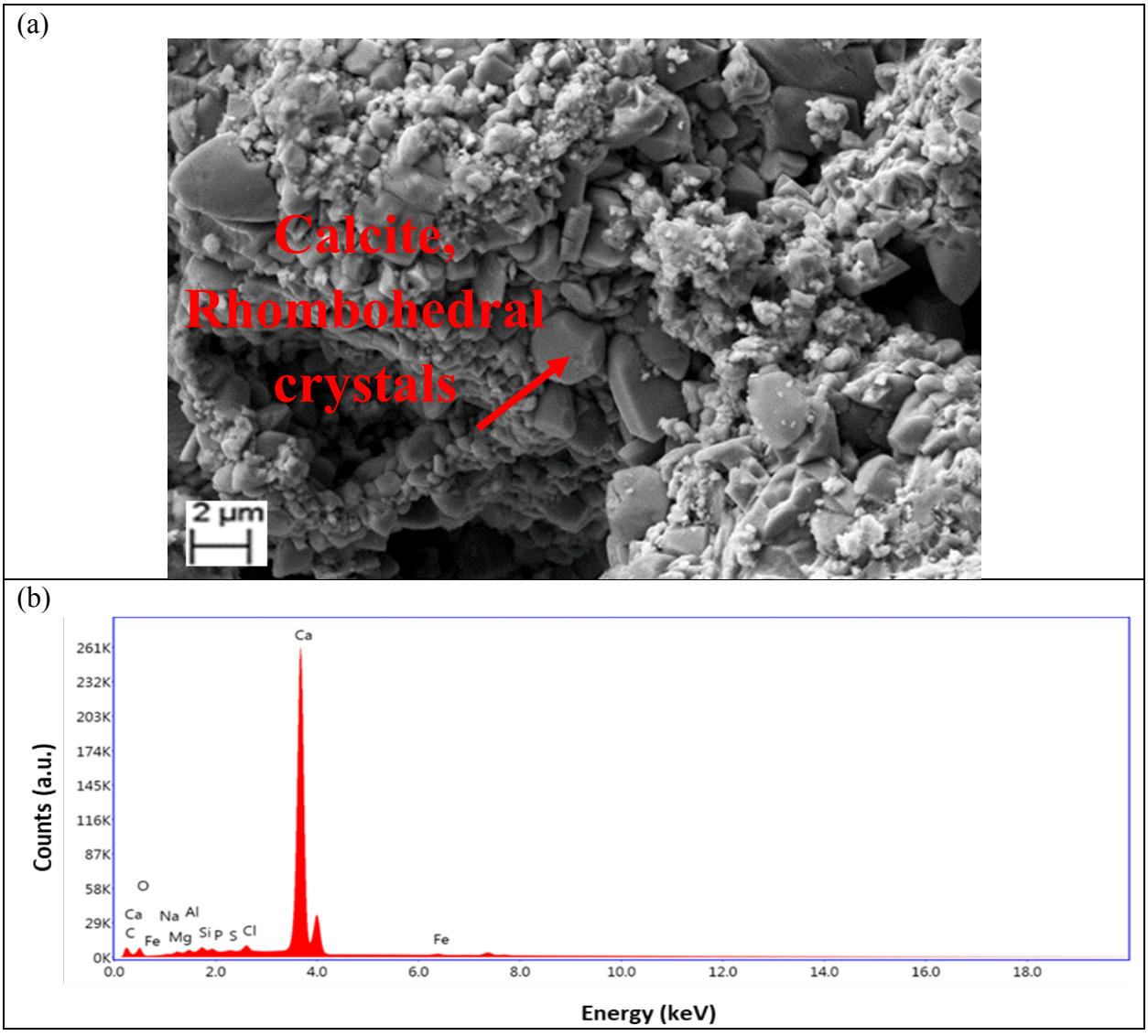

Figure 5.2.8 (a) SEM micrograph of freshly cut stone; (b) EDS analysis results.

Ca and O are the main constituents of limestone, so this was an expected result [11]. This finding from the EDS data is in agreement with XRD data obtained for this sample. The other elements are present only in relatively small quantities. Cl and Na are the main elements of sea salt, therefore small amounts of these present would be reasonably expected. In addition, Fe, Si and Mg are the impurities present in the limestone from sand grains, silt or mud. This material was eroded from nearby land and washed into the sea where it was then mixed with lime muds, shells and corals. The carbon present is due to the preparation of samples using a carbon coater, but may also be from burnt fuel pollutants in the atmosphere. S and P are present due to the atmospheric pollutants from the industrial activities around the site [12].

JOKHDAR HOUSE

The SEM micrograph from the sample showed crystal structures similar to the expected minerals - calcite, halite and gypsum. The morphology of natural halite is largely dominated by cubic forms, however when the crystals grow as a result of evaporation from aqueous solution, the perfection of the cube faces is usually lost. In contrast, the structure of gypsum (a monoclinic system) consists of layers of tetrahedra (Figure 5.2.9a) [5]. The EDS results identified (in order of descending atomic weight %): Ca, O, Si, S, Fe, Al, K, Cl, Na, Mg and C as shown in Figure 5.2.9b. The Ca and O are assigned to limestone and S attributed to the reaction between the $CaCO_3$ and SO_2, indicating that the stone had undergone attack by the pollutant and resulted in corrosion of the building's structural material. C was also found due to the carbon coater and deposition of hydrocarbon pollutants. Na and Cl are components in the stone due to the spray from the sea and their natural presence in limestones. This observation agreed with XRD results that were obtained from the same stone sample.

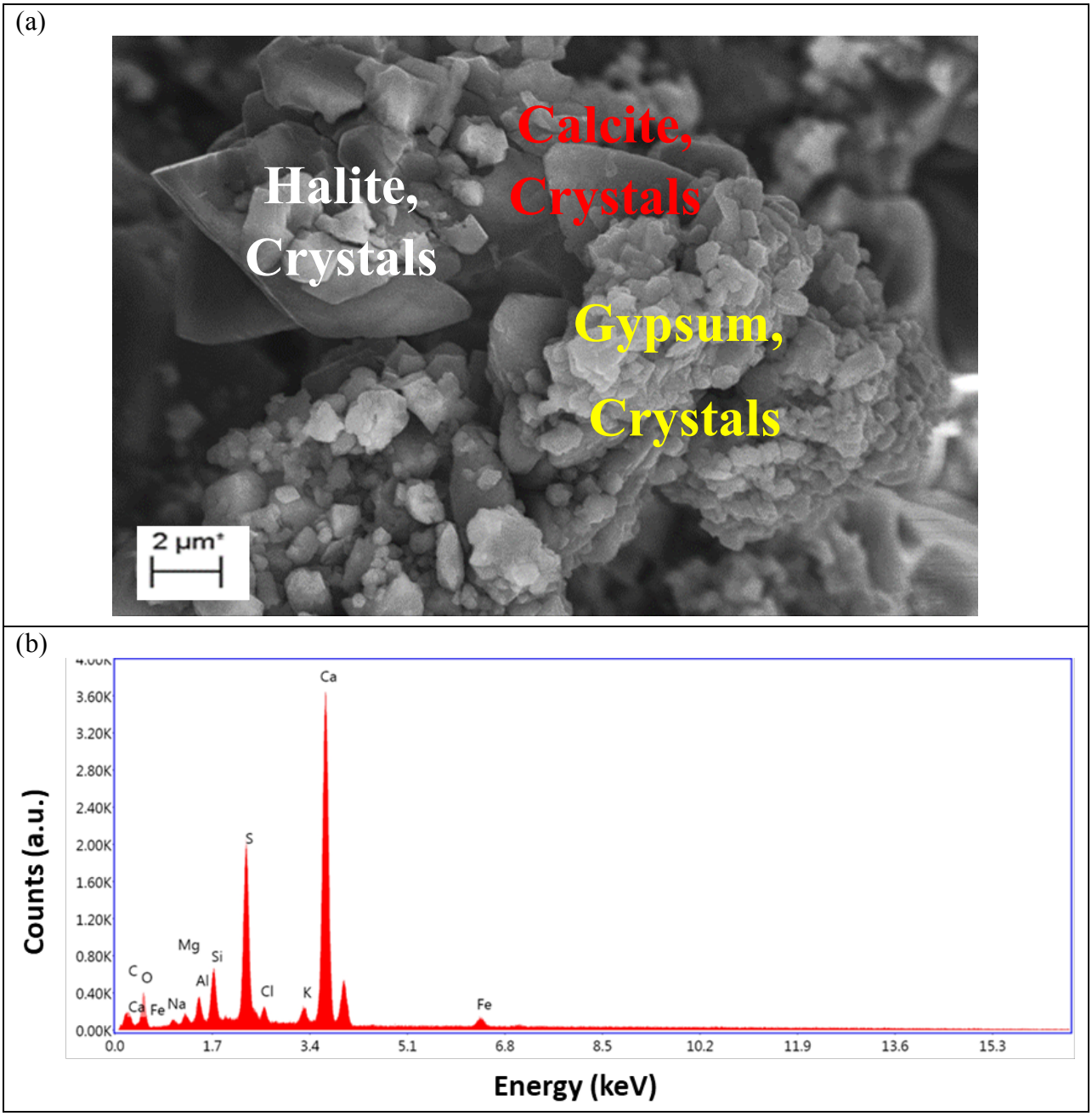

Figure 5.2.9 (a) SEM micrograph from the stone sample collected from Jokhdar house and; (b) EDS spectrum results.

JAMJOOM HOUSE

The SEM micrograph presented in Figure 5.2.10a well-formed crystal structures on the surface of the stone sample. These crystal forms were assigned to be mainly calcite and halite crystals, as with the other stone samples. EDS results identified Ca, O, C, Si, Al, Mg, K, Cl, Fe, Si and Na, in descending atomic weight percentage, as shown in Figure 5.2.10b. These are similar to the results to the other samples. It showed that the stone had undergone corrosion due to presence of S. The other elements making up the composition are expected to be observed with this kind of stone, as the calcite is often deposited from seawater with lime mud, clays and calciferous organisms.

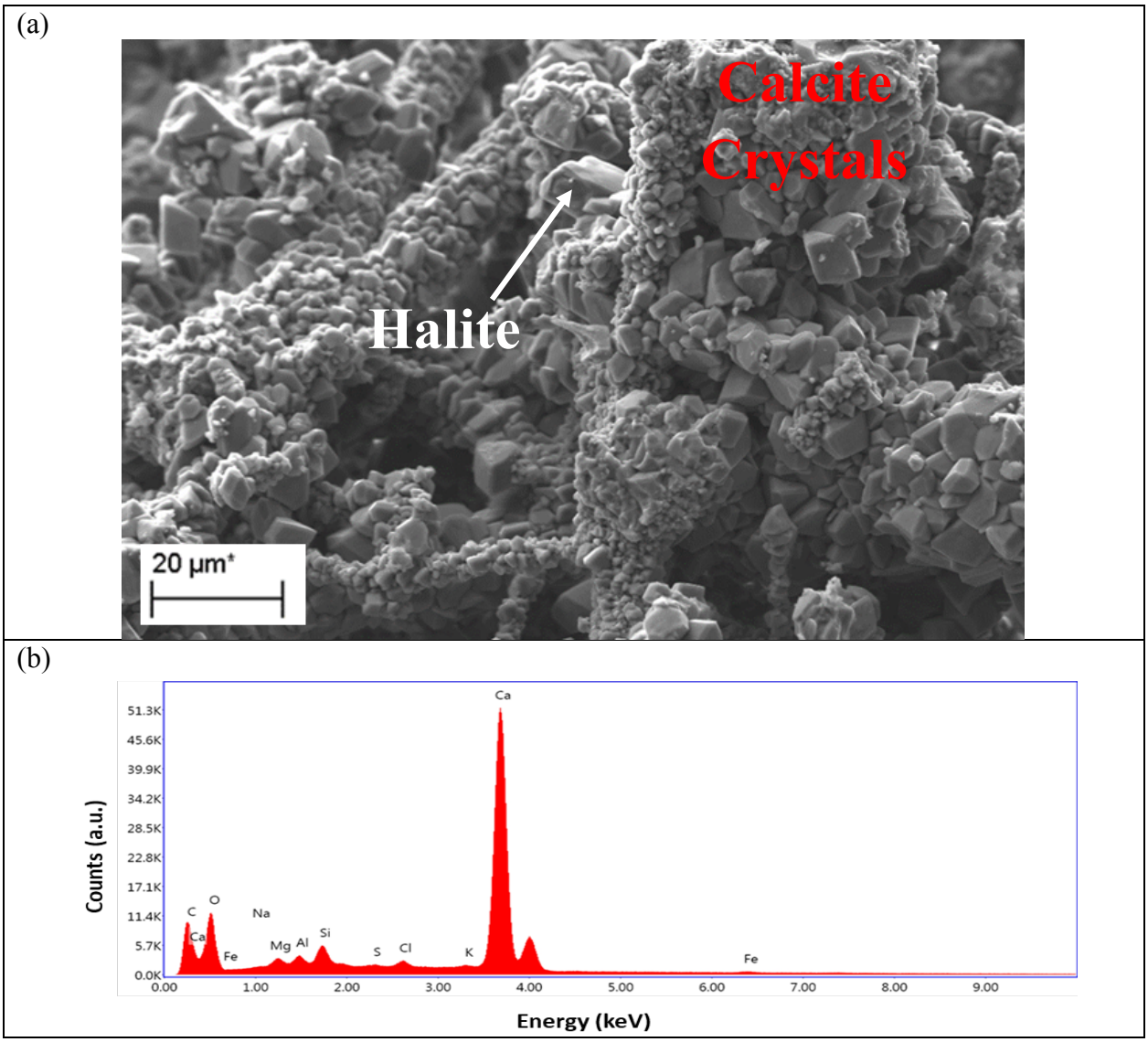

Figure 5.2.10 (a) SEM micrograph from the stone sample collected from Jamjoom house and; (b) EDS spectrum results.

BANAJA HOUSE

Secondary electron micrographs showed mainly calcite and quartz crystal structures formed on the Banaja house stone surface (Figure 5.2.11a). The EDS results identified (in order of descending atomic weight %): O, Ca, C, Si, Al, S, Mg, K, Na, Fe and Cl, as shown in Figure 5.2.11b. This finding is similar to the stone samples observed from Jamjoom and Jokhdar houses and is in agreement with XRD results from these stone samples.

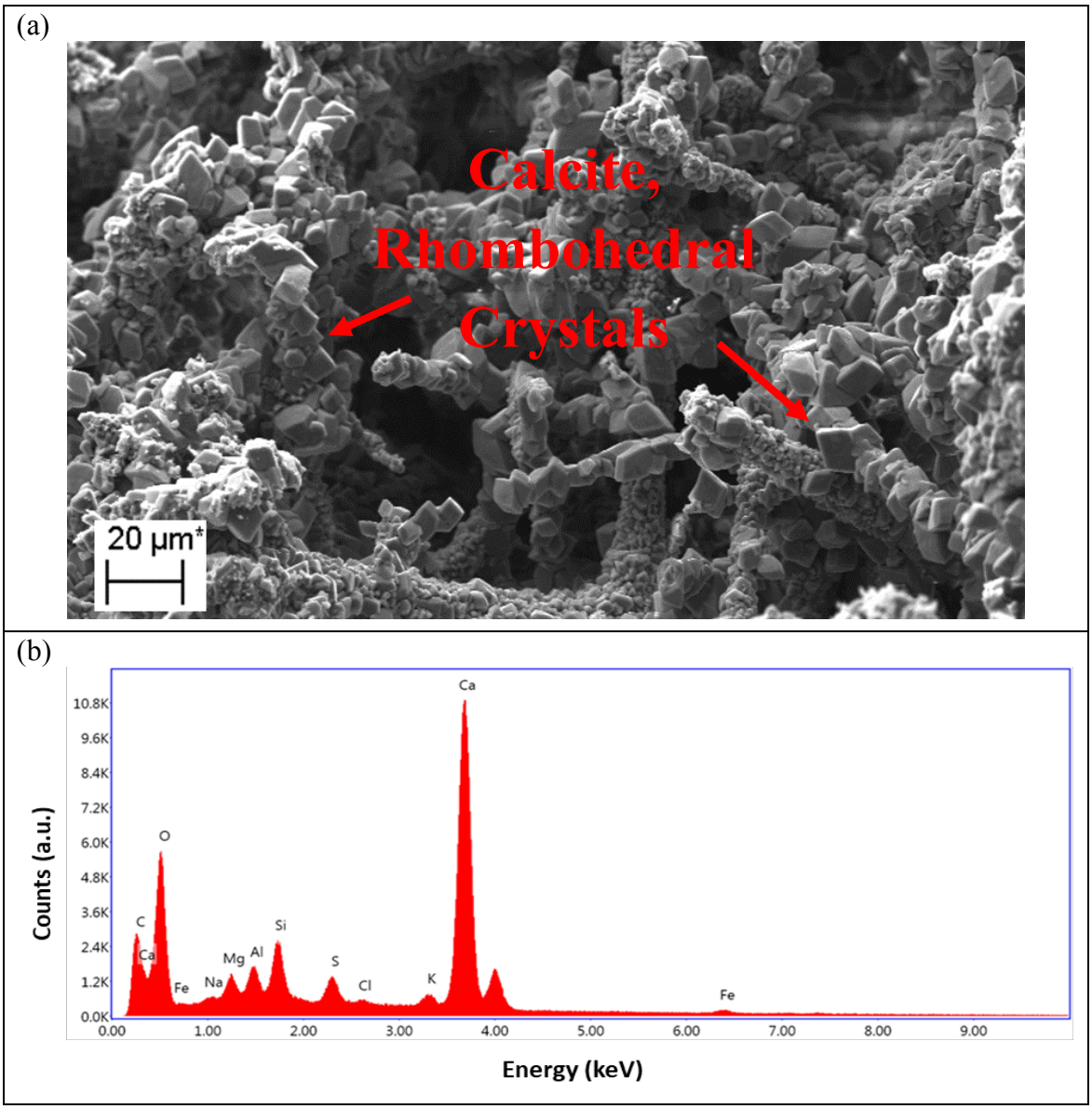

Figure 5.2.11 (a) SEM micrograph from the stone sample collected from Banaja house and (b) EDS spectrum results.

ALSALLUM HOUSE

Figure 5.2.12a is a secondary electron micrograph collected from the stone surface of the Alsallum house. The micrograph revealed similar crystal structures to the previous samples, although with a slightly different texture. These crystals are again attributed to calcite and halite. Figure 5.2.12b shows the EDS results which again identified a majority of Ca, C and O assigned to limestone.

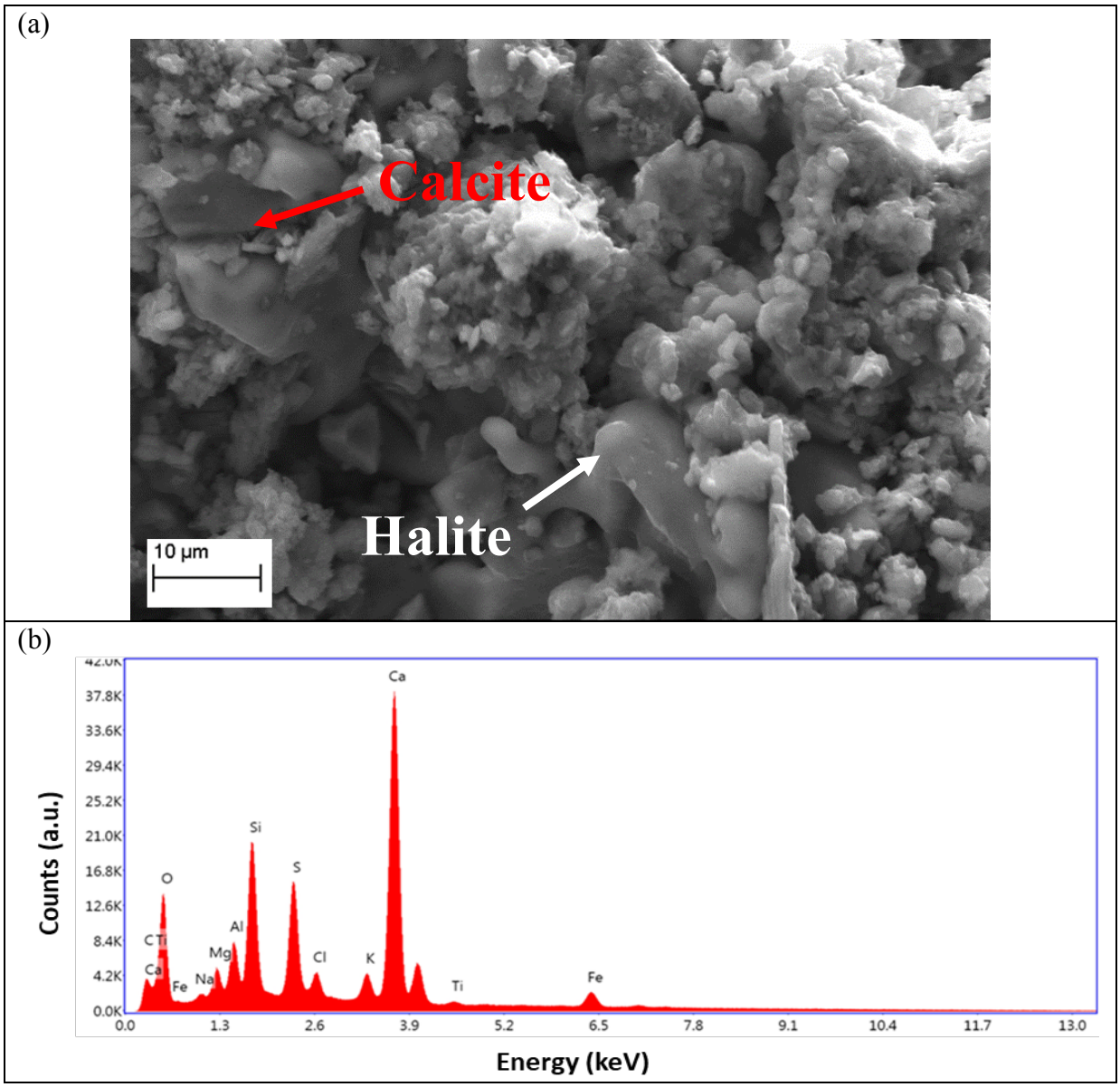

Figure 5.2.12 (a) SEM micrograph from the stone sample collected from Alsallum house and; (b) EDS spectrum results.

Na and Cl (salt) came from the sea. Si was also found to be deposited on the sample surface due to the sand around the site as well as its level as in impurity in limestones from the area. In addition, the EDS showed that the stone had undergone corrosion due to presence of S. Fe, Mg and Ti elements also were identified as trace natural components of these types of limestones. This finding is agreement with the XRD data obtained for this sample. Table 5.2.2 summarises the results of EDS elemental quantitative results obtained from the stone samples.

Table 5.2.2 Summary of the EDS elemental quantitative results identified in the stone samples.

Stone Samples	**Elements (Weight %)**											
	C	**O**	**Na**	**Mg**	**Al**	**Si**	**P**	**S**	**Cl**	**K**	**Ca**	**Fe**
Manqaba Quarry	11.71	31.38	0.99	0.44	0.35	0.61	0.05	0.04	0.62	-	53.68	0.13
Jokhdar House	0.01	33.86	1.05	0.76	1.92	3.86	-	14.01	1.25	1.48	39.76	2.05
Jamjoom House	10.49	36.12	0.03	0.64	0.72	1.53	-	0.06	0.58	0.60	49.64	0.16
Banaja House	8.28	45.16	0.31	1.30	1.74	2.99	-	1.51	0.22	1.02	37.17	0.31
Alsallum House	1.75	44.54	0.97	1.85	2.97	7.90	-	6.93	1.39	1.71	27.24	3.04

5.2.4 Laser Raman Spectroscopy Analysis

Raman spectra collected from the quarry and the four samples from the historical houses are shown in Figure 5.2.13. The spectrum obtained from the quarry specimen identified bands located at 282, 712, 1085 and 1356 cm^{-1}, these bands are assigned to calcium carbonate, calcite. The intense band (ν_1) of the calcite corresponds to the symmetric stretching of the CO_3 group at 1085 cm^{-1}, in addition, the ν_2 (symmetric bending) vibration mode, ν_3 (asymmetric stretching) mode and ν_4 (asymmetric bending) mode have notable peaks at 282 cm^{-1}, 1437 cm^{-1}, and 714 cm^{-1} respectively [13, 14].

Extra bands located at 449 and 465 cm^{-1} are attributed to NaCl, halite [15]. Similar spectra were collected from the Jokhdar, Jamjoom, Banaja and Alsallum houses, however they only identified calcite, as halite peaks were not visible above the background (Figure 5.2.13). As the laser depth of interaction was only a few nanometres from the surface, it was not possible to detect any other species, similar to the results obtained from XRD technique.

The findings showed confidently however that calcite was the main phase from all samples. The presence of calcite affirms that the main constituent of the historic structures in Jeddah is limestone. The halite observed in the spectra was indicative of evaporitic constituents in the limestone, suggesting sea origin, and is in agreement with the other characterisation techniques employed in this study (Table 5.2.13).

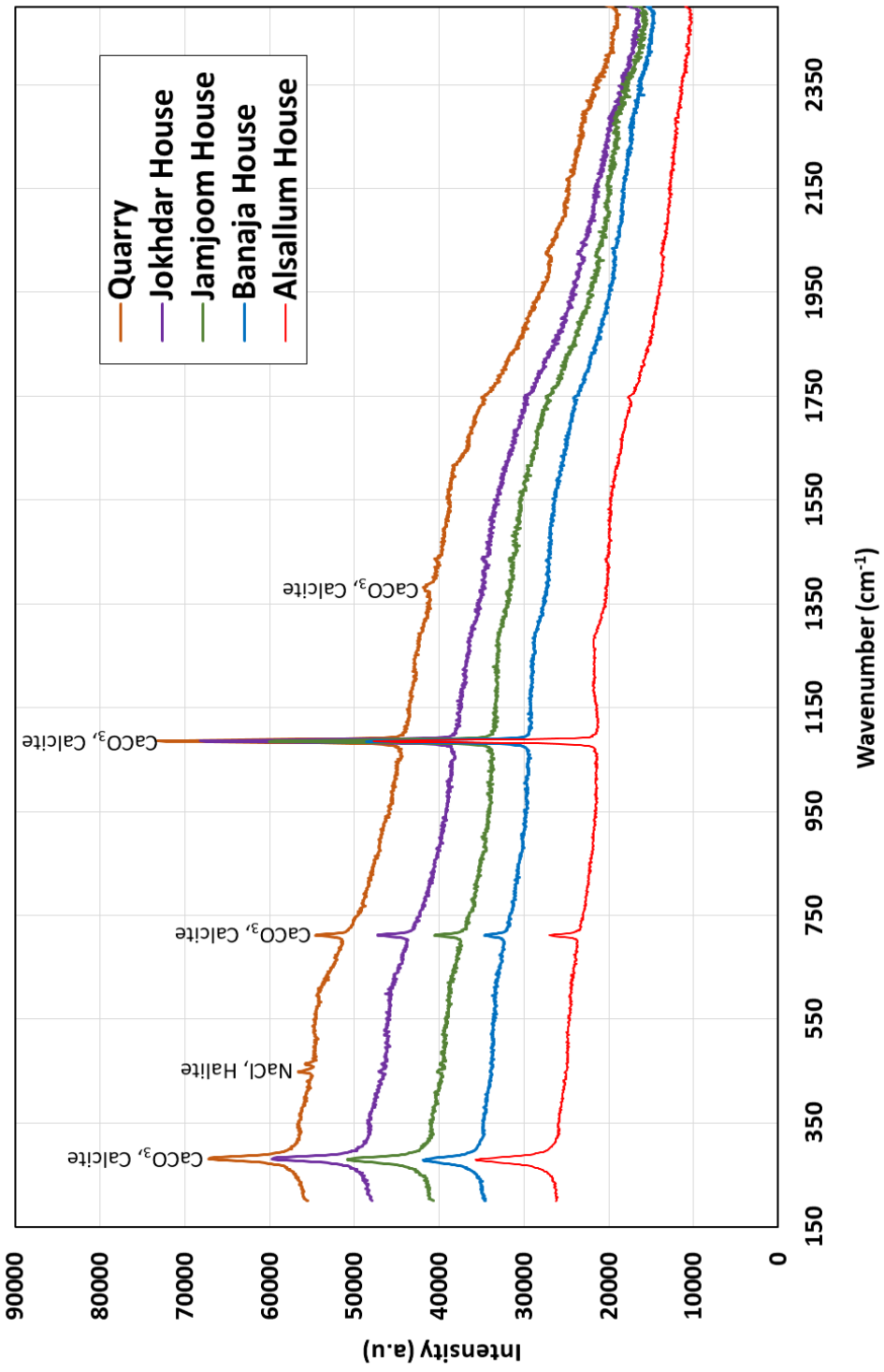

Figure 5.2.13 Raman spectra collected from the Jeddah stone samples.

Overall, the main result from characterisation of the stone materials from the quarry and the stone used to construct the houses confirms that the houses were made from limestone.

5.3 Mortar

The samples collected and their original locations are described in section 4.2.2. The results obtained from the mortar samples collected from five of the historical houses are discussed in this section.

5.3.1 Optical Microscope

Figure 5.3.1 is an optical micrograph obtained from openly exposed mortar surfaces from each of the houses.

The observations made from these micrographs revealed that the surface from Nawwar house contains a black deposit which can be formed from fossil fuel burning nearby, which is likely due to the industrial activities occurring across and around the site. Larger white crystals were also observed (see Figure 5.3.1a), while the Jamjoom and Jokhdar house images show some brownish colours in the matrix which can be assigned to very dense sand grains (Figures 5.3.1b, e). Shelly fragments are very clearly seen on the surface of the Banaja house sample, shown in Figure 5.3.1c. This optical micrograph of the Banaja house sample also demonstrates large sand (quartzitic and feldspathic) grains which are about 200μm in diameter. The sand grains probably came from the original limestone deposit, or were introduced as part of the mortar mixture (Figure 5.3.1d).

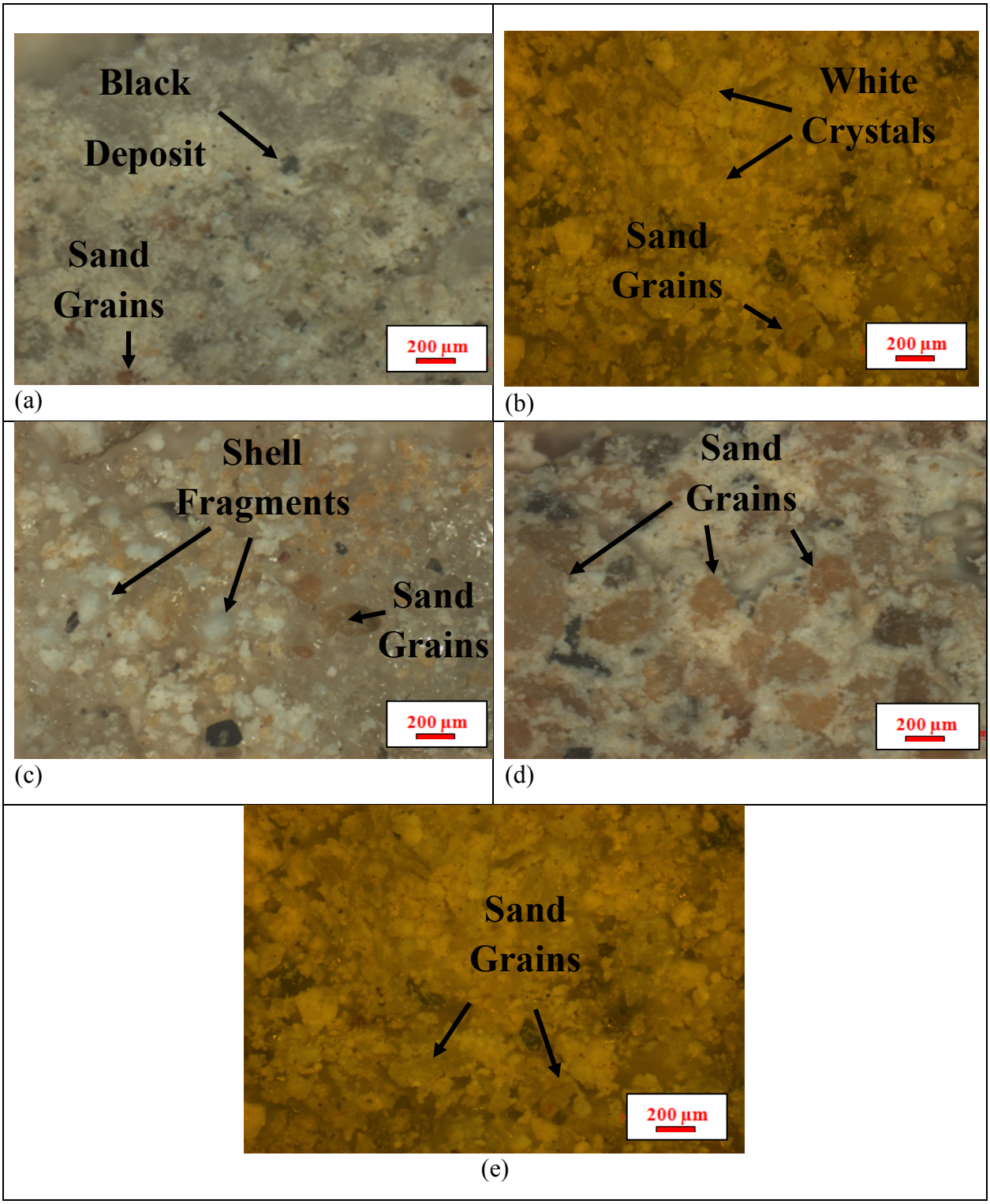

Figure 5.3.1 Optical images from the mortar samples: (a) Nawwar house north facade, (b) Jamjoom house west facade, (c) Banaja house west facade (internal), (d) Banaja house west facade (external) and (e) Jokhdar house south west facade.

5.3.2 X-Ray Diffraction Analysis

XRD identified the mineral phases in the mortar samples collected from the historical houses. This data is summarised in Table 5.3.1.

Table 5.3.1 Summary of the characteristic mineral phases identified in the historical house mortar samples.

Location	Compound
Original mortar from the external north facade of Nawwar house.	SiO_2 √ $KAlSi_3O_8$ $CaCO_3$ NaCl $CaSO_4.2H_2O$
Original mortar from the external west facade of Jamjoom house.	SiO_2 √ $CaCO_3$ NaCl
Original mortar from the indoor east facade of Banaja house.	NaCl √ $CaCO_3$ SiO_2
Original mortar from the external south facade of Banaja house.	SiO_2 √ $KAlSi_3O_8$ NaCl $CaCO_3$ $CaSO_4.2H_2O$
Original mortar from the external west facade of Jokhdar house.	NaCl √ SiO_2 $CaCO_3$ $CaSO_4.2H_2O$

NAWWAR HOUSE

XRD result obtained from the mortar sample collected from Nawwar house identified the phase of SiO_2 (quartz) as the major phase, but a small amount of halite was also observed. In addition, calcite was also identified. $KAlSi_3O_8$, orthoclase feldspar also observed. This mineral phase is a commonly called "potassium feldspar" or simply "K-spar." Orthoclase forms in igneous rocks such as granites, granodiorites and syenites, which weather to become common constituents of sand [16].

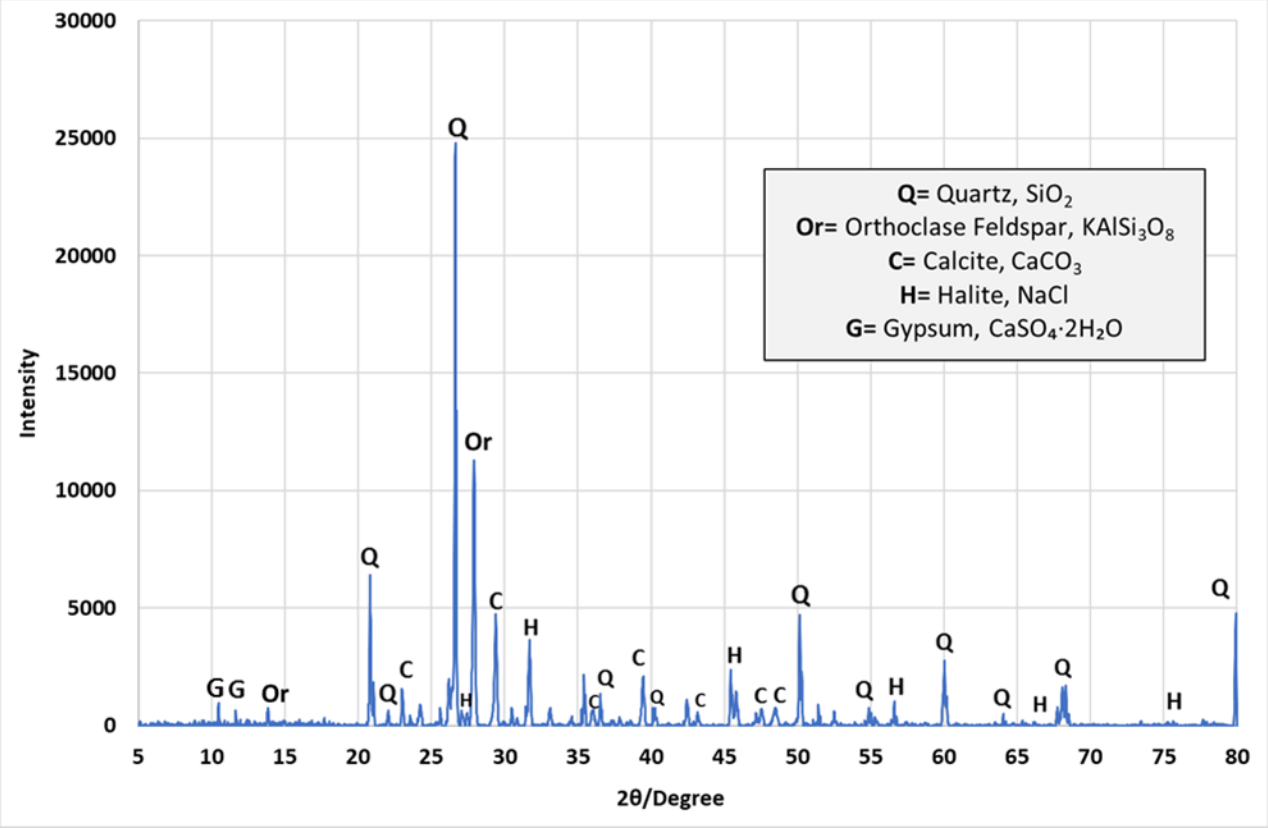

Figure 5.3.2 XRD pattern of the mortar sample collected from Nawwar house.

Small amounts of $CaSO_4.2H_2O$ (gypsum) were also detected. This is most probably due to the reaction between the $CaCO_3$ and SO_2 from emissions from the heavy traffic and industrial areas around the houses (Figure 5.3.2 and Table 5.3.1). The XRD confirmed the presence of quartz, halite and calcite as the main phases, confirming that the binder used to make these mortars was lime. There is no sign of any hydraulic mortar materials such as calcium silicate hydrate (C-S-H). The presence of quartz is attributed to the sand mixed with the mortar, indicating that the binder used to make this mortar is based on a non-hydraulic lime.

JAMJOOM HOUSE

Quartz, halite and calcite were the main mineral phases identified in the mortar sample from the Jamjoom house (Figure 5.3.3). An intense quartz peak was observed in this sample, this is a sign that there was a quartzitic sand used to make the lime base. These mineral phases are similar to the phases observed from Nawwar house.

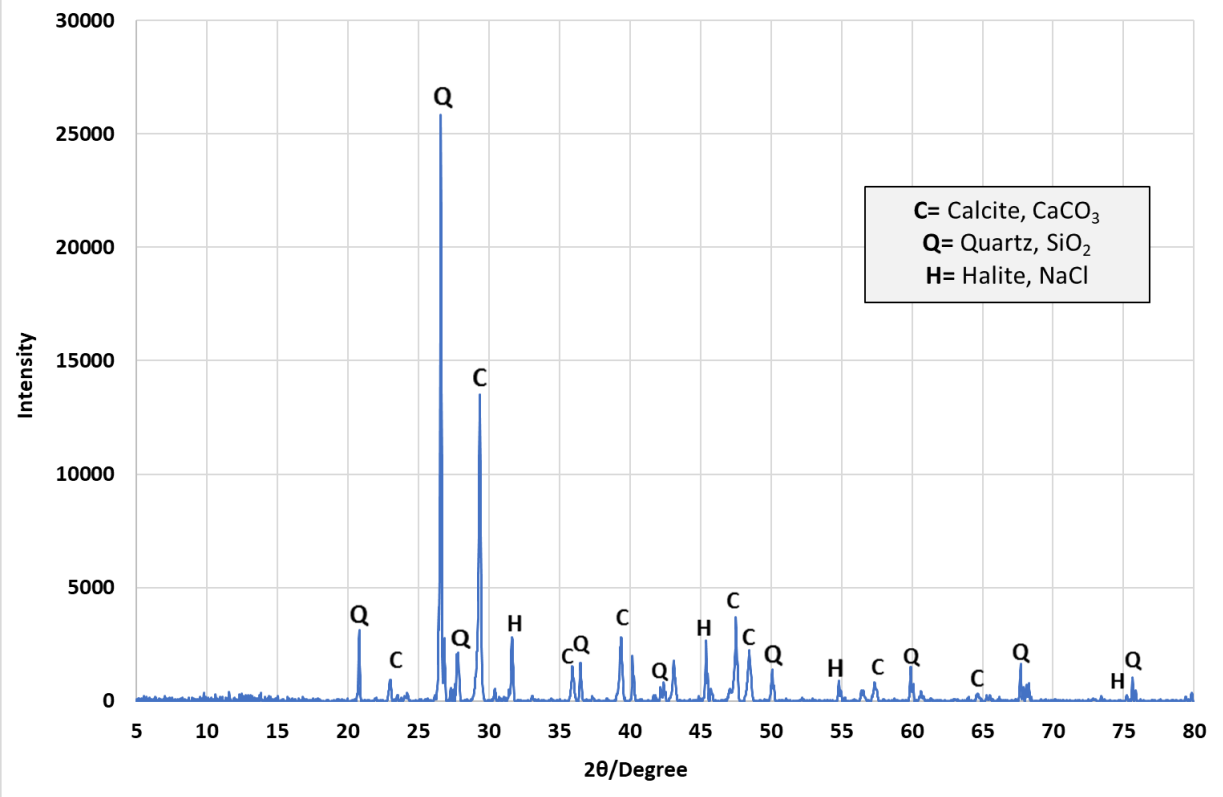

Figure 5.3.3 XRD pattern of the mortar sample collected from Jamjoom house.

BANAJA HOUSE (INTERNAL)

The XRD result from mortar sample collected from the internal face of Banaja house is shown in Figure 5.3.4. The result identified halite as a major phase. $CaCO_3$ and SiO_2 (calcite and quartz) were also identified, as with the other samples. The presence of calcite is attributed to seashell fragments mixed with the mortar to make the matrix stronger (as shown in optical micrograph Figure 5.3.1c). SiO_2 is from the sand and NaCl from the evaporation of sea salt. In comparison with the Nawwar and Jamjoom house samples, a strong halite peak was clearly identified. This could be due to the location of the house, which is facing a marine environment, and therefore receives a greater amount of sea spray, causing repeated wetting and dryness cycles, and a greater amount of salt deposition, ultimately causing damage to the building materials.

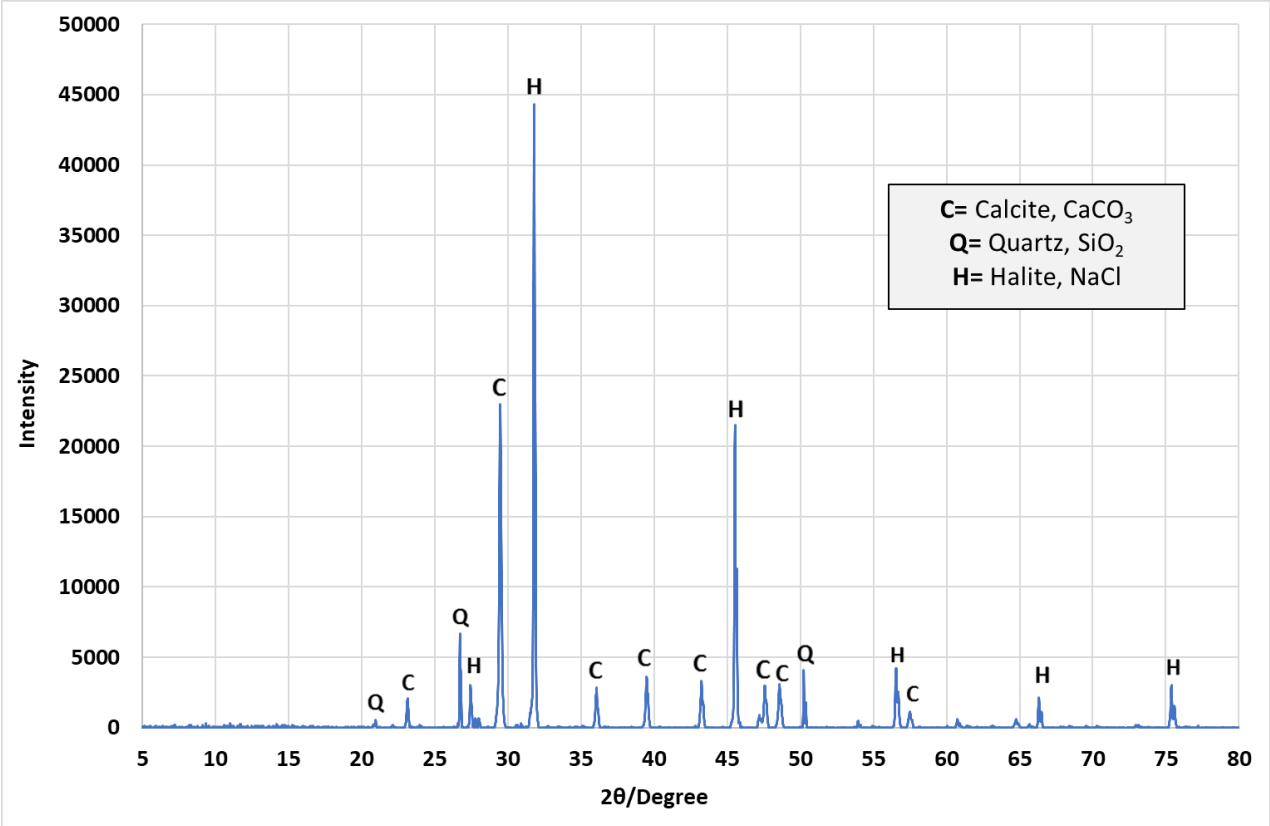

Figure 5.3.4 XRD pattern of the mortar sample collected from Banaja house (internal).

BANAJA HOUSE (EXTERNAL)

Figure 5.3.5 shows the XRD diffraction pattern collected from the external face of Banaja house. The diffraction pattern identified SiO_2 (quartz) as with the other mortars, and $AlKAlSi_3O_8$ (orthoclase feldspar). These phases are attributed to the sand mixed with the mortar. The finding is in agreement with the observation from the optical microscope which showed large (>200µm diameter) grains of sands on the surface of the sample. Halite, calcite and gypsum were also identified. The phases observed were similar compared to the results obtained from Nawwar house.

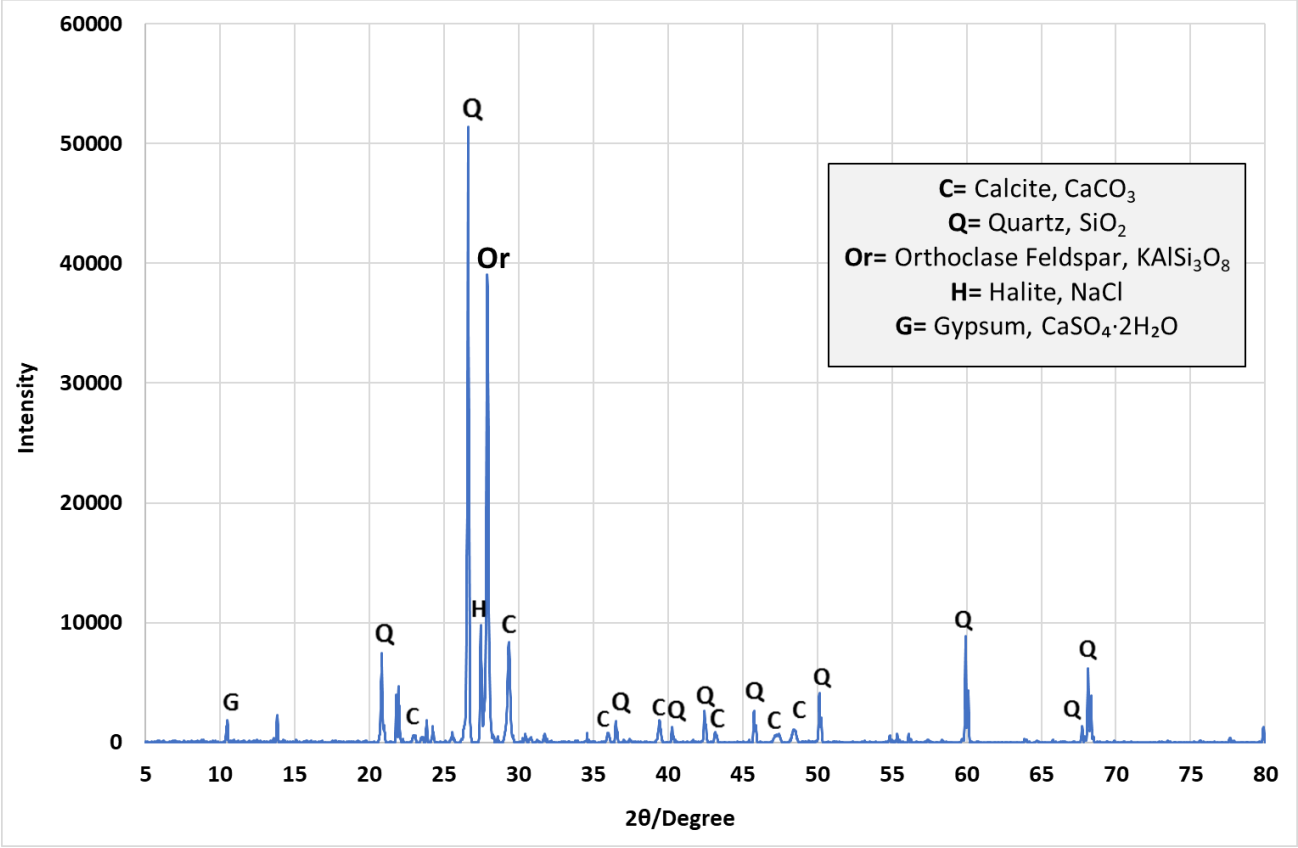

Figure 5.3.5 XRD pattern of the mortar sample collected from Banaja house (external).

JOKHDAR HOUSE

The XRD result for the mortar sample collected from Jokhdar house shown in Figure 5.3.6. Halite was a major phase observed, but quartz, calcite and gypsum were also identified. A strong halite peak is again attributed to the salty sea spray, as the house is close to the shore, just like Banaja house. The quartz peak observed can be attributed to the sand mixture in the mortar as clearly seen in the corresponding optical micrograph (Figure 5.3.1e). This result is similar to the results obtained from the samples collected from Banaja (external) and Nawwar houses.

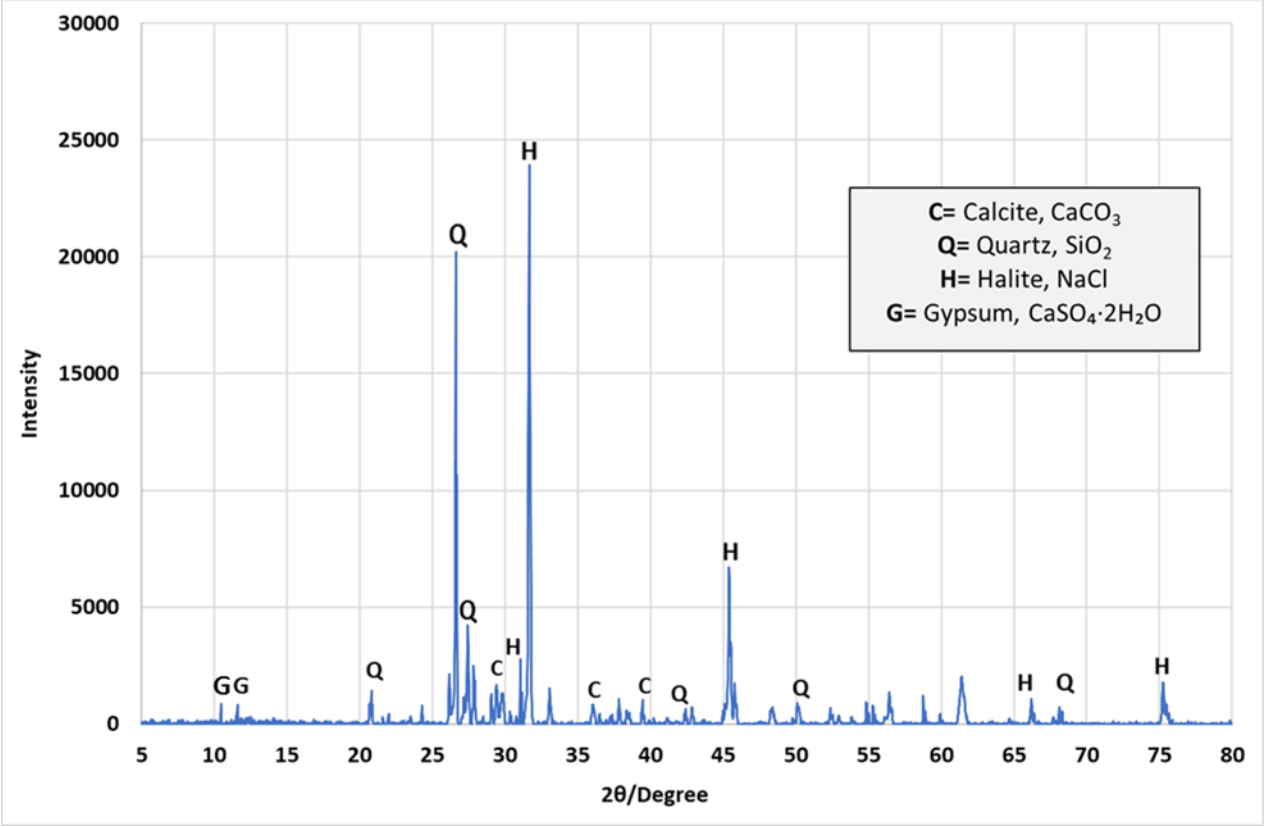

Figure 5.3.6 XRD pattern of the mortar sample collected from Jokhdar house (external).

5.3.3 SEM-EDS Analysis

NAWWAR HOUSE

Figure 5.3.7a is the SEM micrograph obtained from the mortar sample collected from Nawwar house, and here the microstructure reveals the structure of the quartz and calcite crystals in the matrix. The EDS spectrum identified: O, Si, Ca, Al, Na, Mg, K, Fe, Cl, C and S (in order of descending atomic weight %). The spectrum is shown in Figure 5.3.7b.

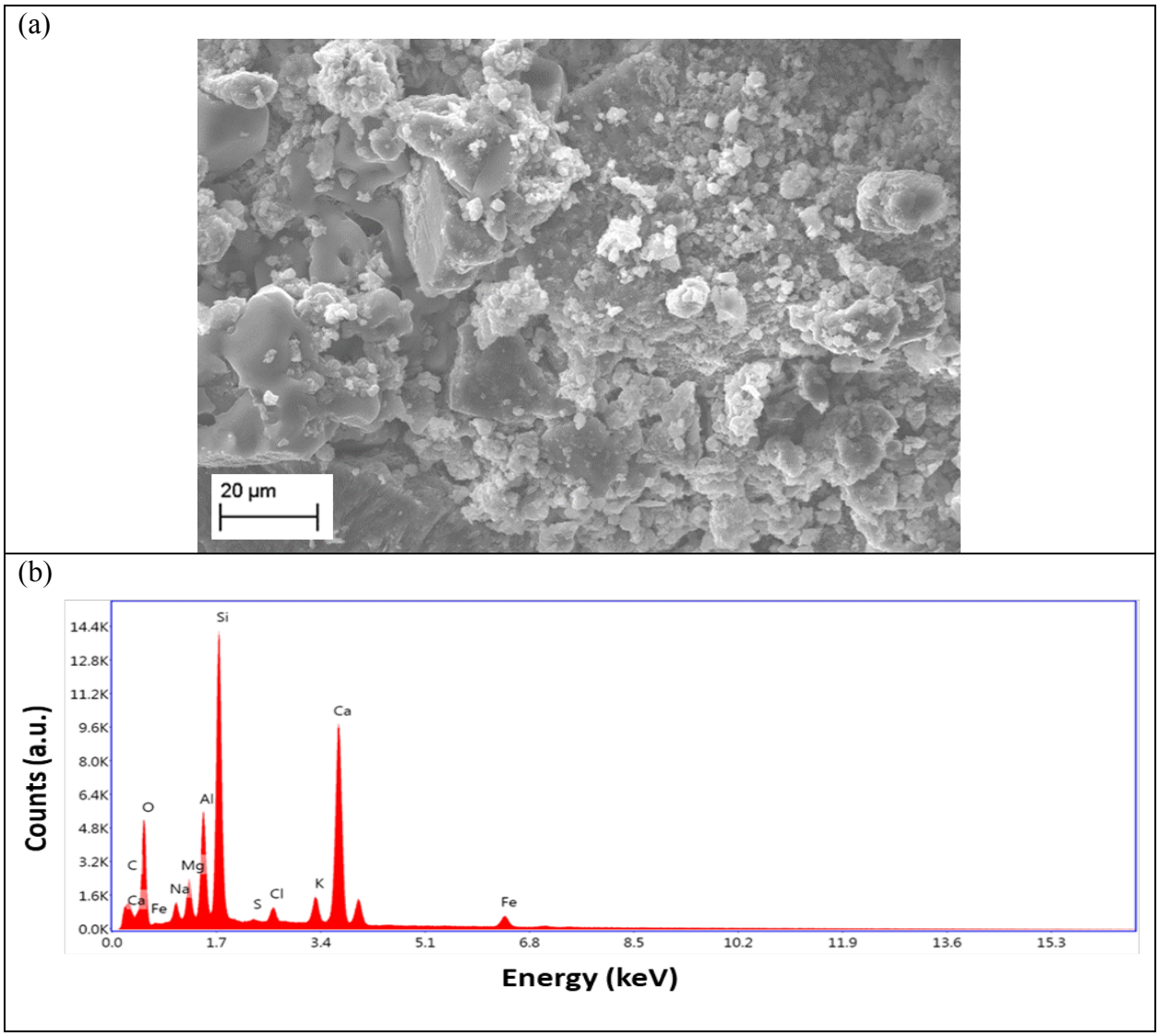

Figure 5.3.7 (a) SEM micrograph from the mortar sample collected from Nawwar house and (b) EDS spectrum results.

JAMJOOM HOUSE

The surface of this sample revealed structures akin to quartz as SEM micrograph showed in Figure 5.3.8a. The mortar has a compact microstructure with aggregates well-embedded in the matrix. It was possible to identify aggregate fragments like quartz, micas and feldspars. Large areas of the surface and pores were filled with well-defined calcite crystals formed possibly by a carbonate dissolution/recrystallisation process of the binder [17]. The EDS results identified (in order of decreasing atomic weight % in the sample): O, Si, Ca, Al, Na, Mg, Cl, Fe, K, S, Ti, and P, as shown in Figure 5.3.8b.

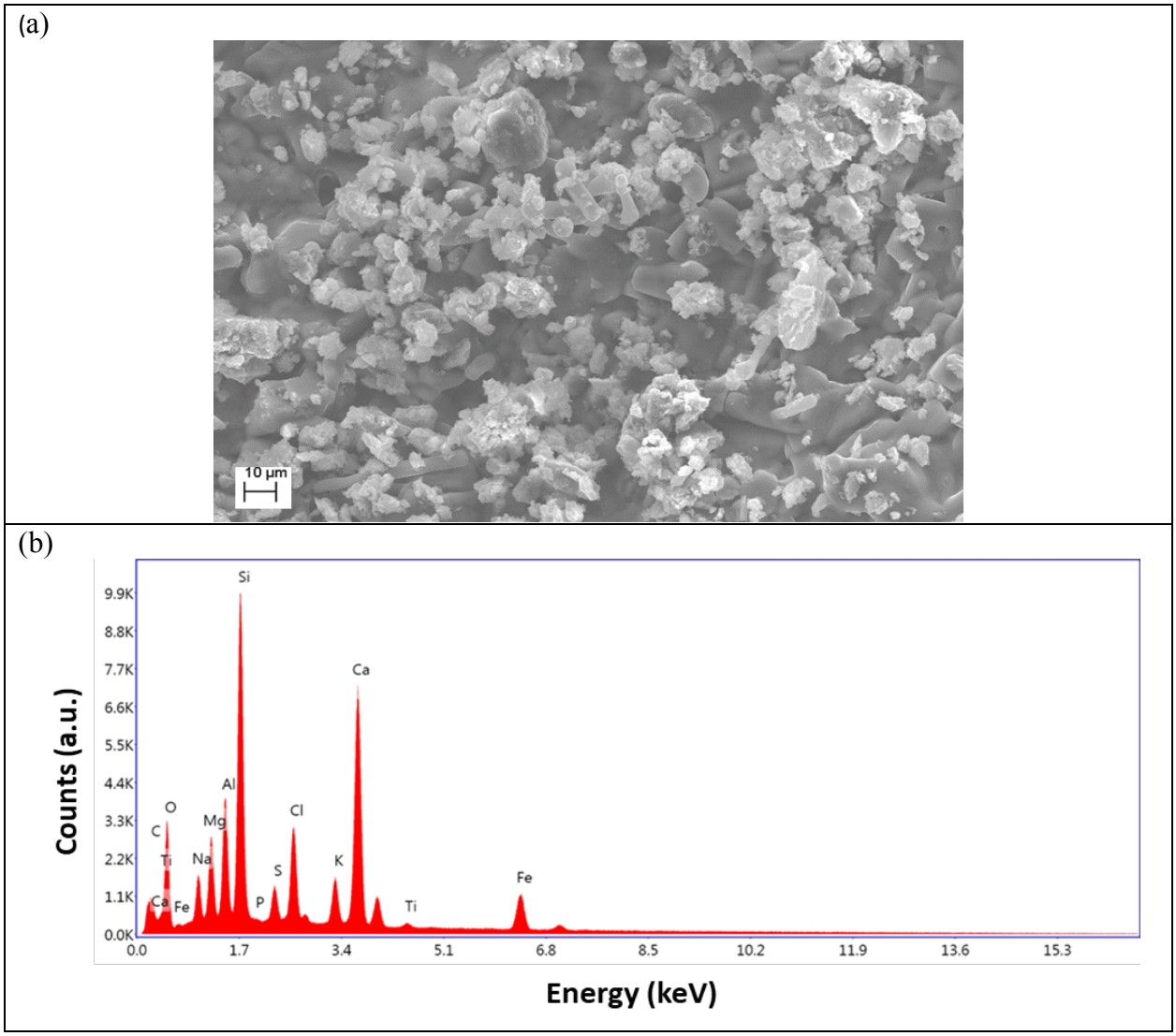

Figure 5.3.8 (a) SEM micrograph from the mortar sample collected from Jamjoom house and (b) EDS spectrum results.

BANAJA HOUSE (INTERNAL)

The surface of the internal Banaja house mortar sample was rich in rhombohedral crystal structures (calcite) as the SEM micrograph shows in Figure 5.3.9a. The EDS results identified: O, Cl, Na, Ca, C, Si, Al, Fe, Mg, K, Si and Ti, in decreasing atomic weight %, as shown in Figure 5.3.9b.

(a)

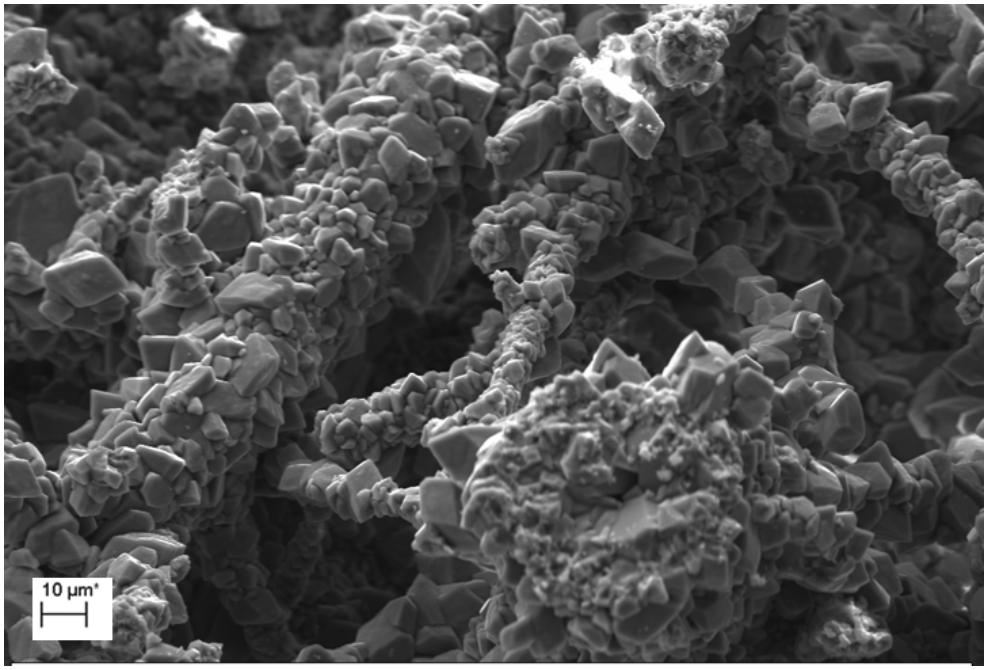

(b)

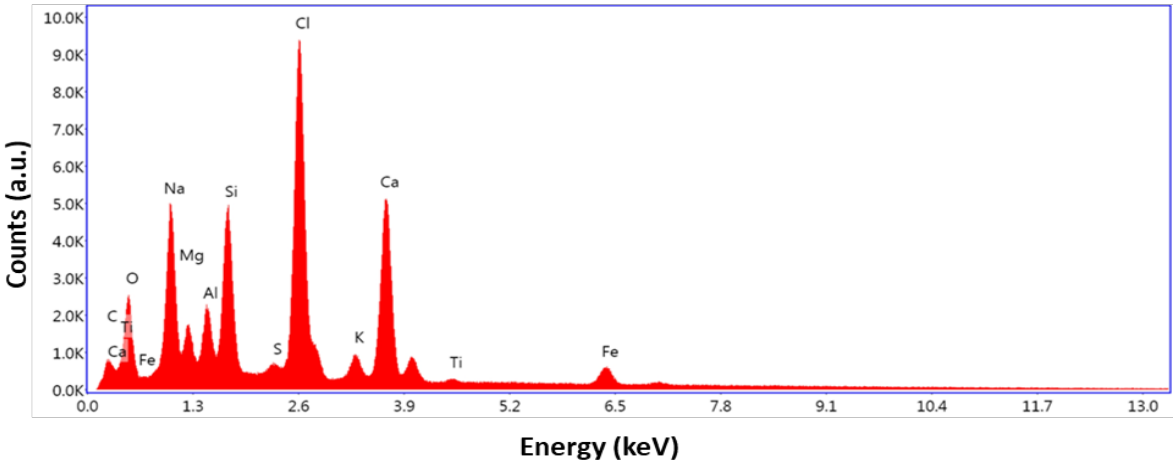

Figure 5.3.9 (a) SEM micrograph from the mortar sample collected from Banaja house from its internal facade and (b) EDS spectrum results.

A large amount of Na and Cl was revealed due to a large amount of evaporation of sea spray. Ca and O being present in large quantities is a clear sign that the mortar was lime-based. In addition, Si was also identified, showing the lime was mixed with sand. This observation is similar to the XRD phases identified in Figure 5.3.4. A small amount of S was observed which can be regarded as being a byproduct of the reaction between $CaCO_3$ and atmospheric SO_2, or possibly because anhydrite was present.

BANAJA HOUSE (EXTERNAL)

The scanning electron micrograph from the external facade of Banaja house sample had quite a different overall texture but still showed that the stone contains crystals with calcite and quartz-like appearances. The calcite structure is aragonitic (orthorhombic), filling the pore spaces within the mortar sample (Figure 5.3.10a) [18]. EDS analysis from the surface revealed the elements: Ca, O, Si, C, Cl, Fe, Al, K, Na and Mg in order of descending atomic weight % (Figure 5.3.10b). Ca and O are the main constituents of lime-based mortars. Si was embedded in the matrix, supporting the idea that sand was used as an aggregate in the mortar mixture. It was possible to identify aggregate fragments like quartz and feldspars in the sample. Na and Cl were again present due to sea salt from the marine environment and again a small amount of S was also observed. These are in a good agreement with the XRD results obtained.

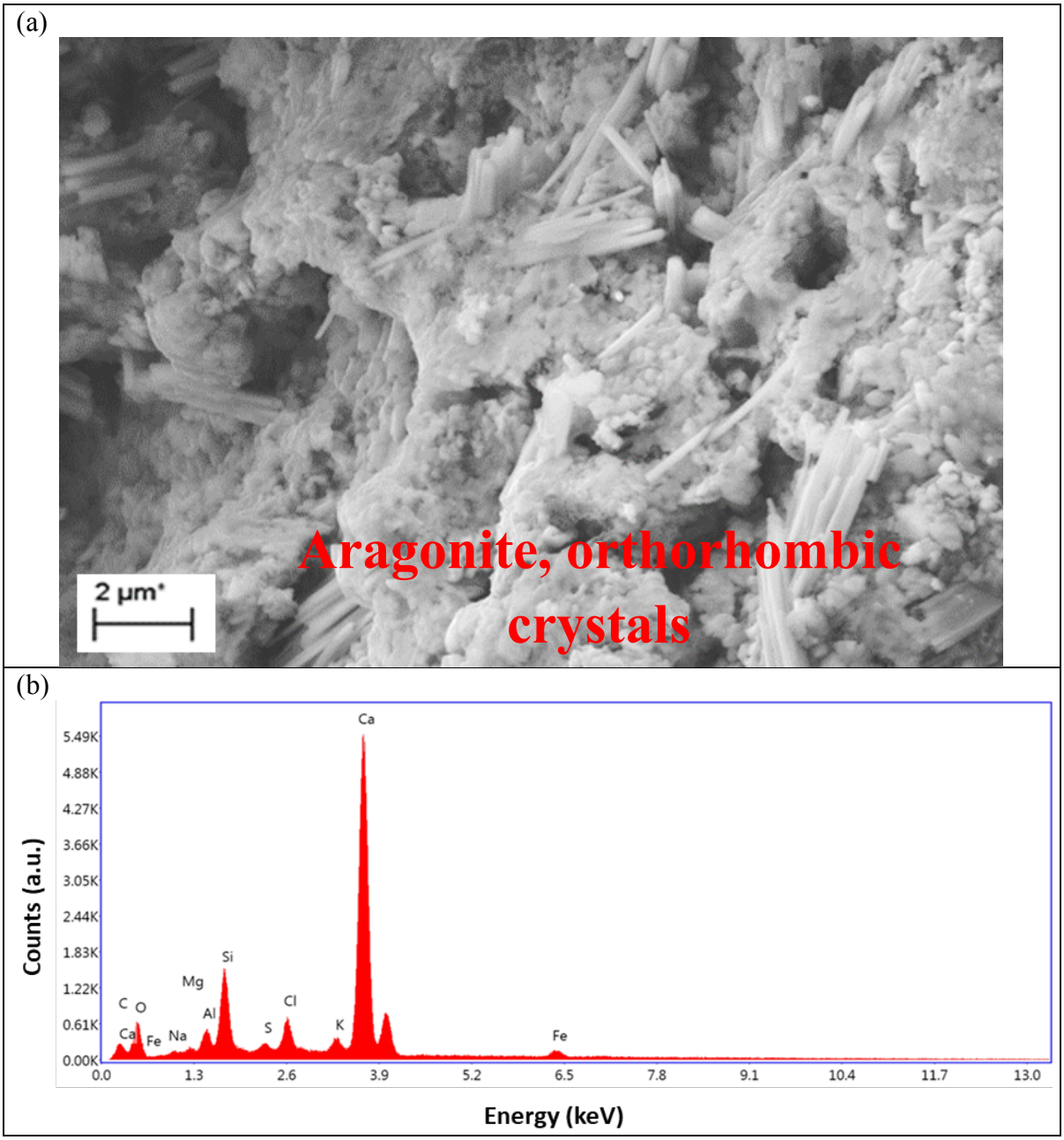

Figure 5.3.10 (a) SEM micrograph from the mortar sample collected from Banaja house from its external facade and (b) EDS spectrum results.

JOKHDAR HOUSE

Figure 5.3.11(a) represents the SEM micrograph obtained from the surface of mortar sample collected from Jokhdar house. The surface contains a large amount of halite deposited on the surface. The EDs spectrum identified O, Cl, Na, Ca, C, Si, Al, Fe, Mg, K, Si and Ti as shown in Figure 5.3.11b.

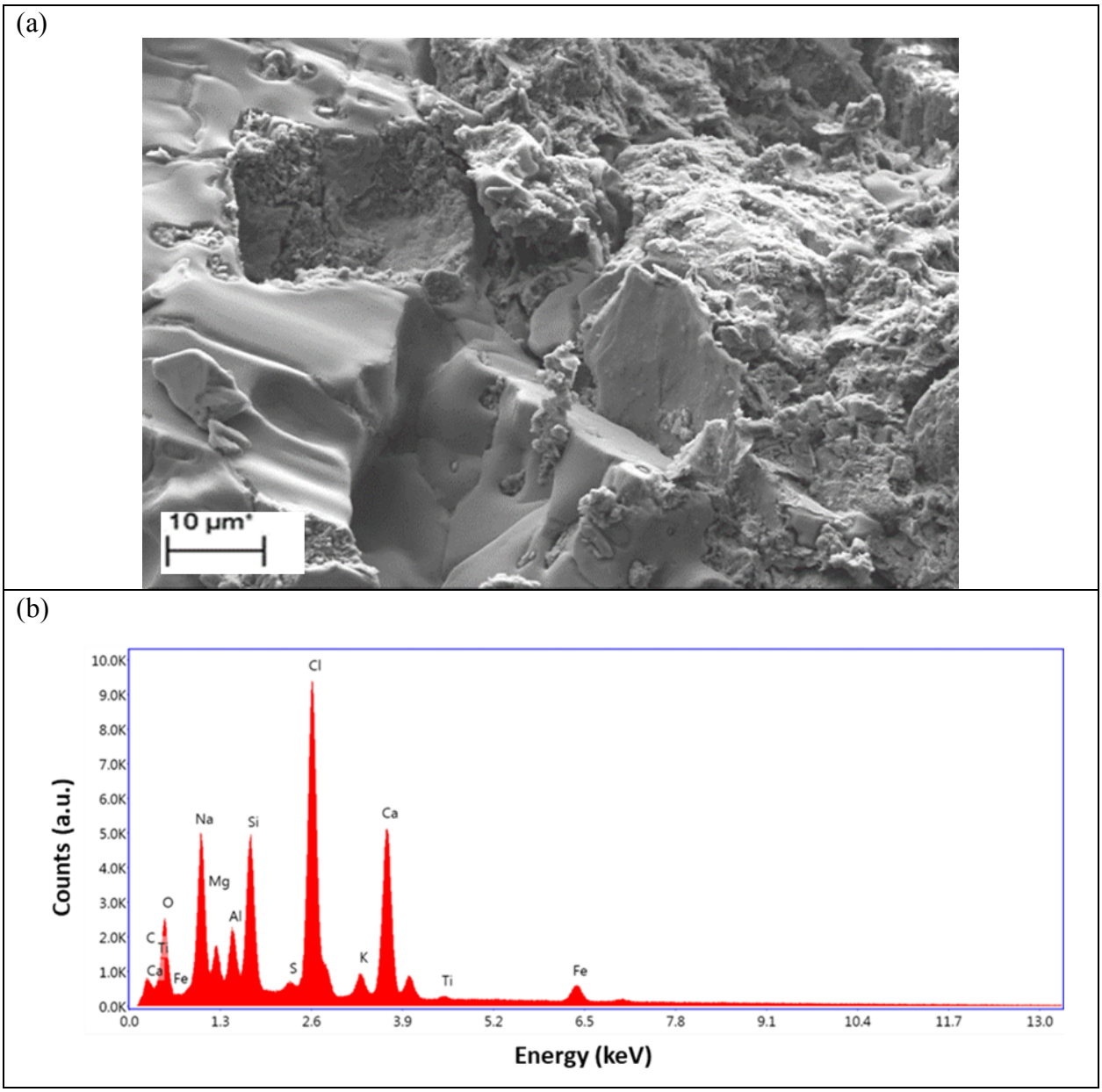

Figure 5.3.11 (a) SEM micrograph from the mortar sample collected from Jokhdar house and (b) EDS spectrum results.

The presence of Na and Cl again confirmed the presence of salt, primarily from the sea. Ca and O indicate the lime-based mortar mixture, and Si was also present from the sand used as an aggregate. These results are, with the rest of the house samples, in agreement with the XRD spectra obtained for each sample, as shown in Figure 5.3.6.

Generally, the EDS analyses from the mortar samples collected revealed that sulphur, and sodium chloride were the main atmospheric pollutants. EDS elemental quantitative results in the mortar samples summarised in Table 5.3.2.

Table 5.3.2 Summary of the EDS elemental quantitative identified in mortar samples.

Mortar Samples	Elements (Weight %)												
	C	**O**	**Na**	**Mg**	**Al**	**Si**	**P**	**S**	**Cl**	**K**	**Ca**	**Ti**	**Fe**
Nawwar House	0.59	43.12	4.08	3.92	7.98	18.46	-	0.32	1.06	1.92	16.85	-	1.70
Jamjoom House	-	34.97	6.20	5.90	7.15	16.64	0.08	1.77	5.00	2.31	15.37	0.12	4.49
Banaja House (Internal)	12.74	24.63	14.43	2.78	3.12	7.10	-	0.50	16.80	1.51	13.49	0.12	2.79
Banaja House (External)	3.29	34.82	0.51	0.17	1.72	6.59	-	0.54	2.90	1.59	45.66	-	2.21
Jokhdar House	12.74	24.43	14.43	2.78	3.12	7.16	-	0.60	16.40	1.61	18.49	0.12	2.79

5.3.4 Laser Raman Spectroscopy Analysis

Raman spectra of the five mortar samples collected from the different houses are shown in Figure 5.3.12. The spectrum from Nawwar house identified calcite bands located at 1085 cm^{-1} and quartz located at 464 cm^{-1}. Small amounts of calcite and orthoclase feldspar had peaks at 514 cm^{-1} in the spectra from the mortar collected from within Jokhdar house [19]. Raman results from the internal wall and external wall of Banaja house showed the presence of calcite bands located at 280, 712 and 1084 cm^{-1}, a quartz band at 464 cm^{-1} and a less intense peak of gypsum located at 1010 cm^{-1} [20]. The spectrum obtained from Jamjoom house sample only identified a calcite band (located at 1084 cm^{-1}).

The results indicate that calcite was the main phase from all samples. The presence of calcite confirms that a lime-based mortar was used to construct the houses. Quartz observed from the spectra was indicated to be from the sand mixed with mortar samples, in addition an orthoclase feldspar band was observed due to the slightly feldspathic nature of the sand used. The existence of gypsum in the Banaja house sample, indicative of the degradation of the mortar, is thought to be present because of the reaction between the limestone ($CaCO_3$) and the atmospheric pollutant, SO_2.

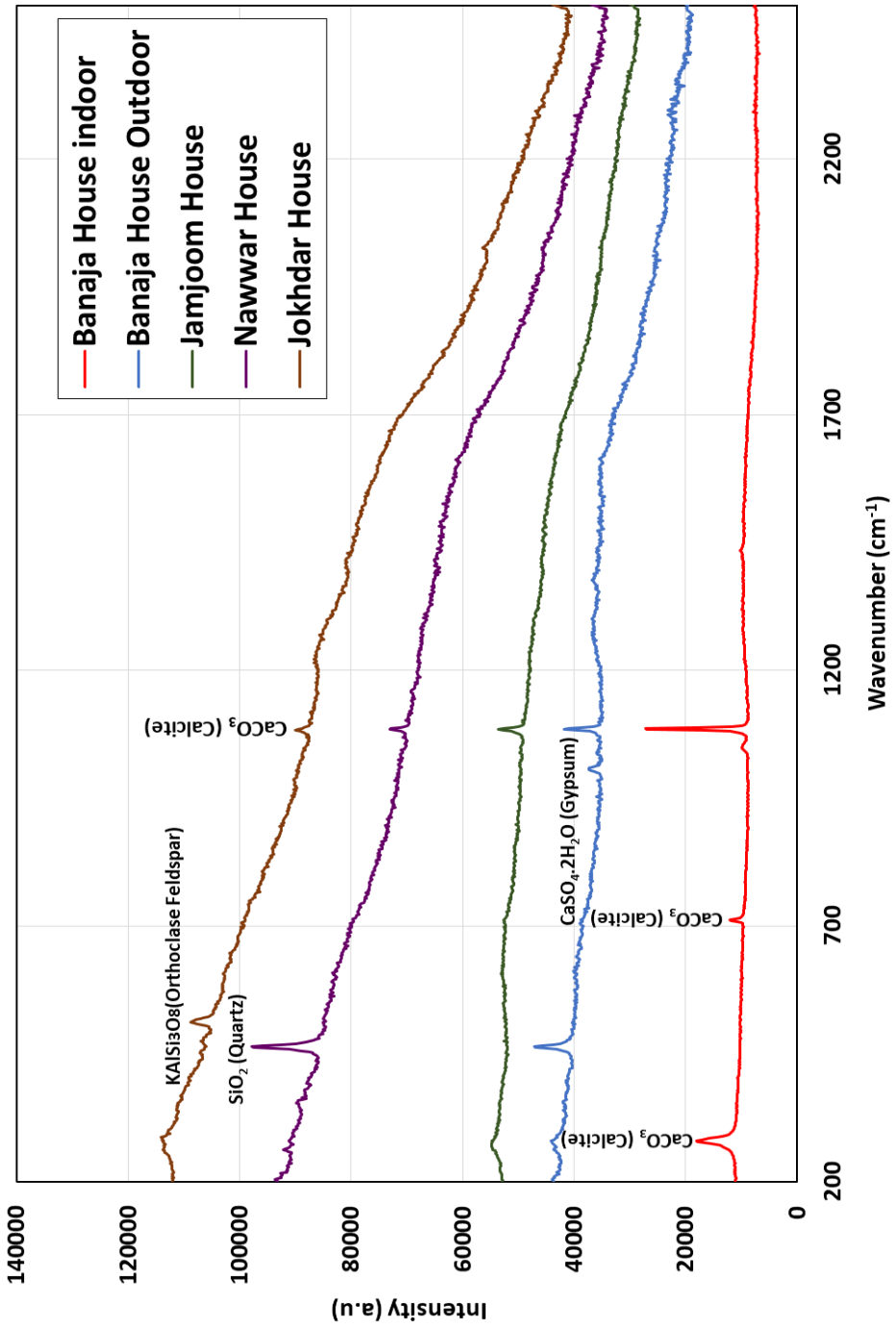

Figure 5.3.12 LR spectra collected from mortar samples for the five houses.

Overall, the mortar samples collected from the five houses showed that they were constructed from mainly non-hydraulic lime, based on the mixes of minerals identified and suggested composition from the combined LR and XRD spectra. The results showed that the mortar had undergone corrosion due to presence of salt and SO_2.

5.4 Plaster

The results obtained from each plaster sample collected from four houses (Jokhdar – west and east facades, Alturkey, Jamjoom, Nawwar) are presented in the following section.

5.4.1 Optical Micrographs

By examining the surface of the corresponding specimens under the optical microscope, it was confirmed that the plaster surfaces consist of a mixture of a white mineral structure, fine sand, green paint, black deposites (Figure 5.4.1). The presence of the black deposit may indicate that the components experienced corrosion due to atmospheric pollution.

The observations made from these micrographs revealed that the plaster surfaces collected from Jokhdar house (west) consisted mainly of a shiny white crystal (Figure 5.4.1a). The dark colour and very dense sand grains were also observed on the surfaces of the Jamjoom and Alturkey house samples, as shown in Figure 5.4.1b and c. This is probably due to a seashell component added to the plaster mixture. In contrast, the exposed plaster surface from Jokhdar house (east) contained dense sand grains and a dark deposit which can be assigned to fossil-fuel burning and emissions from traffic congestion and industrial activities around the site (Figure 5.4.1e).

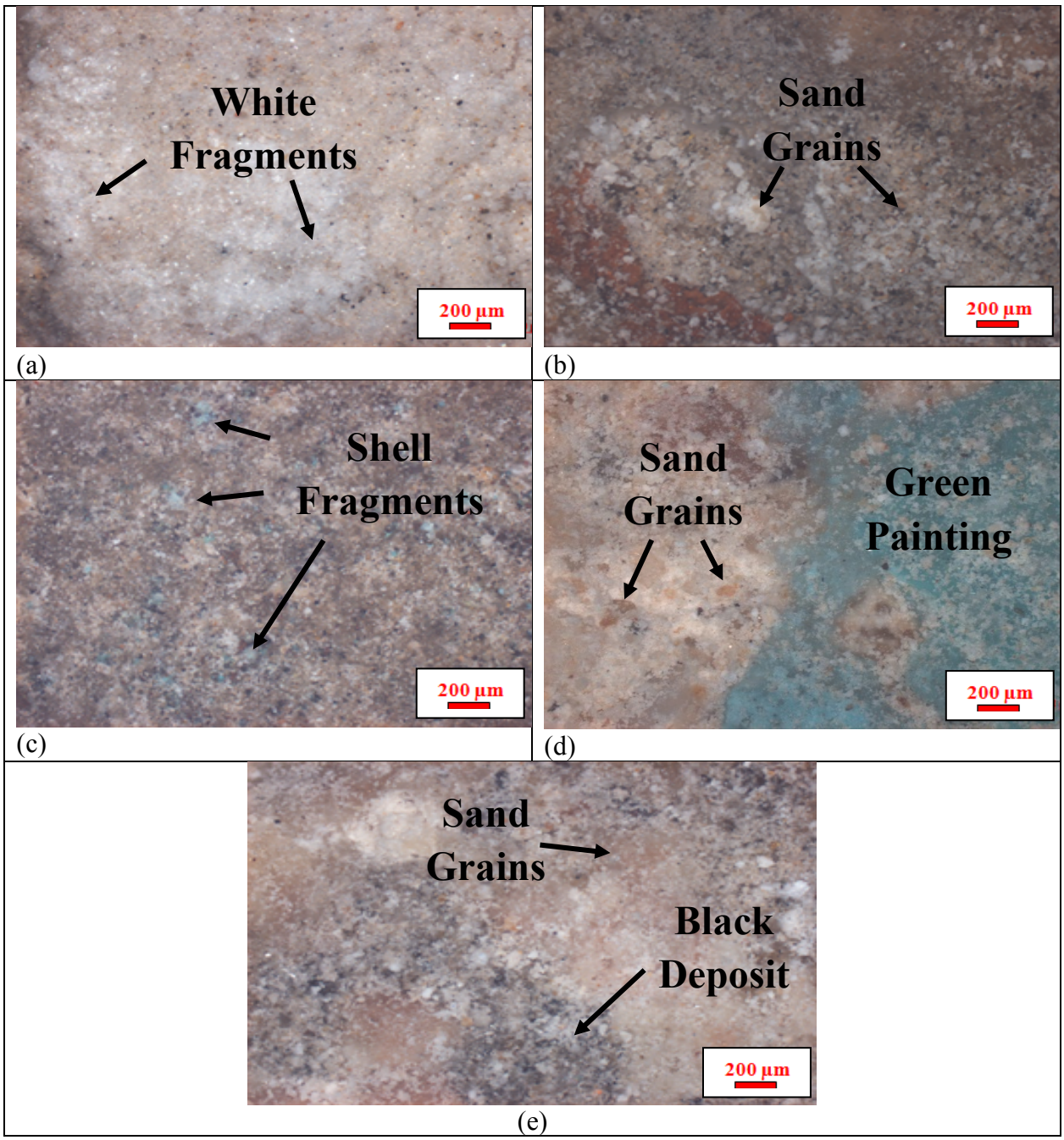

Figure 5.4.1 Optical images from the plaster samples collected from: (a) Jokhdar house west facade (b) Jamjoom house west facade, (c) Alturkey house east facade, (d) Nawwar house north facade and (e) Jokhdar house east facade.

5.4.2 X-Ray Diffraction Analysis

Table 5.4.1 summarises the XRD results obtained from the powdered plaster samples collected from the five historical houses. Different mineral phases were collected from each plaster identified and discussed below.

Table 5.4.1 Summary of the characteristics of the mineral phases identified in the plaster samples collected from the historical houses in Jeddah.

Location	Compound
Original plaster from the external west facade of Jokhdar house.	$CaSO_4.\ 2H_2O$ √
Original plaster from the external west facade of Jamjoom house.	$CaCO_3$ √ NaCl SiO_2 $CaSO_4.\ 2H_2O$
Original plaster from the external east facade of Alturkey house.	$CaCO_3$ √ SiO_2 NaCl $CaSO_4.\ 2H_2O$ $CaCO_3$
Original plaster from the external north facade of Nawwar house.	SiO_2 √ $CaCO_3$ NaCl
Original plaster from the external east facade of Jokhdar house.	SiO_2 √ $CaCO_3$ $CaSO_4.\ 2H_2O$

JOKHDAR HOUSE

A representative XRD pattern collected from the west wall of Jokhdar house is shown in Figure 5.4.2. The results identified only gypsum: this indicates that the plaster is made from gypsum and was for decorative or protective purposes, rather than structural. The use of gypsum plaster for protective or decorative coating of walls and ceilings and for decoration in this house is not suggested in the other samples.

The most common types of plaster mainly contain either gypsum, lime, or cement, but all work in a similar way. It is manufactured as a dry powder and made as a dry powder and mixed with water to form a hard but workable paste directly before it is applied to the surface. The reaction with water releases heat by crystallization and the hydrated plaster then hardens [21].

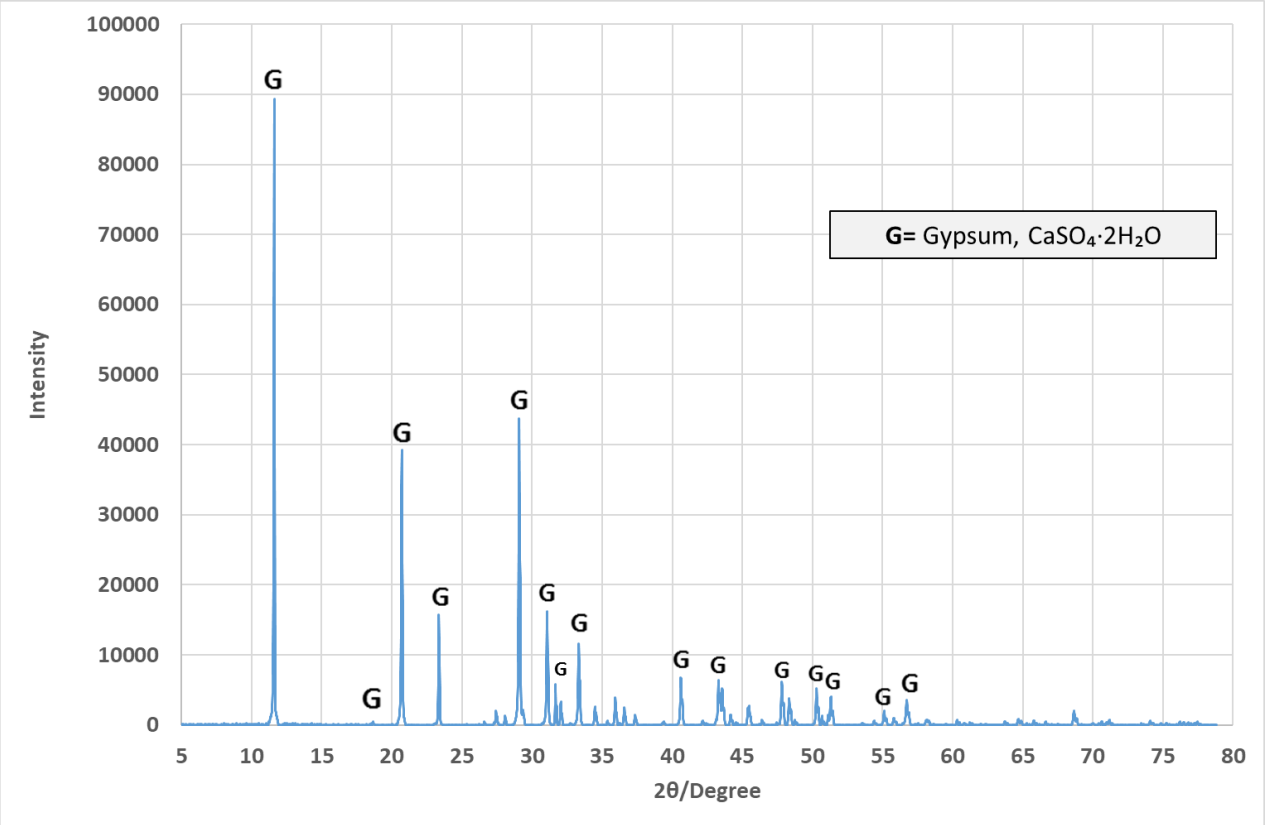

Figure 5.4.2 XRD pattern of the plaster sample collected from the west face of Jokhdar house.

JAMJOOM HOUSE

Figure 5.4.3 presents the mineral phases obtained from the plaster of the Jamjoom house. The result identified that calcite is the main phase, but halite, quartz and gypsum were also identified. The calcite and quartz probably came from the seashell and sand grains as seen in the optical microscope image (Figure 5.4.1b) and mixed with the plaster. Halite forms where salty lakes or sea-beds dry up. This suggested that the plaster type used for this house was made from a lime based mixture. The presence of gypsum is attributed to the reaction between the solid $CaCO_3$ and atmospheric SO_2.

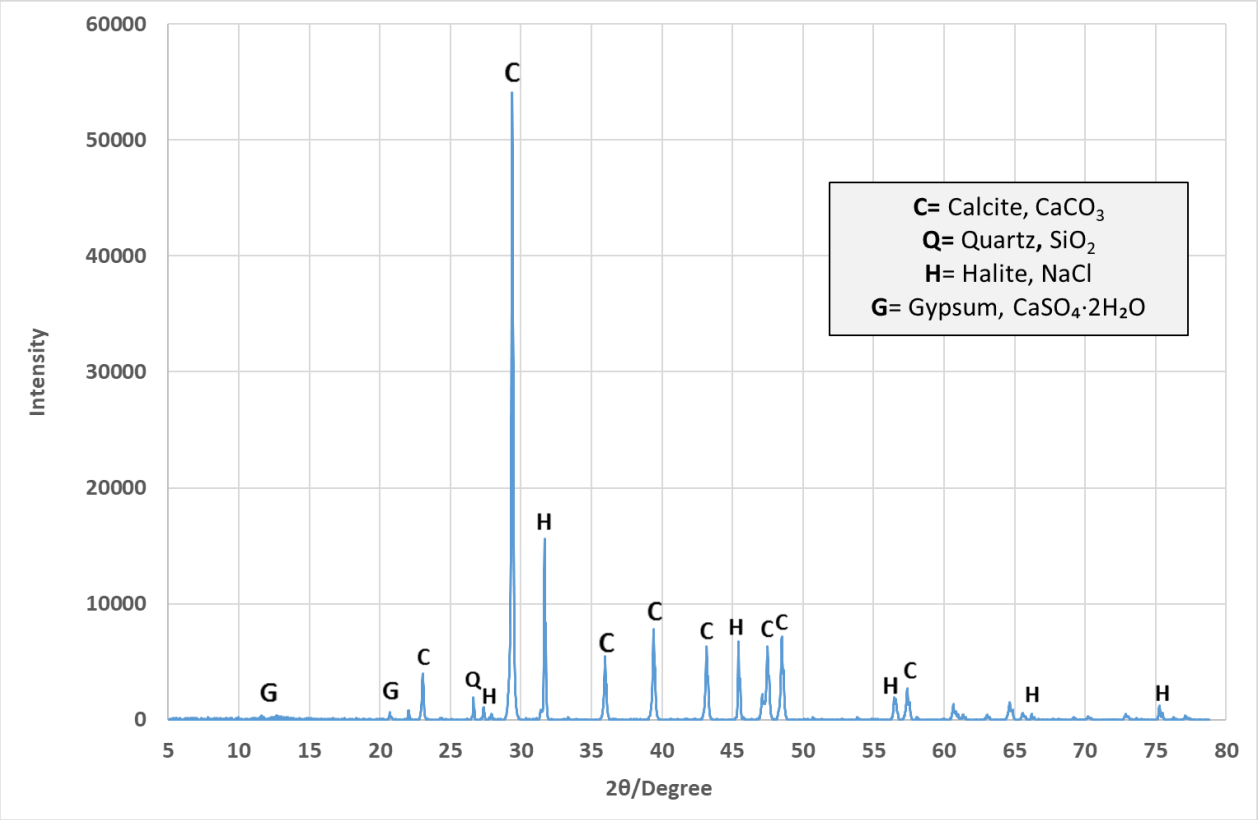

Figure 5.4.3 XRD pattern of the plaster sample collected from the west face of Jamjoom house.

ALTURKEY HOUSE

Figure 5.4.4 represents the mineral phases obtained by XRD and identified calcite as the major phase but also quartz, halite and a small peaks of gypsum. In addition, a small peak for aragonite, another $CaCO_3$ phase, was seen. Analysis of the XRD pattern of the sample collected from Alturkey house revealed that the sample must be composed from a lime-based binder and a sand aggregate, which is confirmed with the optical micrograph findings. Halite was found due to the salt from the sea. The presence of gypsum in the plaster sample can be explained by the carbonation of $CaCO_3$ in lime reacting with SO_2 and H_2O, subsequently precipitating $CaSO_4.2H_2O$. This evidence suggests that the plaster is and has been susceptible to degradation.

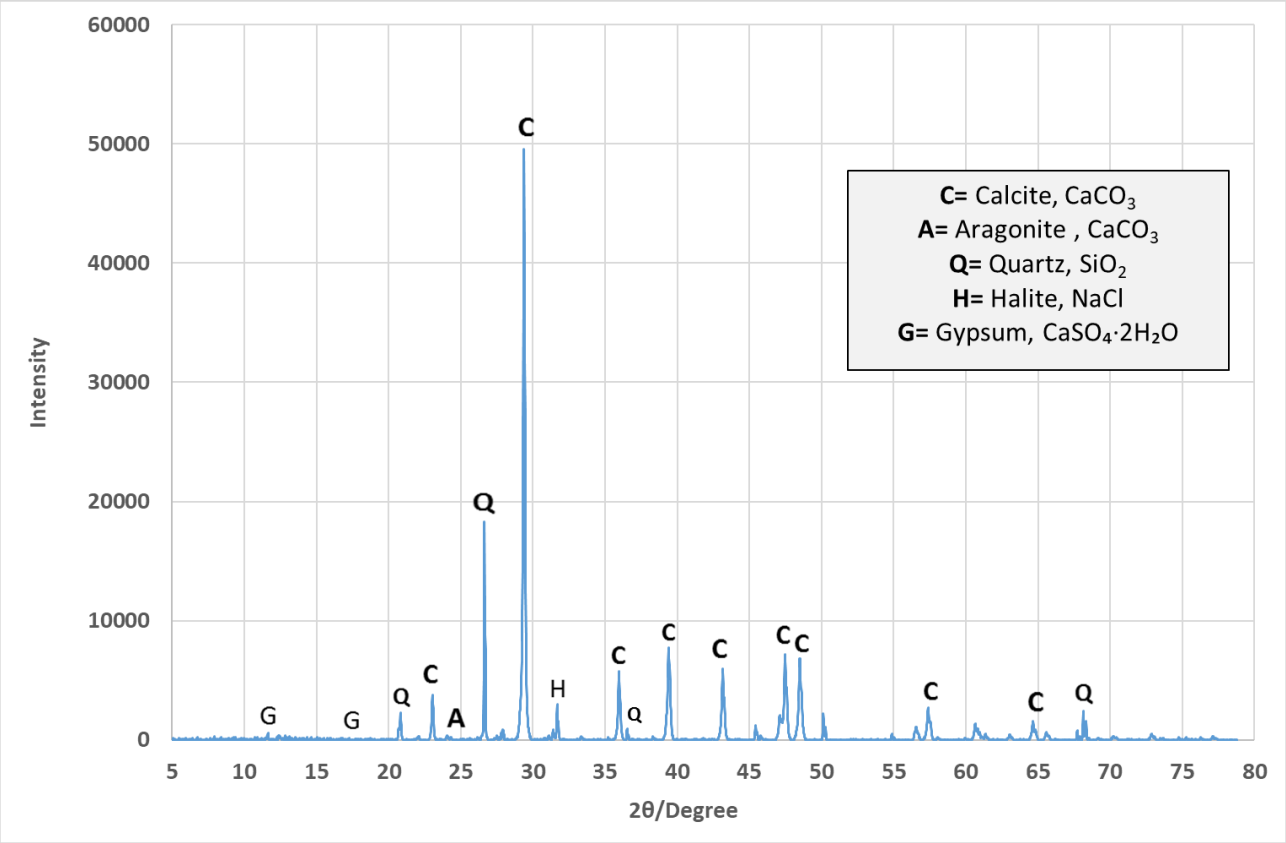

Figure 5.4.4 XRD pattern of the plaster sample collected from the east face of Alturkey house.

NAWWAR HOUSE

The XRD diffraction pattern collected from a plaster sample of Nawwar house is shown in Figure 5.4.5. The result identified quartz as the main phase, and in addition, like the other samples, calcite and halite were observed. The presence of strong quartz peaks was due to the sand mixed with the plaster, confirming like the Jamjoom and Alturkey houses, that the binder was a lime-based mixture with a sand aggregate. Interestingly, there was no sign of any gypsum peaks for this sample, possibly because this sample came from a North-facing wall that did not receive doses of atmospheric pollutants from traffic or industrial activity nearby (see Figure 4.1.1, site d) from prevailing winds that could have damaged or reacted with the plaster.

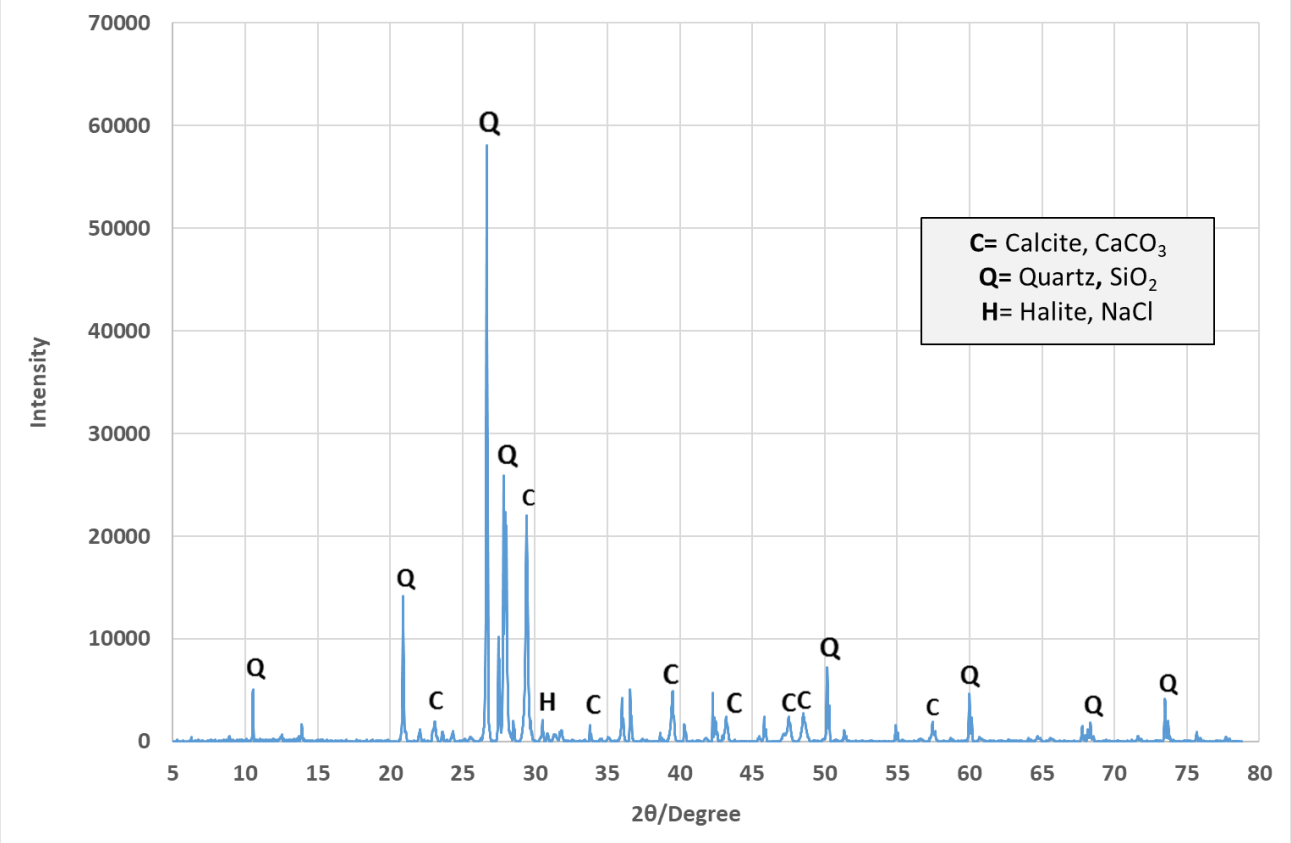

Figure 5.4.5 XRD pattern of the plaster sample collected from the north face of Nawwar house.

JOKHDAR HOUSE

An XRD pattern of the plaster sample collected from Jokhdar house's east face is shown in Figure 5.4.6. The results show that the major phases must be quartz, calcite and gypsum, confirming what is seen in the optical micrograph in Figure 5.4.1e. This is attributed to the sand aggregate that was mixed with the plaster. The presence of gypsum once again is thought to have resulted from carbonation of lime ($CaCO_3$) reacting with SO_2 and H_2O providing the end product, $CaSO_4.2H_2O$. In comparison with the Nawwar house sample which did not show signs of degradation, this result indicates degradation had occurred with the gypsum mineral being the key identifier of this process.

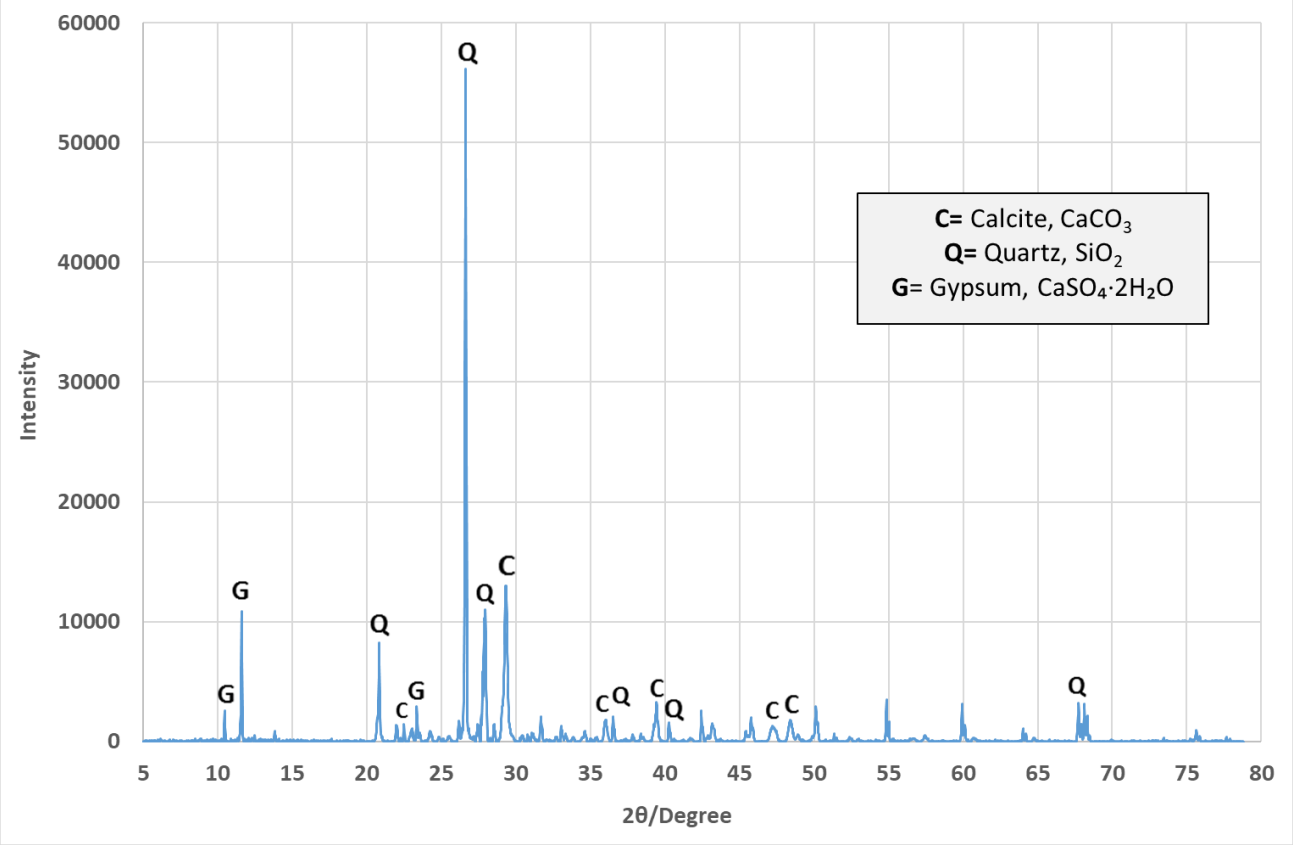

Figure 5.4.6 XRD pattern of the plaster sample collected from the east face of Jokhdar house.

5.4.3 SEM-EDS Analysis

JOKHDAR HOUSE

An SEM micrograph of the plaster surface from the west facade of Jokhdar house showed the typical needle-like shape of gypsum crystals (monoclinic crystal symmetry system), shown in Figure 5.4.7 [22]. The results of EDS maps showed Ca, O and S: the key elements of gypsum, which was used to decorate the house, (Figure 5.4.8). These are in good agreement with the XRD results obtained from the same sample as shown in Figure 5.4.2.

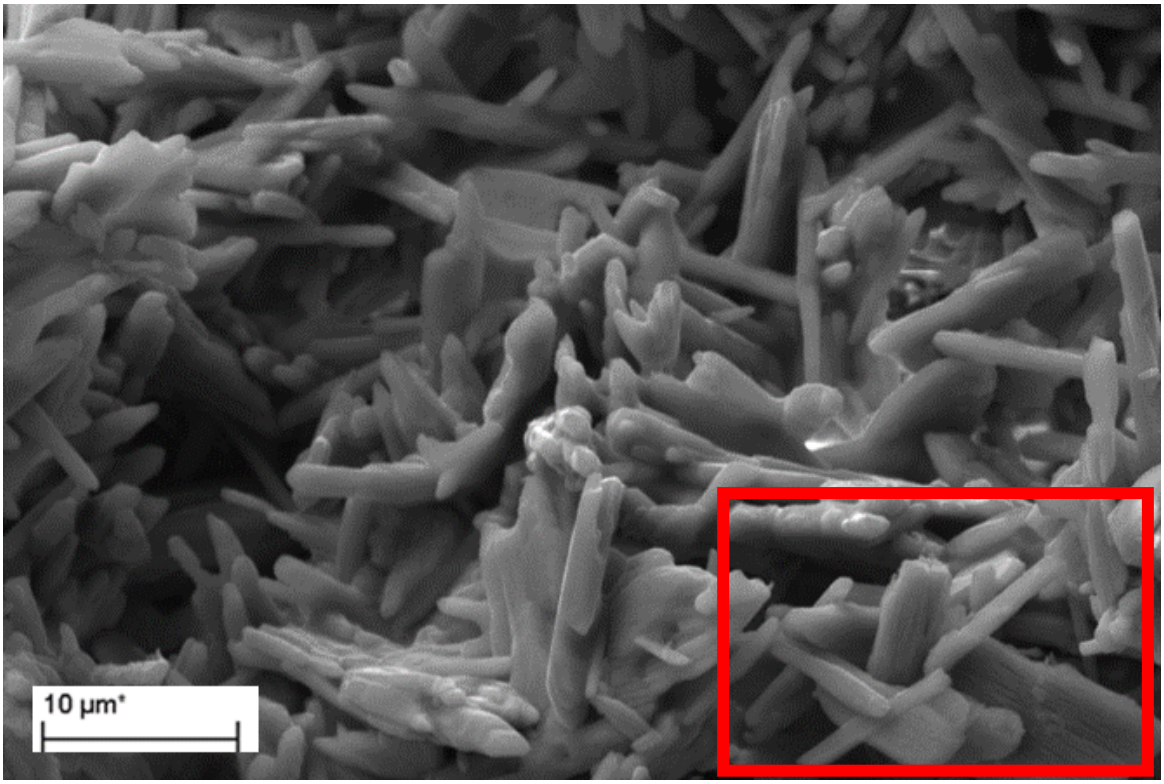

Figure 5.4.7 SEM micrograph from the plaster sample collected from the west facade of Jokhdar house.

The energy-dispersive X-ray maps in this area shows the structure of the gypsum crystals made to cover the limestone (Figure 5.4.8).

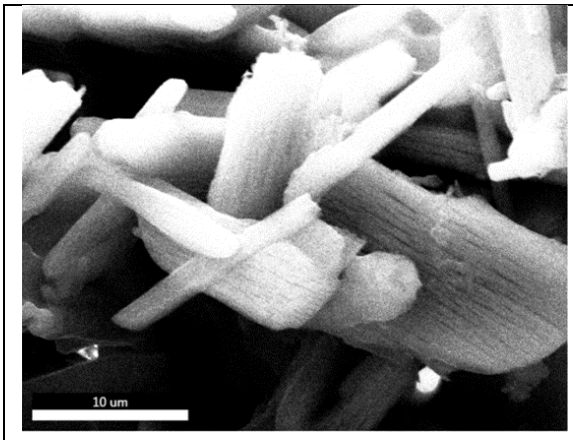

SE

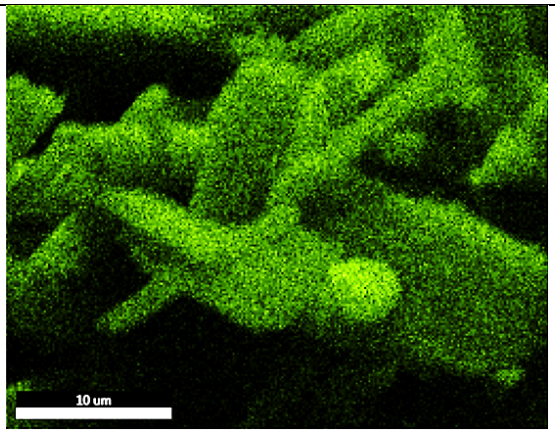

O

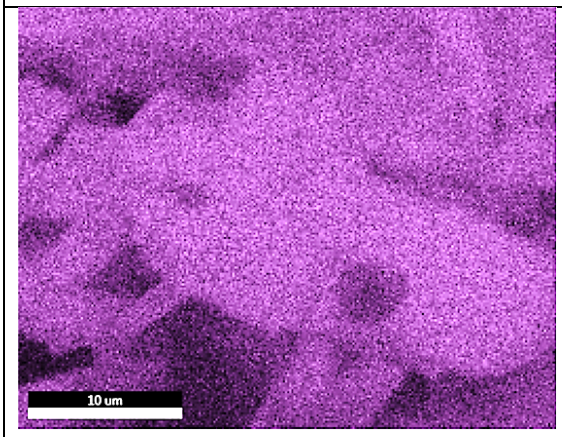

S

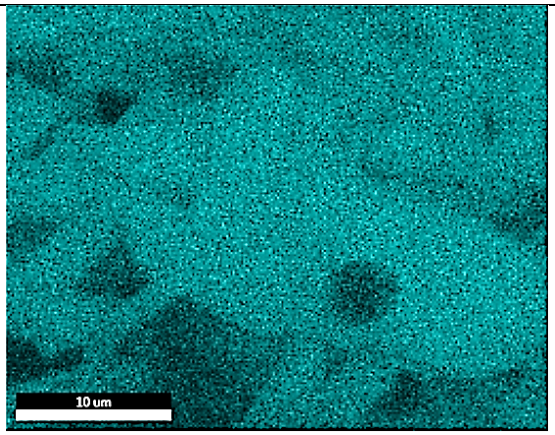

Ca

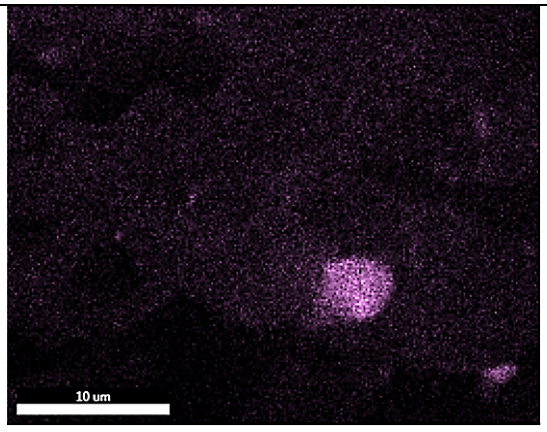

Si

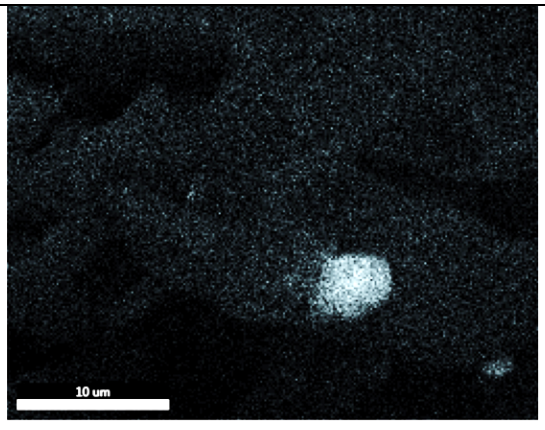

Al

Figure 5.4.8 X-Ray mapping shows the gypsum from Jokhdar house.

JAMJOOM HOUSE

The SEM micrograph of the plaster surface from the west facade of Jamjoom house shows structures akin to the calcite crystals and sand grains on the other samples (Figure 5.4.9a). This result agrees with the XRD mineralogic phases observed (Figure 5.4.3). The EDS results from this area identified O, Ca, Na, C, Fe, Si, K, Si, Al, Cl and Mg (Figure 5.4.9b).

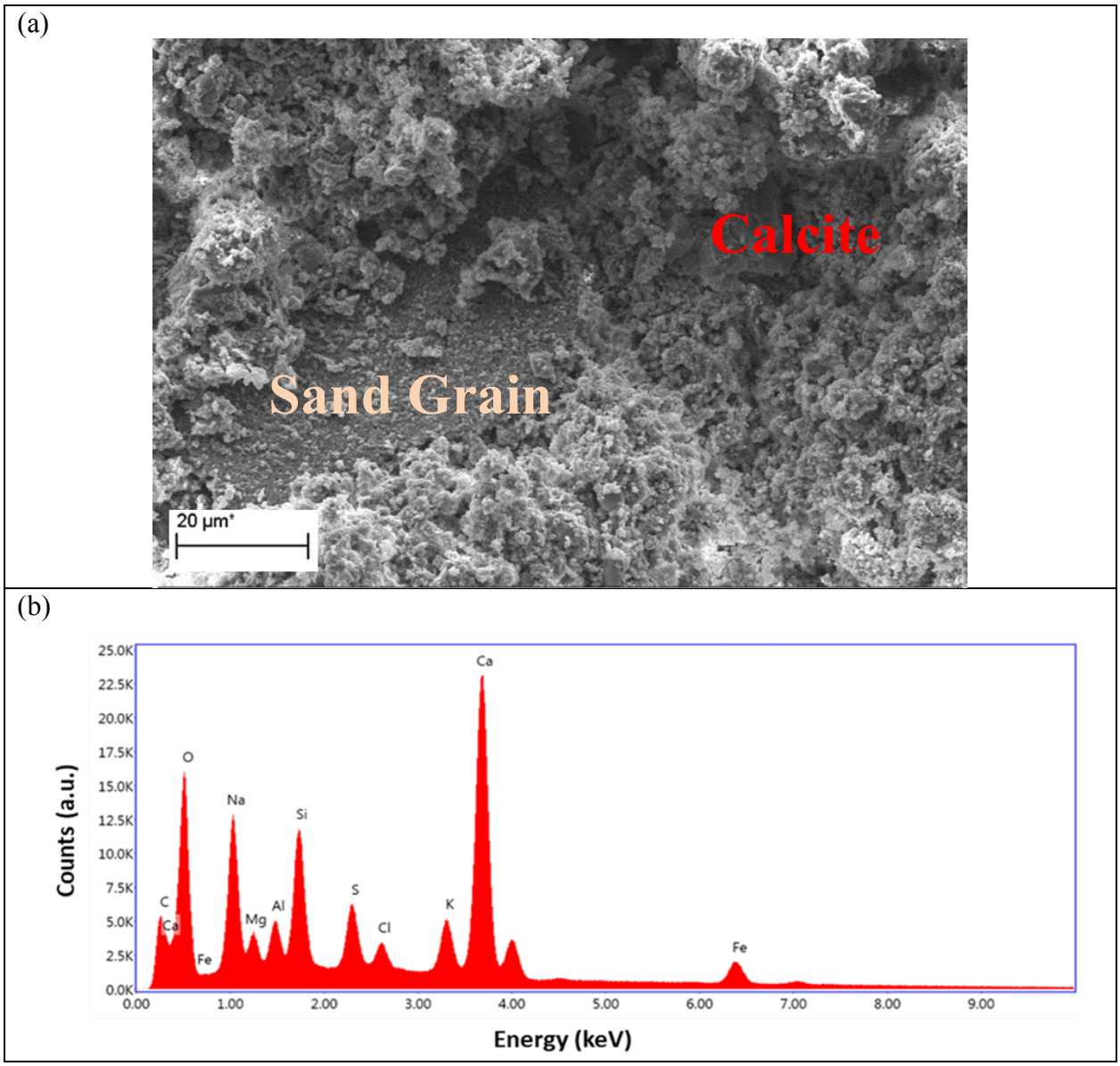

Figure 5.4.9 (a) SEM photograph collected from the plaster sample of Jamjoom house and (b) EDS spectrum results.

Carbon was identified on the surface of sample but because it is present due to the carbon coater as part of sample preparation, it is impossible to discern if it is elemental carbon that truly came from atmospheric pollutants, or as part of carbonate in the calcite crystals already present. Ca and O were certainly due to the lime-based mixture used to build the house, and S is purported to have been sourced by the reaction between the $CaCO_3$ and atmospheric SO_2. Other elements such as Si, Al, K, and Fe are usually from the sand or clays present in the mixtures. Na and Cl were present due to the influence of seawater.

ALTURKEY HOUSE

The SEM micrograph obtained from the surface plaster of Alturkey house revealed different structures of calcite and quartz crystals (Figure 5.4.14a). The EDS results identified Ca and O due to the lime base used to create the plaster (Figure 5.4.10b). The S and P are present due to reactions with atmospheric pollutants. Elemental carbon is attributed to the carbon coater and the other elements are present (Si, Mg, Al, and K) are from the sands and clays mixed with the plaster. Na and Cl are present due to seawater.

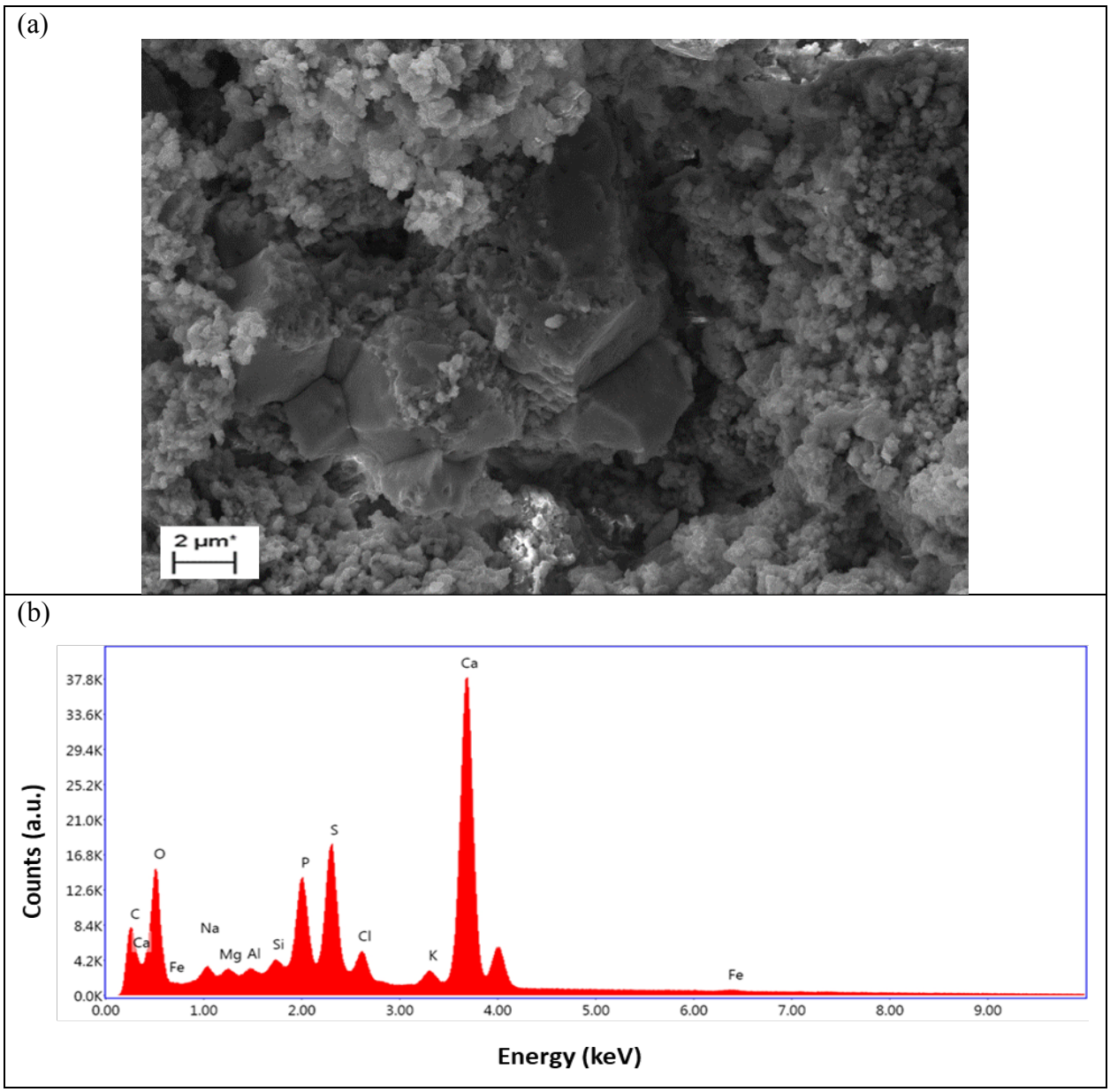

Figure 5.4.10 (a) SEM photograph collected from the plaster sample of Alturkey house and (b) EDS spectrum results.

NAWWAR HOUSE

The SEM micrograph from Nawwar house revealed a quartz and calcite dominant structure, as expected, as shown in Figure 5.4.11a. The EDS results identified a strong Si signal, signifying the large amount of quartz present from the sand aggregate mixed with the plaster.

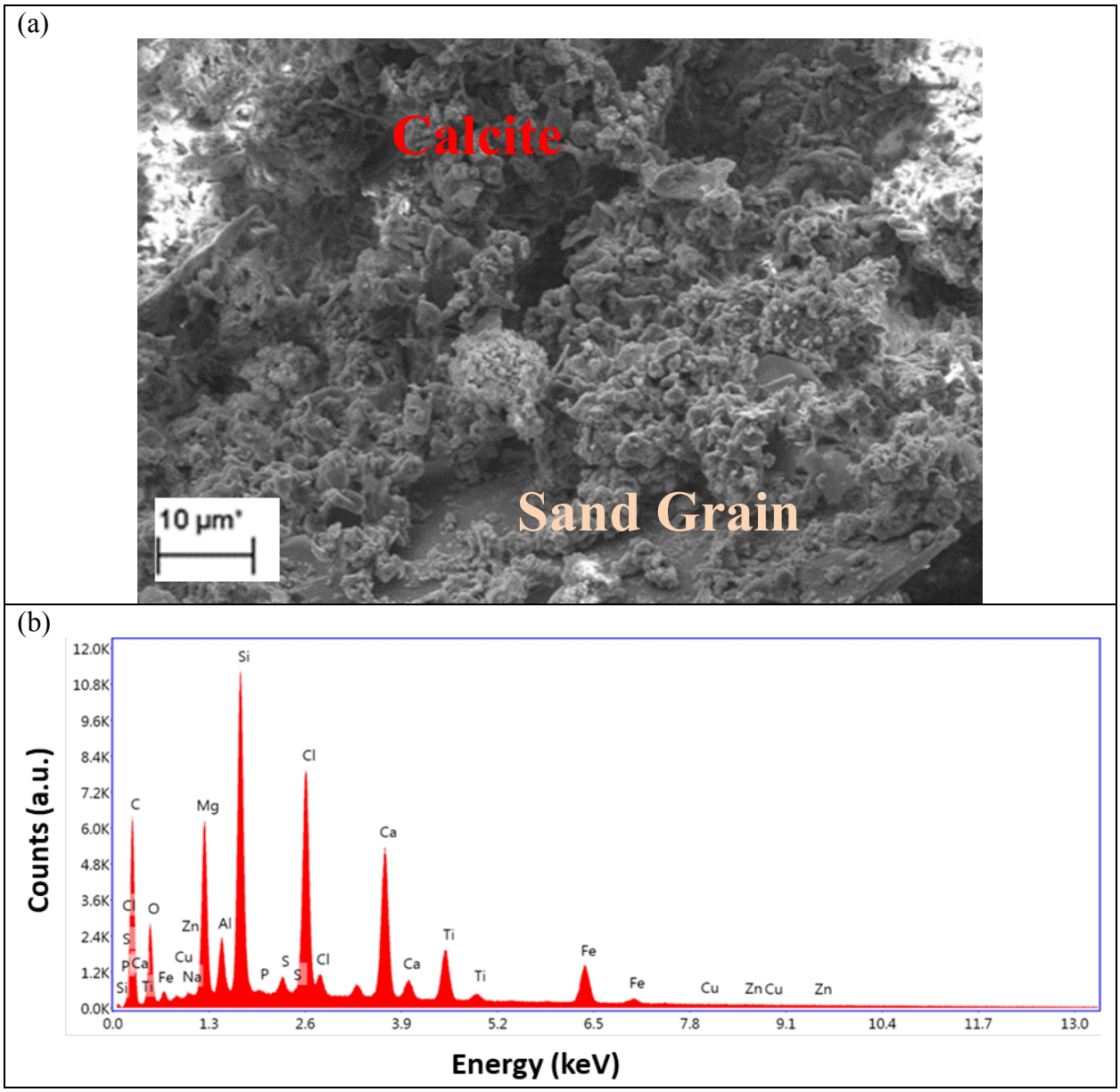

Figure 5.4.11 (a) SEM photograph collected from plaster sample of Nawwar house and (b) EDS spectrum results of the corresponding area.

This finding agreed with XRD peaks seen in the spectrum collected from the Nawwar sample. While the other results were congruent with the other houses, other elements were identified with the EDS scan including Cu and Zn as well as S and P in trace amounts, in addition to the usual oxides and impurities (Mg, Al, K, Ti and Fe), suggesting the presence of industrial activity and deposition of heavy metal pollutants (Figure 5.4.11b).

JOKHDAR HOUSE

During the analysis of the corroded samples, various particles were observed on the surface and others had irregular rough or smooth shapes and high porosity.

The SEM micrograph of the plaster surface from the east facade of Jokhdar house reveals high amounts of quartz, calcite and gypsum crystals, which agrees solidly with the XRD result as shown in Figure 5.4.6. To investigate the distribution of the heavy metal atmospheric pollutant particles, an SEM micrograph (Figure 5.4.12) combined with EDS mapping (5.4.13) was conducted to ascertain which particles were the pollutants and confirming their metallic composition of Fe, Cu and Zn.

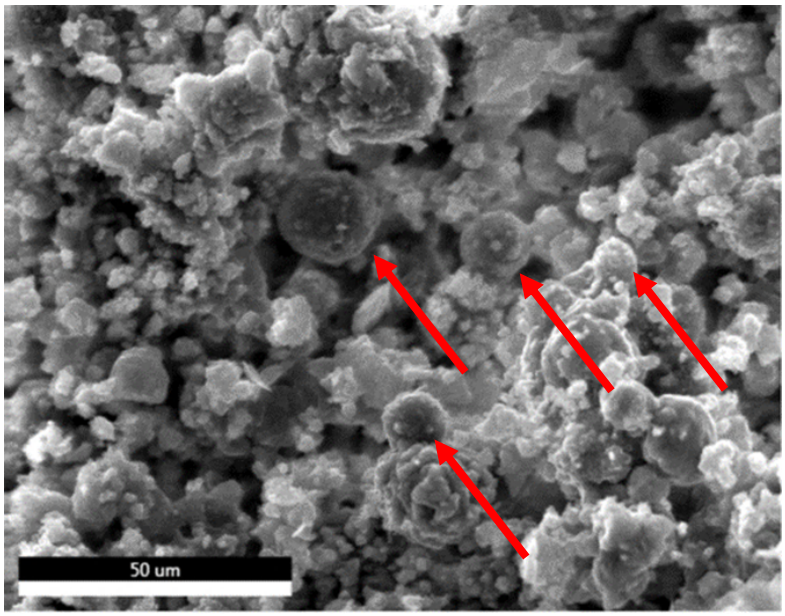

Figure 5.4.12 SEM micrograph showing the plaster surface rich in atmospheric pollutants particles.

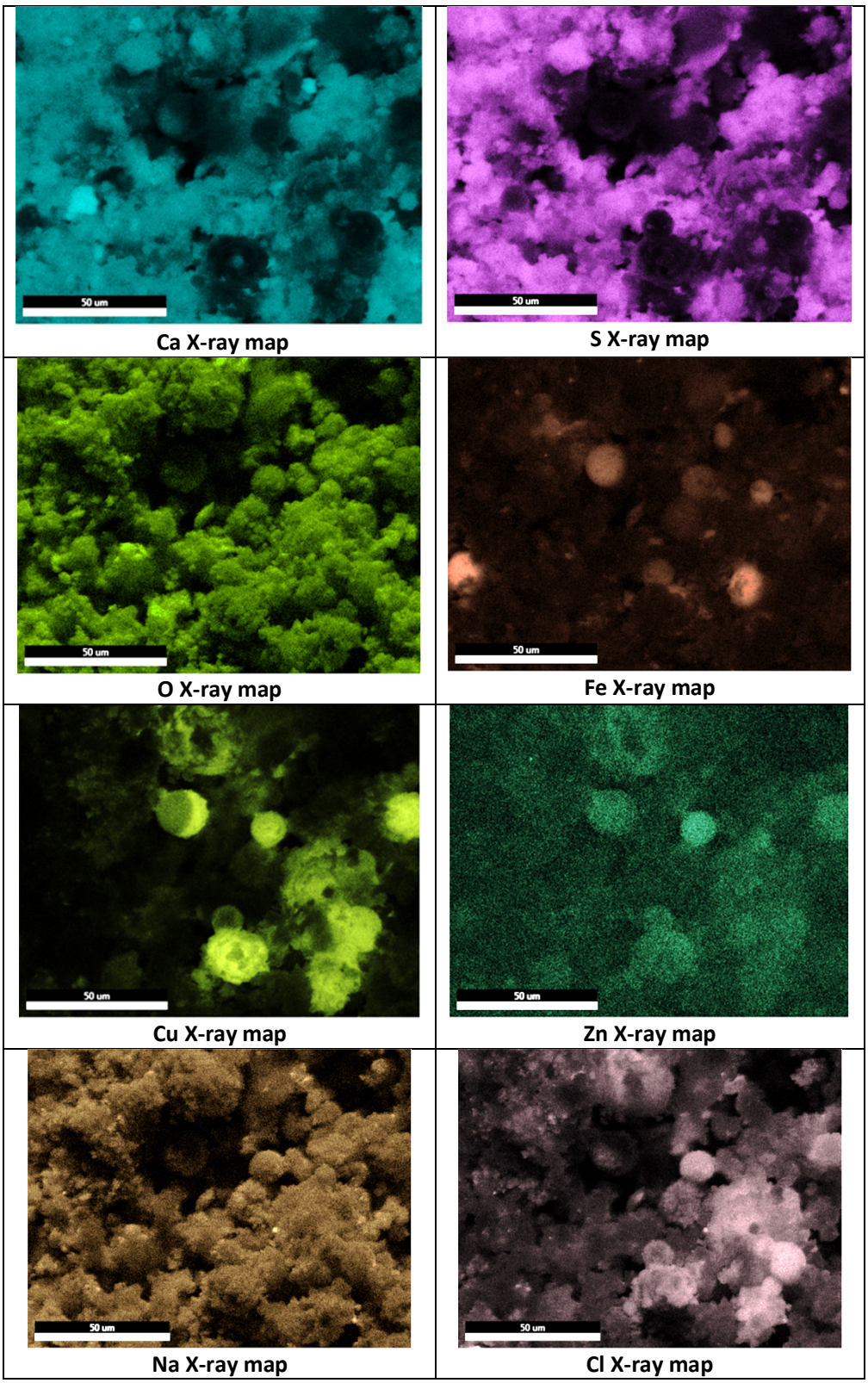

Figure 5.4.13 SEM photograph and x-ray mapping collected from the plaster sample of Jokhdar house from the east facade.

The main anthropogenic substances detected in these microscale particles were Fe, Cu and Zn. During the investigation, SEM examination revealed different types of particles containing different sizes of spheres approximately 10-40 μm. However, the X-ray elemental maps obtained from these particles to further investigate their compositions are presented in Figures 5.4.14 and 5.4.15. Other elements found on these surfaces include Na, Cl, S and P attributed to the interaction of sea salts as well as industrially produced atmospheric pollutants. The site is located near Jeddah port, surrounded by industry and an oil refinery. Further study will be carried out to measure air pollution at the sites to confirm these findings. Table 5.4.2 summarises the EDS elemental quantitative results obtained from the plaster samples.

Table 5.4.2 Summary of the EDS elemental quantitative results identified in the plaster samples.

Plaster Samples	Elements (Weight %)												
	C	O	Na	Mg	Al	Si	P	S	Cl	K	Ca	Ti	Fe
Jamjoom House	7.84	34.83	10.43	1.23	1.60	5.01	-	2.82	1.34	3.60	25.77	-	5.61
Alturkey House	13.16	34.03	0.63	0.13	0.12	0.66	5.68	7.70	1.92	1.04	34.45	-	0.48
Nawwar House	44.44	15.43	-	5.21	1.33	8.64	-	0.38	7.99	-	7.99	3.44	5.06

5.4.4 Laser Raman Spectroscopy (LRS) Analysis

Raman spectra collected from the five plaster samples are shown in Figure 5.3.16. The spectrum from Jokhdar House identified only $CaSO_4.2H_2O$ (gypsum) bands located at 415, 495, 621, 672, 1008 and 1134 cm^{-1}. However, it must be noted as before that the laser depth is only a few nanometres from the surface; similar to the XRD technique, so cannot detect any other structures below the outer gypsum-coating of the samples. The finding is nonetheless in good agreement with the XRD results displayed in Figure 5.4.2.

Raman spectra from Jamjoom, Alturkey, and Jokhdar's east facade show the presence of calcite bands at 277, 710, 1086 cm^{-1}. The Raman spectra from Nawwar house also identified band of calcite located at 1086 cm^{-1} and an additional quartz band at 446 cm^{-1}. These findings are supported by the XRD data shown in section 5.4.2.

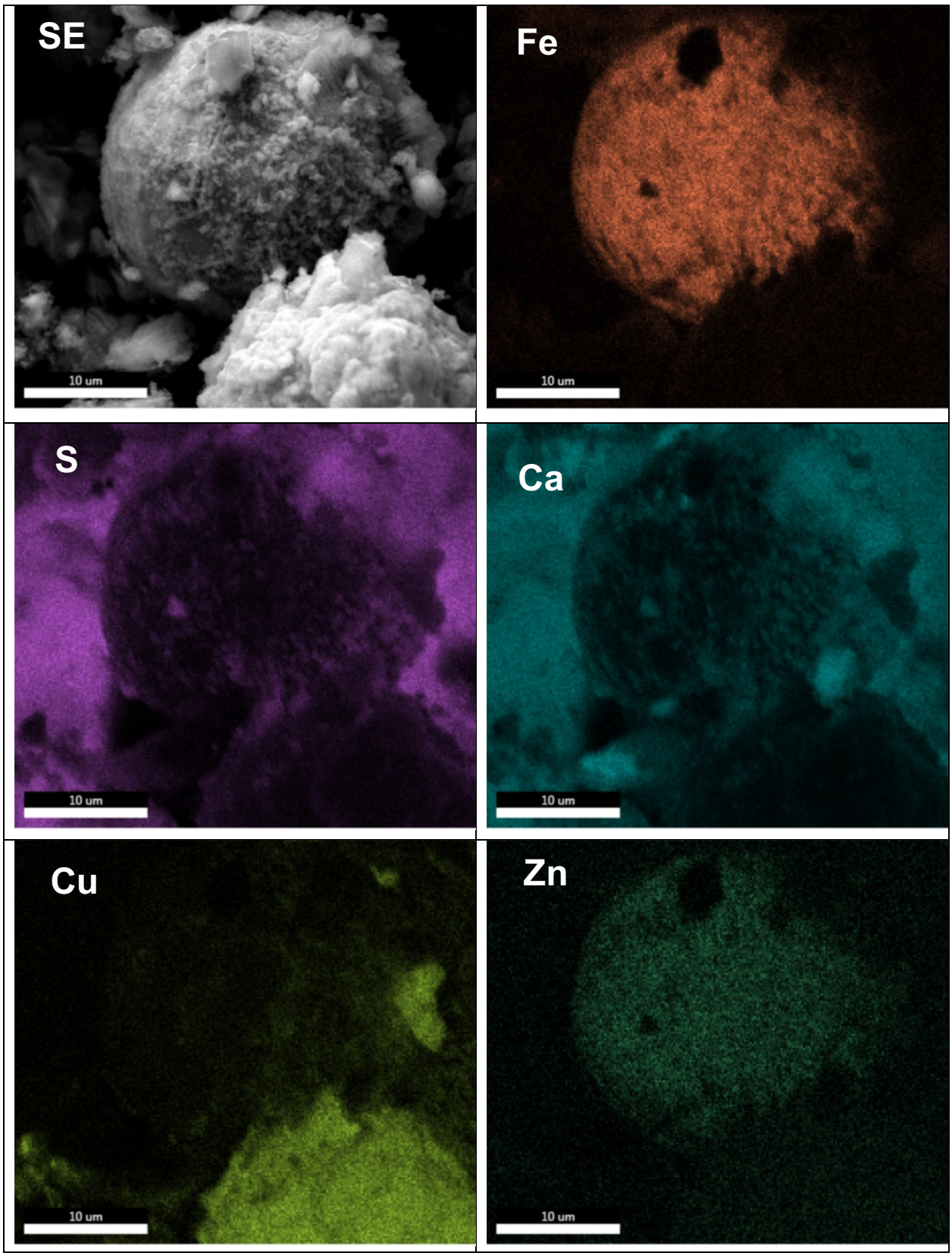

Figure 5.4.14 X-ray mapping of an iron particle deposited on the Jokhdar house plaster.

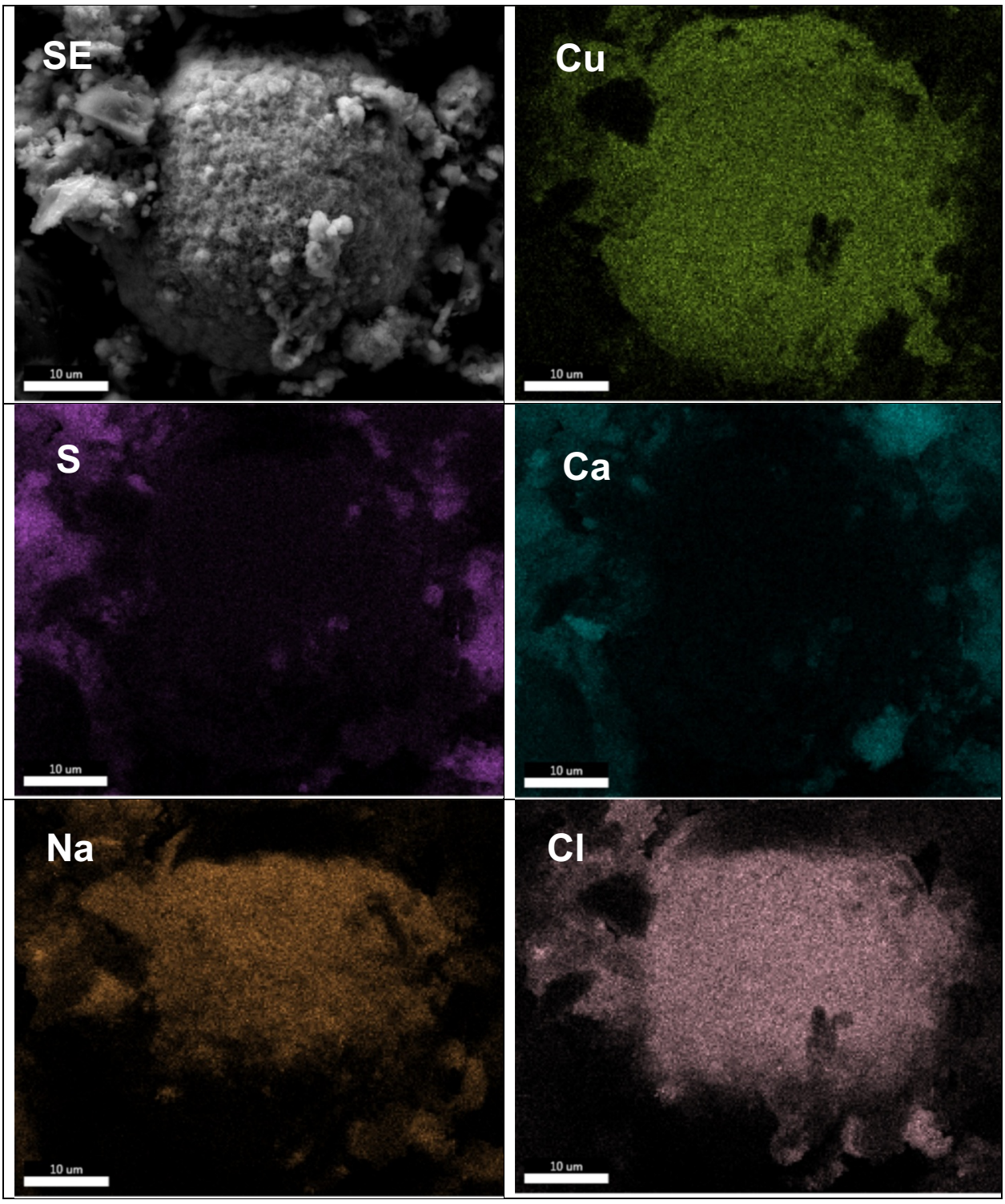

Figure 5.4.15 X-ray mapping of a copper particle was found on the surface of the Jokhdar house plaster.

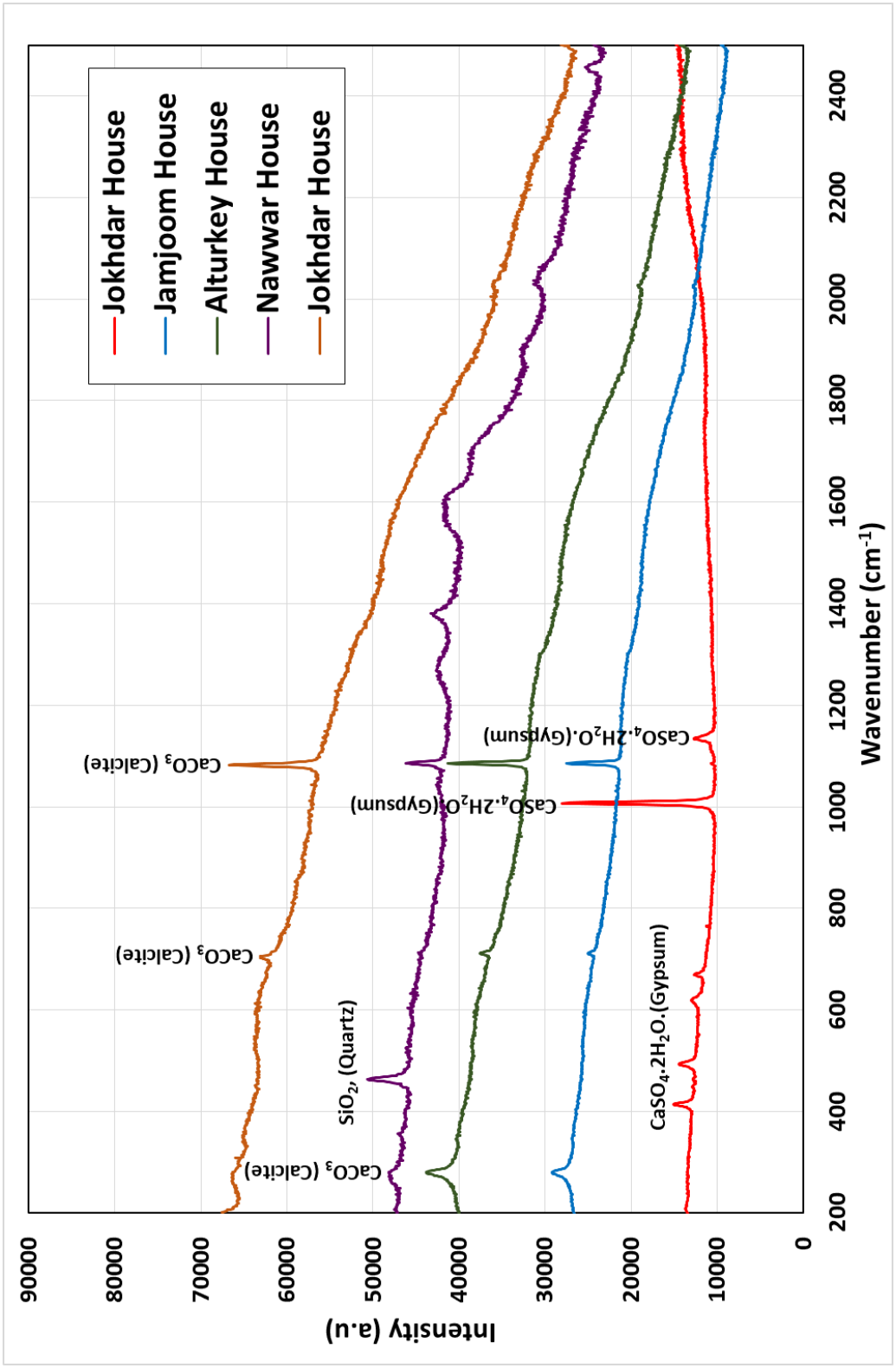

Figure 5.4.16 Laser Raman spectra collected from all five plaster samples.

5.5 FIB-SEM sectioning and Analysis

The result of metallic particles observed on the plaster sample of the east wall of Jokhdar house required further analysis for more detailed structural information. Focused Ion beam (FIB) and the scanning electron microscope (SEM) were used together, conducted by removing the particulates from the plaster surface using a micromanipulator (Figure 5.5.1). The main objective was to identify the inner morphological structure of the spherical particles.

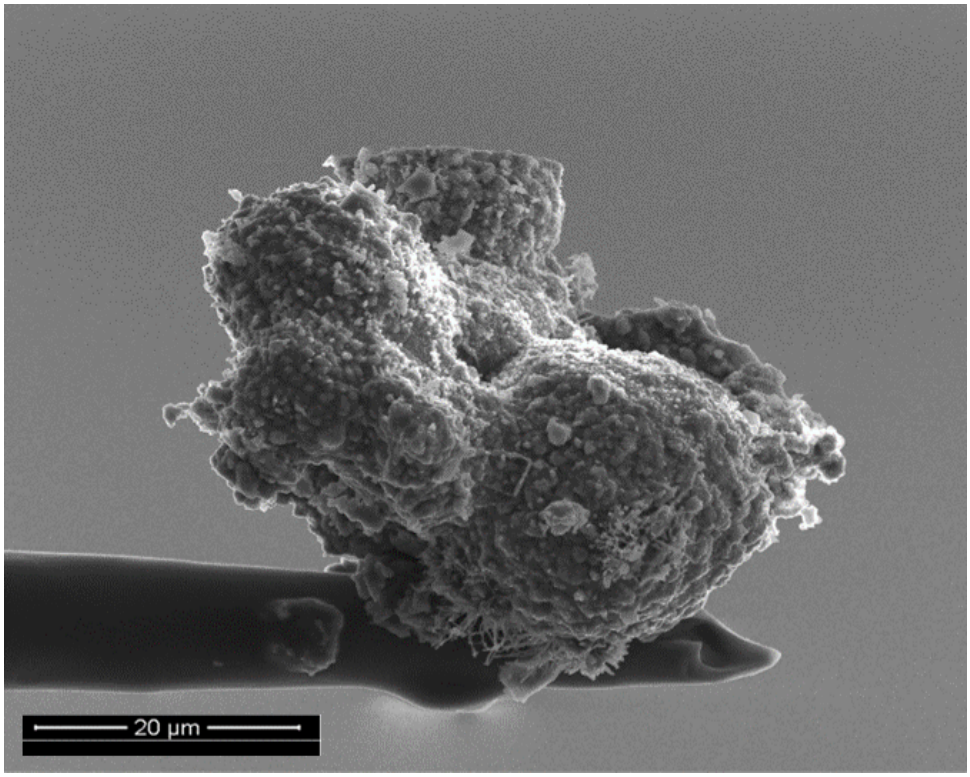

Figure 5.5.1 FEI™ Helios NanoLab™ 600 dual FIB-SEM with Kleindiek™ MM3A-micromanipulator used for particle removal.

The structure showed that the solid inner core of the particle was a mixed Cu-Fe composition with lesser but variable amounts of Zn. These particles were commonly spherical and metallic with a thin outer oxide layer. An example sectioned particle is presented in Figure 5.5.2. The X-ray maps show the presence and distribution of the heavy metals (Fe, Cu and Zn) and the oxide layer.

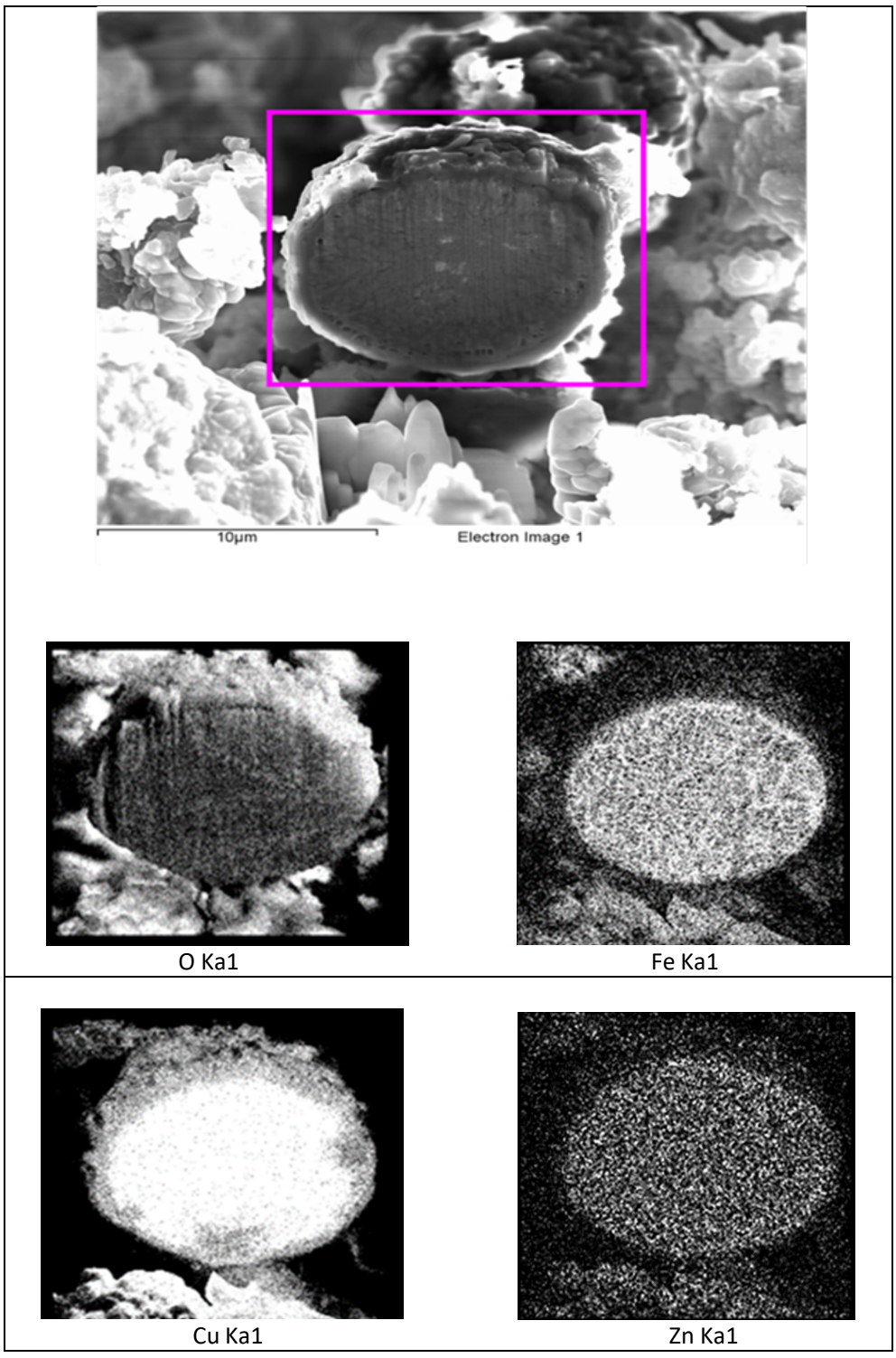

Figure 5.5.2 An example X-ray map of the heavy metal particle when sectioned.

5.6 Summary Discussion

Previous authors reported that the historic buildings located in a marine environment that have been facing sodium chloride bearing sea-spray for centuries and probably from ground water mays suffer severe deterioration of their materials [23]. The present results showed significant effect of the salt due to the crystallisation-dissolution cycling [24, 25, 26]. The results also showed the presence of $CaSO_4.2H_2O$ (Gypsum) as a corrosion product identified in stone, mortar and plaster materials causing the degradation of these materials [27]. These attributed from the atmospheric SO_2 pollutant.

5.7 Summary

Overall, the results from the investigated stone, mortar and plaster materials lead to drawing the following conclusions:

Stone:

- Limestone was the main material used to construct the buildings.
- Sulphur and sodium chloride were the main atmospheric pollutants.

Mortar:

- The binder used was non-hydraulic lime-based material.
- Sulphur and sodium chloride were the main atmospheric pollutants.

Plaster:

- Consisted of densely packed calcite, quartz and gypsum crystals.
- The binder used to make the plaster is comprised of non-hydraulic lime and gypsum-based mixtures.
- Sulphur and sodium chloride were the main atmospheric pollutants. In addition, particles comprised of copper, iron and zinc metals were also observed.
- Heavy metal particles comprised of Fe, Cu and Zn were detected on the outer surface of the east-facing Jokhdar house plaster sample.

5.8 References

[1] Kumar, S.Z., Lin Li, A., (2009). Materials characterization techniques. Boca Raton: CRC Press. ISBN 1420042947.

[2] Middendorf, B., Hughes, J. J., Callebaut, K., Baronio, G. and Papayianni, I., (2005). Investigative methods for the characterization of historic mortars - Part 1: Mineralogical characterization. Materials and Structures, RILEM Technical Committees. 38, pp761-769.

[3] Lindqvist J. E., Sandstrom M., (2000). Quantitative analysis of historical mortars using optical microscopy. Materials and Structures, RILEM Technical Committees. 33, pp 612-617.

[4] Lasemi, Z., Sandberg, P.A., (1984). Transformation of aragonite-dominated lime muds to microcrystalline limestones. 12(7), pp420-423. Available at: https://pubs.geoscienceworld.org/gsa/geology/article/12/7/420/198537/Transformation-of-aragonite-dominated-lime-muds-to [Accessed May 2019].

[5] Aquilano, D., Otálora, F., Pastero, L., García-Ruiz, J.M., (2016). Three study cases of growth morphology in minerals: Halite, calcite and gypsum. Progress in Crystal Growth and Characterisation of Materials. 62(2), pp 227-251. Available at: https://doi.org/10.1016/j.pcrysgrow.2016.04.012.

[6] La Russa, M.F., Ruffolo, S.A., Belfiore, C.M., Aloise, P., Randazzo, L., Rovella1, N., Pezzino, A., Montana, G., (2013). Study of the effects of salt crystallization on degradation of limestone rocks. Periodico di Mineralogia. 82(1), pp113-127. Available at: http://periodicodimineralogia.it/index.php/mineralogia/article/view/199 [Accessed May 2019].

[7] El-Turki, A., Ball, R.J., Wang, C.F., Allen, G.C., (2005). A study of novel lime-based mortars consisting of lime, oyster shell lime, clay, sugar, sand and rice using Focus Ion Beam microscopy, Raman spectroscopy and mechanical testing. Paper presented at: 10th Euroseminar on Microscopy Applied to Building Materials, Paisley, UK United Kingdom. Available at: https://researchportal.bath.ac.uk/en/publications/a-study-of-novel-lime-based-mortars-consisting-of-lime-oyster-she [Accessed May 2019].

[8] Rasmussen, M. H., Wedel, S., Pedersen, K. H., Illerup, J. B., & Dam-Johansen, K., (2015). Initial reaction between CaO and SO_2 under carbonating and non-carbonating conditions. Chemical Engineering Science, 134, pp169-177. Available at: https://sciencedirect.com/science/article/pii/s0009250915003127. [Accessed 13/10/2019].

[9] Shchukarev, A. V. (2007). A study of the SiO_2-aqueous electrolyte (NaCl, CsCl) interface by X-ray photoelectron spectroscopy. 69(4), 514-525. Available at: https://link.springer.com/article/10.1134/s1061933x0704014x. [Accessed October 2019].

[10] Orbasil, A., (2009). The Conservation of Coral Buildings on Saudi Arabia's Northern Red Sea Coast. Journal of Architectural Conservation. 15(1), pp49-64, DOI: 10.1080/13556207.2009.10785039.

[11] Hwidi, R.S., Nuraiti, T., Izhar, T., Mohd Saad, F.N., (2018). Characterization of Limestone as Raw Material to Hydrated Lime. In: International Conference on Civil & Environmental Engineering (CENVIRON 2017) [online] E3S Web of Conferences, 34, 02042. Available at: https://doi.org/10.1051/e3sconf/20183402042 [Accessed October 2019].

[12] Pinho, P., Augusto, S., Martins-Loução, M.A., Pereira, M.J., Soares, A., Máguas, C., Branquinho, C., (2008). Causes of change in nitrophytic and oligotrophic lichen species in a Mediterranean climate: Impact of land cover and atmospheric pollutants. Environmental Pollution. 154(3), pp 380-389. Available at: https://doi.org/10.1016/j.envpol.2007.11.028.

[13] Buzgar, N., Apopei, A. I., (2009). The Raman Study of Certain Carbonates. Geologie, Tomul LV. 2, pp 97-112.

[14] El-Turki, A., Ball, R., Holmes, S, Allen, W.J., Allen , G.C., (2010). Environmental cycling and laboratory testing to evaluate the significance of moisture control for lime mortars. Construction and building Materials. 24(8), pp1392-1397. Available at: https://doi.org/10.1016/j.conbuildmat.2010.01.019

[15] Lafuente B., Downs R T., Yang H., Stone N., (2015). The power of databases: the RRUFF project. In: Highlights in Mineralogical Crystallography, T Armbruster and R M Danisi, eds. Berlin, Germany, W. De Gruyter, pp 1-30, [online] Available at: http://rruff.info/halite/notchem=nacl/display=default/R070586 [Accessed October 2019].

[16] Whyte, E. F. (1921). A study of the extraction of potash from orthoclase feldspar by carbon dioxide and sulphur dioxide. Proceedings and Transactions of the Nova Scotian Institute of Science, 15(3), 145-151.

[17] Santos Silva, A., Ricardo, J.M., Salta, M., Adriano, P., Mirao, J., Candeias, A., (2006). Characterization of Roman mortars from the historical town of Mertola. Heritage Weathering Conservation. 1, pp85-90. Available at: http://cathedral.lnec.pt/publicacoes/l1.pdf [Accessed October 2019].

[18] Ergenç, D., Gómez-Villalba., L. S., Fort, R., (2018). Crystal development during carbonation of lime-based mortars in different environmental conditions. Materials Characterization. 142, pp276-288. Available at: https://doi.org/10.1016/j.matchar.2018.05.043. [Accessed October 2019].

[19] Freeman, J.J., Wang, A., Kuebler, K.E., Jolliff, L.B., Haskin, L.A., (2008). Characterization of Natural Feldspars by Raman Spectroscopy for Future Planetary Exploration. The Canadian Mineralogist. 46, pp1795-1818. Available at: DOI: 10.3749/canmin.46.6.00.

[20] Marszałek, M., (2016). Identification of secondary salts and their sources in deteriorated stone monuments using micro-Raman spectroscopy, SEM-EDS and XRD. Journal of Raman Spectroscopy. 47(12), pp 1473-1485. Available at: https://doi.org/10.1002/jrs.5037. [Accessed October 2019].

[21] Freire, T., Santos Silva, A., do Rosário Veiga, M., de Brito, J., (2012). Characterisation of Decorative Portuguese Gypsum Plasters from the Nineteenth and Twentieth Centuries: The Case of the Bolsa Palace in Oporto. Historic Mortars, Springer Netherlands. RILEM Bookseries 7, pp141-151. Available at: DOI 10.1007/978-94-007-4635-0_11.

[22] Charola, A., Pühringer, J., Steiger, M., (2007). Gypsum: A review of its role in the deterioration of building materials. Environmental Geology. 52(2), pp 339-352. Available at: DOI: 10.1007/s00254-006-0566-9.

[23] Groot, C., Van Hees, R.P.J., Wijffels., T., (2009). Selection of plasters and renders for salt laden masonry substrates, 23(5), pp 1743-1750. Available at: DOI: 10.1016/j.conbuildmat.2008.09.013.

[24] Watt, D., Colston, B., (2000). Investigating the effects of humidity and salt crystallisation on medieval masonry, 35(8), pp 737-749. Available at: https://doi.org/10.1016/S0360-1323(00)00015-9.

[25] Zedef, V., Kocak, K., Doyen, A., Ozsen, H., Kekec, b., (2007). Effect of salt crystallization on stones of historical buildings and monuments, Konya, Central Turkey, 42930, PP 1453-1457. Available at: https://doi.org/10.1016/j.buildenv.2005.12.010.

[26] Gentilini, C., Franzoni, E., Bandini, S., Nobile, L., (2012). Effect of salt crystallisation on the shear behaviour of masonry walls: An experimental study, 37 pp 181-189. Available at: https://doi.org/10.1016/j.conbuildmat.2012.07.086.

[27] Allen, G.C., El-Turki, A., Hallam, K.R., Mclaughlin, D., and Stacey, M., (2000). Role Of NO_2 and SO_2 in degradation of limestone. British Corrosion Journal, (35) No. 135.

CHAPTER 6
IN-SITU CHARACTERISATION OF ATMOSPHERIC AEROSOLS AT HISTORICAL SITE IN JEDDAH

6.1 Background

Based on the results obtained from the characterisation of the building materials presented in chapter 5, the work showed that the surface plaster collected from Jokhdar house has a high number of metallic micro-particles. The main objective of the work in this current chapter was to monitor and identify the presence the metallic atmospheric aerosol particles around the historic quarter of the city, to verify whether the metal micro-particles observed on the building surface were present and deposited from air pollution arising from nearby industrial activities.

6.2 Sampling Location

An image from Google Maps presents the historical site located in the southern part of Jeddah (see Figure 6.2.1). The site is located near the coast and is surrounded by industrial activities. The samples were collected from the western and southern sites (as indicated in Chapter 4, Figure 4.1.1). The western buildings are located just a few kilometres from the Red Sea, and oil-fired desalination plants that produce potable water for the city and surrounding areas, together with the rest of the Port of Jeddah's commercial activities. These activities provide a starting point to suggest what anthropogenic atmospheric particles are likely to be affecting the buildings in Jeddah in western directions. In addition, the south of the historic quarter is bounded by an industrial area and an oil refinery, providing an additional source of possible pollution albeit located in the down-wind direction for predominant trade winds coming from the north west.

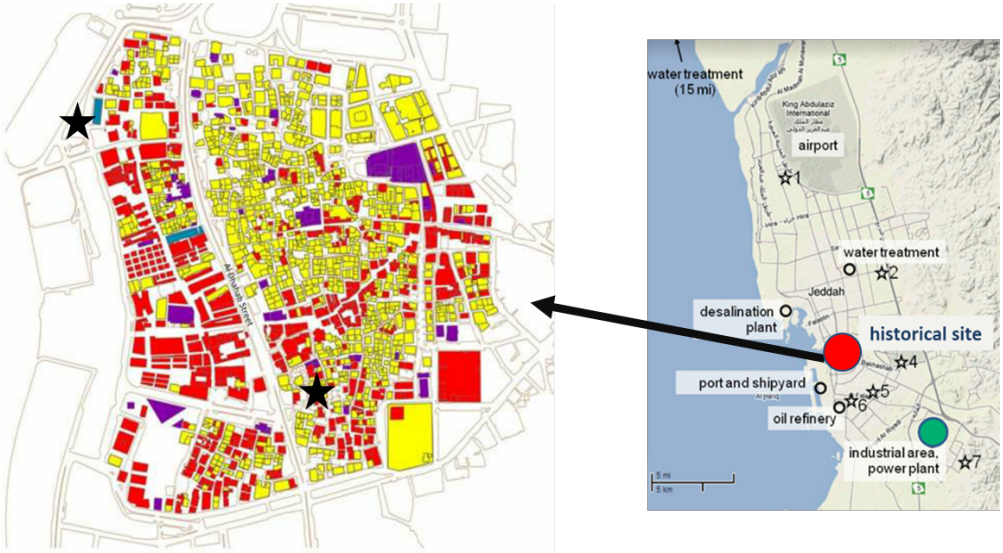

Figure 6.2.1 Sampling locations including the historical site highlighted by a red circle, and the southern industrial site highlighted by a green circle.

6.3 Sample Collection

Samples were collected using a particle impactor supplied by California Measurements Inc (Figure 6.3.1). The impactor is a mass-based inertial impaction system which can be used for sampling airborne or gas-suspended particulates.

Figure 6.3.1 Photograph of the particle impactor being deployed at the historical site.

The device consists of a 3-stage on carbon sticky stubs, 2 lpm flow, and inertial impaction sample collector with particle-size cut-points down to 0.05 microns and deposits samples onto the stubs for electron microscopy analysis. Schematic of the atmospheric aerosol impactor shown in Figure 6.3.2. The mission of field study was conducted from 4th June to 18th July 2018.

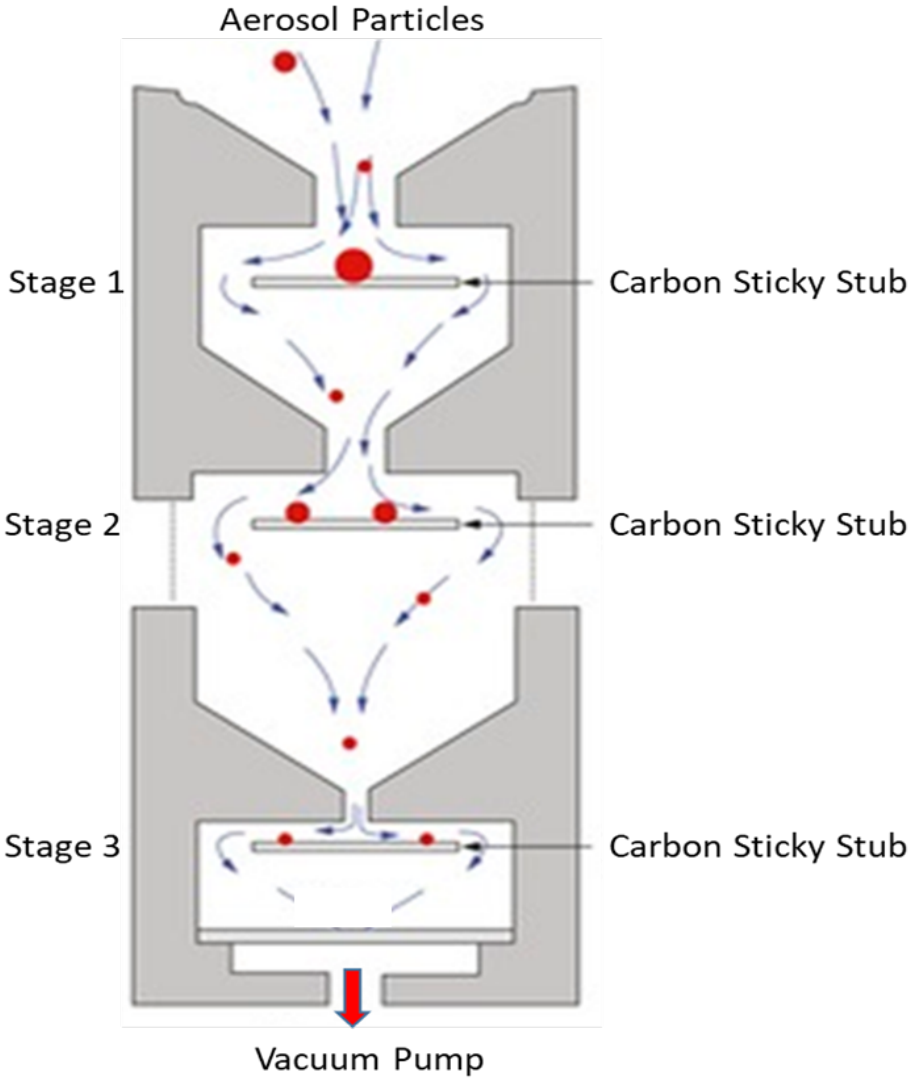

Figure 6.3.2 Schematic of the atmospheric aerosol impactor.

In addition, 60 filtered samples were collected and provided by The General Authority of Meteorology and Environment Protection (GAMEP) at the industrial site. The MP101M analyzer were used to collect the PM25 fraction i.e. particles between 25 µm and ~2.5 µm in diameter. The type of filters were roll of fiber glass autonomy of three years or 1200 cycles (based on 24 daily cycle).

The collected aerosol samples were subsequently analysed at the University of Bristol, Interface Analysis Centre (IAC). The following techniques were used to characterise the elemental composition, size and morphology of collected particles:

- Zeiss Sigma HD, variable pressure field emission scanning electron microscope (FESEM) (see Chapter 4: section 4.3.4). This allowed direct observation of individual particles captured by sampling.

- Thermo Fisher Scientific Niton FXL 950, X-ray Fluorescence (XRF) spectrometer. This allowed bulk analysis of filter papers to get an overall picture of the elemental composition of the aerosol population.

6.4 Results and Discussion

SEM-EDS was used to analyse the range of collected aerosol samples. The results from the western and southern locations are described separately in the following sections.

6.4.1 Western Location

The secondary electron micrograph below presents the aerosol sample, in which various particles of different types with average diameters of 1-10 μm were identified (Figure 6.4.1). Some were spherical and others had irregular rough structures. In general, ambient aerosols are generated from the incomplete combustion of fuels and industrial activities and their composition and size can be influenced by: meteorological factors, atmospheric conditions, types of emissions sources and by parameters such as density, shape and hygroscopicity [1].

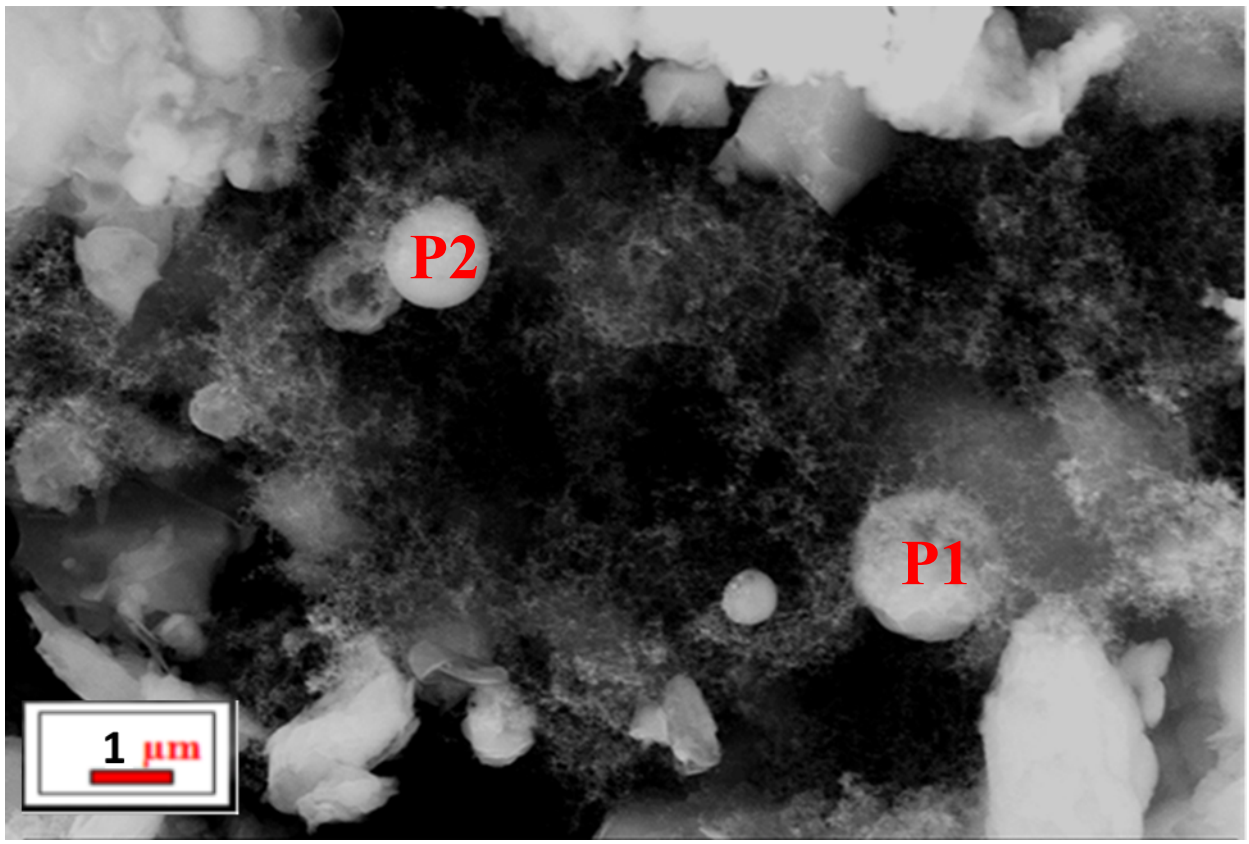

Figure 6.4.1 An example electron micrograph from aerosol samples collected from the western location of the historical site.

SEM-EDS results of the particulates from Figure 6.4.1 show the most commonly occurring particles are spherical. Example spherical particles (P1) and (P2) shown in Figures 6.4.2 and 6.4.3 and EDS analysis demonstrates that there is significant calcium signal from the particles but also significant amounts of Fe and Cu. A tendency for increasing calcium concentration with decreasing particle size was also observed. Calcium enriched aerosol particles may be environmentally significant with implications for our understanding of sea spray aerosol [2]. Carbon was also observed, this was attributed primarily to the carbon tabs used during the preparation of the sample. It is considered that these aerosols are influenced by several complex processes due to the incomplete combustion of fossil-fuels and their waste products in high temperature gas/steam releases containing volatiles rising from the desalination plants [3, 4, 5]. This will be discussed in more detail later in the Chapter.

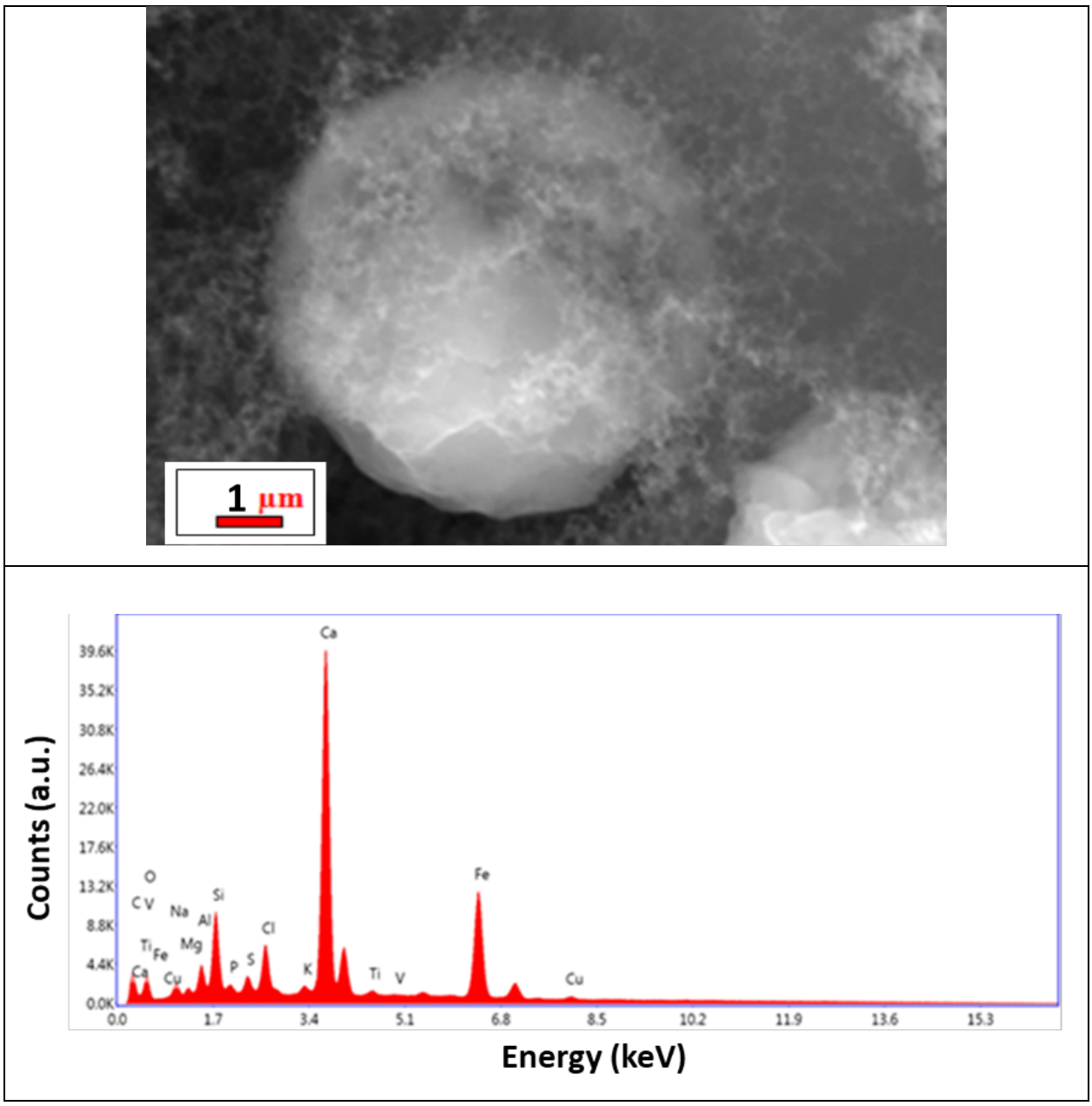

Figure 6.4.2 SEM-EDS of a spherical particle (P1).

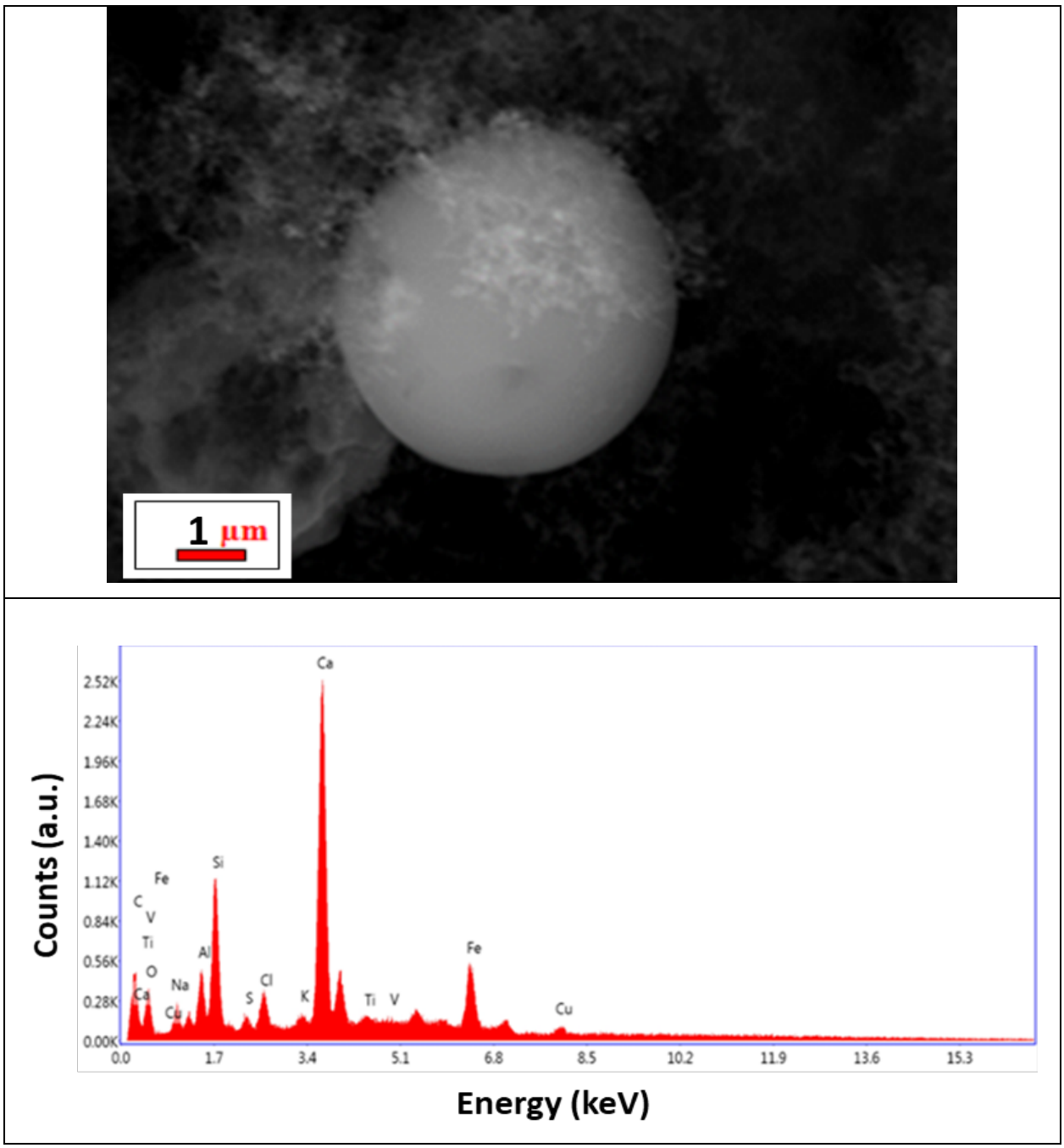

Figure 6.4.3 SEM-EDS of a spherical particle (P2).

Most of the spherical particles analysed contained transition metals. Copper (Cu) is a notable occurrence as it has too high a value to be deliberately released and is too low in natural abundance to be considered to have a natural origin.

The SEM micrograph below shows one such spherical particle (Figure 6.4.4a). The EDS results for this particle show predominantly Fe present as the metal component (Figure 6.4.4.b). Additionally, nanoparticles of adhered silicate, carbonate and sea salt are invoked by the detection of Ca and Si, but also Na, K and Cl, indicating mixing with marine aerosols [6]. These particles are resolved by the micrograph and show as lighter features due to differential charging under the beam due to their insulating properties relative to the metal particle.

(a)

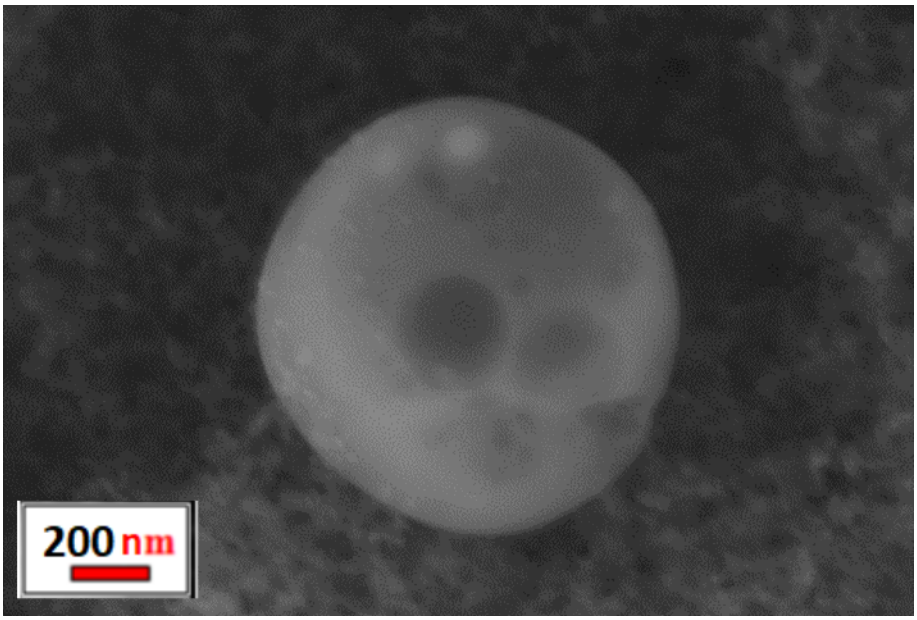

(b)

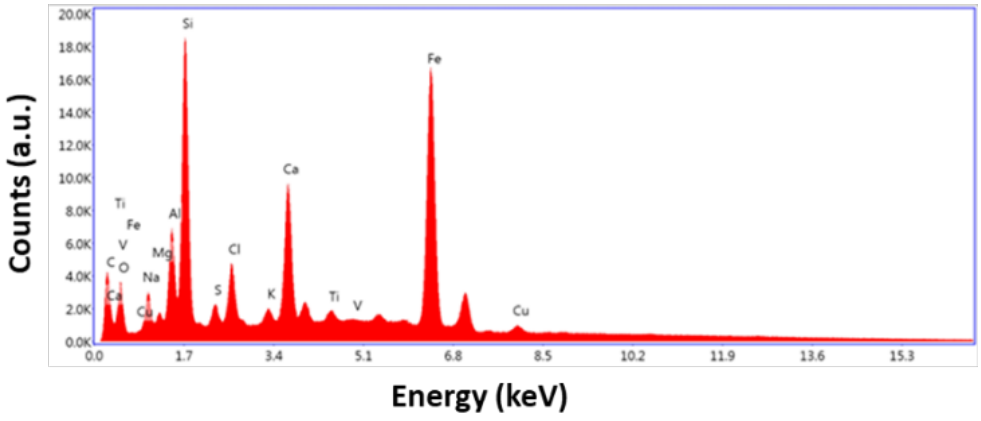

Figure 6.4.4 (a) SEM image of a spherical metal particle and (b) EDS spectrum of corresponding particle.

Given that Jeddah is a coastal city it was not unexpected for the sample analysis to also identify a significant amount of salt (halite) particles. EDX analysis confirmed that salt particles were predominantly sodium chloride (Figure 6.4.5) but with small amounts of calcium (which may come from other matrix materials in the sample). Any historic site located in a marine environment facing sodium chloride spray for times may suffer severe degradation of its structure, due to the recrystallisation of the salt over repeating wetting and drying cycles as the growing and shrinking crystal structure applies stress, damaging these historical site.

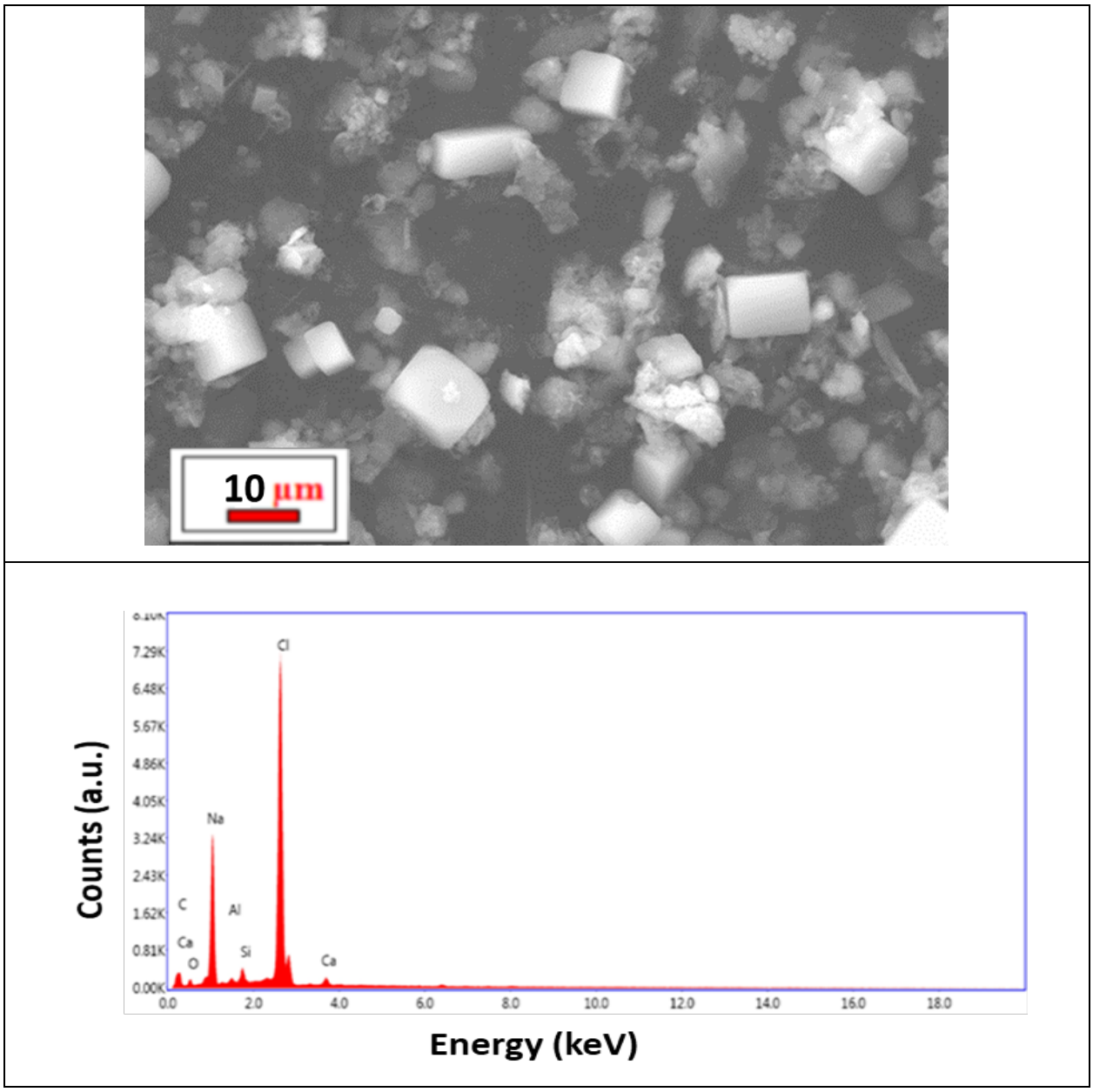

Figure 6.4.5 An SEM micrograph of salt and the matched EDS spectrum from the sample.

The particle grains were characteristically well formed faceted cubic crystals, 10-15 μm in maximum dimension. The observed crystal habit is typical of halite and suggests that crystals formed from a marine source, by evaporation of salt containing water droplets (from sea spray). Sea salt (NaCl) is considered a serious problem for historical structural materials in coastal areas as the salt, carried as aerosols by onshore winds, can attack building materials and steel structures [7]. Salt aerosol deposition is not uniform and instead decreases in concentration away from the coastal zone [8, 9]. Equally, on a very local-scale salt aerosol deposition onto building surfaces will not be uniform, with sea-facing walls expectedly picking up greater salt deposition than walls on the lee side of the buildings. This explains the variation seen for the samples taken from the different buildings in the Jeddah historic quarter.

6.4.2 Southern Location

The results of the samples collected from the southern locations of the historical site are shown in Figures 6.4.6 - 6.4.9. The most commonly occurring particles were spherical, similar to the western location samples. Highly porous particles with an irregular pore distribution were also found at this site. It is speculated that these particles are "spheroidal carbonaceous particles." Spheroidal Carbonaceous Particles (SCPs) are a component of fly-ash formed by the incomplete high-temperature combustion of fossil fuels and are therefore unambiguous indicators of atmospheric deposition from industrial sources, including power generation, as shown in Figure 6.4.6a [10]. EDS analysis of this particle in Figure 6.4.6b indicated that other than carbon, S, Si, Al, Mg Ca and K were the major elements present. Khodier et al reported that these types of particles with similar compositions are emitted from oil-fired power plants [11]. There is considerable experimental evidence that even if most of the mass for the condensational accumulation mode growth of aerosol nuclei comes from hydrocarbon gas-to-aerosol conversion, it is the sulphur from SO_2 that provides the nuclei for the aerosol particles to continue growing in concentrations up to 300 μm^3 cm^{-3} in urban areas, hence it is not surprising to see sulphur as the main element present in most of these particulates [12].

(a)

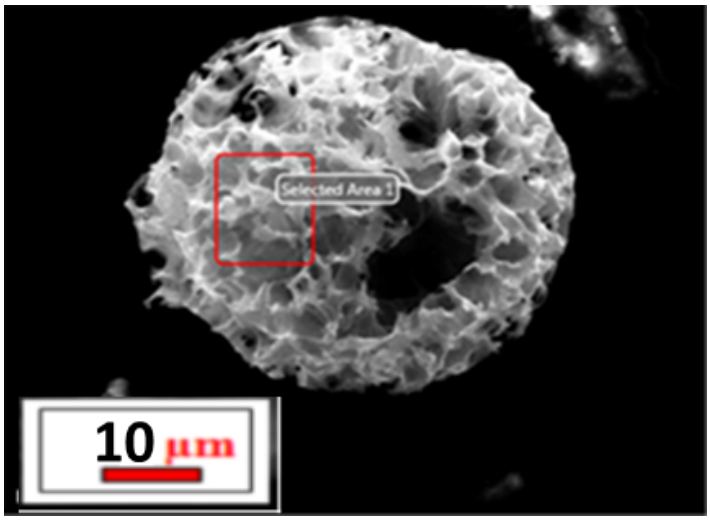

(b)

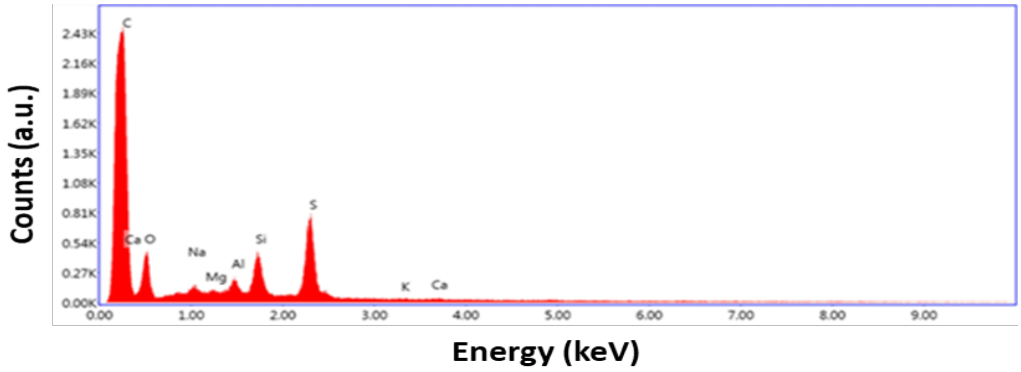

Figure 6.4.6 (a) SEM micrograph of a typical spherical carbonaceous particle from oil fly ash and (b) the particle's EDS composition.

The secondary electron image from other spherical particles found on the sample is shown in Figure 6.4.7a. EDS analysis of these particles (Figure 6.4.7b) identified Si and Al in addition to Fe and Ti. It is not clear if the Si and Al signal is derived from the particles or the underlying material which is likely an alumino-silicate (sand) particle matrix. When considering the small size of the individual particles (~200nm) and the accelerating voltage of the electron beam (10-30kV) the majority of the EDX signal being generated will come from the 'background' material because the bulb volume of electron interaction (from which the X-ray are generated) will be several cubic microns i.e. from a volume much bigger than the individual particles. Whilst Al could be attributed to nearby smelters in the industrial area [13] it is more reasonable to attribute it to natural alumino-silicate materials due to the coincident presence of oxygen.

FIB sectioning followed by TEM analysis (diffraction and/or elemental analysis) would be the only way to fully confirm that individual particles are completely metallic and not metal-oxides. This was achieved in the previous chapter for such particles deposited onto plaster surfaces.

In addition to the spherical particles, Na, Cl and lesser amounts of Ca and Mg were also recorded. Again, the presence of these particles is ascribed to sea spray carried on the wind from the Red Sea near the site, as with the western location samples.

(a)

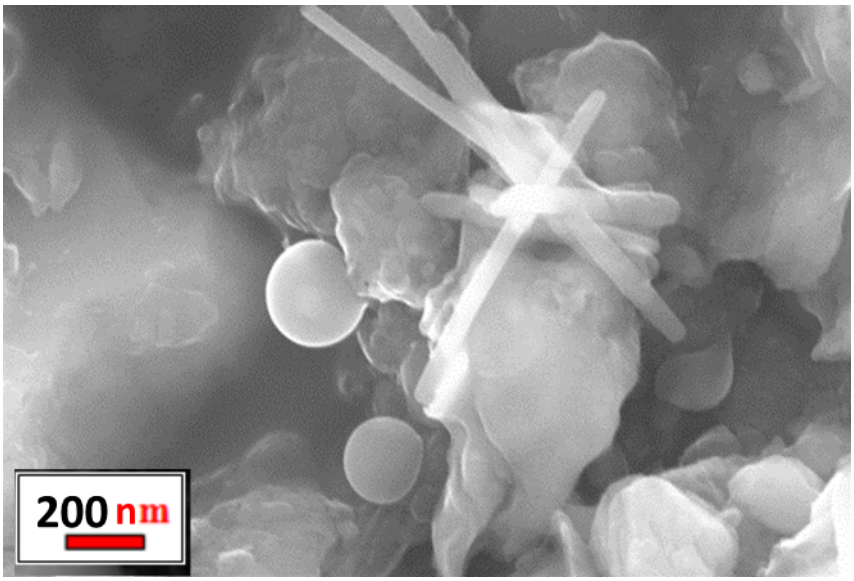

(b)

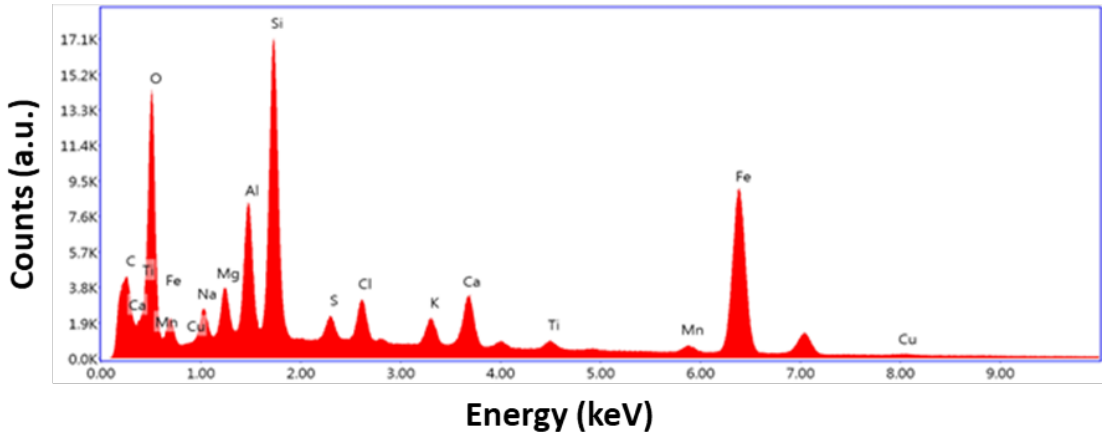

Figure 6.4.7 (a) A secondary electron image of the particulate and (b) EDS spectrum of the imaged area.

The secondary electron image in Figure 6.4.8a showed an aggregated bundle of spherical particles clustered together. EDS investigation (Figure 6.4.8b) found that the particle consisted of O, Si, Al and large amount of Fe [14]. Na and Cl present can be assumed once again to be from sea salt, whereas the presence of Fe is most likely to be due to emissions flaring off of the nearby oil refinery.

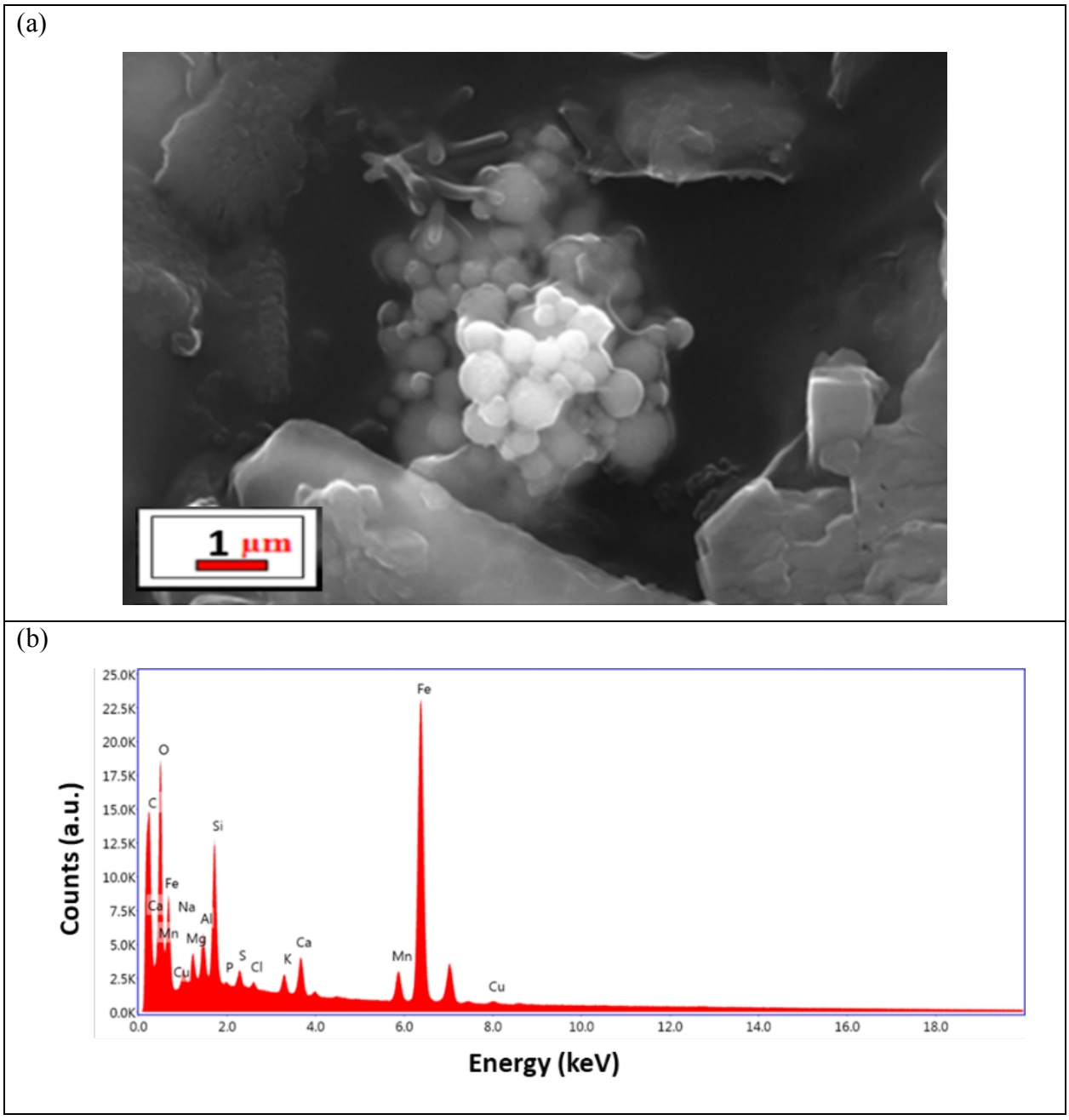

Figure 6.4.8 (a) SEM image of a spherical iron particles and (b) EDS spectrum of the corresponding particle.

This can happen when clusters of particulates are turbulently mixed in the high-temperature gases or vapours emitted from the refineries, especially where additives containing organometallic compounds, metal deactivators, lubricants, corrosion inhibitors and fuel stabilizers are still present in combusted fuel or where reactions have occurred at some point in the pipeline and are released during combustion.

(a)

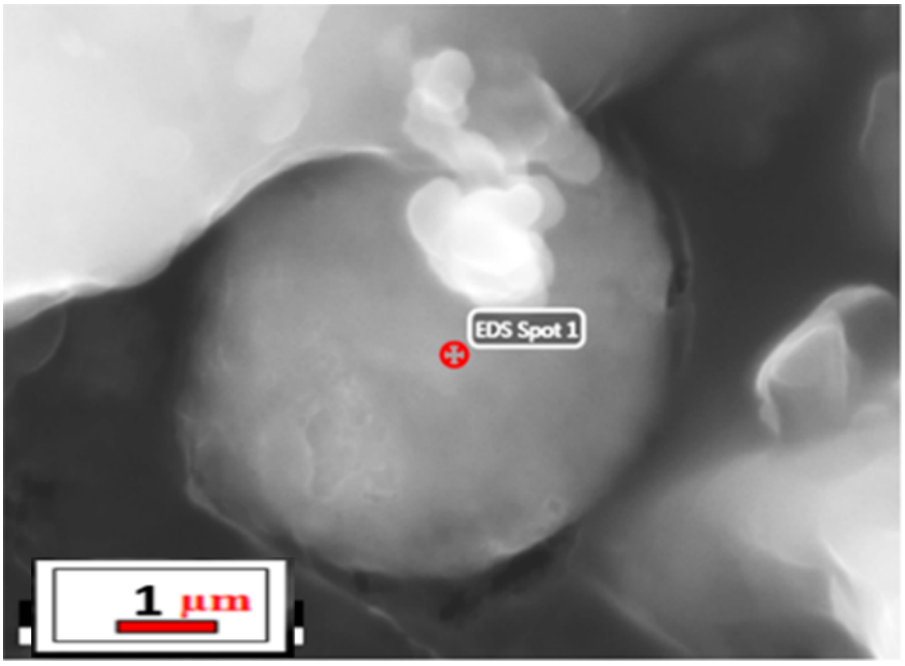

(b)

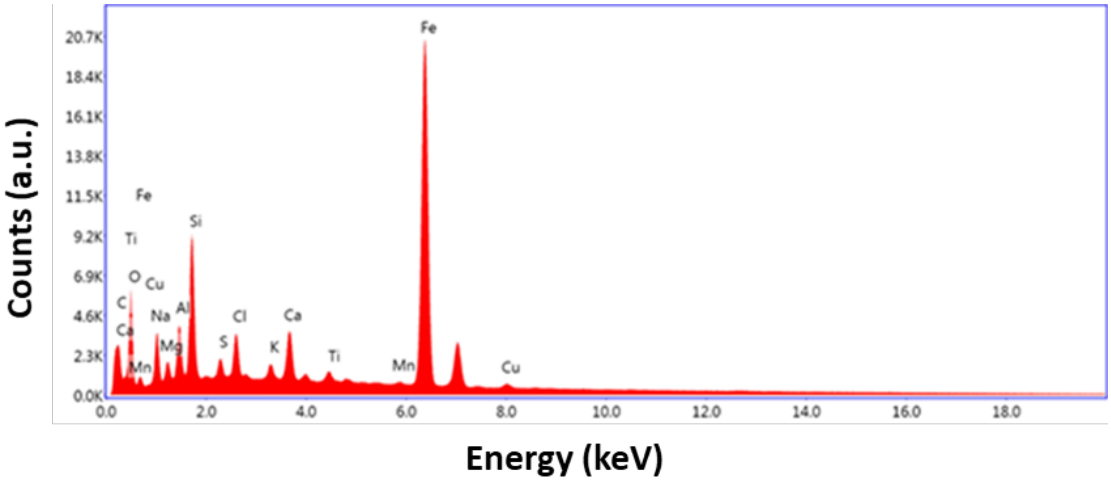

Figure 6.4.9 (a) A secondary electron micrograph of the larger (2micron diameter) spherical iron particle and (b) EDS spectrum from a point on the spherical metallic particle.

The SEM micrograph presented in Figure 6.4.9a demonstrates another typical example of a suspected spherical iron particle found with a diameter of 2 μm. The EDS results confirmed that particle was majority Fe, with trace amounts of Ti and Cu, suggesting it is the same type of metallic particle seen across the samples (Figure 6.4.9b). The source of these particles is expected to be from the emissions of the industrial activities around the area. This is discussed in more detail later in the chapter.

6.4.3 Analysis of the Collected Filter Samples

A total of 60 filtered samples were analysed using XRF. The filter samples were collected by The General Authority of Meteorology and Environment Protection (Figure 6.2.1), as described previously in section 6.3. Fiberglass tape for 60 samples, Dimensions: 483 x 324 x 266 mm (W x D x H).

The Niton FXL field X-Ray Thermo Scientific high-resolution X-ray Fluorescence Spectrometer shown in Figure 6.4.10 was used for these analyses. XRF is a technique that produces characteristic secondary x-rays also called fluorescence from a specimen that have been subjected to bombardment by high-energy x-rays It is a compact and lightweight instrument offering the highest XRF-based analysis performance and lowest detection levels for more than 40 critical elements (including Fe, Ti, Zn, S and Ca, crucial for this study). Test results can be obtained from this instrument within minutes rather than days, which saves both a significant amount of time and the expense of transporting samples offsite for the purpose of separate ex-situ testing and analysis [15].

This study has excluded certain elements for measurements because the results were at the limit of detection for the instrument. It is well understood that the aerosol populations in a given area can change as a function of numerous different parameters, both natural and anthropogenic, that can change seasonally. For example, in Jeddah the predominant wind direction is from the north west, carrying marine aerosols from the Red Sea. However, seasonal shifts in wind direction can reduce the abundance of marine aerosol salts, whilst increasing the amounts of alumino-silicates (from sands) and also salts derived from terrestrial evaporite sources, which have a higher

concentration of light metals e.g. K and Li. The anthropogenic component of aerosols is likely to have less seasonal variation but will have diurnal variation based on traffic patterns and industrial working shifts.

Figure 6.4.10 Showing the Thermo Fisher Scientific Niton FXL 950 X-ray Fluorescence (XRF) spectrometer.

Figure 6.4.11 reports the resultant combined stacked bar chart of the data showing the concentrations identified for the variety of elements tested. Each detected element's daily average is plotted vs its concentration in mg/m^3.

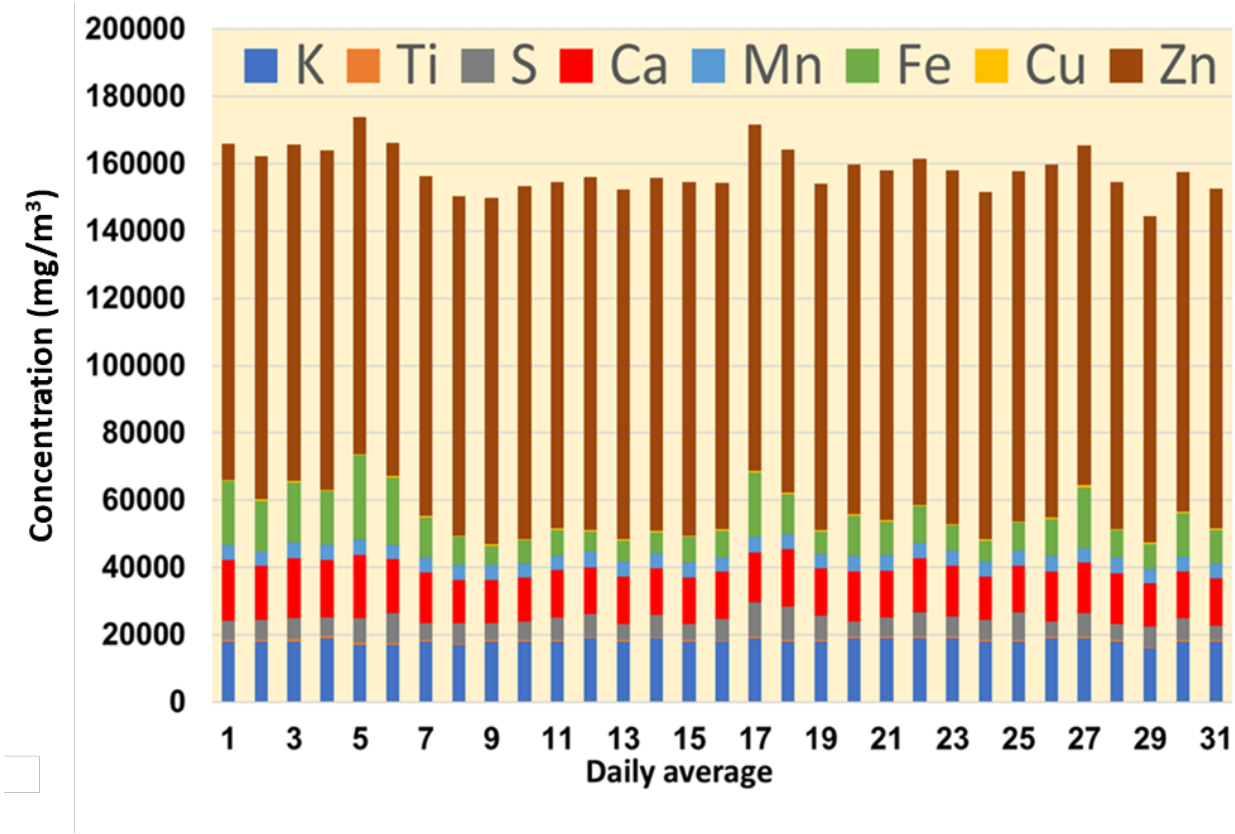

Figure 6.4.11 Bar chart showing the elemental composition of the filter samples.

Concentration of the elements K, Ti, S, Ca, Mn, Fe, Cu and Zn are presented in Figure 6.4.11. Other studies [16, 17, 18] have been conducted and showed that the increase in atmospheric pollution can cause serious damage to living organisms and non-living materials. These studies include pollution from transportation and industrial activities as the main sources for atmospheric pollution, neglecting other possible sources.

It can be seen from the results that Zn is most abundant in these samples, which is unusual and ascribed to incomplete combustion of heavy oil (both Zn & Fe) from local refineries. Cu makes a very small contribution to the overall pollution, but this element is also ascribed to the fossil fuel burning [11]. These results showed the composition of metallic elements expected from the industrial activities near the sampling station.

6.5 Summary Discussion

Previous authors [19, 20] have related spherical aerosol particles to anthropogenic sources (usually high temperature combustion processes), whereas other studies have ascribed an association between particles with irregular morphologies as having a natural source of origin [21, 22]. This would seem to be an oversimplification.

In some studies that have noted Fe-rich particles (PM25 and below), the analysed samples have documented iron both in spherical particles and in irregularly shaped particles, which indicates that this element had its origin in both natural and anthropogenic sources. Manganese is frequently emitted during the combustion of hydrocarbons [23] or from the metallurgical industry [24, 25]. Rounded zinc oxide particles have also been associated with high temperature combustion processes and metallurgical industrial emissions [25].

It is generally accepted that in areas of frequent vehicular traffic; the presence of metallic Cu, Fe, and Zn aerosol particles can be derived from traffic activity. In urban areas, these metals are released as a consequence of tire wear and brake abrasion when vehicles are continuously accelerating and decelerating [21].

Some particles which are irregular shaped, have previously been associated with having a mineral origin [26] which for Jeddah is quite feasible when considering the surrounding desert environment. However, sources such as vehicle emissions can also produce angular particles either from engine emissions (as metal oxides) or from break abrasion (as metal particles).

From the present analysis, where spherical metal particles constituted primarily of Fe and Cu have been observed, we ascribe the source of material to high temperature combustion processes – either from metallurgical manufacturing or from high temperature pyro-processing at the city's oil refinery. The distinguishing feature is the sphericity of the particles which rules out vehicle emissions, which are typically angular.

The analysis in the previous chapter has provided good evidence that these spherical particles observed in both air samples and on building surfaces are metallic rather than metal oxide. Due to the low burning temperatures in combustion engines and the deliberate entrainment of oxygen,

metal-oxides are the primary metal-bearing aerosol constituent from vehicle exhausts and not metallic particle. Hence, these spherical particles can only be derived from a very high-temperature and oxygen poor industrial process, whereby the particles form in a gas flow from condensation of metallic vapours or solidification of metallic melt droplets. If oxygen was present during formation, then metal particles would not form – they would be oxide.

Accordingly, we tentatively attribute this source of metallic micro-pollution to high-temperature industrial plant in the city. Considering the predominant wind direction is from the north west, it is suggested that the primary source may possibly be the coastal desalination plant rather than the large industrial area to the south, which includes a large oil refinery.

6.6 Summary

- Both spherical and irregular aerosol micro-particles were observed in air samples collected from two different parts of the historic quarter of Jeddah.
- Elemental compositions of metal-containing aerosols obtained from the historical site were typically rich in C, Fe, Cu and Zn. In addition, Ca, Al, Si, Na and Cl were identified.
- Elemental compositions of aerosols collected from the city's southern station of the General Presidency of Meteorology and Environment Protection were found comprised predominantly of Zn and Fe with more limited amounts of Mn and Cu. In addition, Ca, K, Ti and S were identified.
- Analysis indicates a mixture of natural and anthropogenic aerosols present in the air during sampling. Natural particulates include both marine salts as well as alumino-silicates derived from the sands of the surrounding desert. Anthropogenic particles included spherical metal micro-particles which are attributed to nearby high-temperature industrial combustion processes.

This finding is agreement with the SEM-EDS results obtained from plaster surfaces across the historic buildings. The results are heavily suggestive of considerable pollution of the historical site in Jeddah due to industrial activity.

6.7 References

[1] Calvo, A.I., Alves, C., Castro, A., Pont, V., Vicente, A.M., Fraile, R., (2013). Research on aerosol sources and chemical composition: Past, current and emerging issues. Atmospheric Research. 120-121, pp1-28. Available at: https://doi.org/10.1016/j.atmosres.2012.09.021.

[2] Salter, M.E., Hamacher-Barth, E., Leck, C., Werner, J., Johnson, C.M., Riipinen, I., Nilsson, E.D., Zieger, P., (2016). Calcium enrichment in sea spray aerosol particles. Geophysical Research Letters. 43, pp1-9, Available at: doi:10.1002/2016GL070275.

[3] Lee Jr., R.E., von Lehmden, D.J., (1973). Trace Metal Pollution in the Environment, Journal of the Air Pollution Control Association, 23(10), pp. 853-857, Available at: DOI: 10.1080/00022470.1973.10469854.

[4] Scott, D., Seifert, W., Westcott, V., (1994). The Particles of Wear. Scientific American Offprints, pp10-11.

[5] Fitch, J., Gebarin, S., (2019). Origin of Spherical Particles in Lubricants. Noria Corporation. [Online] Available at: www.machinerylubrication.com/Read/719/ [Accessed 17/04/2019].

[6] Andreae, M.O., Charlson, R.J., Bruynseels, F., Storms, H., Van Grieken, R., Maenhaut, W., (1986). Internal mixture of sea salt, silicates, and excess sulfate in marine aerosols. Science. 232(4758), pp1620-1623. Available at: https://www.ncbi.nlm.nih.gov/pubmed/17812139.

[7] Voorhees, P.W., Johnson, W.C., (2004). The Thermodynamics of Elastically Stressed Crystals. Solid State Physics – Advances in Research and Applications. 59(C), pp1-201. Available at: https://doi.org/10.1016/S0081-1947(04)80003-1.

[8] Alcántara, J., B, Chico., Iván, D., Daniel de la, F., Manuel, M., (2015). Airborne chloride deposit and its effect on marine atmospheric corrosion of mild steel. Corrosion Science, 2015. 97: p. 74-88. Available at: DOI: 10.1016/j.corsci.2015.04.015.

[9] Feliu, S., Morcillo, M., and B. Chico., (1999). Effect of distance from sea on atmospheric corrosion rate. Corrosion, 55(9): p. 883-891. Available at: https://doi.org/10.5006/1.3284045.

[10] Swindles, G.T., (2010). Dating recent peat profiles using spheroidal carbonaceous particles (SCPs). Mires and Peat. 7(3) pp1-5.

[11] Khodeir, M., Shamy, M., Alghamdi, M., Zhong, M., Sun, H., Costa, M., Chen, L and Maciejczyk, P., (2012). Source apportionment and elemental composition of $PM_{2.5}$ and PM_{10} in Jeddah City, Saudi Arabia. Atmospheric Pollution Research 3, pp331-340. Available at: https://doi.org/10.5094/APR.2012.037.

[12] Whitby, K.T., (1977). The Physical Characteristics of Sulfur Aerosols. Atmospheric Environment. 12(1-3), pp135-159. Available at: https://doi.org/10.1016/0004-6981(78)90196-8.

[13] Höflich, B.L., Weinbruch, S., Theissmann, R., Gorzawski, H., Ebert, M., Ortner, H.M., Skogstad, A., Ellingsen, D.G., Drabløs, P.A., Thomassen, Y., (2005). Characterization of individual aerosol particles in workroom air of aluminium smelter potrooms. Journal of Environmental Monitoring. 7(5), pp419-424. Available at: https://www.ncbi.nlm.nih.gov/pubmed/15877161.

[14] Habeebullah, T. M., (2016) Chemical composition of particulate matters in Makkah – focusing on cations, anions and heavy metals. Aerosol Air Qual Res. 16, pp336–347.

[15] Thermo Fisher Scientific, (2016). Niton FXL Field X-ray Lab.[online] Website available at: https://www.thermofisher.com/order/catalog/product/NITONFXLXRF [Accessed 17/04/2019].

[16] Hussein, T., Alghamdi, M.A., Khoder, M., AbdelMaksoud, A.S., Al-Jeelani, H., Goknil, M.K., Shabbaj, I.I., Almehmadi, F.M., Hyvärinen, A., Lihavainen, H. and Hämeri, K., (2014). Particulate matter and number concentrations of particles larger than 0.25 μm in the urban atmosphere of Jeddah, Saudi Arabia. Aerosol and Air Quality Research, 14(5), pp.1383-1391.

[17] Lim, C.C., Thurston, G.D., Shamy, M., Alghamdi, M., Kohder, M., Mohorjy, A.M., Alkhalaf, A.K., Brocato, K., Chen, L.C., Costa, M., (2018). Temporal variation of fine and coarse particulate matter sources in Jeddah, Saudi Arabia. Published in final edited form as: J Air Waste Manag Assoc. 68(2), pp.123–138.

[18] Lee Jr, R.E., von Lehmden, D.J., (1973). Trace Metal Pollution in the Environment, Journal of the Air Pollution Control Association, 23(10), pp. 853-857, Available at: DOI: 10.1080/00022470.1973.10469854.

[19] González, L.T., Longoria-Rodriguez, F.E., Sánchez-Domínguez, M., Leyva-Porras, C., Acuña-Askar, K., Kharissov, B.I., Arizpe-Zapata, A., Alfaro-Barbosa, J.M., (2018). Seasonal variation and chemical composition of particle matter: A study by XPS, ICP-AES and sequential microanalysis using Raman with SEM/EDS. J. Environmental Science. 74, pp32–49. Available at: https://doi.org/10.1016/j.jes.2018.02.002.

[20] Li, W., Shao, L.Y., (2009). Transmission electron microscopy study of aerosol particles from the brown hazes in Northern China. J. Geophysical. Research, 114, 1–10. Available at: https://doi.org/10.1029/2008JD011285.

[21] Aragón-Piña, A., Campos-Ramos, A.A., Leyva-Ramos, R., Hernández-Orta, M.; Miranda-Ortiz, N.; Luszczewski-Kudra, A., (2006). Influencia de las emisiones industriales en el polvo atmosférico de la Ciudad de San Luis Potosí, México. Rev. Int. Contam. Ambient, 22, pp5–19.

[22] Buseck, P.R., Jacob, D.J., Posfai, M., Li, J., Anderson, J.R., (2000). Minerals in the air: An environmental perspective. International Geology Review., 42, pp577–594. Available at: https://doi.org/10.1080/00206810009465101.

[23] Pacyna, J.M., Semb, A., Hanssen, J.E., (1984). Emission and long-range transport of trace elements in Europe. Tellus: Chemical and Physical Meterology., 36, pp163–178. Available at: https://doi.org/10.3402/tellusb.v36i3.14886.

[24] Querol, X., Alastuey, A., Rosa, J., Sánchez-De-La-Campa, A., Plana, F., Ruir, C.R., (2002). Source apportionment analysis of atmospheric particles in an industrialized urban site in Southwestern Spain. Atmospheric Environment, 36, pp3113–3125. Available at: https://doi.org/10.1016/S1352-2310(02)00257-1.

[25] Alastuey, A., Querol, X., Plana, F., Viana, M., Ruiz, C., Sanchez de la Campa, A., De la Rosa, J., Mantilla, E., Garcia dos Santos, S., (2006). Identification and chemical characterization of industrial particulate matter sources in Southwest Spain. J. Air Waste Manag. Assoc., 56, pp993–1006. Available at: https://doi.org/10.1080/10473289.2006.10464502.

[26] Breed, C.A., Arocena, J.M., Sutherland, D., (2002). Possible sources of PM_{10} in Prince George (Canada) as revealed by morphology and in situ chemical composition of particulate. Atmos. Environ., 36, pp1721–1731. Available at: https://doi.org/10.1016/S1352-2310(01)00500-3.

CHAPTER 7
THE ROLE OF METALLIC AEROSOL MICRO-PARTICLES IN THE DEGRADATION OF BUILDING MATERIALS

7.1 Background

In the previous chapters it has been identified from analysis of field samples, that plaster surfaces have a notable population density of micro-scale metallic particles. This observation also correlates with results obtained from aerosol particulate sampling conducted in the Historical District of Jeddah. The combined data confirms that this district of Jeddah suffers heavy air pollution, with an unusual portion of this pollution as metallic particles which are often spherical in form. When deposited onto building surfaces (as observed) these metallic particles may subsequently act to enhance the natural rate of building material degradation. Specifically, these particles when situated within the micro-cracks or micron-scale depressions on the material surface may cause accelerated degradation via chemical or mechanical means.

The observation of metallic aerosol particles is somewhat unusual. Previous research, examining particulate air pollution from different cities around the world have frequently reported metal oxide particles as a common constituent of air pollution [1].

The objective of this work is to use accelerated ageing to investigate how these observed micro-particles will evolve as a function of time and temperature, to provide an understanding of the mechanisms by which surface degradation might be accelerated due to the presences of the particles as they age. It is expected that volumetric expansion of the metal micro-particles during progressive corrosion will cause a mechanical degradation of building material surfaces.

The role of the effect of metallic aerosol particles in the degradation of building material surfaces has rarely been studied and that is what makes this research work novel.

7.2 Experimental Procedure

The specific aim of this experimental work was to conduct a to-scale test of metal micro-particle oxidation, when said particles were entrapped in micro-scale holes on a limestone surface. This allows for direct observation of the oxidation process and any degradation it causes on the host material; thereby confirming the mechanism (or mechanisms) by which degradation occurs. It is well documented that the climate in Jeddah is both hot and humid for the majority of the year. Under such conditions, metal oxidation is strongly promoted and expected to occur at a rate notably higher than in temperate climatic zones like the UK.

7.2.1 Samples Preparation

Two types of base materials were used for this experiment, calcite single crystal and limestone from Manqabah Quarry. To simulate the observed metallic aerosol particles observed in earlier chapters, high-purity metallic iron powder from Alfa Aesar (99.9% pure Fe) was used. The powder comprised of spherical particles of <10 microns in diameter, with the smallest particles measured at 500nm diameter and the average particle diameter being 2.5 microns, as shown in Figure 7.2.1.

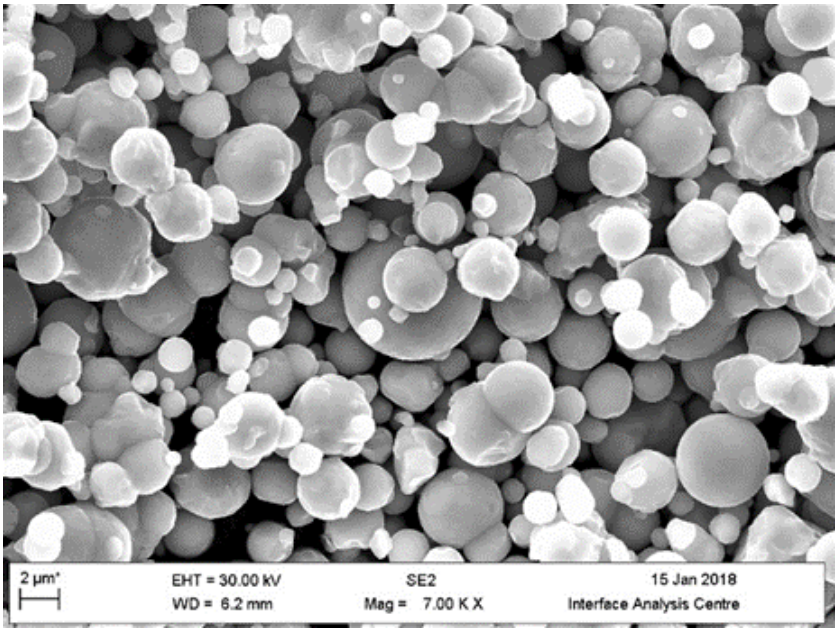

Figure 7.2.1 Shows SEM micrograph of the spherical iron powder.

7.2.1.1 Calcite Single Crystal

A single calcite crystal ($CaCO_3$) was used in initial experimental work. This was to provide a very simple but conservative test scenario. The sample was coated with gold avoiding any beam charging effects in the FIB-SEM instrument. The calcite crystal underwent FIB milling to create a series of square holes (10 x10x 15 μm). Figure 7.2.2 represents an ion-induced secondary electron micrograph showing the three holes before inserting the particles.

The Fe particles were subsequently inserted in the three holes using a Kleindiek micromanipulator in conjunction with an optical microscope. This was a difficult and time-consuming task, requiring significant trial and error testing on multiple samples due to the small size of samples and component micro-beads, required to undertake the experiment.

An example secondary electron micrograph obtained from the calcite crystal surface with the inserted iron particles before oxidation is shown in Figure 7.2.3. From this typical example, it is clear that multiple (rather than single) particles were inserted into the cavities, ascribed to electrostatic adhesion effects.

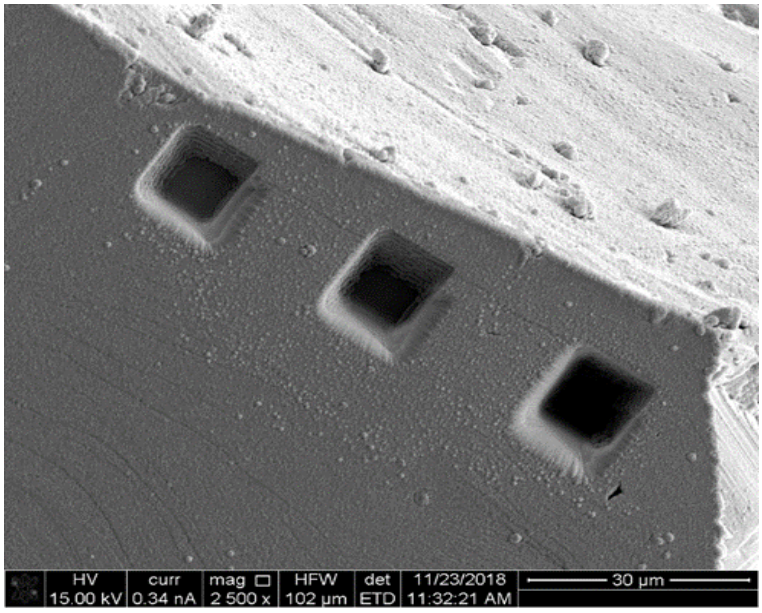

Figure 7.2.2 Ion-induced secondary electron micrograph showing the notch on the surface of calcite crystal.

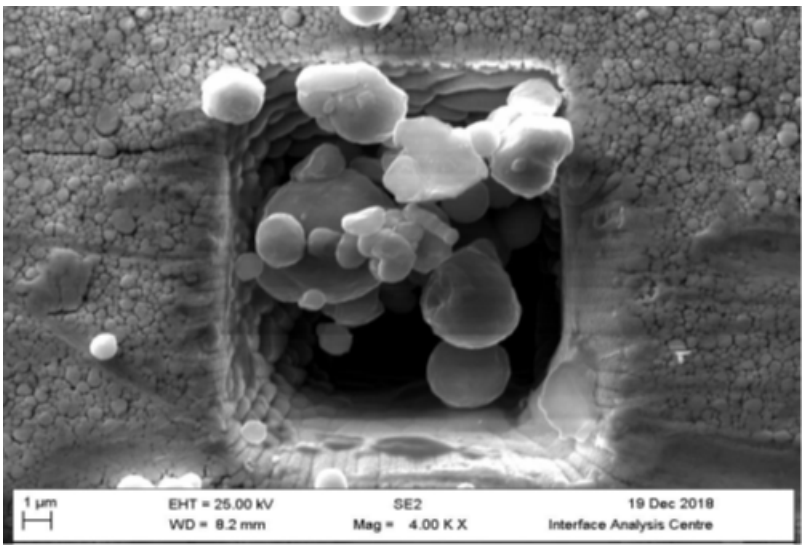

Figure 7.2.3 Secondary electron micrograph represents the spherical iron particles inside the notch on the surface of calcite crystal.

7.2.1.2 Limestone

Limestone material from Manqabah Quarry was also used for further experiments, representing the actual material of the Historic Buildings of Jeddah. Before the experiment, the material was coated with gold (as per the calcite sample) to a 5nm thickness by thermal evaporation in vaccuo to prevent surface charging in the FIB-SEM. A square hole measuring approximately (15 x 15x 25 µm) was made using the ion beam instrument. Figure 7.2.4 shows a SEM micrograph of the milled hole in the limestone sample.

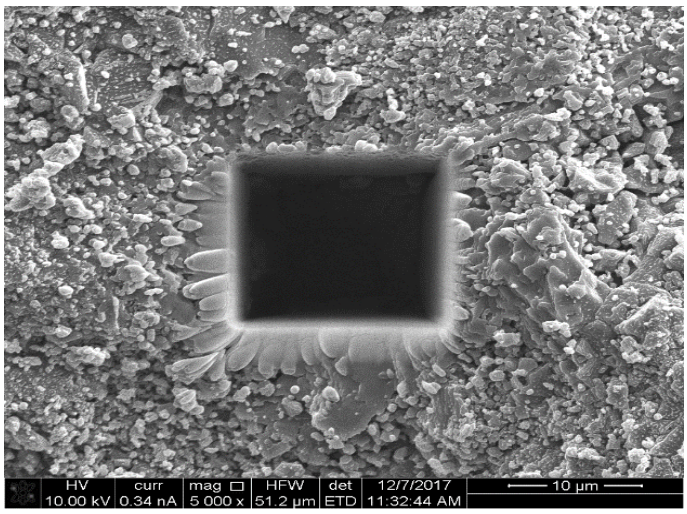

Figure 7.2.4 SEM micrograph of the hole created in limestone using FIB.

Subsequently the high purity spherical iron particles were inserted into the hole, following the process previously detailed; see Figure 7.2.5. The natural micro-scale roughness of the surface made it very easy to identify small surface deformations by comparing electron micrographs before and after particle insertion and before and after subsequent thermal oxidations.

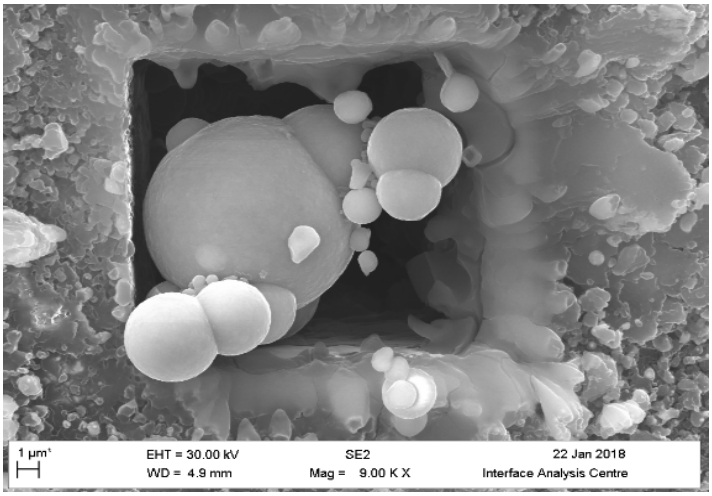

Figure 7.2.5 SEM micrograph of the iron particles inside the hole.

The difference between calcite and limestone is that calcite is a very widely distributed crystalline form of calcium carbonate, $CaCO_3$, found as limestone, chalk and marble while limestone is an abundant rock of marine and fresh-water sediments; primarily composed of calcite ($CaCO_3$); it occurs in a variety of forms, both crystalline and amorphous.

7.2.2 Thermal Oxidation Conditions

After preparation, the particle-impregnated samples were thermally aged using a Lenton furnace with a maximum operating temperature of 1200°C. The samples were exposed at 400°C in air, to induce controlled oxidation of the iron particles over a period of days. The exposure time condition is presented in Table 7.2.1. The thermal treatment was utilized as a method of accelerating the rate of metal particle oxidation and 400°C was selected as a temperature to induce relatively rapid oxidation but was below the 700°C thermal breakdown initiation temperature of $CaCO_3$ [2].

Table 7.2.1 Oxidation exposure time.

Exposure time/Hours	
Calcite Single Crystal	Limestone
12	12
24	24
48	48
72	72
96	96
196	196
-	288
-	672
-	1056

In addition, a Mettler-Toledo thermogravimetric analyzer with differential scanning calorimetry (TGA/DSC) was used to determine the oxidation rate of the iron powder more accurately under the same conditions. An iron powder sample weighing ~200 mg was placed in alumina crucible and heated to 400°C using a 10°C min^{-1} heating ramp using a dry nitrogen flow of 50 cm^3 min^{-1}. Once at the 400°C reaction temperature, a flow of air was passed through the instrument and the oxidation was measured by weight-gain and calorimetric change.

The relationship between the weight gain of the iron powder and period of exposure (time) was observed to follow a parabolic relationship, as shown in Figure 7.2.6. This indicated rapid initial oxidation followed as a surface oxide was established followed by more gradual oxidation as the oxide thickened and the metal was progressively consumed.

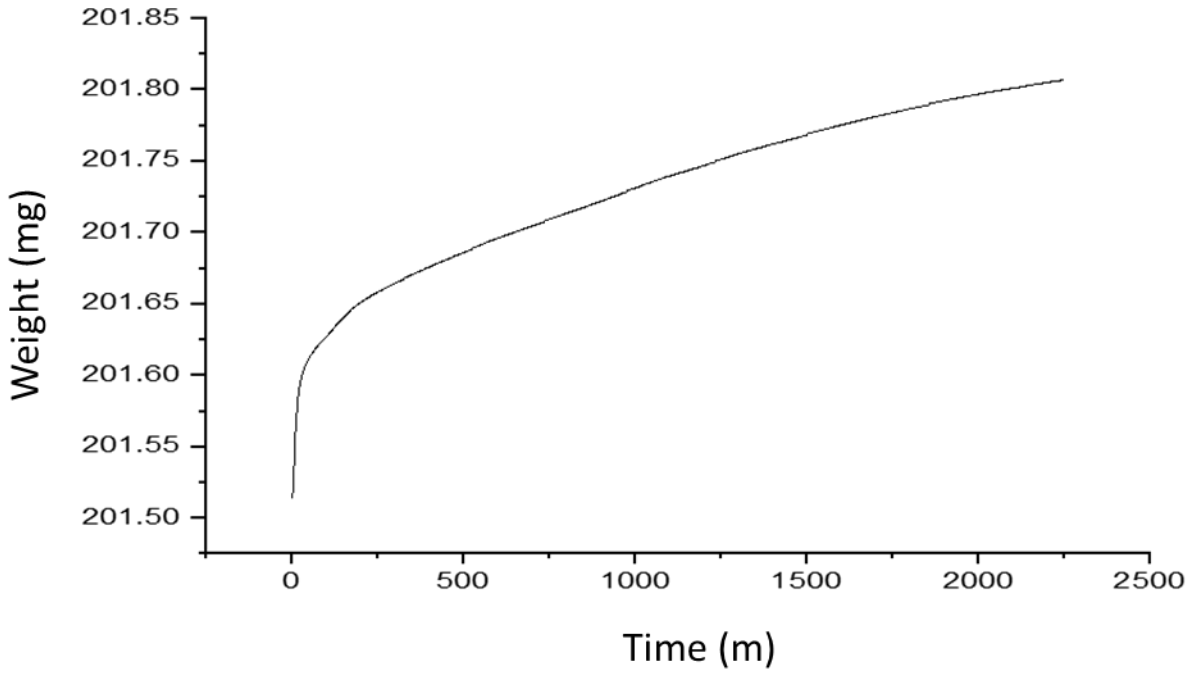

Figure 7.2.6 TGA result show the oxidation rate of Fe powder particles over ~40 hours.

7.3 Results and Discussion

The results from the calcite single crystal and limestone materials are described separately in the following sections. The former, single crystal material provides a conservative approximation of the true material properties of the Jeddah building materials, specifically the yield strength.

7.3.1 Calcite Single Crystal

7.3.1.1 SEM Results

Figure 7.3.1 shows the SEM micrograph of the ion-milled hole with inserted iron particles, before the thermal treatment. It can be seen that multiple particles are present in the hole, which was found to be an unavoidable limitation of the experimental setup. Particles are seen clearly sitting at different depths down to the bottom of the hole.

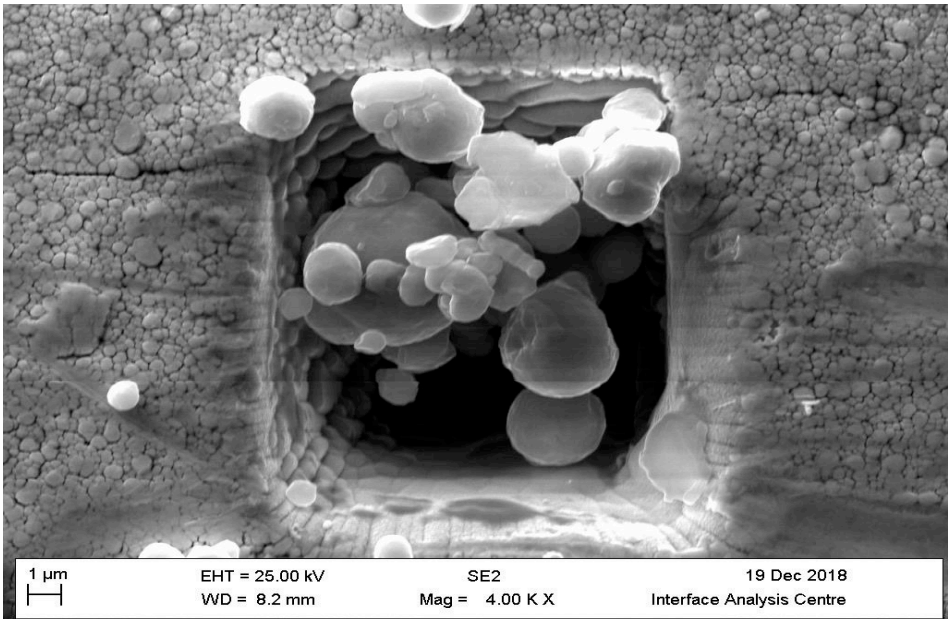

Figure 7.3.1 SEM micrograph of the as prepared sample with the embedded spherical Fe particles before oxidisation.

The SEM micrograph depicted in Figure 7.3.2 provides a magnified view of the inserted iron particles within the ion-milled in the top surface of single crystal after 48 hours of thermal treatment. The iron particles have clearly undergone oxidation, with a clear volume expansion. On spherical particles, small outwardly projecting nano-blades are evident, typical of haematite (Fe_2O_3).

In addition, by comparison of the surrounding surface features between micrographs, the onset of micro-cracking can be evidenced, indicating that the hydraulic forces generated by the volume expansion of the metal particles was sufficient to overcome the critical yield strength of the calcite crystal.

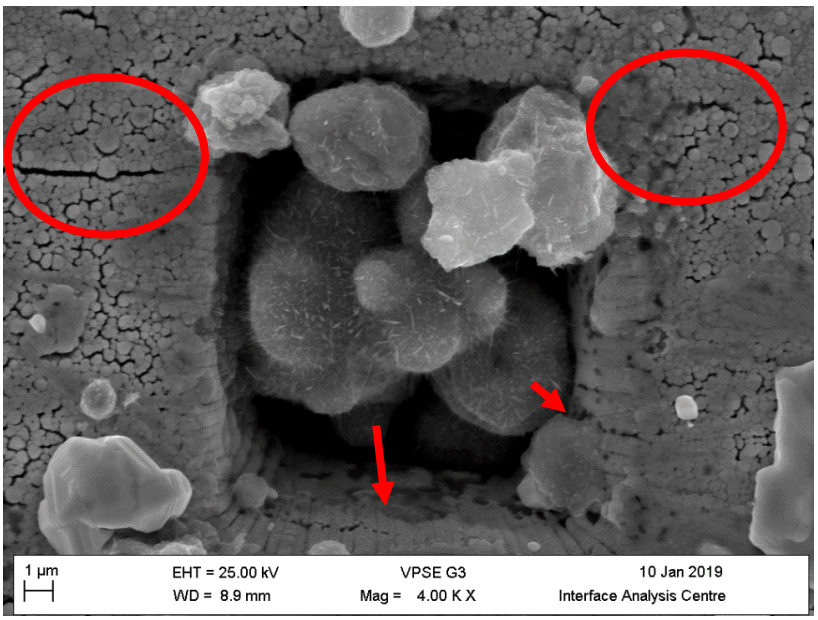

Figure 7.3.2 SEM micrograph showing the particles expansion after 48 hours oxidised at 400^0C. Red circles indicated areas where micro-cracking has developed most obviously.

Figure 7.3.3 shows a SEM micrograph of the single crystal after being thermally treated for 96 hours at 400^0C. It shows considerable further volume expansion of the Fe particles by oxidation, with some deformation occurring for the particles located deeper inside the hole.

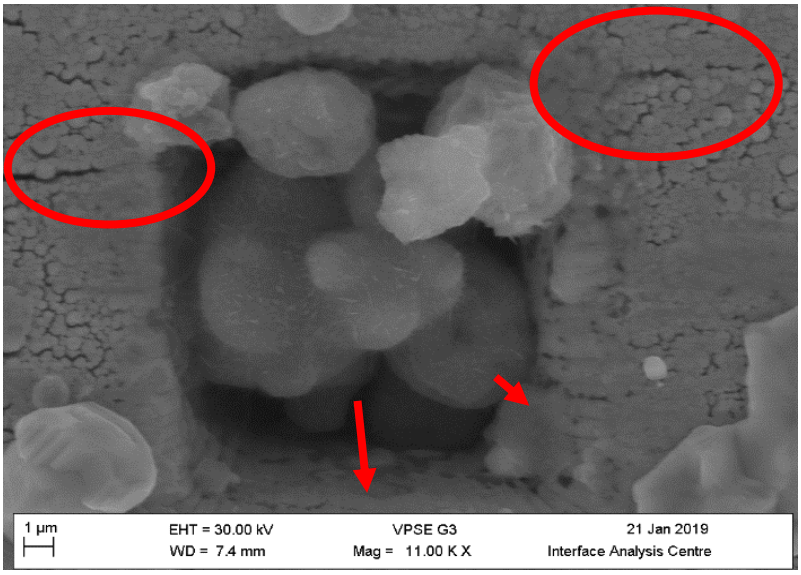

Figure 7.3.3 SEM micrograph showing the oxidation-related growth of the Fe particles after 96 hours exposure in air at 400^0C.

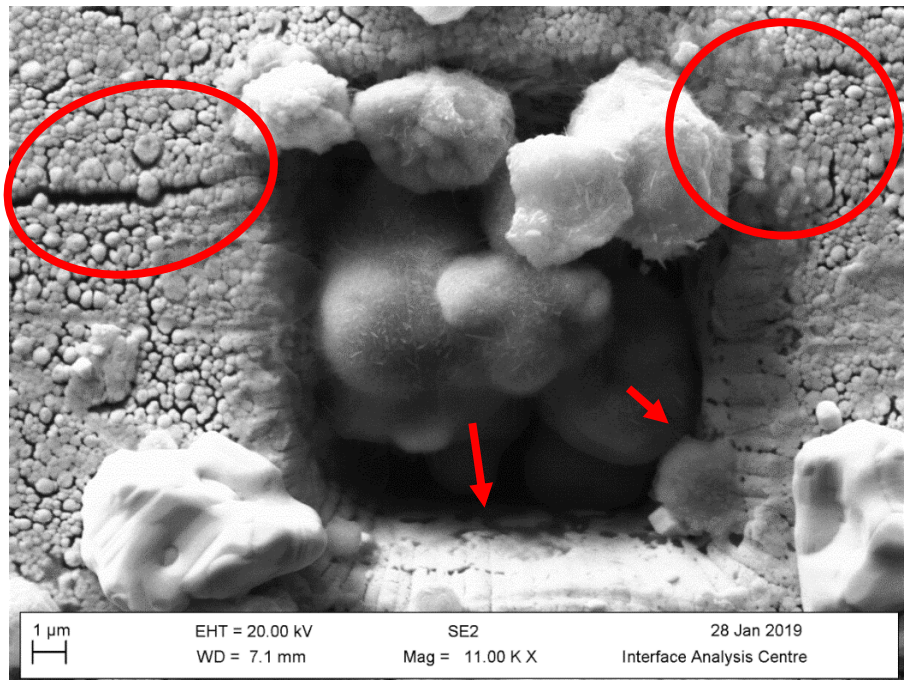

Figure 7.3.4 SEM micrograph of oxidation growth of Fe in the sample after 196 hours at 400^0C.

After 196 hours at 400^0C the Fe spheres are ascribed to have fully oxidised, due to the lack of any significant particle growth between 96 and 196-hours thermal treatment. The oxidation of the particles had caused an almost total infilling of the free space in the milled holes. What is also noteworthy is that the micro-cracks first observed to be opening after just 48 hours have further opened to 196 hours. Figure 7.3.4 shows the cracks on the surface, with the crack on the left-hand side showing the most significant opening.

7.3.1.2 X-Ray Tomography (XRT) Results

The technique of X-ray computed tomography (XRT) allows a 3D visualization of samples based on the processing of stacks of numerous angularly rotated 2D radiographs to create a computed tomogram. Radiography and XRT allows the viewing of the structure inside an inhomogeneous opaque object on the basis of density differences which cause differential X-ray attenuation. There are three possible mechanisms for the interaction of x-rays with solid matter namely, absorption, coherent or Compton scattering. The mechanism most likely to occur is based on the energies of the incident X-rays. Regardless, the primary intensity (or flux) of the incoming X-ray beam is

lowered after penetrating the object as a proportion of the photons are stopped, either by adsorption of scattering interactions within with the sample material [3, 4].

In this study, a Zeiss Xradia 520 Versa 3D x-ray microscope was used for analysis, with a purported 1µm resolution for resolving individual features. Example XRT 3D projections from the calcite single crystal sample with inserted Fe particles are shown in Figure 7.3.5, for 3 different periods of thermal treatment: 0 hours, 96 hours and 196 hours. The data clearly shows:

a) The sample before the application of heating. The iron micro-particles can be observed in the milled hole and are suitably resolved due to the large density difference between the calcite (2.71 g/cm^3) and metallic iron (7.87 g/cm^3). The particles are on the resolution limit of the X-ray microscope (Figure 7.3.5-A).

b) The sample after having been subjected to heat at a temperature of 400^{0}C for 96 hours. The tomogram shows the iron particles beginning to oxidise which is indicated by the changes in density as the metal (7.87 g/cm^3) is converted to the oxide haematite (5.26 g/cm^3). The surface of the calcite crystal has a significant number of micro-scale quasi-spherical particles on the crystal surfaces which make analysis of the FIB-pits very challenging. It is considered that these protrusions are an unexpected product of the thermal treatment (Figure 7.3.5-B).

c) The sample is now considered to be fully oxidised after being in the furnace at 400^{0}C for 196 hours. The density contrast between the residual Fe_2O_3 (5.26 g/cm^3) and calcite (2.71 g/cm^3) was not sufficiently high to be able to resolve the individual particles. Equally, the XRT did not have sufficient resolution to resolve the micro-cracks in the calcite that were observed by high magnification electron microscopy. However, the XRT does indicate the formation of what appears to be a more distinct linear crack running outwards from the 3 holes (Figure 7.3.5-C).

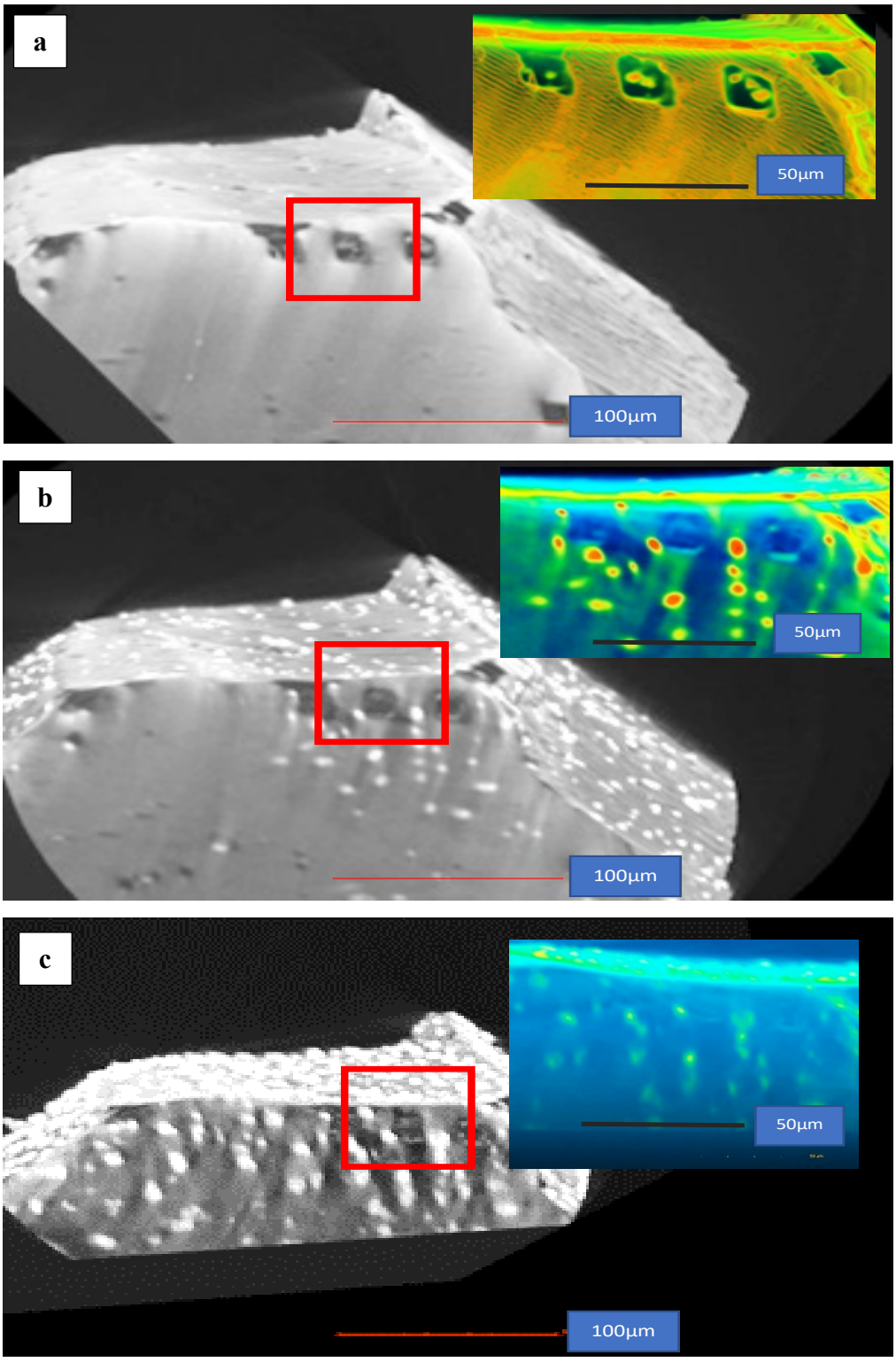

Figure 7.3.5 XRT imaging of calcite crystal with Fe particles oxidised at 400^{0}C; (a) As prepared, (b) After 96 hours and; (c) After 196 hours.

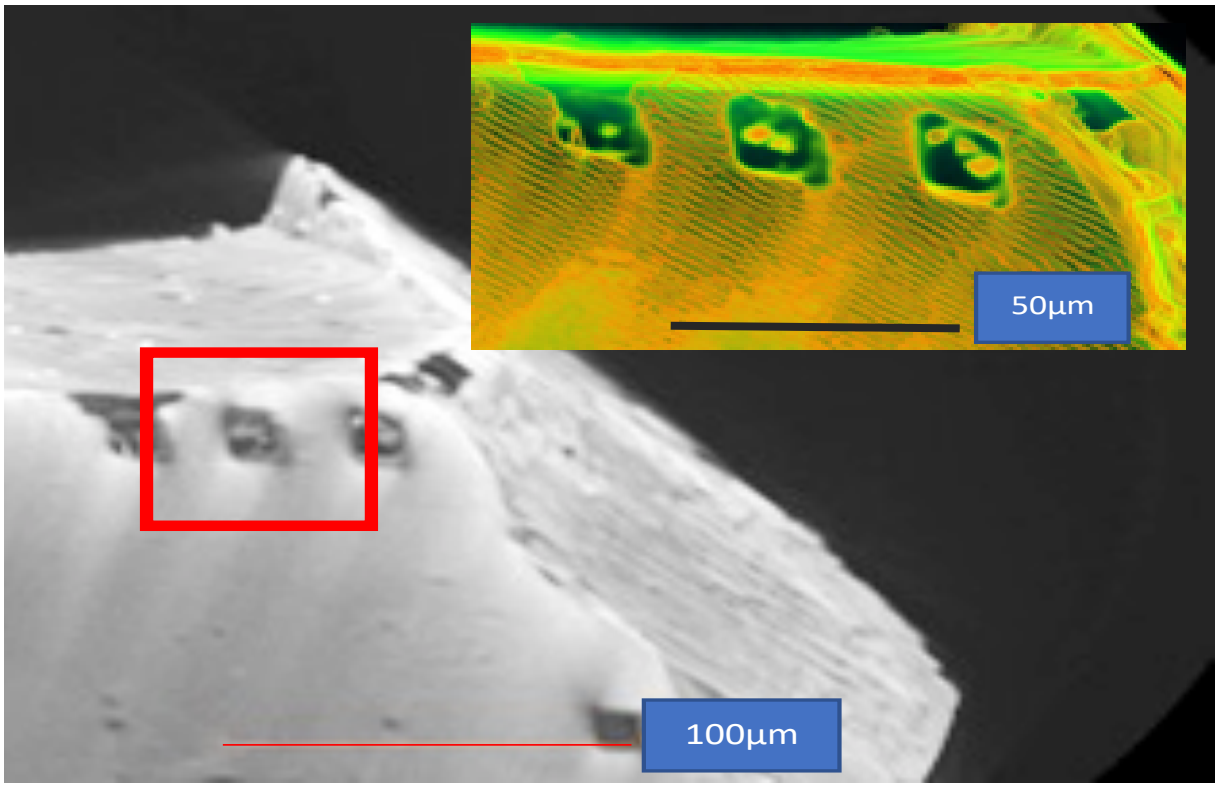

Figure 7.3.5-A XRT imaging of the initial calcite crystal with Fe particles before oxidation.

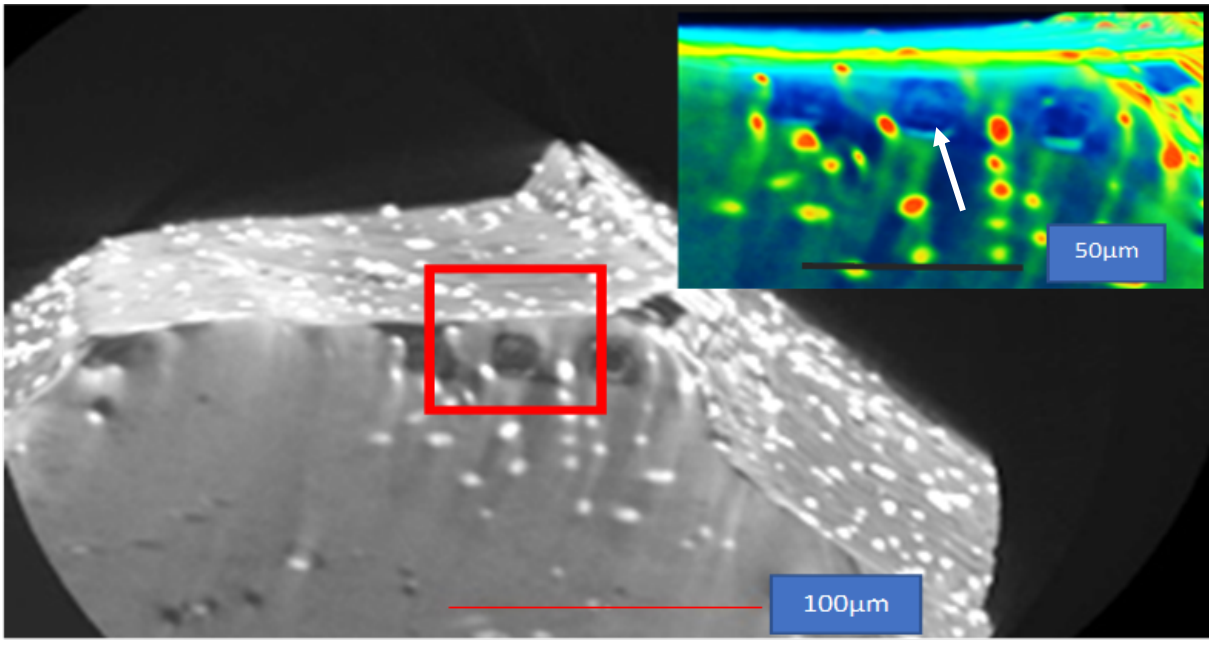

Figure 7.3.5-B XRT imaging of the initial calcite crystal with Fe particles after 196 hours oxidation.

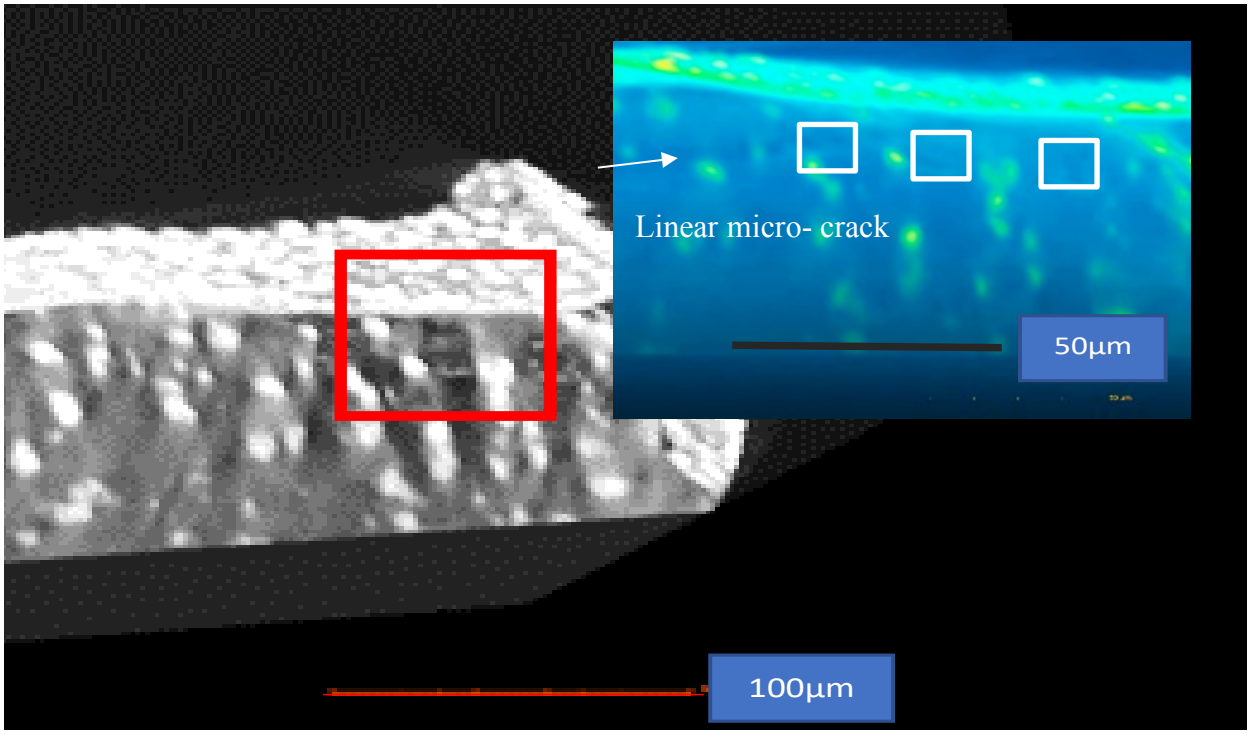

Figure 7.3.5-C XRT of the calcite crystal after 196 hours oxidation. A linear low-density feature is observed in the XRT data, which is ascribed to a possible linear micro-crack.

7.3.1.3 Dual Beam Results

In order to understand the extent of particle oxidisation and volume expansion following XRT analysis, the FIB-SEM instrument was used to conduct serial ion beam sectioning. This allowed direct observation of the particles infilling the milled holes on the calcite surface. Imaging of different cut sections of the particle-filled holes following thermal exposure at 400^0C for 196 hours is shown in Figure 7.3.6.

To undertake this sectioning, platinum was deposited over the hole and the immediately surrounding area to protect the sample from ion implantation damage. This is essential to enable smooth section faces to be cut into the material and allow differentiation of phase contrasts and micro-structures.

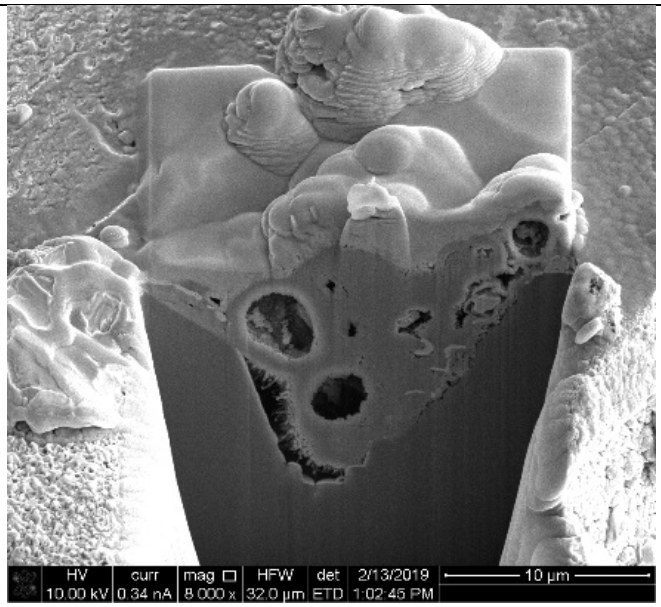

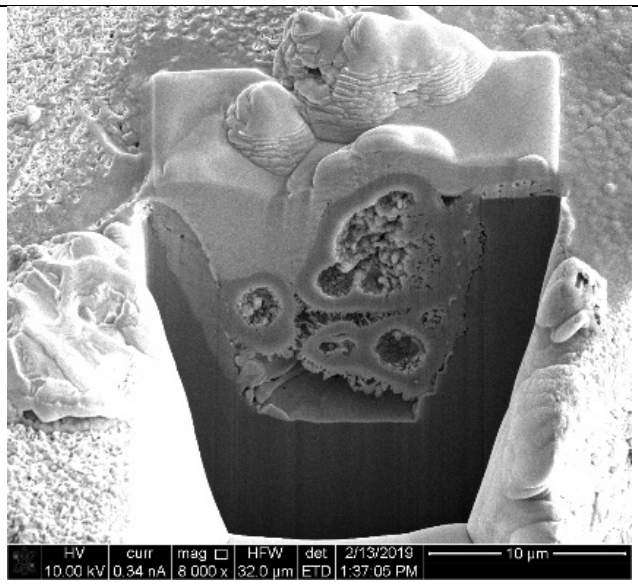

Figure 7.3.6 An example of Ion- induced secondary electron micrographs of the particles sectioning using FIB.

During the sample sectioning, the results showed that the expansive growth of the iron particles during oxidation filled the majority of the free space in the milled hole (Figure 7.3.6.). The EDS mapping of Fe and O allows clear identification that the iron particles achieved full oxidation (Figure 7.3.7). Interestingly the core of the particles showed a distinct porosity in some cases. This was attributed to the diffusional process for iron oxide formation, facilitated by cation (Fe) diffusion from the metallic core outwards through the oxide to the particle surface.

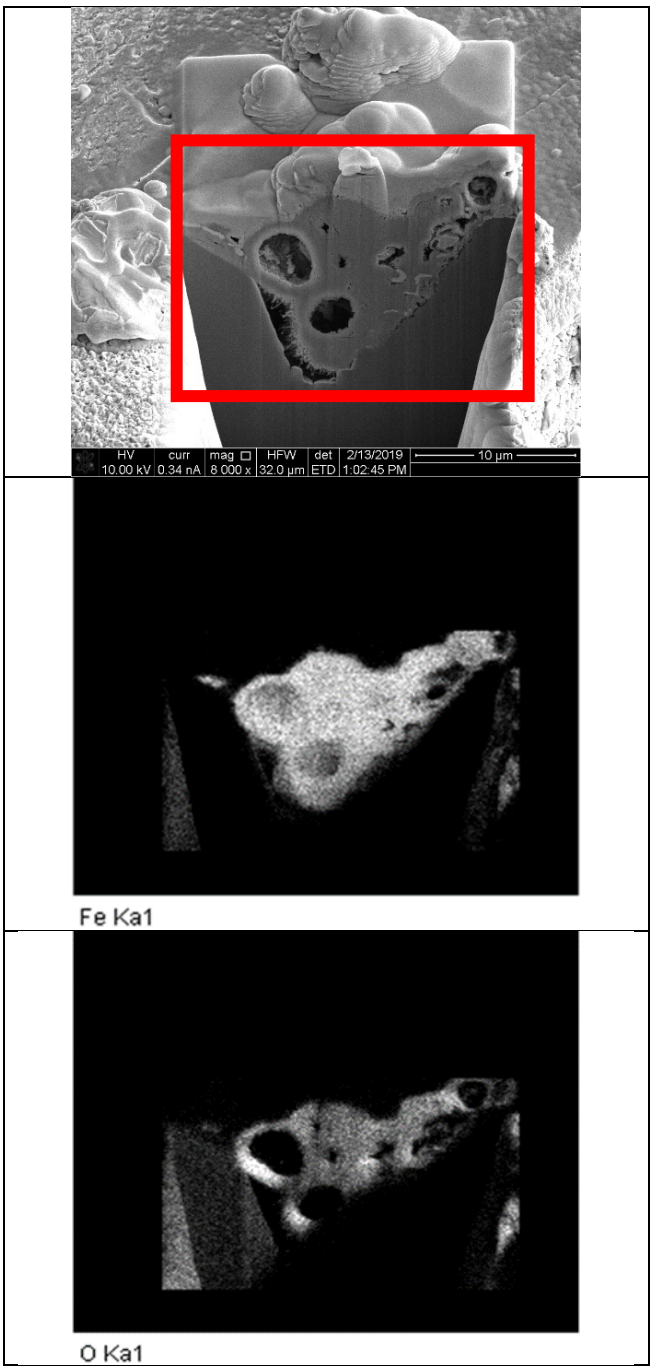

Figure 7.3.7 Elemental (EDX) mapping showing a section face through an infilled hole.

It is notable that the ion-milled holes did not have a flat bottom. Instead the holes had an angled base to provide a 'wedge' shape that would be more representative of a simulated pre-existing crack in the material surface. This is illustrated in the serial FIB sections (Figure 7.3.6).

7.3.2 Ion-Milled Cavities in Limestone

7.3.2.1 SEM-EDS Results

A similar set of experiments was conducted on the limestone sample substrates obtained from Manqabah Quarry. From the experiments on calcite it was determined that the XRT analysis did not quite have sufficient spatial resolution to provide a detailed observation of the in-hole oxidation process. Accordingly, this method of analysis was dropped from the experiments on the Manqabah Limestone.

As prepared Fe micro-particles were inserted in the ion-milled holes as shown Figure 7.3.8, then the sample was heated at 400°C in air for a series of sequential exposure times (See Table 7.2.1). The SEM-EDS analysis of the as prepared substrate and the particles is shown in Figure 7.3.8.

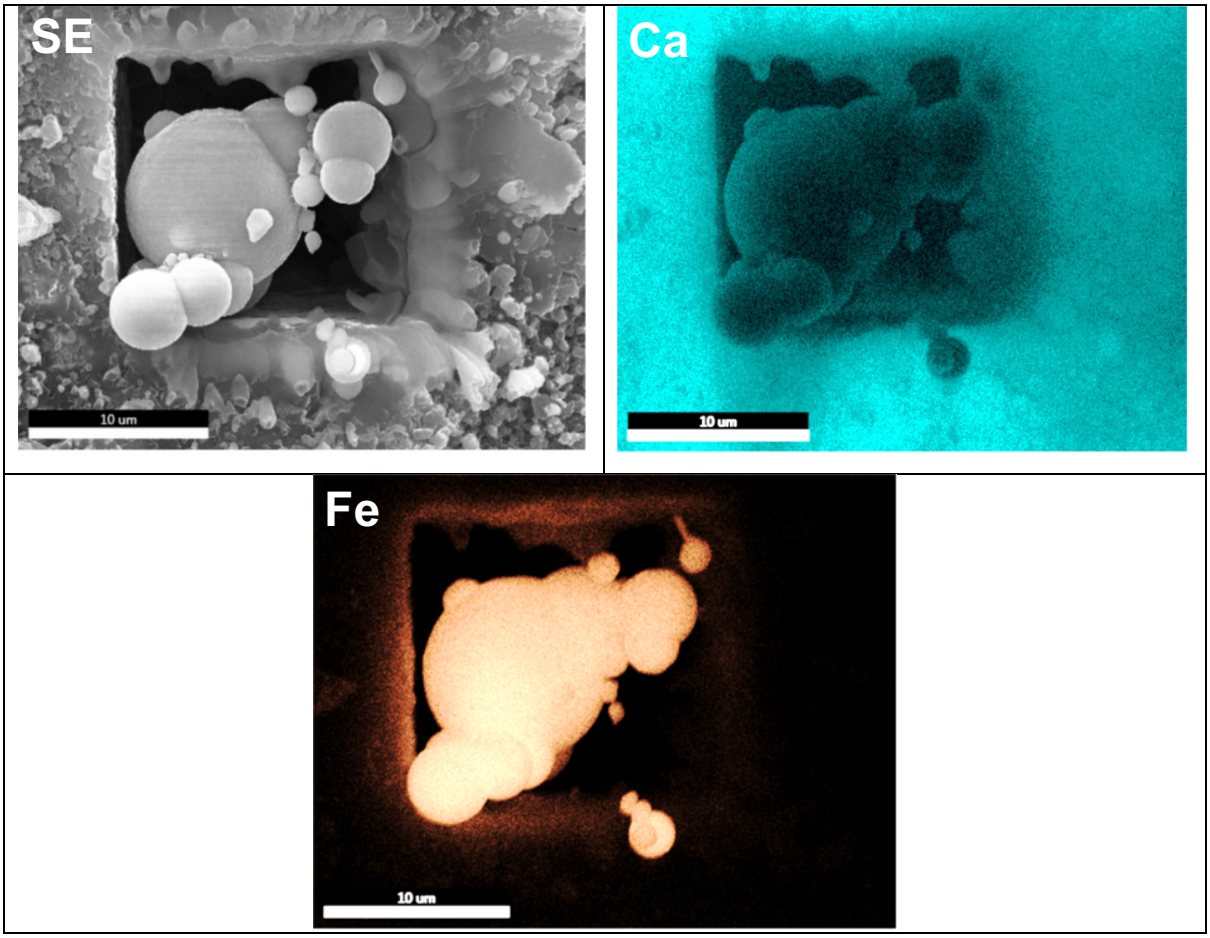

Figure 7.3.8 SEM micrograph and EDX (Ca & Fe) mapping of an infilled hole in the limestone.

Following thermal exposure of 12, 24 and 48 hours, the iron micro-particles showed significant volume expansion. Development of micro-cracking was also observed, which was not present on the as-prepared sample.

A typical SEM micrograph obtained from the thermally oxidised sample after 48 hours is shown in Figure 7.3.9. EDS mapping clearly shows the distribution of Fe, O and Ca, with Ca attributed as the main constituent of limestone and was not present in the metal particles.

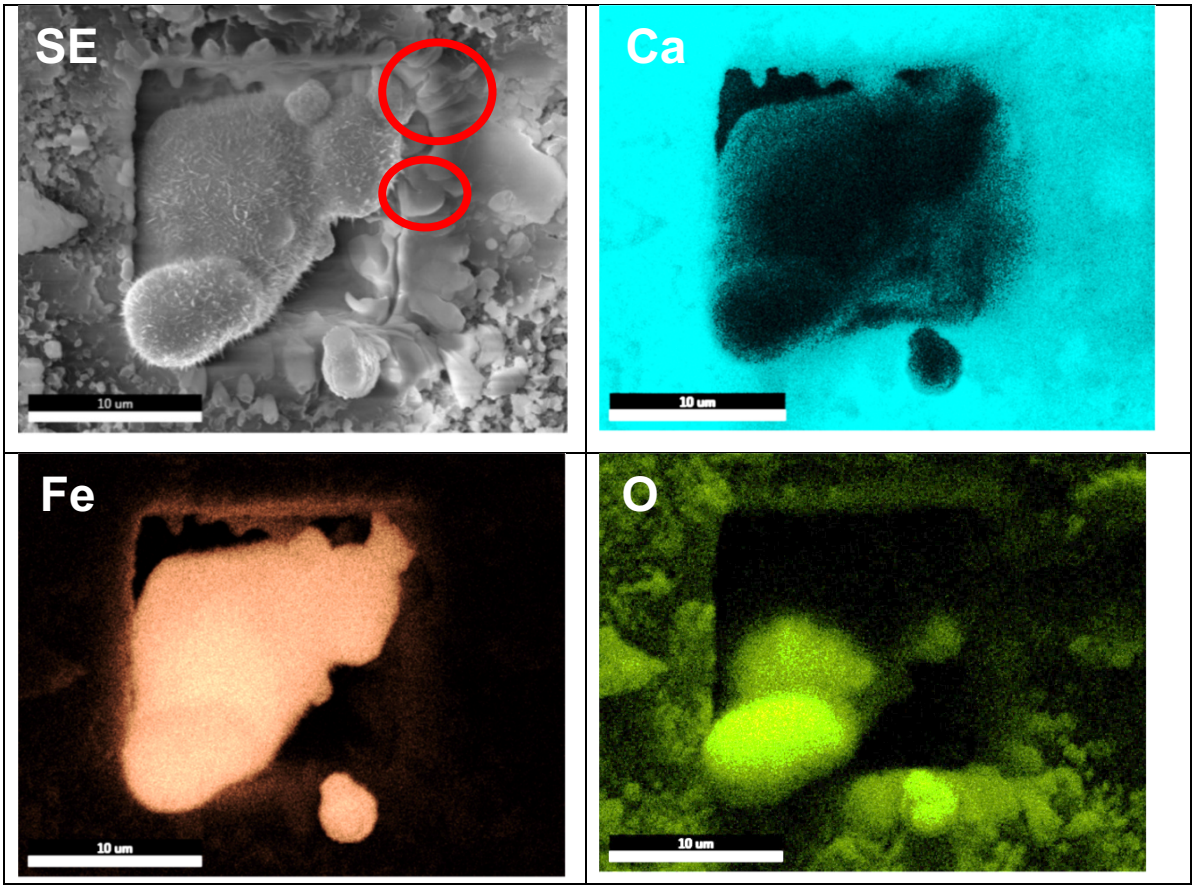

Figure 7.3.9 SEM micrograph and coincident EDX elemental mapping of the Fe particles after 48 hours of in-hole oxidation.

Further development of the initiated micro-cracks was observed after thermal exposure for 1056 hours, which evidenced completion of particle oxidation.

The resulting SEM micrographs were collated before and then after each thermal treatment step to chart the progression of oxidation and cracking. The overall comparison showed that the particles expanded (through oxidation) to fill the hole, subsequently creating cracks on the material sample as shown in Figure 7.3.10. This cracking can be attributed to stress generated by the expanding particles and this is defined under ASTM D883, as “stress cracking” - an external crack [5].

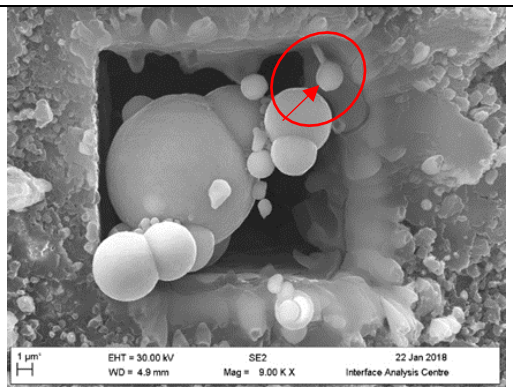

As prepared

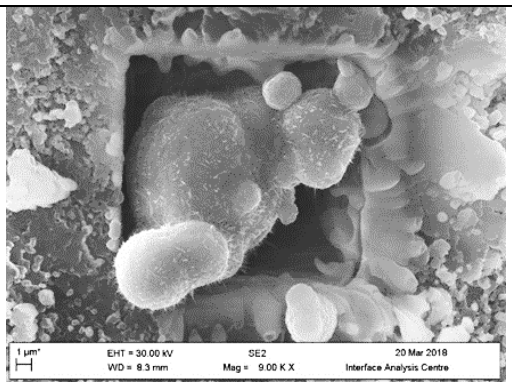

After 12 Hours

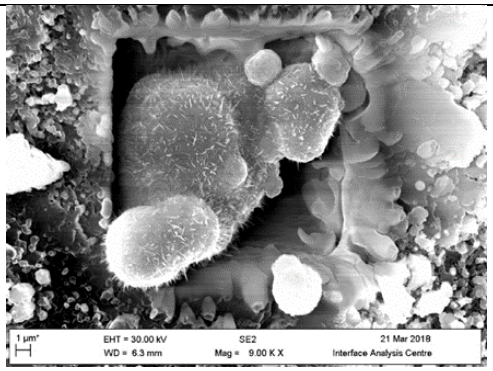

After 24 Hours

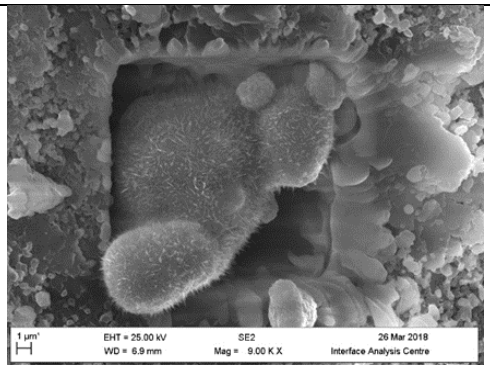

After 48 Hours

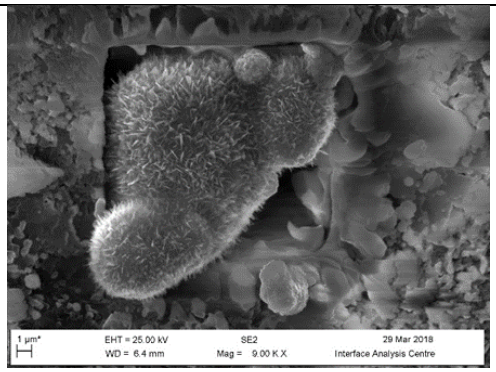

After 96 Hours

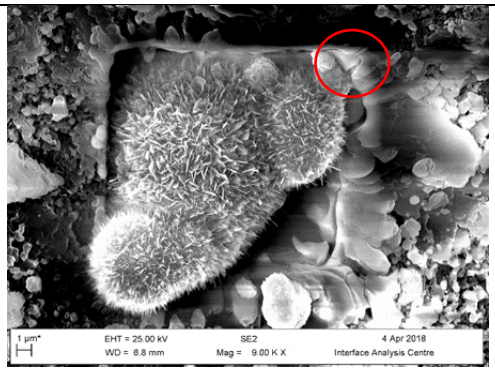

After 196 Hours

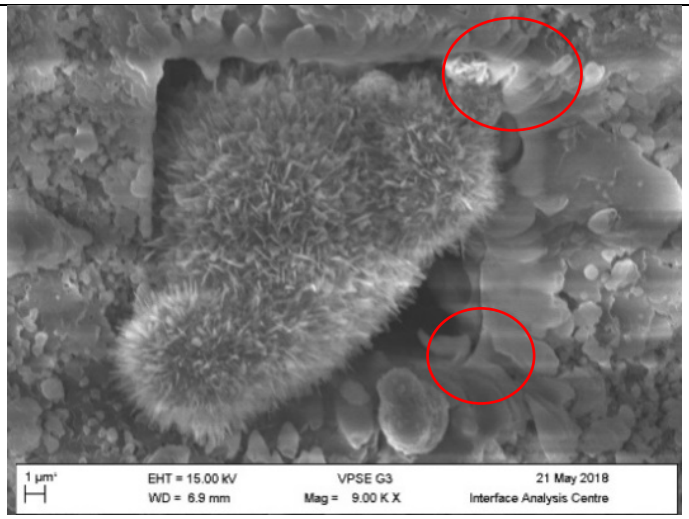

After 1056 Hours

Figure 7.3.10 A sequence of SEM-Micrographs showing progressive particle oxidation.

The sequence shows that the majority of the volume expansion had completed within 48 hours, which is commensurate with the TGA-DSC study. The micrographs at 96, 196 and 1056 hours show very little difference in the volume and extent of the particles. As in the previous experiments on calcite, the particle surfaces exhibited a nano-bladed surface texture typical of thermally grown hematite. Fine plate-like structure is observed from volume expansion of the Fe particles by oxidation. It is similar to the morphologies of the rust product formed on the skyward and earthward surfaces after 3 years of exposure in the marine-urban-industrial environment [6].

The size of the largest iron particle subjected to thermal treatment was determined to be ~9 µm in diameter. By charting its subsequent volume expansion and assuming that it was solid throughout a comparison of oxidation rate for different heating period could be calculated. It can be observed that the iron particle increases in volume with increase thermal period following a parabolic reaction rate, in good agreement with the TGA-DSC experiments. This indicates that the oxidation of the particles was not apparently hindered by the down-hole location, which was as expected. Coefficient of correlation has been applied in this study to find out the relationships between the particle diameter in (µm) and exposure time in (hours). In general, positive correlation have been recorded with R-value ranges at 0.92 and is shown in Figure 7.3.11.

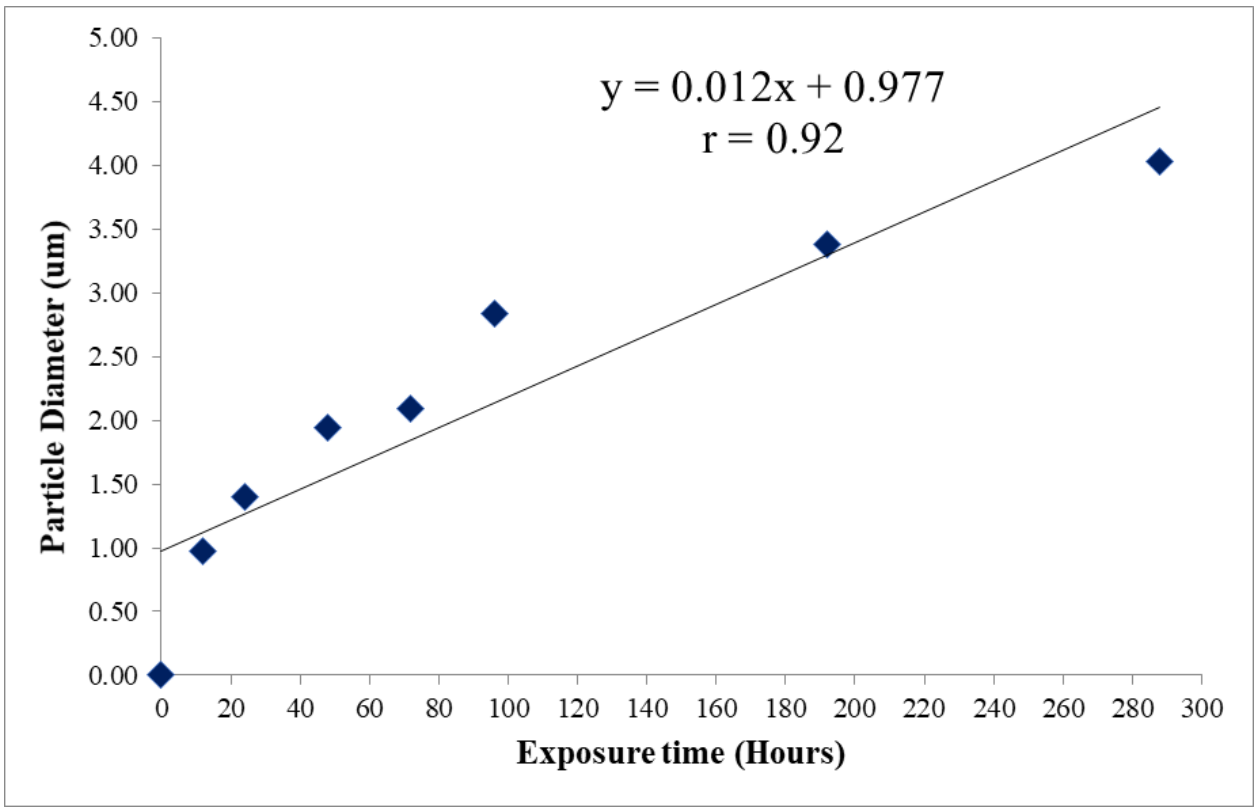

Figure 7.3.11 Determined oxidation rate of iron particle inside the limestone.

In both the calcite single crystal experiments and the limestone experiments it was observed that the Fe particles underwent significant volume expansion; of more than 50% in most cases. This expansion, when confined by the ion-milled holes was expected to exert a significant force on the surrounding material. From the observed micro-cracking it is evidenced that this applied stress was sufficient to overcome the critical yield strength of both the calcite, and more easily the limestone.

7.4 Summary Discussion

The combined experimental work presented in this chapter has provided compelling evidence to validate the hypothesis that aerosol metal particles deposited (wet or dry) onto building surfaces can potentially accelerate the surface degradation if, during deposition, they become wedged or entrapped in cavities or pre-existing cracks and subsequently undergo oxidation with an associated volumetric expansion. The data presented in Chapters 5 and 6 clearly demonstrates that (1) in the city of Jeddah a proportion of the air pollution is constituted by spherical metallic micro-particles (≤PM25) derived from industrial high temperature thermal processes occurring in the city and (2) in the Historic Quarter of the city, the building surfaces are clearly evidenced as having received deposition of these metallic aerosol particles which are well embedded on the building surfaces and especially on coarse building plaster which has a more pronounced micro-roughness.

The experiments presented have demonstrated that even with partial oxidation of the metal particles it is feasible that the associated volume expansion could generate strains in the material surface exceeding the yield strength – hence causing cracking and potential delamination of the outermost surface. The climatic conditions present in Jeddah are some of the most extreme to be experienced anywhere in the world in terms of temperature and humidity. This combined with marine aerosol salts, means that corrosion of the metal particles would be expectedly rapid. Corrosion would not be anywhere near as rapid as the thermal treatments used to accelerate the corrosion process but based on previous literature studies a rate 30-70 μm per year could be expected [7].

Specifically, it is reported that corrosion of carbon steel and mild steel occurs when the relative humidity of the air is above 70% to 80% and the air temperature is above 32 F (0 degrees Celsius). Corrosion rates will accelerate with increasing temperature and may be accelerated further by air impurities e.g. salts, that dissolve in condensed water or rainwater and by dust and dirt settling on the metal surface to facilitate galvanic corrosion or dissolution.

An excellent review of environmental factors affecting steel corrosion is provided by Okonkwo et al [8] which assesses the different environmental factors from temperature and humidity through to aerosol salts and acid rain.

Drawing parallels with Lan et al. [9] who studied the concentration of some environmental factors in Vietnam, which has a high climatic temperature, relative humidity and frequent rainfall. The concentration of sulphur dioxide (SO_2) in the study areas in Vietnam was found to be high compared to other environmental factors and was high compared to values recorded for Jeddah. Regardless, the study revealed that steel was very sensitive to acidic pollutants especially sulphur dioxide and acid rain [9].

For a coastal region like Jeddah where temperatures will expectedly be ~50°C between July and October with high humidity, the ambient temperature and other environmental factors may have influential roles in the corrosion process of the observed Fe-Zn-Cu microparticles. Environmental factors can change from one country to another as some countries have high temperature, high humidity, frequent rainfall, and several pollutants availability [10].

There are several environmental factors that can influence the corrosion (and corrosion rate) of steel materials exposed to the atmosphere. The degree of impact of these factors depends on the intensity and concentration of these factors at each location and can also be a combined effect of interrelated environmental factors [Okonkwo et al].

For example, Chloride ions are often found in industrial areas and exist as one of the most vital and common atmospheric corrosive agents [11, 12]. For example, in the gulf states it is well documented that the presence of the chloride ions in the atmosphere can influence the corrosion of carbon steel used for oil pipelines and can even lead to the failure of the entire pipeline system [13, 14, 15].

Certainly, for Jeddah which is coastally located, the historic as well as our own aerosol analysis clearly evidences the presence of chloride. This chloride could either be derived from the sea (which is most likely given predominant wind directions) or from nearby desert areas derived from aeolian erosion and pickup of surficial evaporite salt deposits. A study by Syed [16] suggested that sea wind can release up to 0.45kg of sea salt per cubic mile into the air, which poses the expectation that chloride co-deposited with the metal micro-particles could help to accelerate the rate of subsequent corrosion.

Indeed, other studies have also shown that sea-salt aerosols will also contain measurable quantities of magnesium chloride ($MgCl_2$) as well as sodium chloride (NaCl) which can promote steel corrosion even at low humidity [17, 18]. The second study [18] also revealed that sea water can also be a significant source of SO_2 and this is corroborated but further work that has shown the concentration of atmospheric SO_2 is often greater in coastal areas [19], and consequently will affect the corrosion rate of steels more in coastal towns, cities and industrial facilities. In a moist environment, the SO_2 is absorbed onto steel surfaces which is converted to $FeSO_4$. This process occurs because sulphur dioxide has a high solubility in water and has the affinity to form sulfuric acid in atmospheric moisture films which subsequently attached the steel causing enhanced corrosion.

Several studies have examined the corrosion behaviour of different steel-types exposed to chloride-rich environments [20, 21, 22]. The generally accepted viewpoint is that the steel corrosion rate increases after exposure to chloride contaminated atmospheric conditions for a certain time period. For example, Castaño et al. [23] studied the effect of chloride on the corrosion behaviour of carbon steel at six test sites in Colombia, specifically examining the relationship between exposure time and environmental characteristics of each site. Chlorides were found to be most influential environmental factor affecting steel corrosion.

The ambient temperature has also been shown to influence the rate of steel corrosion [24, 25]. If the humidity is constant, an increase in the surface temperature will increase the rate of chemical reaction. Nevertheless, the effect of temperature on atmospheric corrosion is relatively complex. Increase in the ambient temperature will tend to increase both electrochemical and diffusion processes, thereby increasing the rates of corrosion by enhancing the kinetics. On the other hand, increasing the temperature towards the extremes sometimes recorded in Jeddah, will locally decrease the humidity and increase the evaporation of surface adsorbed water layers thereby drying out the steel surfaces [Behrangi et al]. This latter effect is not considered to be significant in Jeddah where relative humidity remains high throughout the year due to the city's coastal aspect.

In the future, with rising atmospheric CO_2 levels the rate of metallic iron corrosion, as well as building surface degradation, is likely to increase further due to the formation of carbonic acid at higher concentrations [26]. This will be an inevitable and detrimental result of ongoing anthropogenic CO_2 releases that is often completely overlooked by governments and the public.

To curb the accelerating rates of metal corrosion and materials degradation on historic (and other) building structures it is therefore important to have cleaner air, both from the standpoint of having fewer metallic aerosol particles but also from gaseous pollutants including CO_2.

7.5 Summary

In summary, the work presented in this chapter has identified and verified that corrosion of micro-scale metallic particles deposited onto building surfaces can act as a mechanism to cause accelerated surface degradation. This will be most pronounced on material surfaces which have a roughened surfaces and relatively low yield strength. For example, a granite or marble surface would expectedly be more resistant to this mechanism of degradation than a calcite-cemented sandstone or limestone. The following key points can be highlighted:

- The results show that the iron micro-particles expand during oxidation to fill the ion-beam milled cavities and subsequently generated sufficient hydraulic force to create cracks in the host (calcite and limestone) materials.

- Cracks were formed in both the calcite single crystal sample and the limestone sample.

- Only limited corrosion (and volume expansion) is likely to be necessary to cause hydraulically induced cracking of the building material surfaces.

- The overall conclusion is that the observed metallic aerosol pollutant particles are detrimental for the historical buildings of Jeddah and the mechanism by which degradation is caused, has been demonstrated with experiments.

7.6 References

[1] Lorelei de Jesus, A., Rahman, M.M., Mazaheri, M., Thompson, H., Knibbs, L.D., Jeong, C., Evans, G., Nei, W., Ding, A., Qiao, L., Li, L., Portin, H., Niemi, J.V., Timonen, H., Luoma, K., Petaja, T., Kulmala, M., Kowalski M., Morawska, L., (2019). Ultrafine particles and PM2.5 in the air of cities around the world: Are they representative of each other? Environmental International, 129, pp 118-135 Available at: https://doi.org/10.1016/j.envint.2019.05.021.

[2] Karunadasa, K.S.P., Manoratne, C.H., Pitawala, H.M.T.G.A., Rajapakse, R.M.G., (2019). Thermal decomposition of calcium carbonate (calcite polymorph) as examined by in-situ high-temperature X-ray powder diffraction, Journal of Physics and Chemistry of Solids, 134, pp 21-28. Available at: https://doi.org/10.1016/j.jpcs.2019.05.023.

[3] Drakopoulos, M., Connolley, T., Reinhard, C., Atwood, R., Magdysyuk, O., Vo, N., Hart, M., Connor, L., Humphreys, B., Howell, G., Davies, S., Hill, T., Wilkin, G., Pedersen, U., Foster, A., De Maio, N., Basham, M., Yuan, F., Wanelik, K., (2015). The Joint Engineering, Environment and Processing (JEEP) beamline at Diamond Light Source. J Synchrotron Radiat; 22:828–38. Available at: doi:10.1107/S1700577515003513.

[4] Bock, R., (1979). A Handbook of Decomposition Methods in Analytical Chemistry. International Textbook Company, Limited. T. & A. Constable Ltd., Great Britain.

[5] Hsuan, Y.G., Koerner, R.M., (1993). Stress-Cracking Resistance of High-Density Polyethylene Geomembranes, Journal of Geotechnical Engineering, volume 119, Issue 11.

[6] Dhaiveegan, P., Elangovan, N., Nishimura, T., Rajendran, N., (2016). Weathering Steel in Industrial- Marine-Urban Environment: Field Study. MATERIAL TRANSACTION 57(2), Available at: DOI: 10.2320/matertrans.M2015345.

[7] American Galvanizers Association. Corrosion Rate. https://galvanizeit.org/corrosion/corrosion-process/corrosion-rate. Retrieved February 25, 2020.

[8] Okonkwo, P., Shakoor, A., Mohamed, A.M.A., (2015). ENVIRONMENTAL FACTORS AFFECTING CORROSION OF PIPELINE STEEL: A REVIEW, International Journal of Mechanical and Production Engineering Research and Development (IJMPERD) ISSN(P): 2249-6890; ISSN(E): 2249-8001 Vol. 5, Issue 5, pp 57-70.

[9] Lan, T., Nguyen, T., Nishimura, R., Tsujino, Y., Yokoi, M., Maeda, Y., (2006). Atmospheric corrosion of carbon steel under field exposure in the southern part of Vietnam. Corrosion Science, Volume 48, pp 179-192, Available at: https://doi.org/10.1016/j.corsci.2004.11.018.

[10] Rodríguez, J.J.S., F.J.S. Hernández., J.E.G. González., (2003). The effect of environmental and meteorological variables on atmospheric corrosion of carbon steel, copper, zinc and aluminium in a limited geographic zone with different types of environment. Corrosion Science, 45(4): p. 799-815. Available at: http://hdl.handle.net/10553/53006.

[11] Iakovleva, E., Makila, E., Salonen, J., Sitarz, M., Sillanpaa, M., (2015). Industrial products and wastes as adsorbents for sulphate and chloride removal from synthetic alkaline solution and mine process water. Chemical Engineering Journal, 259: p. 364-371. Available at: DOI: 10.1016/j.cej.2014.07.091.

[12] Wojnicki, M., Luty-Blocho, M., Socha, R.P., Mech, K., Pedzich, Z., Fitzner, K., Rudnik, E., (2015). Kinetic studies of sorption and reduction of gold (III) chloride complex ions on activated carbon Norit ROX 0.8. Journal of Industrial and Engineering Chemistry, 29: p. 289-297. Available at: DOI10.1016/j.jiec.2015.03.036.

[13] Kale, A., Thacker, B.N., Sridhar, N., Waldhart, C.J., (2008). A probabilistic model for internal corrosion of gas pipelines. in Proceedings of the Biennial International Pipeline Conference, IPC. Paper No: IPC2004-0483, pp. 2437-2445. Available at: https://doi.org/10.1115/IPC2004-0483.

[14] Singh, M., Markeset, T., (2014). Simultaneous handling of variability and uncertainty in probabilistic and possibilistic failure analysis of corroded pipes. International Journal of Systems Assurance Engineering and Management, 5(1): p. 43-54.

[15] Ossai, C.I., Boswell, B., Davies, I.J., (2015). Pipeline failures in corrosive environments – A conceptual analysis of trends and effects. Engineering Failure Analysis, 53: p. 36-58. Available at: https://doi.org/10.1016/j.engfailanal.2015.03.004.

[16] SYED, S., (2006). ATMOSPHERIC CORROSION OF MATERIALS. Emirates Journal for Engineering Research, 1(11): p. 1-24.

[17] Feliu, S., Morcillo, M., (1993). The prediction of atmospheric corrosion from meteorological and pollution parameters—I. Annual corrosion. Corrosion Science, 34(3): p. 403-414. Available at: https://doi.org/10.1016/0010-938X(93)90112-T.

[18] Ericsson, R., (1978). The influence of sodium chloride on the atmospheric corrosion of steel. Materials and Corrosion, 29(6): p. 400-403. Available at: https://doi.org/10.1002/maco.19780290604.

[19] Chen, W., Hao, L., Dong, J., Ke, W., (2014). Effect of sulphur dioxide on the corrosion of a low alloy steel in simulated coastal industrial atmosphere. Corrosion Scienc. 83: p. 155.

[20] Liu, Q.Y., Mao, L.J., Zhou S.W., (2014). Effects of chloride content on CO2 corrosion of carbon steel in simulated oil and gas well environments. Corrosion Science, 84: p. 165-171. Available at: DOI: 10.1016/j.corsci.2014.03.025.

[21] Wang, Y., Cheng, G., Wu, W., Qiao, Q., Li, Y., Li, X., (2015). Effect of pH and chloride on the micro-mechanism of pitting corrosion for high strength pipeline steel in aerated NaCl solutions. Applied Surface Science, 349: p. 746-756. Available at: DOI: 10.1016/j.apsusc.2015.05.053.

[22] Yeğen, I., Usta, M., (2010). The effect of salt bath cementation on mechanical behavior of hot-rolled and cold-drawn SAE 8620 and 16MnCr5 steels. Vacuum, 85(3): p. 390-396 Available at: DOI: 10.1016/j.vacuum.2010.07.013.

[23] Castaño, J.G., Botero, C., Restrepo, A., Agudelo, E., Correa, E., Echeverria, F., (2010). Atmospheric corrosion of carbon steel in Colombia. Corrosion Science, 52(1): p. 216-223. Available at: DOI: 10.1016/j.corsci.2009.09.006.

[24] Jiang, G., Keller, J., Bond P.L., (2014). Determining the long-term effects of H2S concentration, relative humidity and air temperature on concrete sewer corrosion. Water Research, 65: p. 157-169. Available at: doi: 10.1016/j.watres.2014.07.026.

[25] Behrangi, A., Nguyen, H., Lambrigtsen, B., Schreier, M., Dang, V., (2015). Investigating the role of multi-spectral and near surface temperature and humidity data to improve precipitation detection at high latitudes. Atmospheric Research, 163: p. 2-12. Available at: DOI: 10.1016/j.atmosres.2014.10.019.

[26] Yin, Z.F., Feng, Y.R., Zhao, W.Z., Bai, Z.Q., Lin, G.F., (2009). Effect of temperature on CO_2 corrosion of carbon steel. Surface and Interface Analysis, 41(6): p. 517-523. Available at: https://doi.org/10.1002/sia.3057.

CHAPTER 8

GENERAL DISCUSSION AND CONCLUSION

8.1 Material Characterisation

Increasing levels of atmospheric pollution have been observed to accentuate and accelerate the degradation of building surfaces in the historical quarter, over the last few decades in Jeddah, Saudi Arabia. The site located in the south of Jeddah city, is surrounded by industrial activities such as the oil refinery and Jeddah port, which are considered to constitute major local pollution sources.

This study investigates the chemical and mineralogical characteristic of the building materials used to construct the declared UNESCO world heritage site located in Jeddah. Stone, mortar and plaster samples were collected from six historic buildings as well as from the quarry from which the stone blocks were originally produced. The main objective of this work was to identify the composition and alteration of the stone, mortar and plaster to provide information about the degradation mechanisms. Light Optical Microscopy (OM), X-ray Diffraction (XRD), Laser Raman Spectroscopy (LRS) and Scanning Electron Microscopy combined with Energy-Dispersion X-ray Spectroscopy (FEGSEM-EDS) were all utilized as analytical tools to determine the chemical composition of the corresponding materials.

The results revealed that the stone used throughout the historic buildings, is calcareous limestone ($CaCO_3$). Where the binder in mortar mix is determined to have been non-hydraulic lime ($Ca(OH)_2$). Equally, the associated binder in 'standard' plaster is also lime based, made with non-hydraulic lime and local sand, whilst the decorative plaster is made of gypsum ($CaSO_4.2H_2O$). On degraded surfaces of plaster samples, it was possible to detect the deposition of sea salt and not oxide metallic particles, of Fe, Cu and Zn. The observation of metallic particles was unusual and not to our knowledge, previously reported in any aerosol pollution survey in Jeddah or elsewhere.

8.2 Sampling of Aerosol Pollutants

The results gathered from detailed characterisation of the collected building materials showed that exposed surfaces in the historical quarter contained ~150-200 particle/mm² spherical metallic aerosol particles that were particularly abundant on plaster surfaces located on the west face of Jokhdar house contained ~200-300 particle/ mm² and size of the particles (5-40μm).

Atmospheric particle samples were collected from two locations at the world heritage site and from the southern industrial areas using a particle impactor made by California Measurements Inc. In addition, sampling filters from the industrial area using MP101M analyzer were provided for analysis by The General Authority of Meteorology and Environment Protection (GAMEP) in Jeddah.

The collected filter samples were analysed using SEM-EDS and XRF. The results from impactor samples collected at the historical site identified C, Fe, Cu and Zn. In addition, Ca, Al, Si, Na and Cl that were all identified in minor quantities. Aerosol particles were commonly spherical and metallic, rather than metal oxides.

The filters provided from The General Authority of Meteorology and Environment Protection (GAMEP) identified Zn and Fe. In addition, a small amount of Mn, Cu, Ca, K, Ti and S were also identified, provide a good correlation with our own sampling results.

The analysis showed that both the historical and industrial sites in Jeddah city are heavily polluted. This finding is in a good agreement with the results obtained from the building materials characterisation. A key observation is that the spherical micro-sized metal particles found on building surfaces are derived from the air, as aerosol pollution particles.

8.3 The Role of the Metallic Particles in the Degradation of Building Materials

Having confirmed that the metallic micro-particles were being deposited on building surfaces, the next phase of the research aimed at examining the mechanism by which their environmental corrosion accelerate the degradation of building surfaces. The hypothesis was that these particles can affect the building surfaces by opening micro cracks, upon oxidation with time, and thus damaging the buildings.

Experiment attempted to recreate the degradation process by using calcite single crystal and limestone samples. High purity spherical iron powder of grain sizes <10 micron were inserted into micro-machined holes created by a Focused (gallium) Ion Beam instrument. This was to mimic the aerosols entering micro-cracks or depressions on the building surfaces. Then, the samples were heated at 400°C for different exposure times to induce accelerated oxidation, with associated volume expansion. The result showed that the particles expanded in volume to fill the holes, subsequently creating cracks in the surrounding material. More frequent cracking was observed in single crystal calcite than limestone which was attributed to the single crystal having no grain boundary networks or particle interfaces within which the accumulated strains might better be dispersed. This finding showed that the metallic pollutants can cause accelerated damage on building material surfaces especially, for historical buildings.

8.4 Conclusion

The aim of this work is to identify the type of atmospheric pollutants at the historical quarter in Jeddah, Saudi Arabia and the influence of different aerosol components on the degradation of the building materials. The results will underpin the generation of new guidelines for the Meteorological, Health departments and the Saudi Commission for Tourism and National Heritage, which is responsible for the preservation and management of all historical sites in Saudi Arabia.

Furthermore, this study will afford significant data on particulate air pollutants and their role in the degradation of these historical buildings. Subsequently, this will inform strategies for protecting, preserving or restoring these historical quarters.

It is expected that this study, focused on Jeddah city will be applicable to most any city in the same climatic zone and will therefore have a wide-ranging international consequence. An exception is the source of metallic aerosols, which would seem to be characteristic of high temperature pyroprocessing such as that conducted in oil refineries.

Overall, the current research revealed that there is a significant effect of the oxidation of metallic particles on the degradation of building material surfaces in the city of Jeddah. There is also a wider consideration and evaluation that needs to be made with respect to human health. This will be discussed in the following final chapter.

CHAPTER 9
FUTURE WORK

Based on the results obtained from this research, it can be determined that the historical quarter of Jeddah city is heavily polluted with salt and metallic aerosol particles and toxic gases. Jeddah city is geographically surrounded by numerous industrial activities, such as the production of steel, paper, glass and an oil refinery. The atmosphere in Jeddah city is also laden with sea salt from the red sea, soil dust generated from exposed soils and nearby desert areas. In summer, temperatures reach up to 52^{o}C with a relative humidity of > 90%. All these parameters will have an effect on human health as well as the degradation of building materials.

Future studies are necessary to provide further reliable data to help the Saudi Arabia government to manage and mitigate the effects of the air pollution in their cities. Future studies should cover:

- Protection of the environment by the application of research and environmental policies to protect habitats and to control hazardous emissions. Implementation of an environmental management systems and procedures would allow identification and evaluation of the environmental impacts arising from pollution and the major sources of pollution themselves. Limiting industrial emissions, via more stringent regulations would be an important objective, but only when the primary sources of the pollution have been thoroughly and scientifically confirmed.

- Research into public awareness and raising public awareness of air pollution issues in Jeddah, the negative effect it has on human health as well as historic buildings that are considered as national treasures. This will be in coincidence with raising awareness about the global challenges and concerns about climate change and rising atmospheric CO_2 levels.

- Develop an assessment mechanism to better evaluate and tackle local climate-change related challenges in Jeddah city and around the historical quarter.

- Investigate the filtering systems used by local industries to limit particulate aerosol emissions and propose enhanced methods to reduce both toxic gas and aerosol particle emissions into the environment.

- Continued city-wide monitoring of air pollution in Jeddah, establishing a wireless network which provides real-time data such that daily, seasonal and other temporal patterns of pollution level variation can be captured and understood. Any enhanced monitoring campaign should be underpinned by regular impactor-type sampling to understand the types of aerosol particles present in the air around Jeddah and the risk factors they pose.

- Based on this proposed data network and working with The General Authority of Meteorology and Environment Protection a detailed environmental impact assessment needs to be constructed and evaluated before establishing any major new industrial activities in the city, to ensure they follow the international specification and do not significantly add to the existing pollution burden.

- Finally, it is recommended to work with the Ministry of Education to develop a full understanding in the student population of the importance of the environment and the need for good and responsible custodianship.

In the longer term, if atmospheric CO_2 levels are to rise still further, then it is expected that acid effects will further accelerate building degradation, especially in climatic areas with very high humidity.

Consequently, further research is required to establish degradation rate experiments for different simulated atmospheric CO_2 levels, to quantitively establish just how much faster degradation of buildings will occur, historic or otherwise.